Study of catalysts for isobutene and alcohols transformation in view of biomass valorization

Aleksandra Lilic

N°d'ordre NNT : 2017LYSE1084

THESE de DOCTORAT DE L'UNIVERSITE DE LYON

opérée au sein de
l'Université Claude Bernard Lyon 1

Ecole Doctorale ED 206
(Chimie, Procédés, Environnement)

Spécialité de doctorat : Catalyse hétérogène, Calorimétrie d'adsorption
Discipline : Chimie

Soutenue publiquement le 09/06/2017 par
Aleksandra LILIĆ

Title: **Study of catalysts for isobutene and alcohols transformation in view of biomass valorization**

Titre: **Valorisation de la biomasse par l'étude de catalyseurs pour la transformation de l'isobutène et d'alcools**

Devant le jury composé de:

M. FONGARLAND Pascal Professeur *d'Université Lyon 1* et Directeur à *LGPC*	**Président**
M. CAPRON Mickaël Maitre de conférences (HDR) à *l'Université Lille 1*	**Rapporteur**
M. DUBOIS Jean-Luc Directeur Scientifique à *ARKEMA*	**Rapporteur**
M. VÉDRINE Jacques Directeur de recherche à *l'UPMC-Paris 6*	**Examinateur**
Mme BENNICI Simona Chargée de recherche (HDR) à *l'IS2M (CNRS)*	**Directrice de thèse**
Mme AUROUX Aline Directrice de recherche à *l'IRCELYON (CNRS)*	**Co-directrice de thèse**
M. DEVAUX Jean-François Chercheur sénior à *ARKEMA*	**Membre invité**

UNIVERSITE CLAUDE BERNARD - LYON 1

Président de l'Université	**M. le Professeur Frédéric FLEURY**
Président du Conseil Académique	M. le Professeur Hamda BEN HADID
Vice-président du Conseil d'Administration	M. le Professeur Didier REVEL
Vice-président du Conseil Formation et Vie Universitaire	M. le Professeur Philippe CHEVALIER
Vice-président de la Commission Recherche	M. Fabrice VALLÉE
Directrice Générale des Services	Mme Dominique MARCHAND

COMPOSANTES SANTE

Faculté de Médecine Lyon Est – Claude Bernard	Directeur : M. le Professeur G.RODE
Faculté de Médecine et de Maïeutique Lyon Sud – Charles Mérieux	Directeur : Mme la Professeure C. BURILLON
Faculté d'Odontologie	Directeur : M. le Professeur D. BOURGEOIS
Institut des Sciences Pharmaceutiques et Biologiques	Directeur : Mme la Professeure C. VINCIGUERRA
Institut des Sciences et Techniques de la Réadaptation	Directeur : M. X. PERROT
Département de formation et Centre de Recherche en Biologie Humaine	Directeur : Mme la Professeure A-M. SCHOTT

COMPOSANTES ET DEPARTEMENTS DE SCIENCES ET TECHNOLOGIE

Faculté des Sciences et Technologies	Directeur : M. F. DE MARCHI
Département Biologie	Directeur : M. le Professeur F. THEVENARD
Département Chimie Biochimie	Directeur : Mme C. FELIX
Département GEP	Directeur : M. Hassan HAMMOURI
Département Informatique	Directeur : M. le Professeur S. AKKOUCHE
Département Mathématiques	Directeur : M. le Professeur G. TOMANOV
Département Mécanique	Directeur : M. le Professeur H. BEN HADID
Département Physique	Directeur : M. le Professeur J-C PLENET
UFR Sciences et Techniques des Activités Physiques et Sportives	Directeur : M. Y.VANPOULLE
Observatoire des Sciences de l'Univers de Lyon	Directeur : M. B. GUIDERDONI
Polytech Lyon	Directeur : M. le Professeur E.PERRIN
Ecole Supérieure de Chimie Physique Electronique	Directeur : M. G. PIGNAULT
Institut Universitaire de Technologie de Lyon 1	Directeur : M. le Professeur C. VITON
Ecole Supérieure du Professorat et de l'Education	Directeur : M. le Professeur A. MOUGNIOTTE
Institut de Science Financière et d'Assurances	Directeur : M. N. LEBOISNE

To my parents

and

family.

Acknowledgements

This work has been accomplished from April 2014 to Mai 2017 as a part of the project BioMA+, carrying out the research work in *IRCELYON (Institut de Recherches sur la Catalyse et l'Environnement de Lyon)* and *CRRA ARKEMA (Centre de Recherche Rhône-Alpes, ARKEMA, Pierre Bénite).* At the beginning, I would like to thank everyone who supported me during this period of my life and without whom this thesis could not have been fulfilled.

French Environment and Energy Management Agency (ADEME) is greatly acknowledged for financial support of this project within the framework of the program "Investment for the Future" ("Investissements d'Avenir"). I deeply appreciate the opportunity to collaborate with all the partners of the BioMA+ project, and I am grateful for all the helpful discussions during our meetings.

I am grateful to Mr. Michel Lacroix, director of *IRCELYON*, and his successor Mrs. Catherine Pinel, for welcoming me in *IRCELYON* during my PhD.

I want to thank Mrs. Simona Bennici, my thesis director, for her patient guidance, precious help in the articles and thesis redaction process, and for accepting to follow this thesis until the end, even if she moved to another institute in the meantime.

Certainly, the greatest acknowledgement and appreciation is reserved for Madame Aline Auroux, co-director of this PhD. I am sincerely grateful and honored for the opportunity to be under your supervision and I have learned so much from you. Indeed, your unique skills and character make you an extraordinary mentor, scientist, and research group manager.

I would like to thank Mr. Jean-Luc Dubois for his valuable comments and suggestions during these three years which greatly improved the quality of the research and articles resulted from this thesis, and served me as inspiration and motivation on my scientific path.

Mr. Jean-François Devaux is acknowledged for welcoming me in *CRRA ARKEMA* and providing me everything needed to perform catalytic tests. Thank you for all the help and suggestions, and for generously sharing your knowledge and experience with me.

I would like to thank the jury members of my PhD defense: Mr. Pascal Fongarland, Mr. Jean-Luc Dubois, Mr. Mickaël Capron, Mr. Jacques C. Védrine, and Mr. Jean-François Devaux for having accepted to judge this thesis and for all the constructive remarks they have made.

I had a real pleasure to work with all my colleagues who were in the *ATARI group* (former *Energy*) at *IRCELYON* during my stay in France, and especially with Jingxuan Cai, Amira Jabbari-Hichri, Nicolas Brodu, Cécile Nicoli, Dario Bozzo, Georgeta Postole, Kamel Amzal, Vincent Folliard, Basile Galey, Vu Tung Lam Tran, Flora Som, and Qi Shen.

The biggest "THANK YOU" I want to say to the best student trainees in the world: Tiantian Wei, Audrey Bouvier, and Theo Maconi. Your hard work directly contributed to my PhD thesis and I had a pleasure to collaborate with you.

Special thanks are addressed to the *Technical services of IRCELYON* for valuable technical contributions in XRD, BET, NMR, XPS, TG-DTA-MS, and chemical analyses. Thank you all for your time and willingness to additionally and patiently explain every result or technique when needed.

Genuine gratitude is reserved for Bruno Palatin, Anne Le Gall, Fabienne Vauloup, and all dear colleagues from *CRRA ARKEMA.* Your kind acceptance, meaningful collaboration and help during my stay are highly appreciated and won't be forgotten.

Special acknowledgement goes to Carole Mutschler and Prof. Pascal Fongarland from the *Laboratoire de Génie des Procédés Catalytiques* (*LGPC*, Lyon, France) for their generous help with the thermodynamic calculations.

French Chemical Society (SCF) is greatly acknowledged for the financial grant provided to present my work at *6th EUCHEMS Chemistry Congress* (Seville, Spain).

Very special place in my heart have the dearest colleagues from the *ING* team at *IRCELYON* which always accepted me and supported me during my stay in France and among whom I found some great friends for a lifetime. I was blessed to know you all and thank you for all the great time that we had together.

I would like to thank Prof. Ljiljana Damjanović, without whom I would not have come into this research group; and Prof. Vesna Rakić for her friendly encouragement during the thesis period.

Especially, I use this opportunity to express my deepest gratitude to my best “French” friends Cécile Nicoli, Mirela Tsagkari, Yoldes Khabzina, Anita Borowiec, Natalia Potrzebowska, and Alexandre Legrand. Thank you for your sincere friendship, constant support, and all the good and bad situations that we have survived together. I enjoyed all our “deep philosophical” discussions about life, science, and business.

My dear friends, Tamara Radulović, Katarina Živković, Dušica Jovanović, Ružica Kovrlija, Miljana Gligorijević, Stefan Preković, and Marko Todorović, you were always there for me in every situation and always ready to encourage me, even if far away, and I am truly blessed to have you in my life.

And the last, but not the least, my dear, parents, thank you for all that I am today and I love you so much. The greatest appreciation goes to my dear mother for her continuous support, love, dedication, and understanding.

.

Table of Contents

List of Publications 1

List of Communications 2

Preface and overview of the thesis manuscript 5

Chapter 1. Introduction 9

1.1. Project BioMA+: valorization of sugars 9

1.2. Objectives of the thesis 11

References 15

Chapter 2. State of the art: Catalytic reactions 17

2.1. Oxidation of isobutene (IBN) to methacrylic acid (MAA) 17

2.2. Acrolein 18

2.2.1. Introduction. 18

2.2.2. Acrolein synthesis overview 20

2.3. Methanol and ethanol production 25

2.4. Oxidation of methanol to formaldehyde on FeMoOx catalysts 26

2.5. Oxidation of ethanol to acetaldehyde 29

2.6. Vapor-phase methanol and ethanol coupling reactions in absence of oxygen 34

2.7. Acrolein production by oxidative coupling of methanol and ethanol 36

References 40

Chapter 3. State of the art: Catalysts acidity/basicity 45

3.1. Influence of acid/base properties of the catalysts on the gas-phase aldol condensation of acetaldehyde and formaldehyde 45

3.2. Acid/base properties of the catalysts investigated by gas-solid adsorption microcalorimetry coupled with volumetric line. 59

3.2.1. Bulk, mixed and supported oxides 60

3.2.2. Bulk and supported Keggin type heteropolyacids. 83

References 90

Chapter 4. Experimental part 95

4.1. Catalyst preparation. 95
4.1.1. Catalysts involved in isobutene production 95
4.1.1.1. Bulk oxides 95
4.1.1.2. Bulk heteropolyacids 96
4.1.2. Catalysts involved in acrolein production 96
4.1.2.1. Basic oxides supported on silica and alumina 96
4.1.2.2. Mixed Mg/Al oxides (CHTs) 97
4.1.2.3. Silica-supported heteropolyacids 97
4.1.2.4. Various catalysts 97
4.1.3. List of catalytic materials 98
4.2. Characterization of the catalysts 100
4.2.1. X-ray diffraction (XRD). 100
4.2.2. Chemical analysis (ICP-OES) 101
4.2.3. Thermal analysis techniques 102
4.2.4. BET surface area and pore size determination. 103
4.2.5. X-ray photoelectron spectroscopy 105
4.2.6. ^{27}Al MAS NMR 106
4.2.7. Adsorption microcalorimetry coupled with volumetric line. 108
4.2.8. Liquid phase adsorption calorimetry 112
4.3. Catalytic tests. 114
References 116
Chapter 5. The impact of bio-sourced isobutene impurities on the catalysts used for methacrylic acid production: adsorption microcalorimetry study 117
Abstract 117
5.1. Introduction 118
5.2. Results and discussion 119
5.2.1. Characterization of the commercial catalysts used for the oxidation of isobutene to methacrylic acid 119
5.2.2. Adsorption microcalorimetry performed on model catalysts 123
5.2.2.1. Adsorption microcalorimetry on the bulk oxides 123
5.2.2.2. Adsorption microcalorimetry on the bulk Keggin-type heteropolyacids 127

5.3. Conclusions 134

References 135

Chapter 6. Influence of catalyst acid/base properties in acrolein production by oxidative coupling of ethanol and methanol *(Publication I)* 137

Chapter 7. A comparative study of acidic, amphoteric and basic catalysts in the oxidative coupling of methanol and ethanol for acrolein production *(Publication II)* 163

8. Conclusions 193

List of Abbreviations 199

Abstract (English, French) 201

Résumé substantiel en français 203

List of publications

Results of this thesis have been published or submitted in several international journals which are listed below:

I. A. Lilić, S. Bennici, J.F. Devaux, J.L. Dubois, A. Auroux, "Influence of catalyst acid/base properties in acrolein production by oxidative coupling of methanol and ethanol", *ChemSusChem* **2017**, *10*, 1916-1930. DOI:10.1002/cssc.201700230.

II. A. Lilić, T. Wei, S. Bennici, J.F. Devaux, J.L. Dubois, A. Auroux, "A comparative study of basic, amphoteric and acidic catalysts in the oxidative coupling of methanol and ethanol for acrolein production", accepted in *ChemSusChem.* DOI: 10.1002/cssc.201701040.

III. A. Borowiec, A. Lilić, J.C. Morin, J.F. Devaux, J.L. Dubois, M. Capron, S. Bennici, A. Auroux, F. Dumeignil, "Acrolein production starting from methanol and ethanol over FeMo-doped with La and Ce catalysts", to be submitted to *Applied catalysis A: General*.

List of communications

Oral presentations:

I. A. Lilić, T. Wei, S. Bennici, J.F Devaux, J.L. Dubois, A. Auroux, "Gas-phase production of acrolein from a mixture of alcohols on silica-supported basic oxide catalysts: influence of acid/base features", *Journée Scientifique de la SCF 2016 (Section Rhône-Alpes)*, Grenoble (France), 9/06/2016.

II. A. Lilić, S. Bennici, J.F Devaux, J.L. Dubois, A. Auroux, "Acrolein direct synthesis from methanol and ethanol on hybrid FeMoOx - Na,K,Ca,Mg/SiO2 oxide catalysts", *6th EUCHEMS Chemistry Congress*, Sevilla (Spain), 11-15/09/2016.

III. A. Lilić, V. Folliard, T. Wei, S. Bennici, J.F. Devaux, J.L. Dubois, A. Auroux, "Comparison of basic, amphoteric and acidic catalysts in the oxidative coupling of a mixture of methanol and ethanol for acrolein production", *13th European Congress on Catalysis (EUROPACAT 2017)*, Florence (Italy), 27-31/08/2017.

- -

Poster presentations:

IV. A. Lilić, D. Bozzo, S. Bennici, A. Auroux, "Investigation of the acid-base properties of a series of heteropolyacids by adsorption calorimetry in gas phase and liquid phase", *46th French Conference on Calorimetry and Thermal Analysis (JCAT 2015)*, Montpellier (France), 20-23/05/2015.

V. A. Lilić, D. Bozzo, S. Bennici, A. Auroux, "Acidity of heteropolyacids measured by probe adsorption calorimetry: NH_3 in gas phase and PEA in n-decane", *Journée Scientifique de la SCF 2015 (Section Rhône-Alpes)*, Villeurbanne (France), 11/06/2015.

VI. A. Lilić, D. Bozzo, S. Bennici, A. Auroux, "Comparison of gas phase and liquid phase adsorption calorimetry for evaluating the acid-base properties of various heteropolyacids", *12th Conference on Calorimetry and Thermal Analysis of the Polish Society of Calorimetry and Thermal Analysis* (CCTA12-*PTKAT)*, 6-10/09/2015, Zakopane (Poland).

VII. A. Lilić, S. Bennici, J.F Devaux, J.L. Dubois, A. Auroux, "SO_2 and NH_3 adsorption calorimetry in the study of the surface acid/base properties of oxide catalysts for acrolein production", *47th French Conference on Calorimetry and Thermal Analysis (JCAT 2016)*, Anglette (France), 17-20/05/2016.

VIII. A. Lilić, S. Bennici, J.F Devaux, J.L. Dubois, A. Auroux, “Acrolein production from a mixture of alcohols in gas phase on silica–supported basic oxides catalysts: on which sites?”, *1st French Conference on Catalysis (FCCat 2016)*, Frejus (France), 23-27/05/2016.

IX. A. Lilić, O. Otman, V. Folliard, S. Bennici, A. Auroux, “Understanding catalytic performances in biomass-derived reactions from the acid/base sites strength point of view”, *The International Symposium on Green Chemistry (ISGC 2017)*, La Rochelle (France), 16-19/05/2017.

Preface and overview of the thesis manuscript

Renewable energy sources and sustainable policies, including the promotion of energy efficiency and energy conservation, offer substantial long-term benefits to industrialized, developing and transitional countries. They provide access to clean and domestically available energy and lead to a decreased dependence on fossil fuel imports, and a reduction in greenhouse gas emissions. Renewable resources present a solution to the increased scarcity and price of fossil fuels. Additionally they help to reduce anthropogenic emission of greenhouse gases and their impacts on climate changes. In the chemistry sector, petroleum chemistry can be replaced by sustainable or green chemistry. In agriculture, sustainable methods that enable soils to act as carbon dioxide sinks can be used. In the construction sector, sustainable building practice and green construction can be used, replacing for example steel-enforced concrete by textile-reinforced concrete. Research and development and capital investments in all these sectors will not only contribute to climate protection, but also stimulate economic growth and create millions of new jobs. [1]

Biomass offers a source of carbon from the biosphere, as an alternative to fossilized carbon. Anything that grows and is available in non-fossilized form, can be classified as biomass, including arable crops, trees, bushes, animal by-products, human and animal waste, waste food, and any other waste stream that rots quickly, and it can be replenished on a rolling timeframe of years and decades. One of the attractions of biomass is its versatility: under the right circumstances, it can be used to provide a sustainable supply of electricity, heat, transport fuels or chemical feedstock, in addition to many other uses. Petrochemicals are widely used to make many of the materials associated with modern-day living and biomass can be converted to petrochemicals using different chemical, thermochemical and biochemical methods. As populations in developing countries grow, and expectations around lifestyle increase, the demand for these products is increasing. [2]

This PhD thesis was carried out as part of the project BioMA+ funded by *French Environment and Energy Management Agency (Agence de l'Environnement et de la Maîtrise de l'Energie- ADEME)* within the framework of the program "Investment for the Future" ("Investissements d'Avenir"). The project gathered industrial and academic French partners with various fields of expertise including biochemistry, catalysis, and engineering in order to scale up the isobutene production process from biomass (developed by *Global Bioenergies*) to industrial pilot scale. The project also sought to convert this bio-sourced isobutene into methacrylic acid, a compound widely used in paints. For the first time, bio-sourced methacrylic acid was effectively produced from bio-isobutene, and the success obtained in the industrial pilot allowed the preparation of the next step of scaling-up, which will take place in the demo plant recently set up in the *Leuna refinery* (Germany). [3] But the heart of this thesis was devoted to the study of a new route to produce acrolein from methanol and ethanol. Such a process performed on FeMo-like catalysts, has been recently proposed by *ARKEMA and UCCS (Unité de Catalyse et Chimie du Solide),* and its scale-up from a micropilot to industrial size opens new perspective in replacing the current fossil-based acrolein production process. The results obtained

during the project will permit to deeper understand the reaction mechanism thus allowing improvements in the acrolein yield for future applications.

The study presented in this manuscript was achieved thanks to a specific partnership between *IRCELYON (Institut de Recherches sur la Catalyse et l'Environnement de Lyon)* and *CRRA ARKEMA (Centre de Recherche Rhône-Alpes, ARKEMA, Pierre Bénite)* during the BioMA+ project. The research performed during this PhD thesis was linked to the reactions of isobutene oxidation to methacrylic acid, and to acrolein production by alcohols oxidative coupling of methanol and ethanol. Considering the two step gas-phase production of bio-methacrylic acid (consisting in two successive oxidations: isobutene to metacrolein followed by methacrolein to methacrylic acid) the focus was to investigate the impact of possible impurities contained in bio-isobutene on the acid/base sites of industrial and model catalysts. Concerning acrolein production, originally this method was developed to take place in a single reactor on FeMo-like catalysts. However this reaction consists in two successive steps: oxidation of alcohols to formaldehyde and acetaldehyde, and aldol condensation of aldehydes to form acrolein. During this PhD thesis the reaction was decoupled and performed in two consecutive reactors. Numerous catalytic tests using the reference FeMoOx redox catalyst in the first reactor (oxidation), and various aldolization catalysts in the second reactor (aldolization), were performed and correlated to the surface acid/base properties. In particular, the acid/base features of the catalysts were for the first time correlated to the yields in acrolein obtained in oxidizing conditions. The main technique used for studying the interaction of impurities with the surface of the catalysts and for the investigation of their acid/base properties, was gas-phase adsorption microcalorimetry. Other complementary techniques were used for the characterization of the catalysts as X-ray diffraction (XRD), chemical (ICP-OES) and thermal analyses (TG and TG-DTA-MS), liquid nitrogen adsorption, X-ray spectroscopy (XPS), and nuclear magnetic resonance (^{27}Al MAS NMR).

The project BioMA+ is covered by a confidentiality accord until 19/12/2026. However, due to the agreement between the project participants, the content of this manuscript can be disclosed.

Thesis subject and results are presented in eight chapters.

The first chapter entitled "Introduction" presents the BioMA+ project and the role of this PhD thesis in the project is stated (Section 1.1.). The main objectives of this thesis are then defined in Section 1.2. Chapter 2 deals with the state of the art of the catalytic reactions involved with this research project. Section 2.1. provides short bibliographical insight on the problematic considering (bio)-isobutene oxidation to (bio)-methacrylic acid. In Section 2.2 an overview of the acrolein applications and methods of synthesis proposed up to now is given. Sections 2.3. to 2.6. are dedicated to production of methanol and ethanol; methanol oxidation to formaldehyde over FeMoOx catalysts; ethanol oxidation to acetaldehyde; and methanol and ethanol coupling reactions in absence of oxygen. Finally, in Section 2.7. the new process for acrolein synthesis starting from methanol and ethanol is thoroughly described. Chapter 3 presents the state of the art of catalysts acidity and basicity. In Section 3.1. a literature survey of the influence of the acid/base properties of the catalysts on the gas-phase aldol-condensation of acetaldehyde and formaldehyde, is reported. Aditionally, a

detailed summary of the literature dealing with the measurement of the acid/base properties of oxide catalysts by adsorption microcalorimetry is reported in Section 3.2.

Chapter 4 (Experimental part) summarizes the information about the preparation of the catalysts (Section 4.1.), the experimental techniques (Section 4.2.) and catalytic tests (Section 4.3.) performed during the presented research.

In chapters 5, 6 and 7, the experimental results obtained during the thesis are reported and discussed. Chapter 5 describes the results connected to the production of bio-methacrylic acid by oxidation of bio-isobutene. The most valuable results of this thesis are presented in chapters 6 and 7 and are dealing with the influence of catalyst acid/base properties on acrolein production by oxidative coupling of methanol and ethanol, and more precisely with the impact of surface acid/base properties of the aldolization catalysts on the aldol-condensation of acetaldehyde and formaldehyde in gas-phase in presence of oxygen. Results obtained using silica-supported oxides as aldolization catalysts, are presented in chapter 6, while chapter 7 reports on the effect of different basic, acidic and amphoteric catalysts on acrolein production.

Finally, the main conclusions of this PhD thesis are summarized in chapter 8.

Chapter 1.

Introduction

1.1. Project BioMA+: valorization of sugars

Four partners and two subcontractors were involved in the BioMA+ project. The coordinator of the project consortium was *Global Bioenergies* (Evry, France), a company founded in 2008 with a unique goal: to develop a process converting renewable resources (sugar, crops, agricultural and forestry waste) into isobutene. The importance of developing new processes for isobutene production, and especially from bioresources, lies in the fact that isobutene is one of the major building blocks of the petrochemicals industry, representing a market of $25 billions, and may in the future address additional markets, up-to $400 billions. 15 million tonnes are produced every year and transformed into fuels, plastics, organic glass and elastomers, as summarized in Scheme 1.1.1. [4] During the project two subcontractors closely collaborated with *Global Bioenergies* in the field of fermentation of sugar *(Agro-industrie Recherches et Développements- ARD,* Pomacle, France*),* and purification and conditioning of bio-isobutene *(PROCINTECH,* Lyon, France).

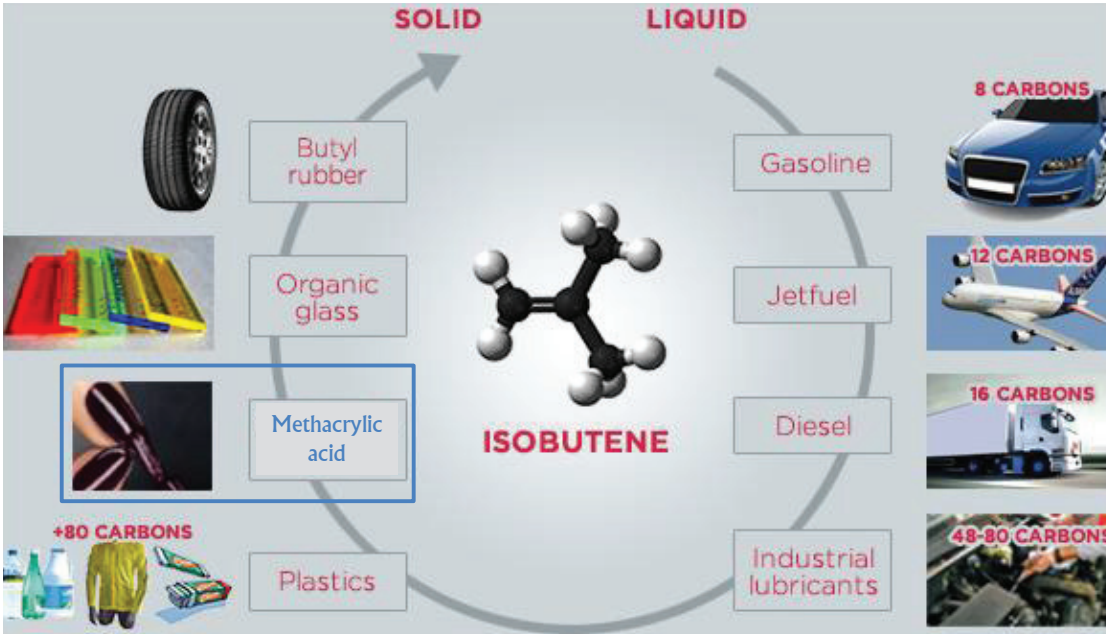

Scheme 1.1.1. Products derived from isobutene. Adapted from reference 5.

ARKEMA (Colombes, France) is one of the leading international companies for specialty chemicals and advanced materials. It was created in 2004 after the reconstruction of French oil major *Total.* The group has three complementary business segments: “High performance materials”

(specialty adhesives, technical polymers, performance additives); "Industrial specialties" (thiochemicals, fluorochemicals, PMMA, hydrogen peroxides); and "Coating solutions" (acrylics, coating resins and additives). According to the sales data from 2016 [6] *ARKEMA* is a world No. 1 to No. 3 on 90% of the portfolio. In the project BioMA+, this company focuses its attention on the developement of new methods for the production of methacrylic acid and acrolein (acrylic acid) from bio-resources. To achieve this goal, close collaboration with two *CNRS* (*Centre National de la Recherche Scientifique*) institutes, in the field of heterogeneous catalysis and materials, was established. *UCCS* (*Unité de Catalyse et Chimie du Solide*, *Université Lille 1*; Lille, France) is a laboratory of catalysis and solid state focused on process and chemical engineering. *IRCELYON* (*Institut de Recherches sur la Catalyse et l'Environnement de Lyon*, *Université Claude Bernard Lyon 1*, Lyon, France) brings together competences in heterogeneous catalysis and environment, being one of the largest catalysis laboratories in France and Europe. Both laboratories include permanent research staff from *CNRS* and university, many PhD students, post-docs, and invited scientists from all over the world.

This PhD thesis was carried out at *IRCELYON* and *ARKEMA*. To clarify its context within the project BioMA+ the organization chart of the project is presented in Scheme 1.1.2. and the tasks in which this manuscript is directly involved are highlighted in orange color. The activities of the project were organized in five principal parts (lots) which are divided into tasks. The main contribution of each partner is also indicated in the scheme. *IRCELYON* was involved only in Lot 5: Oxidation.

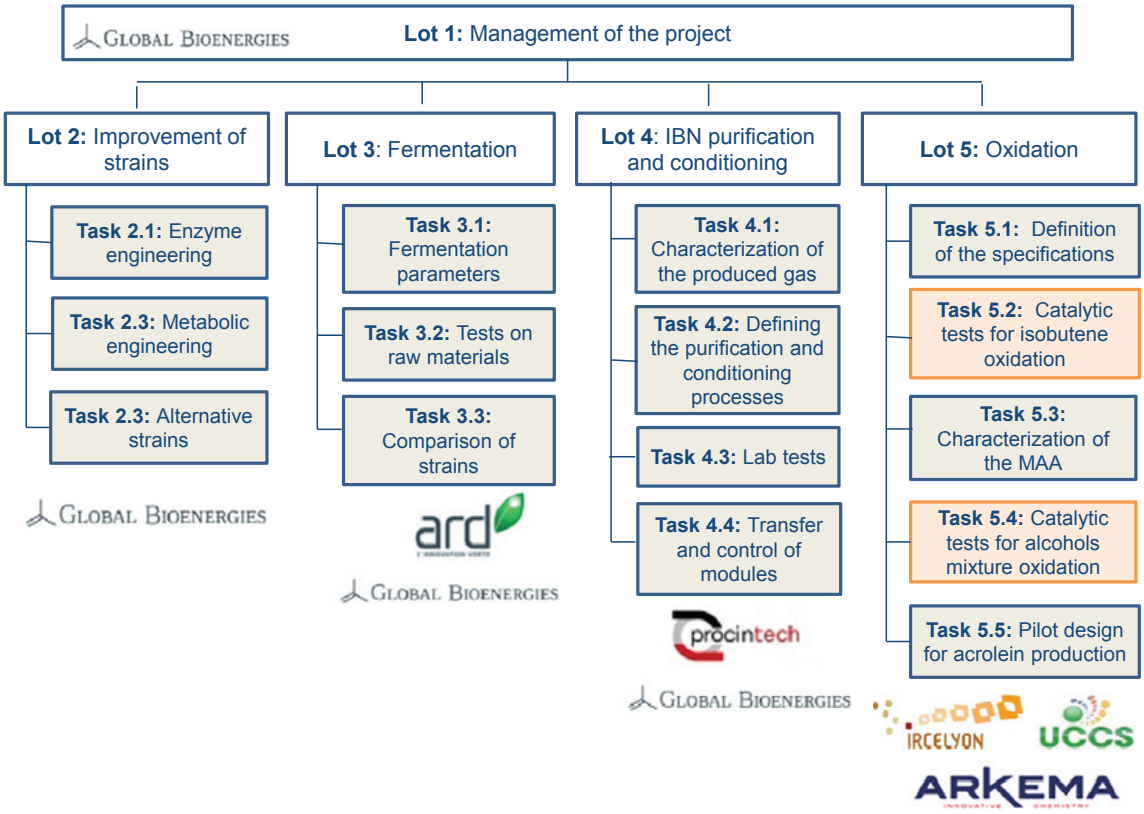

Scheme 1.1.2. Organization chart of the project BioMA+ with contribution of each participant.

Although the principal goal of the project BioMA+ was to develop the process for production of methacrylic acid from bio-sourced isobutene, other scientific and industrial subjects were also developed, all connected with valorization of biomass. Scheme 1.1.3. summarizes the reactions of valorization of sugars for production of petro-chemicals carried out during the BioMA+ project.

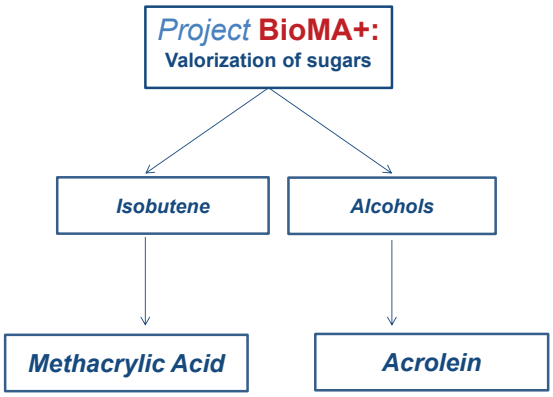

Scheme 1.1.3. Valorization of sugars for the production of methacrylic acid and acrolein (BioMA+ project).

In the next section, the objectives of this PhD thesis will be defined, and the further bibliographical research will be linked to the process of bio-methacrylic production from isobutene and new route for acrolein production by oxidative coupling of methanol and ethanol.

1.2. Objectives of the thesis

1) Oxidation of (bio)-isobutene to (bio)-methacrylic acid: impact of the impurities on the catalysts

The objective was to determine the impact of the gaseous impurities present in bio-isobutene on the industrial and model catalysts, used for production of methacrylic acid. Adsorption microcalorimetry was used as main technique. First, the identification of the phases able to interact with SO_2, CO_2 and NH_3, has been performed. The bonding probe molecule-site is characterized by the value of the differential heats of adsorption (Q_{diff}). The heats of probe molecule adsorption on industrial and model catalysts (single oxides or bulk heteropolyacids) were then compared. The catalysts were also characterized by BET, XRD, TG-DTA-MS and chemical analyses. The steps undertaken during the research are shown in Scheme 1.2.1.

Ex-situ studies were compared with in-situ studies performed by the other project partners to arrive to common conclusions and to set-up new methodology for production of bio-isobutene.

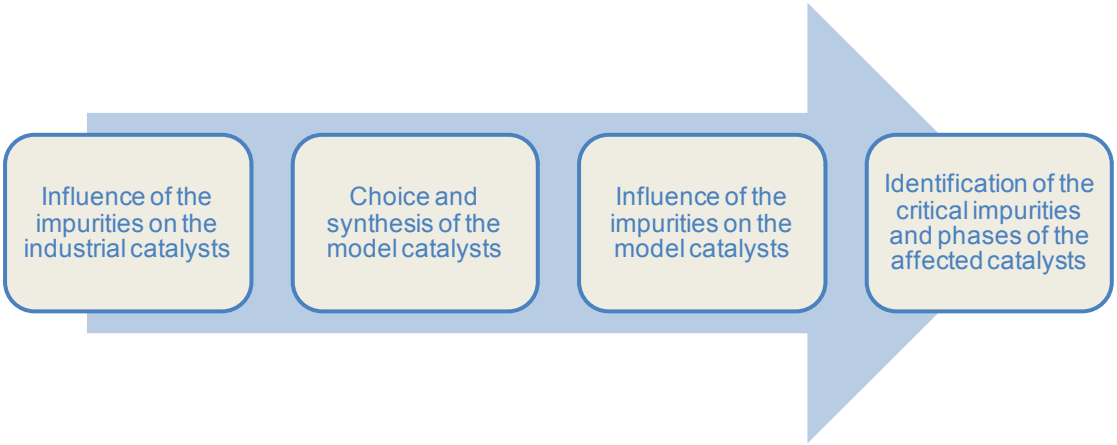

Scheme 1.2.1. Principal objectives for the ex-situ investigation of the impact of the chosen impurities present in the bio-isobutene.

2) Acrolein production by oxidative coupling of methanol and ethanol: impact of the acid/base properties of the catalyst on acrolein production

Production of acrolein, by oxidative coupling of methanol and ethanol, was recently proposed as a potential bio-sourced process. In this gas-phase process, acrolein can be directly synthesized in a single reactor over redox iron molybdate (FeMoOx) catalyst. [7,8] However, the process is constituted of two steps. The first consists in the oxidation of methanol and ethanol to produce formaldehyde and acetaldehyde, then the second step implies the aldol-condensation of formaldehyde and acetaldehyde and the dehydration of the two aldehydes to acrolein in presence of oxygen. Knowing that aldolisation reactions are generally catalyzed by basic and/or acidic sites, the objective of this thesis is to show how the improved yield and selectivity towards acrolein can be obtained by enhancing the cross-aldolization reaction on acid/base catalysts.

The main objective of the work was to study the influence of the acidity/basicity of the catalysts on the aldol condensation of acetaldehyde and formaldehyde to acrolein in oxidizing conditions, and then to describe the optimal acid/base surface properties by selecting an optimized aldolization catalyst to be used in a single reactor with a FeMoOx as oxidation catalyst.

The oxidative coupling of alcohols was performed in two separated consecutive flow fixed bed reactors (simplified scheme is given in Scheme 1.2.2.). In the first reactor, a mixture of methanol, ethanol, nitrogen and oxygen was introduced, and the oxidation to formaldehyde and acetaldehyde was carried out over the iron molybdate (FeMoOx) catalyst. All the products exiting from the first reactor were then directly sent to the second reactor, where the aldol condensation of the two aldehydes, and the further dehydration to acrolein proceeded over different acid/base catalysts. At first, the optimal operating conditions were determined for each catalyst, by identifying the maximum temperature and the appropriate contact time, to attain the maximum acrolein yield at fixed conditions: ($CO+CO_2$) yield remaining below 10 mol%.

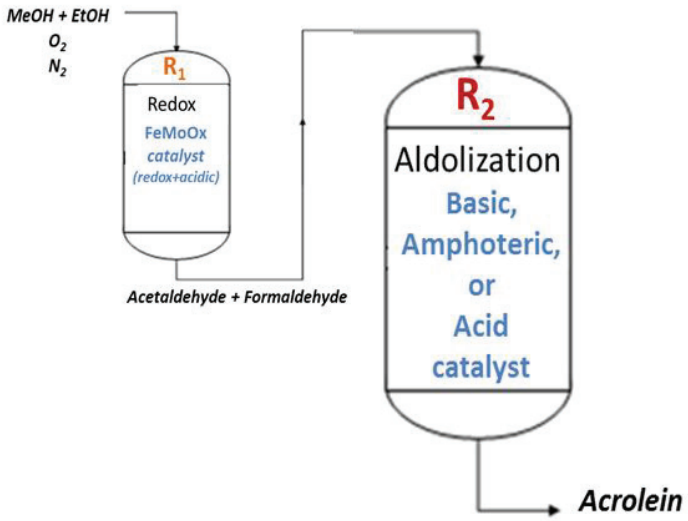

Sheme 1.2.2.Simplified scheme of the two reactors on line: oxidative coupling of methanol and ethanol decoupled in two steps.

To our knowledge, aldol-condensation of acetaldehyde and formaldehyde in gas-phase has not been yet studied in oxidizing conditions. Various research groups studied this reaction in the absence of oxygen, and reported that the main differences in the catalytic results are connected to the surface acid/base properties of the catalysts used. It was shown that acrolein production occurs on both acidic and basic sites, and that acid-base sites cooperation is a key point in acrolein production. However, the proper strength and amount of acidic and basic sites is still unknown, as well as the exact mechanism of this reaction. [9-11] The quantification of the acid/base sites concentration and strength on the surface of the oxide catalysts is even more crucial when the reaction is carried out in presence of oxygen, since it can create over-oxidation reactions.

Solids, with a wide range of the acidic, basic and amphoteric surface properties, were chosen and prepared as catalysts for the second step (aldolization) of the described process. As basic oxides, alkali and earth alkali oxides supported on silica were selected. MgO was also studied as basic oxide. Heteropolyacids supported on silica and niobium phosphate were studied as acidic catalysts. Mg/Al oxides, derived from commercial hydrotalcites with different Mg/Al ratios, as well as MgO supported on alumina, were chosen as amphoteric catalysts.

The acid-base properties of the involved catalysts were investigated by adsorption microcalorimetry using gaseous ammonia, sulfur dioxide, and methanol vapor as probe molecules. Other physico-chemical properties were determined by XRD, NMR, thermal and chemical analyses, and N_2-adsorption at -196 °C. Scheme 1.2.3. summarizes the connection between different steps undertaken to fully investigate the influence of the acidic and basic sites of the catalysts on acrolein production.

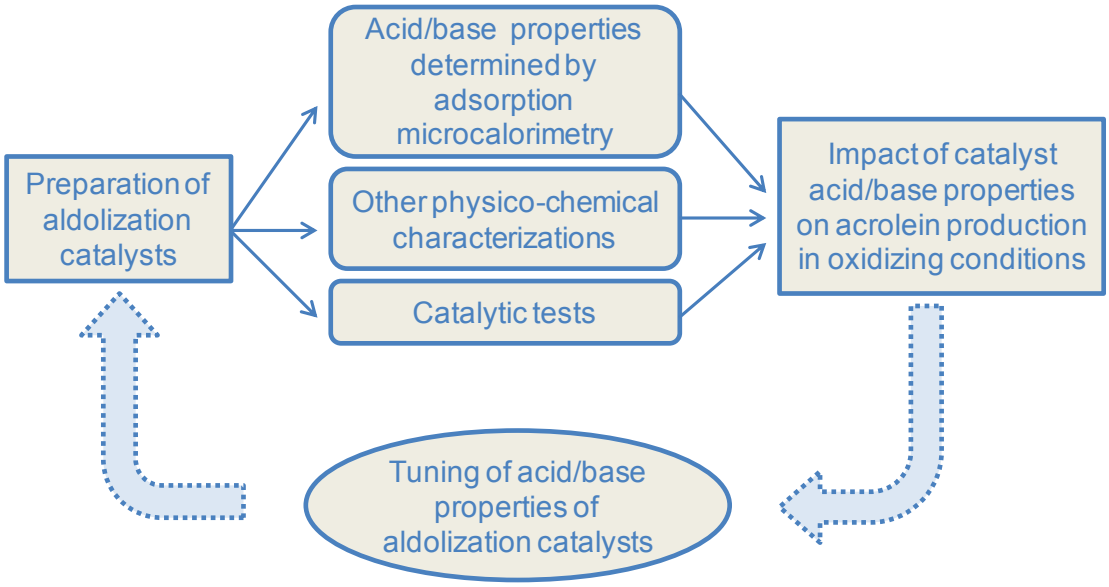

Scheme 1.2.3. Objectives and research methodology applied in studying the impact of acid/basesites of the aldolization catalysts in acrolein production.

3) Acid/base properties of catalytic solids determined by gas-phase adsorption microcalorimetry

After performing adsorption microcalorimetry analysis on all solid samples used during the thesis to determine the number, strength and strength distribution of the acidic and basic surface sites, the obtained data have been implemented and added to acidity/basicity scales. These scales allow the acidity and basicity of solid catalysts to be easily known before applied in a specific reactions. [12]

References

[1] J. Bundschuh (Series Ed.), *About the book series* in *Biomass as Energy Source: Resources, Systems and Applications* (Ed. E. Dahlquist), CRC Press (Taylor & Francis Group), London, **2013**.

[2] D.J. Roddy, *Interface focus* **2013**, *3(1)*, doi: 10.1098/rsfs.2012.0038.

[3] http://www.global-bioenergies.com/success-and-last-payment-in-the-bioma-project-financed-by-the-french-state/?lang=en.

[4] http://www.global-bioenergies.com/our-groupe/isobutene-process/?lang=en.

[5] http://www.chemwinfo.com/articles/42121657/120352_1313643503.

[6] http://www.arkema.com/en/arkema-group/profile/.

[7] J.L. Dubois, M. Capron, F. Dumeignil (Arkema France), WO2014/068213A9**, 2014**.

[8] A. Borowiec, PhD thesis (*Order number: 42244)*, University Lille 1 (FR), **2016**.

[9] M. Ai, *Bull. Chem. Soc. Jpn.* **1991**, *64*, 1342-1345.

[10] E. Dumitriu, V. Hulea, C. Chelaru, C. Catrinescu, D. Tichit, R. Durand, *Appl. Catal. A: Gen.* **1999**, *178*, 145-157.

[11] A. Azzouz, D. Messad, D. Nistor, C. Catrinescu, A. Zvolinschi, S. Asaftei, *Appl. Catal. A: Gen.* **2003**, *241,* 1–13.

[12] Lj. Damjanović, A. Auroux, Chapter 11: *Heterogeneous Catalysis on Solids* in *Handbook of Thermal Analysis and Calorimetry* ,Vol. 5: Recent Advances, Techniques and Applications (Eds.: M.E. Brown, P.K. Gallagher), Elsevier, Amsterdam, **2008**.

Chapter 2.

State of the art: Catalytic reactions

2.1. Oxidation of isobutene (IBN) to methacrylic acid (MAA)

MAA is the main material for the production of methyl methacrylate (MMA). MMA is an important monomer, which is widely used for producing acrylic plastics (polymethyl methacrylate) or producing polymer dispersions for paints and coatings. Methacrylic polymer, which has the characateristics of good transparency and mechanical resistance, is used in many fields such as signboards, building materials, vehicles and lighting equipments. [1,2]

Current industrial production of methacrylic acid is based on the use of acetone or isobutene from fossil resources. The majority of methacrylic acid is currently synthesized via the acetone-cyanohydrin (ACH) route commercialized in 1932, which consists of an initial reaction between acetone and hydrogen cyanide to give the ACH, which is then reacted with excess concentrated sulfuric acid to form the methacrylamide acid sulfate. In a successive stage, the methacrylamide sulfate is treated with excess aqueous methanol. The amide is hydrolyzed and esterified, with formation of a mixture of methylmethacrylate and methacrylic acid. The main drawbacks of this process are the utilization of highly toxic raw materials (hydrogen cyanide) and the coproduction of 1 mol of NH_4HSO_4 for each mole of methylmethacrylate, which also causes environmental problems. [1,3] Different alternative processes have been proposed since 1980s to replace the ACH technology; they are summarized in Scheme 2.1. [3]

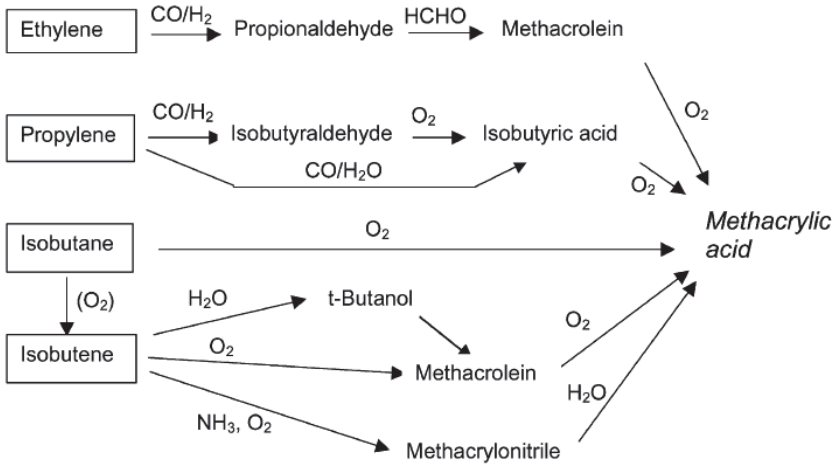

Scheme 2.1. Synthetic routes for methacrylic acid alternatives to the ACH route. [3]

Another well-developed industrial process for methacrylic acid production, adopted today, is a two-step selective oxidation of isobutene, a cheap raw material, to MAA via methacrolein (MAL). [1]

This new process has been developed for an environmentally friendly production of MMA and thereby the development of high performance oxidation catalysts is the key technology. [1] Literature describing the proper catalysts for both steps of this process is vast. [1,2,4-14] It is generally reported that the first step of the process, oxidation of isobutene to MAL, is performed in the 300-450 °C temperature range and the catalysts used are always multicomponent oxide Mo-Bi based catalysts, eventually doped with other elements as Fe, Ni, Co, Cs, K, P, Si, Cr, W. [1,4-9] The second step, the oxidation of MAL to MAA is usually performed at temperature in the 200-400 °C range on catalysts generally composed of a mixture of P-Mo oxides and heteropolyacids (or their salts). Additional presence of elements such as As, K, Cs, Fe, Sb, Ni, Co, B, Ru, Bi, W was also reported. [1,4,10-14]

Relatively cheap isobutene currently used for this process is produced at large scale by petrochemical cracking of crude oil. Selective oxidation of lower alkanes by molecular oxygen is of great importance in the petroleum and petrochemical industries. The content of isobutene in the fraction of C_4 alkanes is about 45-47%. [1,4,15] However, with limited fossil feedstocks and increased demand of the market for methacrylic acid and its derivates, it becomes to use biomass as a source of isobutene. Bio-isobutene produced by sugar fermentation by *Global Bioenergies* can be employed in the process for methacrylic acid production leading to a complementary source of bio-methacrylic acid and potentially total replacement of this petrochemical process by a renewable and sustainable one. Possible industrialization of the process for MAA production using bio-isobutene will depend among many factors, principally on the price of the feedstock.

However, the composition of petrochemicaly and bio-resourced isobutene is not the same. Bio-isobutene, produced by fermentation, usually contains different impurities, such as water vapor, sulfur containing molecules, CO_2, NH_3 and other organic pollutants. A purification step is needed after fermentation. [15] In parallel with the development of the purification process, it is important to examine the influence of the impurities of bio-isobutene on the catalysts, by different in-situ and ex-situ approaches. The influence of these impurities on the catalysts is still unknown.

2.2. Acrolein

2.2.1. Introduction

Acrolein, the simplest unsaturated aldehyde, is a colorless liquid (b.p. 53 °C) at room temperature with a pungent and piercing odor. The conjugation of a carbonyl group with a vinyl group provides acrolein with a high degree of reactivity. [16,17] It has attracted considerable attention of many research groups because of its many industrial applications. Acrolein is an important intermediate for the chemical industry, and is converted to acrylic acid and its esters, glutaraldehyde, methionine, polyurethanes, polyester resins, 1.2.6-hexanetriol, quinoline, etc. [16-19] Scheme 2.2.1. shows the chemicals derived from acrolein.

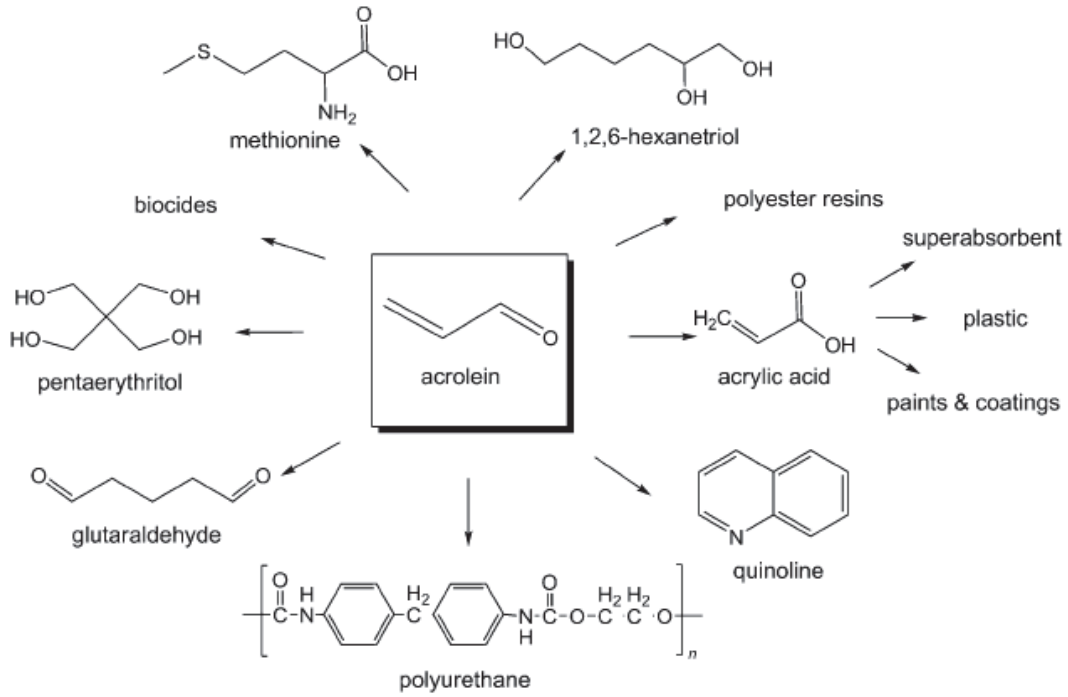

Scheme 2.2.1. Chemicals derived from acrolein. [16]

Acrylic acid is a valuable commodity chemical with a profitable market. Super-absorbent materials for diapers, acrylate plastics, paints and coatings can be produced from polyacrylic acid. The demand of acrylic acid is increased and a shortage of acrylic acid supply was identified in the market since 2010, due to the shutdown of some plants. [16] Industrial production of acrylic acid is principally based on gas-phase oxidation of propylene. [17]

Although a big part of crude acrolein goes to the manufacture of acrylic acid, the main part (approx. 80%) of refined acrolein is consumed for the synthesis of methionine. [16,17,20] Methionine, a sulfur-containing essential amino acid, is required in animal and human nutrition. [16] Commercial methionine production started in 1950s and today's global demand is estimated to be around 500 000 tons per year, with a projected annual growth rate of more than 5%. [16,17]

Also, acrolein can be directly used as an effective aquatic biocide by injection into water to control the growth of undesired microbial material and aquatic weeds. [16,17,21]

Currently, acrolein is obtained in the petrochemical industry from the partial oxidation of propylene. Therefore, there is a great deal of interest in the production of acrolein from renewable sources (glycerol, propanol, ethanol, methanol), developing greener and environmentally friendly processes accompanied by economic improvements in the oleochemical platform. [18] Production of acrolein by glycerol dehydration was almost commercialized, but the huge investments that are needed discouraged the companies up to now to invest into this technology. The latest proposed method for acrolein production by oxidative coupling of methanol and ethanol is still at the level of fundamental researches, but promises to be more favorable for the eventual commercialization than glycerol dehydration method. A short review on the applied and proposed acrolein synthesis methods

is given here below, while the newest proposed method for acrolein production by oxidative coupling of methanol and ethanol will be fully described in Section 2.7.

2.2.2. Acrolein synthesis overview

Acrolein production by condensation of acetaldehyde and formaldehyde

Acrolein was at first industrially produced by gas-phase cross-condensation of acetaldehyde and formaldehyde (Equation 2.1.). [16,17,19,22,23]

$$HCHO + CH_3\text{-}CHO \rightarrow CH_2{=}CH\text{-}CHO + H_2O \quad (2.1.)$$

The technology was developed and commercialized by Degussa between 1935 and 1945. Aldol condensation remained the standard industrial process up to the late 1950s. However, problems as the incomplete conversion complicated the downstream separation, as the product and reactants had similar physical properties. The process was consequently replaced by propylene oxidation since cheap propylene became available in the middle of the 20th century. [16,17,19,22-24] The reaction continued to be studied even when the industrial production stopped and it was generally acknowledged that aldol condensation can occur on both acidic and basic catalysts. It was also described that during the reaction, acetaldehyde can react in two different ways: by cross-condensation with formaldehyde giving acrolein or by self-condensation with another acetaldehyde molecule forming crotonaldehyde. The pathway direction is governed by the ratio of acid and base sites. [25-31] As it will be further explained (Section 3.1), this reaction represents the second step of the recently proposed synthetic route to acrolein by oxidative coupling of methanol and ethanol. [23,32] Details about the catalysts used and the mechanism of this reaction are thoroughly reported in Section 3.1.

Acrolein production by condensation of formaldehyde and ethanol

Ai [33] reported that acrolein can be formed by formaldehyde reaction with ethanol. This method is based on the similar principles as for formaldehyde and acetaldehyde aldol-condensation and research was inspired by the possibility to use bio-ethanol as reactant. The reaction occurs in two steps. First, ethanol reacts with formaldehyde to form acetaldehyde and methanol. Then, the unreacted formaldehyde forms acrolein by aldol condensation with acetaldehyde. The following equation (Equation 2.2.) describes the overall reaction:

$$CH_3\text{-}CH_2\text{-}OH + 2HCHO \rightarrow CH_2{=}CH\text{-}CHO + CH_3\text{-}OH + H_2O \quad (2.2.)$$

Metal oxides supported on silica gel (W, Ti, Fe, Zn, Ni, Bi, Mg, Ca, Li, K) and metal (Fe, Co, Ni) phosphates were tested as catalysts to perform this reaction. The catalytic performances were evaluated at 240-320 °C in a continuous flow system with a constant formaldehyde/ethanol ratio of 2. In all cases, the formaldehyde conversion reached 100% and the highest measured acrolein yield was 52% for nickel phosphate at 320°C. Author reported that the acrolein yield increased with increasing the electronegativity value of the alkaline/alkaline earth metal contained in the active phase (*i.e.* Mg>Ca>Li>K). Other products identified were acetaldehyde, methanol, and carbon dioxide.[33]

Propylene oxidation

Propylene oxidation (Equation 2.3.) is currently the main industrial method for acrolein production. [16,17,19] Propylene gas-phase oxidation was commercialized by Shell in 1959 using copper oxide supported on silicon carbide as a catalyst. Propylene conversion was only around 15%. Further evolution of the catalysts and optimization of reaction conditions led to a propylene conversion higher than 90%. [17]

$$CH_2{=}CH_3\text{-}CHO + O_2 \rightarrow CH_2{=}CH\text{-}CHO + H_2O \qquad (2.3.)$$

Nowadays the reaction is usually operated at 250-400 °C in a multitubular fixed-bed reactor on packed beds of multicomponent metal catalysts presented in the general formula Mo-Bi-X^{II}-X^{III} (-X^{I}-Y-Z)-O, where Mo-Bi-X^{II}-X^{III} are the basic structures containing four necessary metal components: Mo, Bi, X^{II} (Co, Ni, Me, Mg, Pb), and X^{III} (Fe, Cr, Ce, Al). Bismuth molybdates are located on the surface of the catalyst particles and act as active sites; but, the highest activity occurs only with the simultaneous presence of divalent (*e.g.,* Co^{2+}) and trivalent (*e.g.*, Fe^{3+}) metal components. The lifetime of the industrial catalysts is in the two to five years range. Typically, acrolein yield reaches about 80-90%, and the main by-product is acrylic acid (yield of around 10%). Acetaldehyde, acetic acid, CO and CO_2 are also produced in small quantities. [16,19,34] Steam is commonly co-fed with the reactant gases in the industrial process, due to its benefits to the acrolein production. It was reported that water competitively occupies the strong oxidation sites and prevents over oxidation of acrolein to CO_2, and consequently increases the rate of acrolein formation. Moreover, water can create new sites for propylene adsorption on the catalyst surface, thus enhancing the partial oxidation. [16,35-37] It was estimated that approximately 350 kt of acrolein are worldwide annually produced by vapor-phase oxidation of propylene, and the catalyst developments, which are using the actual processes have been primarily driven by the acrylic acid manufacturers. [38]

The reaction is highly exothermic, so one of the major issues for the reactor design is how to efficiently release the generated heat. [16,19] Heat release is essential to maintain isothermal reaction conditions and to prevent temperature runoff and explosion. Usually a molten salt bath is used to control the temperature. Many researches proposed other solutions, such as use of circulating fluidized bed reactor, “wall reactor”, distributive membrane reactor, or improvement of the multitubular reactor (by employing the heat transfer effect of CO_2 during the reactor operation). [16]

It is generally accepted that partial propylene oxidization to acrolein is initiated by the coordination of the propylene C=C double-bond to the Bi-Mo site on the catalyst, leading to the formation of a Mo-bound allyl intermediate surface species as, shown in Scheme 2.2.2. This is the rate-determining step, which can occur on both the carbonyl ("bismuthyl") site of the Bi atom, or on the bridging O atom, depending on the nature of the specific catalysts involved. The C-O bond is then formed through O-insertion, followed by a second hydrogen abstraction. Generally, the lattice oxygen atom on the catalyst surface contributes to the specific selectivity, whereas the adsorbed oxygen radical/molecule contributes to the total oxidation, leading to CO_x. The gaseous molecular oxygen supplied to the reaction re-oxidizes the catalyst, and provides sufficient availability of lattice oxygen atoms. CO_x could also be formed from both propylene and acrolein precursors, due to the rather large mobility of the lattice oxygen atom. Therefore, the mobility of the lattice oxygen, determined by the structure of catalyst, is critical to both propylene conversion and acrolein selectivity. [16]

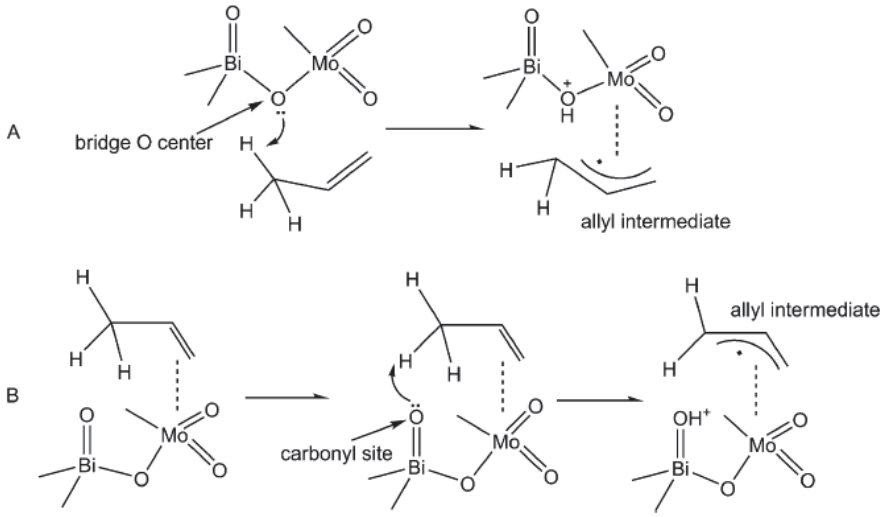

Scheme 2.2.2. Mechanism of the formation of allyl intermediates (initial/rate-determining steps of the partial propylene oxidation). [16]

Propane oxidation to acrolein

Acrolein can be produced from partial oxidation of propane (Equation 2.4.). [16]

$$CH_3\text{-}CH_2\text{-}CH_3 + 3/2\ O_2 \rightarrow CH_2\text{=}CH\text{-}CHO + 2H_2O \qquad (2.4.)$$

Acrolein production from propane was studied in parallel with propylene oxidation and it is still investigated because of propane's considerably low cost. Propane is the by-product of both natural gas production and oil refining, and it is only consumed commercially as fuel. In contrast, the carbon–carbon double bond of propylene makes it an important intermediate for the production of a number of value-added chemicals, such as polypropylene, acrylonitrile, propylene oxide, and isopropyl alcohol. This high demand in many processes brought up the propylene price, making the development of the propane route more attractive. However, despite decades of work on acrolein synthesis from propane,

the yield of acrolein prepared through partial oxidation of propane has not still reached the level for of commercial viability. [16]

The acrolein production from propane was studied mostly using different catalysts containing molybdenum. Generally, catalytic tests were performed in a quartz tubular fixed-bed reactor at high temperatures (up to 520 °C) and under atmospheric pressure. As example, research on magnesium vanadates, vanadia bismuth molybdates and vanadia antimony was reported by Kim et al. The most active material was Ag-Bi-V-Mo-O with acrolein selectivity of 63.5% and propane conversion of 13.1% (at 500 °C). Propylene, CO_x and C_2-hydrocarbons were also detected as well as by-products. [32,39-41]

Zhang et al. [42,43] reported the highest acrolein selectivity of 28.7% with a propane conversion of 15.3% (at 500 °C) on Ce-doped Ag-Mo-P-O catalysts. The other detected products were propylene (up to 25.7% of selectivity), propionaldehyde, acetone, acetaldehyde and CO_x. Same authors also studied the mechanism of this reaction on a $Ce_{0.1}Ag_{0.3}Mo_{0.5}P_{0.3}O_x$ catalyst. Three possible propane oxidation pathways were considered as shown in Scheme 2.2.3. Some quantities of propionaldehyde and acetone were detected among the products, which indicate that pathways I and III can actually occur. However, the yields of propionaldehyde and acetone are lower than that of acrolein, thus suggesting that route II (*via* propylene) is the most favorable. [43]

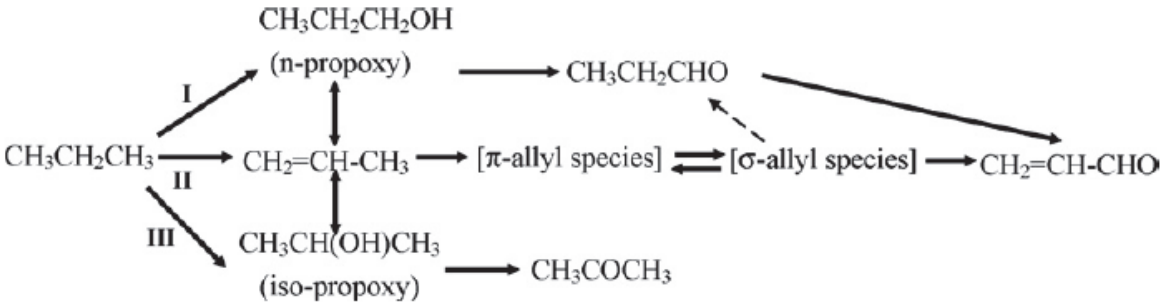

Scheme 2.2.3. Possible pathways for selective propane oxidation to acrolein on $Ce_{0.1}Ag_{0.3}Mo_{0.5}P_{0.3}O_x$ catalyst. [43]

Glycerol dehydration

Recently, glycerol dehydration (Equation 2.5.) became the most studied method for acrolein synthesis. Its development is close to commercialization and represents a bio-sourced alternative to the current industrial fossil based production of acrolein by propylene oxidation. This reaction can be performed either in gas or liquid phase and it is catalyzed exclusively by acid catalysts. [16,44] Biodiesel is now being used worldwide as an alternative fuel to replace, at least partially, diesel obtained from oil. This renewable fuel is mainly produced from transesterification of vegetable oils using methanol or ethanol, resulting in high amounts of glycerol obtained as a coproduct. However, the economic viability of biodiesel production also depends on the destination of this coproduct. Since its purification for pharmaceutical or cosmetic applications is very expensive, glycerol could be

catalytically converted to many interesting chemicals or intermediates. Acrolein is the most interesting glycerol-derived product. [44] Currently, the price of the feedstock and the process investments greatly influence its industrialization and prevent to replace the fossil based acrolein production. [16]

$$CH_2OH\text{-}CHOH\text{-}CH_2OH \rightarrow CH_2{=}CH\text{-}CHO + 2H_2O \quad (2.5.)$$

Liu et al [16] compared and reviewed glycerol liquid and gas-phase dehydration to acrolein and defined the principal drawbacks and problems to be solved in order to achieve commercial implementation. Generally liquid phase glycerol dehydration is described to be difficult and expensive to scale up and industrialize, due to numerous drawbacks (eg. reactors corrosion). [16,32,45] Considering the gas phase process, numerous studies using different acidic catalysts (such as supported mineral acids, supported heteropolyacids, zeolites, and mixed metal oxides) were conducted. The reaction typically occured in the 260-350 °C temperature range, using a vaporized aqueous glycerol solution. Presence of water vapor in the reaction conditions has positive influence on the process and therefore hydrothermaly stable catalysts are required. [16]

The acrolein yield is competitive if compared to the currently applied process starting from propylene, but catalyst deactivation was faster on glycerol dehydration to acrolein. [16] Priority is to extend the catalyst life to the timescale of months to years. The negative influence of catalyst deactivation was usually reflected in the decrease of glycerol conversion along with reaction time, which lowered the overall acrolein yield. Catalyst deactivation is caused by coke formation on the catalyst surface that blocks the pores, thus preventing the reactant contact with active sites. Stronger Brønsted acid sites favor acrolein formation, but also lead to more severe coking and catalyst deactivation. [16]

Some other methods proposed for acrolein synthesis

Acrolein can be, also, synthesized by oxidation of allyl alcohol,[46-48] decomposition of allyl ether [49], or partial oxidation of ethane.[50-54] However, these routes have numerous drawbacks for application on a larger scale, as low availability and high cost of the reactants, high energy consumption, or low selectivity. [16]

Acrolein can be synthesized also through biological routes. From the 1900s, acrolein formation was described during alcoholic fermentation from grains by certain bacterial strain.[16,55-57] Considering alcoholic fermentation, acrolein represented an undesirable compound, and the target of these studies was to minimize or prevent the associated acrolein production. Only recently, researchers started to investigate the possibility of using this “undesired” route for possible chemical production of acrolein. The potential of the solely biological route of acrolein production was described, but bacterial methods were not scaled-up to a production level.

2.3. Methanol and ethanol production

Both alcohols used for acrolein synthesis by oxidative coupling of alcohols (described in Section 2.7.) can be produced from biomass at relatively low price. Therefore a large scale production in the future has to be considered to replace the existing fossil based acrolein production from propylene.

Current industrial production of ethanol is based on direct hydration of ethylene (commercialized in 1948 by Shell company). Nowadays, ethylene and deionized water are used in the ratio 1:0.3-1:0.8, and heated at 250-300 °C under a 6-8 MPa pressure. Many catalysts were considered for this process, but today only supported phosphoric acid catalysts (*e.g.* on silica gel, Volga sandstone or bentonite) are used in industry. The obtained product is an azeotrope mixture containing 95% of ethanol. [58-60] Also bio-ethanol is currently largely produced from biomass. The world total ethanol production during 2014 reached almost 100 billion liters.[61,62]

Bio-ethanol produced by fermentation using yeasts was described to have numerous advantages such as a high selectivity, a low by-products accumulation, a high ethanol yield, a low pH. [58] Many factors influence the productivity of the fermentation process. The first is the substrate concentration, which has to be between 14 and 18 wt%. The concentration cannot be too high due to plasmolysis (*i.e.*, a water loss by cells in a hypertonic solution). [63] Oxygen concentration is the other important factor. Depending on the microorganism's type, ethanol is produced under aerobic or anaerobic conditions. For the aerobic conditions, an optimized level of oxygen is necessary to maintain high ethanol productivity. Temperature and pH have also a strong influence. Standard pH value is between 4 and 6 and temperature around 40 °C. The raw materials for ethanol production are classified in two main groups: fermentable carbohydrates, for a direct use, and organic materials (as starch) that must be pretreated before the fermentation. Substrates deriving from three main sources can be considered: agriculture, forest and industrial by-products. It is estimated that more than 60% of bio-ethanol is produced in the USA, India and Brazil. These are the countries with the optimal climate conditions for the growth of the crops used as feedstock. [58,62]

Current methanol industrial production is based on the catalytic conversion of syngas, and the majority of methanol is consumed for formaldehyde synthesis. This process consists of three steps: production of syngas, synthesis of methanol, and processing of crude methanol. [64,65] The synthesis can be performed applying three different pressure levels: low-pressure methanol process (5-10 MPa), medium-pressure methanol process (10-25 MPa), and high-pressure methanol process (25-30 MPa). The standard catalysts for methanol production are Cu-ZnO-Al_2O_3 or Cr_2O_3-based systems, with different additives.

It is, also, possible to obtain methanol from different biosources (*e.g.* biogas, wastes, and biomass) by pyrolysis, gasification, biosynthesis, electrosynthesis and photo electrochemical processes. Pyrolysis technology is more suitable for the large-scale production of methanol for diesel engines and gas turbine applications, whereas the cost-effective gasification processes are preferred

for the production of gaseous fuel. The feedstock for methanol production can come from organic wastes, municipal solid wastes, sewage sludges or primary and secondary agriculture wastes. However, the bio-methanol production is still not productive enough to compete with traditional fossil based methods, despite the numerous studies performed. [65-67]

2.4. Oxidation of methanol to formaldehyde on FeMoOx catalysts

Due to its high chemical reactivity, formaldehyde ($H_2C=O$ or HCHO) is an important C_1 building block for added-value products. The main use of formaldehyde and its polymers is in synthetic resins industry, such as production of thermosetting resins, oil-soluble resins and adhesives. The rest of formaldehyde is consumed in the manufacture of textiles, paper, fertilizers, miscellaneous resinous products and others chemicals. [68]

In the past (1888) methanol was commercially dehydrogenated to formaldehyde. Nowadays, all of the world production of formaldehyde is based on heterogeneous catalytic processes using methanol as feedstock. Formaldehyde can be manufactured from methanol via two different reaction routes: *i)* dehydrogenation (or oxidative dehydrogenation) in presence of Ag or Cu catalysts, or *ii)* oxidation in presence of Fe-containing MoO_3 catalysts. [68,69] Here the focus will be on the mechanism of oxidation of methanol to formaldehyde over Fe-Mo catalysts.

In the oxidation process a mixture of 18-19 wt% Fe_2O_3 and 81-82 wt% MoO_3 is employed as catalyst and under carefully controlled conditions, converted into catalytically active iron (III)-molybdate. Excess MoO_3 is frequently added in order to supply to losses of MoO_3 due to the formation of molybdenum blue. This compound accumulates at the bottom of the catalyst bed (that is at the lowest temperature), decreasing both the catalytic activity and selectivity. Cr and Co oxide can be used as promoters. The by-products are CO, CO_2 and formic acid. [69]

Excess air is used in the process to ensure an almost complete conversion and to avoid reaching the explosive limits of methanol. Reaction temperature should be lower than 400 °C to insure the stability of the catalyst and limit the side reactions. On Fe-Mo catalysts, formaldehyde yield can reach 95% and conversion 98-99%. The average lifetime of an industrial catalyst is 6-12 months. [68] There are two stoichiometric iron-molybdates: ferric ($Fe_2(MoO_4)_3$) and ferrous ($FeMoO_4$). Only the first one can catalyze the selective oxidation of methanol to formaldehyde, while the second one is formed during the redox catalytic process, and can be found in the used catalysts. The commercial formulations of those catalysts always present a large excess of molybdenum. Some authors attribute the catalytic activity only to $Fe_2(MoO_4)_3$ phase [70,71] while others consider as active phase the mixed oxides with a slight Mo excess. [72,73] Finally, it can be concluded that the active phase is stoichiometric iron molybdate, but a Mo excess is needed to prevent the formation of Fe rich phases on the catalyst surface during reaction, due to loss of MoO_3. [68]

Most of the authors agree that oxidation of methanol to formaldehyde over Fe-Mo catalysts is a redox type mechanism. [68] The reduction of the bulk catalyst by methanol seems to occur only at

temperatures higher than 230 °C, while reoxidation only starts at temperatures higher than 270 °C. The reduction and reoxidation rates increase when temperature rises. B-$FeMoO_4$ is the reduced catalyst phase. Carabucicchio and Trifiro [74] report about diffusion of oxygen ions from the bulk to the catalyst surface, where they can react with the gas phase molecules. Therefore, the rate of the catalyst reduction depends on the diffusion rate of oxygen atoms. [74]

Burriesci et al [71] also investigated the reduced phases of Mo-Fe catalysts and concluded that the catalyst reduction can occur at 200 °C, being practically completed at 270 °C. The formed reduced phase depends on the temperature at which the methanol enters in contact with the catalyst. For temperature lower than 225 °C, α-$FeMo_4$ phase is formed while for temperature higher than 310 °C β-$FeMoO_4$ is the present phase. The total reoxidation of α-$FeMoO_4$ phase is achieved at 355 °C.

In a review, Soares et al [68] reported that most of authors propose a Mars-van Krevelen type reaction mechanism , while only few refer to Langmuir-Hinshelwood/Hougen-Watson mechanism for the methanol oxidation over Fe-Mo catalysts. The first proposed mechanism is:

$$CH_3OH + Cat_{ox} \rightarrow HCHO_{(g)} + H_2O_{(g)} + Cat_{red} \quad (k_1) \qquad (2.6.)$$

$$Cat_{red} + O_{2(g)} \rightarrow Cat_{ox} \quad (k_2) \qquad (2.7.)$$

In the Mars-van Krevelen mechanism hydrogen abstraction from methoxy species, adsorbed on the catalyst surface, is the limiting step. But, depending on the reaction conditions, the desorption of formaldehyde can also be the slower step.

Pernicone et al [75] studied the mechanism of this reaction and reported that formaldehyde and, especially, water act as inhibitors of the reaction. A competitive adsorption was observed between methanol and water. The catalyst studied was constituted of MoO_3, and $Fe_2(MoO4)_3$. It is confirmed that the lattice oxygen of the catalyst participates in methanol oxidation: the same reaction products are obtained by flowing methanol over the catalyst, in the presence or not of oxygen; the reaction rate in the pulse reactor was the same in both cases. The reaction mechanism can follow the classical pathway: *(1)* adsorption of the reactants; *(2)* surface reaction; *(3)* desorption of the products. Therefore, surface lattice oxygen is, in practice, oxygen adsorbed and reduced to O^{2-} ion. Adsorption of methanol should be a dissociative adsorption on centers constituted by anionic vacancies and O^{2-} ions. Finally, the reaction will depend on the catalyst acid-base properties. The anionic vacancy would have the function of a Lewis acid center, while the O^{2-} ion would behave as a Brønsted basic center. Therefore, the proposed mechanism considers that the O^{2-} ion is a stronger Brønsted base than the CH_3O^- ion. In conclusion, a hydroxyl should be formed and an anionic vacancy should be occupied by a methoxyl. They excluded methanol adsorption as the rate-determining step. After this step, the surface reaction should occur by transfer of a H^+ ion from the methoxyl to a near O^{2-} ion, with the formation of the second hydroxyl and electron transfer to the reducible cation (either Mo^{+6}or Fe^{+3}). This is similar to HCHO formation on a reduced anionic vacancy, and this reaction step is also not a limiting one. The reaction is reversible: water is removed from the two neighboring hydroxyls, with the formation of a new methanol adsorption center, constituted by an anionic vacancy and by an O^{2-} ion.

Reaction continues with desorption of formaldehyde from the reduced anionic vacancy, which then acts as an oxygen adsorption center (reoxidation of the catalyst). The rate-limiting step seems to be the desorption of the products, but catalyst reoxidation represents also a slow step. Liberti et al [76] also pointed out the formaldehyde desorption as the rate limiting step. Some other authors proposed similar mechanisms of reaction like Pernicone et al. involving adsorption of methanol and oxygen on different active sites of the catalyst. Water has inhibition effect on the reaction. Some authors argue that the desorption of formaldehyde is not the limiting step of the reaction, favoring the reaction between adsorbed methanol and oxygen as the limiting step. [68]

In spite of the high selectivity on iron molybdate catalysts, other products are also formed, depending on the catalyst type and reaction conditions. The formation of dimethylether (DME), methylformiate (MF), dimethoxymethane (DMM), CO and CO_2 is often reported. Formic acid is scarcely referred, but can act as a strong poison in many formaldehyde applications. Side reactions are more important at low reaction temperature and low methanol conversion. CO is considered as the major by-product. The selectivity towards formaldehyde increases with methanol conversion, except for high conversion levels, at which the formation of CO starts to be important. Generally, reactions from methanol can be divided into two main types: *i)* oxidation reactions (which need oxygen); and *ii)* dehydration reactions (which do not need oxygen). [68]

Tatibouët [77] proposed a scheme for methanol oxidation and dehydration reactions. According to this scheme, except for DME, the formation of all products needs at least one oxidation step (Scheme 2.2.4.). He stated that methanol oxidation is a structure sensitive reaction, and summarized the formation of the different products in an acid-base-strength diagram (Scheme 2.2.5.).

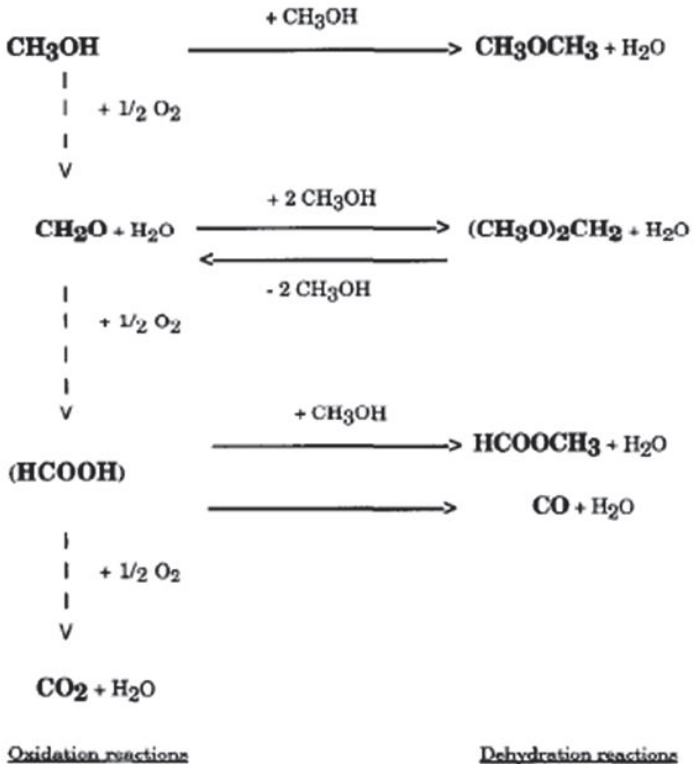

Scheme 2.2.4. A scheme for methanol oxidation and dehydration reactions. [77]

Formaldehyde formation only, requires redox dehydrogenation sites, while the selective formation of DMM involves a dual site (redox dehydrogenation site and Lewis acid site). An important variation, in the DMM selectivity or in the DMM to formaldehyde selectivity ratio, indicates a change in the Lewis acidity of the catalyst. The formation of dimethyl ether is related to the presence of strong acid sites. [77]

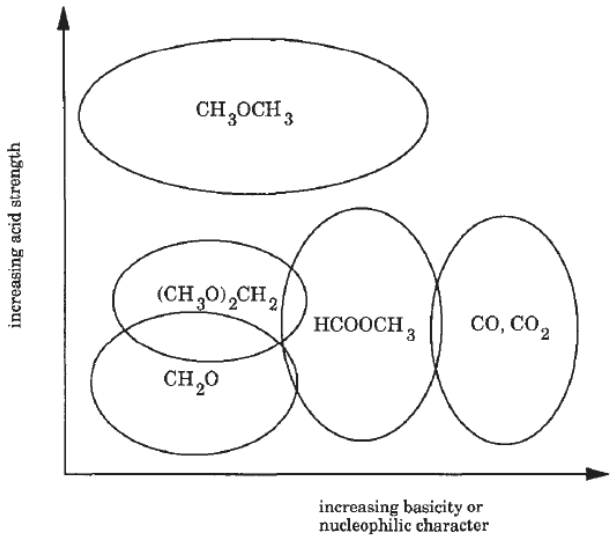

Scheme 2.2.5. Schematic representation of the main reaction products as a function of the acido-basic character of active sites. [77]

Cheng [78] mentioned that water (that is coproduced with formaldehyde) slows down the further oxidation of formaldehyde, thus contributing to the high selectivity of methanol to formaldehyde.

2.5. Oxidation of ethanol to acetaldehyde

As ethanol can be produced from a large range of agricultural feedstocks, it is rapidly becoming an important reactant for production of renewable fuels and chemicals as acetaldehyde and acetic acid. [79]

For the heterogeneous oxidation of ethanol to acetaldehyde different catalysts have been proposed in literature. Takei and co-workers [80] have recently reviewed the various processes used to transform bioethanol to acetaldehyde and acetic acid. A large number of catalytic systems were studied for the oxidative dehydrogenation of ethanol to acetaldehyde (metal oxides, noble and non-noble metal nanoparticles). Gold nanoparticle catalysts have been identified as higly promisisng.

By selecting suitable catalysts and the best reaction conditions, ethanol can be selectively transformed into acetaldehyde, acetic acid, ethylene oxide, ethylene, diethyl ether, and ethyl acetate. In principle, ethanol is oxidized into acetaldehyde, and then to acetic acid (or directly to CO_2 and H_2O). These routes are shown in Scheme 2.2.6, with the related catalyst. Acetaldehyde is selectively produced when $k_2 >> k_3, k_4$. A rough classification is that supported noble metal catalysts lead to acetic acid, while base metal oxides favor acetaldehyde. Cu-based oxides are known to be active and

selective for the dehydrogenation to acetaldehyde. V- and Mo-based oxides and heteropolyacids are the most often studied and, in general, they are selective towards acetaldehyde. Catalysis on gold is specific, because it results to be selective to acetic acid in liquid phase, while selective to acetaldehyde in gas phase (when deposited on metal oxide supports). It was found that on Al_2O_3, Au enhances dehydration to ethylene and diethyl ether, while on SiO_2 and CeO_2 it promotes dehydrogenation to acetaldehyde and hydrogen. Over Au/SiO_2 and Au/CeO_2 catalysts, ethanol is adsorbed on the Au surfaces and then accumulated on the support surfaces as ethoxy species. Then these species are transformed on Au NPs and desorbed as acetaldehyde and H_2. [79-84]

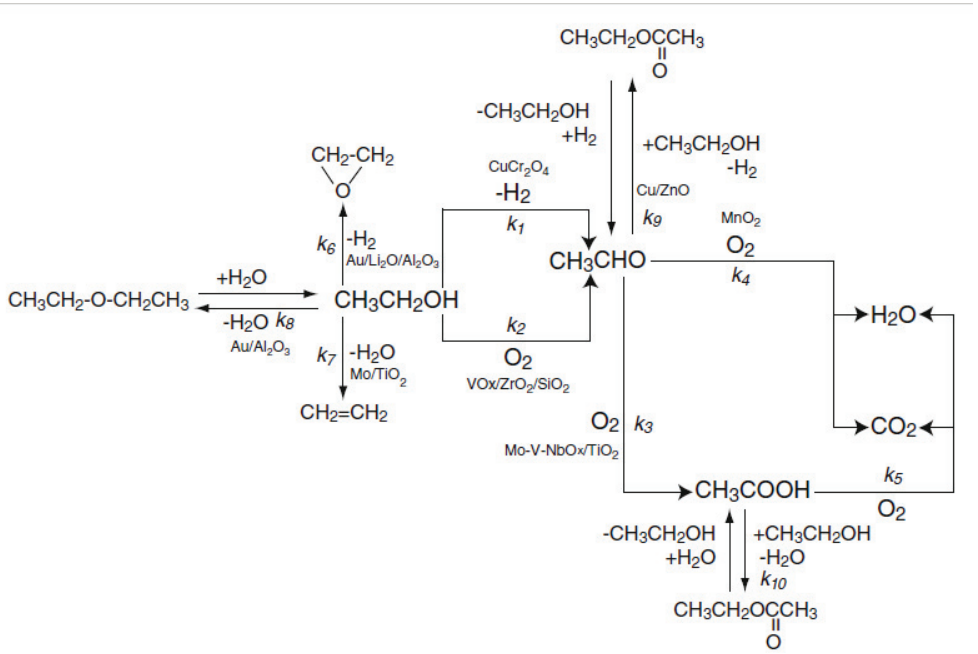

Scheme 2.2.6. Successive reactions involved in ethanol transformation. A typical catalyst for each reaction is presented. [80]

In gas phase, mixed oxides have been widely studied. [80,85-87] Catalysts containing redox-active metal oxides of V, Mo, Cu, and Ce, among others, are active and applied to the commercial production of acetaldehyde and acetic acid from ethanol, via oxidative dehydrogenation processes (ODH).[85] Many articles describe methanol oxidative dehydrogenation over metal oxide catalysts (see Section 2.4.), but only few studies have focused on reaction pathways using ethanol. Methanol and ethanol ODH probably react through an alkoxide intermediate. Studies, over supported molybdenum and vanadium oxide catalysts, suggest that the rate-limiting step is the H-atom abstraction from the CH_2 group. However, the universality of this mechanism for the different transition metal oxides (both acidic and redox) has not been demonstrated. [85,88]

Nair et al. [85] described catalytic pathways for reactions of ethanol to acetaldehyde by oxidative dehydrogenation and of ethanol to diethyl ether by condensation, over VO_x/Al_2O_3, MoO_x/Al_2O3, and WO_x/Al_2O_3. Isotopic labeling showed that acetaldehyde formation occurs via C-H bond cleavage of the CH_2 group (rate-limiting step) in an adsorbed alkoxide, followed by removal of

surface oxygen in a “Mars and van Krevelen” redox mechanism. Diethyl ether formation occurs in parallel via coupling and condensation of two adjacent ethoxy species. A study of the activity of catalysts with MoO_x supported on Al_2O_3, TiO_2, and CeO_2 and binary oxides of MoO_x and WO_x on Al_2O_3 proved that the active redox oxygen, for acetaldehyde formation, is the oxygen atom linking the active metal oxide to the support oxide. Ether formation ability of the metal oxide is related to the electronegativity of the active metal atom.

Ethanol ODH reactions over alumina-supported VO_x, MoO_x, and WO_x catalysts, performed at 180 °C result in two products - acetaldehyde and diethyl ether. Formation of acetaldehyde indicates the presence of redox sites on the catalyst, while diethyl ether formation indicates the presence of acid sites. No variation in the ethanol ODH rate is seen with either 0,25–2,0 mol% ethanol or 1,5–5,0 mol% oxygen. The absence of any effect of oxygen concentration on the oxidation rate suggests that oxidation occurs either through chemisorbed oxygen or through the “Mars–van Krevelen” redox mechanism. [85]

The first step for both acetaldehyde and ether formation is the adsorption of ethanol as an ethoxy species (probably formed concurrently with protonation of terminal oxygen-O_T):

$$CH_3CH_2OH + M{=}O_T \longleftrightarrow CH_3CH_2O\text{-}M\text{-}O_TH \quad (k_1) \qquad (2.8.)$$

The next step in acetaldehyde formation is the rate-limiting abstraction of a H-atom from the ethoxy species and concomitant reduction of the catalyst surface, via the removal of a redox-active bridging lattice oxygen (O_B), in a “Mars–van Krevelen” redox mechanism. The catalyst is then immediately reoxidized using oxygen from the gas phase.

C-H bond scission:

$$CH_3CH_2O\text{-}M\text{-}O_TH + O_B \longrightarrow CH_3CHO\text{-}M\text{-}O_TH + O_BH \quad (k_2) \qquad (2.9.)$$

Acetaldehyde desorption:

$$CH_3CHO\text{-}M\text{-}O_TH \longleftrightarrow M\text{-}O_TH + CH_3CHO \quad (k_3) \qquad (2.10.)$$

Adsorption site regeneration:

$$O_BH + M\text{-}O_TH \longleftrightarrow M{=}O_T + H_2O_B \quad (k_4) \qquad (2.11.)$$

Loss of lattice oxygen:

$$H_2O_B \longleftrightarrow \blacksquare + H_2O_B \quad (k_5) \qquad (2.12.)$$

Reoxidation of the catalyst:

$$\blacksquare + \tfrac{1}{2}\, O_2 \longleftrightarrow O_B \quad (k_6) \qquad (2.13.)$$

Legend: M represents a metal site; O_T represents a terminal oxygen; O_B represents a bridging oxygen; ■ represents a vacancy.

For diethyl ether (DEE) formation, the mechanism involves condensation between two adsorbed ethoxy species. Lattice oxygen is not removed during this reaction. Desorption of the products (ether and water) subsequently regenerates the adsorption sites. [85]

Condensation of ethoxy species:

$$2C_2H_5O\text{-}M\text{-}O_TH \longrightarrow O_T\text{-}M\text{-}H_2O + (CH_3CH_2)_2O\text{-}M\text{-}O_T \quad (k_7) \qquad (2.14.)$$

Ether desorption:

$$(CH_3CH_2)_2O\text{-}M\text{-}O_T \longleftrightarrow (CH_3CH_2)_2O + M{=}O_T \quad (k_8) \qquad (2.15.)$$

Water desorption:

$$O_T\text{-}M\text{-}H_2O \longleftrightarrow M{=}O_T + H_2O \quad (k_9) \qquad (2.16.)$$

Acetaldehyde formation rates depend linearly on ethoxy coverage, while ether formation rates show a non-linear dependence on ethoxy coverage. Acetaldehyde formation thus involves a single ethoxy species, while the condensation of two ethoxy species is required for ether formation. Acetaldehyde formation requires the removal of an O atom from the catalyst surface, to produce an oxygen atom linked to the active metal atom of the support. While the electronegativity of the active metal atom is important for both acetaldehyde formation and ether formation, the support atom electronegativity plays a role in the availability of lattice oxygen in acetaldehyde formation. [85]

Sobolev et al. [82] prepared a set of nanostructured gold catalysts with Au loadings ranging from 0,5 to 7,0 wt% on a TiO_2 support, and evaluated (in gas-phase) the oxidation of ethanol with molecular oxygen (in a flow reactor under atmospheric pressure). In summary, nanostructured Au/TiO_2 catalysts with gold loadings varying from 2 wt% to 7 wt% were extraordinary active in the gas-phase selective oxidation of ethanol. The temperature, at which the catalytic activity occurs, around 125 °C, is unusually low for gas-phase reactions of primary alcohols. These catalysts show an intermediate decrease in activity with subsequent increase of temperature to give a “double-peak” profile of ethanol conversion. This increased activity provides a predominant acetaldehyde production. Total oxidation to CO_x becomes significant only at temperatures above 250 °C. In contrast, gold supported on Al_2O_3 and SiO_2, showed a conventional behavior with a continuous increase of ethanol conversion at temperatures above 200 °C. The main product of all these reactions is acetaldehyde, while small amounts of by-products like acetic acid, ethyl acetate, diethyl ether, ethylene, methane, CO and CO_2 were present. TiO_2 mainly acted on acid-catalyzed reactions, producing diethyl ether and ethylene, rather than acetaldehyde. The most efficient catalyst for acetaldehyde production is $5Au/TiO_2$ (in the low-temperature region- 125 °C), and $2Au/TiO_2$ and $3Au/TiO_2$ catalysts (at higher temperature- 225 °C). [82]

To explain the decrease in ethanol conversion at temperatures above 125 °C, the strong deactivation of these catalysts has to be taken in account. Additionally, hysteresis in the activity profile for $5Au/TiO_2$ was revealed. The increase of the reaction temperature gives a rise to “double-peak” catalytic activity, whereas the low-temperature activity peak is not reproduced during reverse decrease of temperature. The reverse profile of ethanol conversion remained “valid” only at temperatures above

220 °C. Accumulation of organic molecules on the catalyst surface, could be the reason of the catalyst deactivation. The initial catalytic activity is completely restored upon reactivation of the catalyst in oxygen atmosphere at 300 °C. Another possible reason for the double-peak activity could be divergent, oxidative and non-oxidative, reaction pathways for ethanol dehydrogenation, depending on the temperature. Thus, a predominant contribution either of aerobic or anaerobic oxidation might be responsible for the high initial catalytic activity of Au/TiO_2 and its fast decreasing at temperature above 125 °C. In absence of oxygen, the conversion of ethanol is notably lower than in the case where molecular oxygen is present in the feed [82]. Guan and Hensen [81] reported that molecular oxygen is intrinsic promoter of ethanol dehydrogenation in gas-phase aerobic and anaerobic reactions catalyzed by gold particles supported on silica.

Guan and Hensen [79] also investigated the selective oxidation of ethanol to acetaldehyde over Au-Ir catalysts. Acetaldehyde and traces of acetic acid were the main products detected at 180 °C. $Ir(100)/SiO_2$ is more active in ethanol conversion than $Au(100)/SiO_2$. However, the selectivity to C_2-oxygenated species, is significantly lower for the Ir-catalyst. This can be related to the strong metal-carbon bond strength, which results in an increased rate of the carbon–carbon bond cleavage reactions. The selectivity of the Au-catalyst was above 90% in the temperature range of the reaction. Interestingly, a strong synergetic effect between Ir and Au is observed in ethanol oxidation. All Au-Ir catalysts were more active than the relative monometallic, with $Au(26)Ir(74)/SiO_2$ being the most active. With increasing Au content, the conversion slightly decreased but with a concomitant increase in the C_2-oxygenates selectivity. The selectivities for the Au-Ir bimetallic catalysts are typically above 90% and higher than the selectivity of the Ir-catalyst.

The effect of the temperature of the oxidative pretreatment was studied by the same authors [79]. Clearly, high-temperature oxidation, which results in substantial oxidation of the Ir-nanoparticles, resulted in significant loss of the catalytic activity. The activity of the bimetallic catalyst also decreases, but to a much lower extent, compared to that of $Ir(100)/SiO_2$ catalyst. The selectivity to C_2 oxygenates increases also with increasing oxidation temperature. These catalytic results show the beneficial impact of bimetallic Au-Ir nanoparticles in the oxidation of ethanol to acetaldehyde. The nanoparticles consisted of a metallic core and a surface shell, in which the surface Ir-atoms were oxidized. The uncovered Au-atoms, being the adsorption sites for ethanol, probably dissociated ethanol to ethoxide and the oxidized Ir-atoms provided the O-atoms required for the oxidative dehydrogenation. [79,81]

The catalytic activity of surface-modified single-walled carbon nanotubes (SWCNTs) for partial oxidation processes was tested by Abdulahi et al. [89] The results indicate a strong link between ketonic surface groups (C=O) on the SWCNTs surface and the catalytic activity in partial oxidation processes. Weinstein et al. [90] used three types of graphite nanofibers (GNFs), obtained by varying orientations of the graphene sheets (herringbone, platelet, and ribbon), as catalysts for the gas-phase oxidative dehydrogenation of ethanol to acetaldehyde and ethyl acetate, in presence of oxygen. Herringbone fibers produced higher conversions of ethanol compared to platelet and ribbon fibers. Longer contact time between the ethanol and the fibers resulted in higher conversion, as well as in a different products distribution due to increased production of ethyl acetate. Varying the equilibrium

conditions by increasing the oxygen concentration, brought to the increasing of the conversion as well as to higher percentage of acetaldehyde produced. Excess of oxygen regenerates the active sites.

2.6. Vapor-phase methanol and ethanol coupling reactions in absence of oxygen

Products from methanol and ethanol reactions can be divided in two groups, those that do not form C-C bonds (non-C -C coupling products, *e.g.*, formaldehyde, methyl acetate, etc.) and those that form C-C bonds (C-C coupling products, *e.g.*, C_{3+} alcohols, C_{3+} aldehydes, C_{3+} esters, etc.). Higher alcohols synthesis from methanol and ethanol has been explored in the past using homogeneous and heterogeneous catalysts (via Guerbet chemistry). Guerbet type coupling of alcohols typically consists of a series of reactions including: *(1)* lower alcohols dehydrogenation, *(2)* aldol addition (C-C coupling), and *(3)* C-C coupled aldehyde hydrogenation to higher alcohols. [91]

In vapor-phase, the main reported reaction pathways for the C-C coupling of lower alcohols to higher alcohols on multimetallic mixed oxides include the following steps presented in Eq. 2.17. to 2.19. [92]

Alcohol oxidation (dehydrogenation) to aldehyde:

$$2RCH_2CH_2OH \longleftrightarrow 2RCH_2CHO + 2H_2 \quad (2.17.)$$

Aldol condensation of aldehydes with elimination of water (C-C bond forming) to an α,β-unsaturated aldehyde:

$$2RCH_2CHO \longleftrightarrow RCH_2CH{=}CRCHO + H_2O \quad (2.18.)$$

And allylic aldehyde reduction (hydrogenation) to alcohol

$$RCH_2CH{=}CRCHO + 2H_2 \longleftrightarrow RCH_2CH_2CHRCH_2OH \quad (2.19.)$$

Other reactions proposed include direct alcohol and aldehyde condensation (to C-C coupled intermediate species), hydroxy aldehyde keto-aldol interconversion, reverse aldol coupling (to keto form) [93,94], esterification reactions from aldehydes and surface alkoxides [94], and methanol decarbonylation (decomposition) [93].

Some authors in the 1930s reported the use of CuO, MgO, and Al_2O_3 mixtures for the vapor phase C-C coupling of methanol + ethanol and ethanol. The presence of all oxidic components (CuO, MgO, and Al_2O_3) was claimed to be essential for high yields of C-C coupling alcohols and catalyst stability [91]. Mechanistic studies of alcohol (methanol + n-propanol, ethanol) coupling reactions on mixed metal oxides ($MgAlO_x$) by Di Cosimo et al. [91,93,95] have revealed that an optimum distribution of weak Lewis acid and strong Brønsted base sites (deriving from an intimate contact of Mg and Al oxide phases) is required for maximizing the C-C coupling reaction rate, and that are not reached with only one of the monometallic oxides. It is shown that, on $MgAlO_x$ mixed metal oxides (atomic Mg/Al = 1), the maximum ethanol coupling formation rate to n-butanol corresponded to the maximum density of basic sites in the catalyst. It is suggested that more active catalyst for C-C

coupling reactions might be produced by introducing a hydrogenation-dehydrogenation catalyst metal (like Cu).

Bravo-Suárez and co-workers [91] studied the effects of catalyst composition on methanol and ethanol coupling reactions on $CuMgAlO_x$ mixed metal oxides, with Cu contents between 4 and 38 at%. The catalysts (around 3g) were tested between 175 and 250 °C, 0.1 MPa, alcohols gas-hourly space velocities (GHSVs) of 1000-3000 std $cm^3\ g_{cat}^{-1}\ h^{-1}$, and a feed MeOH/EtOH molar ratio of 4. Pretreatment of catalysts was carried out in He at approximately 470 °C for 5 h before reaction. The samples were then treated in 25 vol% H_2 in He at approximately 330 °C for 3 h and cooled down to reaction temperature in He. The resulting He/MeOH/EtOH gas mixture had a volumetric ratio of 75/20/5, corresponding to an alcohols GHSV of 1000 std (25 °C, 101 kPa) $cm^3\ g_{cat}^{-1}\ h^{-1}$.

The authors [91] broadly grouped reaction products as: *(i)* C-C coupling (*e.g.*, C_{3+} alcohols; C_{3+} aldehydes; C_{3+} esters); *(ii)* non-C-C coupling (*e.g.*, H_2CO, HAc, $HCOOCH_3$, MeOAc); and *(iii)* decomposition (*e.g.*, CO_x) products. Based on the Guerbet-chemistry, and previously published mechanistic and kinetic results on alcohol coupling reactions, Scheme 2.2.7. represents a simplified reaction network of the formation of the main products obtained from methanol and ethanol coupling reactions on $CuMgAlO_x$ catalysts. The top panel shows the reactions typically proposed for Guerbet alcohols coupling for MeOH + EtOH (*e.g.*, methanol and ethanol dehydrogenation to H_2CO and HAc, aldol condensation with loss of H_2O to acrolein, and acrolein hydrogenation to propanal and n-propanol), ethanol, and methanol and n-propanol. The absence of hydroxyaldehydes and unsaturated aldehydes (formed upon water elimination, *e.g.*, acrolein) suggests that the desorption rates are low. They rapidly react to form the corresponding saturated aldehyde (*e.g.*, propanal), which is also consistent with the favorable thermodynamics of dehydration and hydrogenation of these intermediates. The lower panel includes other reactions in which formation of C-C (*e.g.*, methyl propionate, methyl butyrate) and non-C-C coupled (*e.g.*, methyl formate, methyl acetate) esters occured from aldehydes and alcohols via oxidative esterification (*i.e.,* Tischenko-type reactions); and CO and CO_2 as a result of methanol decomposition, and the water-gas shift (WGS) reactions, respectively. [91]

Same authors [91] reported that the presence of Cu in the MMOs drastically changed the product distribution of vapor-phase methanol + ethanol coupling reactions. On $MgAlO_x$, C_{3+} alcohols were the predominant products, but with low methanol and ethanol conversions, and with fast catalyst deactivation. On $CuMgAlO_x$, C-C coupling (C_{3+} aldehydes, alcohols, and esters), non-C-C coupling (*e.g.*, acetaldehyde, methyl formate, methyl acetate, ethyl acetate), and decomposition products (*i.e.* CO_x) were observed at significantly larger methanol and ethanol conversions, and with slower catalyst deactivation. On $CuMgAlO_x$ catalysts, the production of non-C-C coupling and decomposition products was also high, because metallic Cu does not only catalyzed esterification reactions of non-C-C (*e.g.*, methyl acetate) and C-C coupling (*e.g.*, methyl propionate) intermediate products, but also dehydrogenation (*e.g.*, acetaldehyde), methanol reverse synthesis ($CH_3OH \rightarrow CO + 2H_2$), and the water-gas shift ($CO + H_2O \rightarrow CO_2 + H_2$) reactions. Intermediate Cu contents, intermediate temperatures, and high space velocities appear to favor the STY (g $kg_{cat}^{-1}\ h^{-1}$) C-C coupling products,

without significant production of non-C-C coupling and decomposition products. The results of this study suggest that $CuMgAlO_x$ is a multifunctional catalyst in which M-O-Al (M=Mg, Cu) acid–base pair sites catalyze C-C coupling reactions, while metallic oligomeric Cu catalyzes esterification of C-C, non-C-C coupling intermediate products, and methanol decomposition reactions.

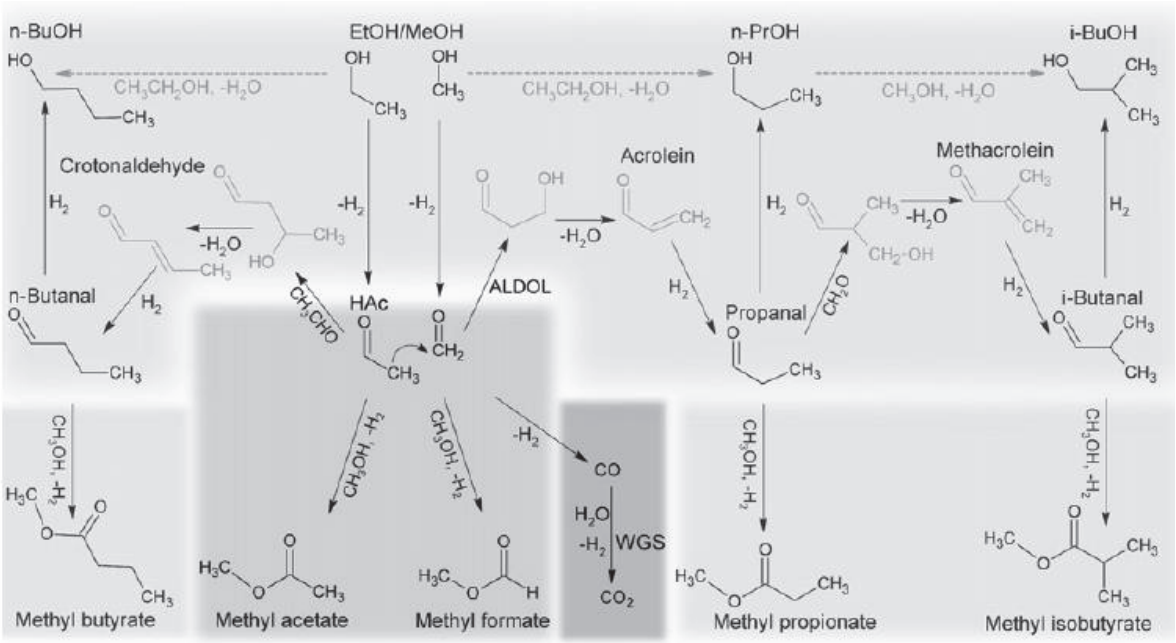

Scheme 2.2.7. Increasing shades of gray indicate grouped C-C coupling, non-C-C coupling, and decomposition products. Dashed arrows on top panel added to indicate start and end products in a specific combination of alcohols for Guerbet-like reactions. [91]

2.7. Acrolein production by oxidative coupling of methanol and ethanol

Oxidative coupling of ethanol and methanol represents the latest method proposed for acrolein synthesis. This process was described for the first time in the patent filled in 2012 which was assigned to *ARKEMA*. The process for direct acrolein synthesis is constituted of two successive steps. In the first step reactions of oxidation are taking place over selective redox catalyst: methanol and ethanol are simultaneously transformed to formaldehyde and acetaldehyde, respectively (Eq. 2.20). Then, in the second step, aldol condensation of the produced formaldehyde and acetaldehyde and dehydration to acrolein proceeds over aldolization (acid-base) catalyst (Eq. 2.21). It was discovered that the two steps can be carried out successfully in the presence of a single catalyst-commercially available redox iron molybdate catalyst (MoO_3-$Fe_2(MoO_4)_3$). [23]

$$CH_3OH + CH_3\text{-}CH_2\text{-}OH + O_2 \rightarrow HCHO + CH_3\text{-}CHO + 2\ H_2O \quad (2.20.)$$

$$HCHO + CH_3\text{-}CHO \rightarrow CH_2{=}CH\text{-}CHO + H_2O \quad (2.21.)$$

This two-step gas-phase reaction was conducted in a single reactor at temperatures between 200° and 400 °C at atmospheric pressure. Typical reaction mixture consisted of methanol+ethanol mixture in the ratio between 0.8 and 2 (around 10%), oxygen (max. 10%) and helium (around 80%).

GHSV was reported to be between 2000 and 40 000 h^{-1}. Alternatively it was described that reaction could take place in two consecutive reactors. In this case, at the exit of the first reactor, the condensation step could be carried out in parallel to eliminate water before the mixture enters into the aldolization (second) reactor because water could affect aldol condensation reaction. It can also remove the other impurities produced in the first reactor, such as acetic acid, propionic acid, formic acid, or acrylic acid, which could also react in the aldol condensation reaction performed in the second reactor. [23]

The second step of this reaction (aldol condensation of acetaldehyde and formaldehyde) was already mentioned in one of the previous Sections (2.2.2.). In Section 3.1, it will be fully described considering the impact of the acid/base properties of the catalysts on the reaction mechanism. It is also important to underline that in the case of methanol and ethanol oxidative coupling the reaction of aldol condensation occurs in presence of oxygen. Impact of the acid-base properties was not studied (up to now) in oxidizing conditions.

Dubois and co-authors reported in the patent that FeMoOx catalyst (200 mg) alone had relatively good selectivity for acrolein at 325 °C, and that the methanol/ethanol ratio in the reaction mixture strongly influenced the results. The highest selectivity towards acrolein (57%) was for MeOH:EtOH ratio of 0.8. When MeOH:EtOH ratio in the alcohols mixture was 1.2 acrolein selectivity was lower (48%) for a total conversion of methanol and ethanol. In the same conditions selectivity towards acrolein diminished to 40% when three times bigger quantity of catalyst was used (600mg). The carbon yields, selectivites and conversions were calculated as a function of the moles of carbon (from both alcohols) involved in the reaction (see Section 4.3.). Mo-Bi based catalyst (typically used for the oxidation of propanol in acrolein) was also tested in this reaction, but showed much lower activity (acrolein yield of only 18%). [23]

Later the same authors [23] studied the production of acrolein from methanol and ethanol in a single reactor configuration using the mixture of two catalysts. MeOH and EtOH ratio was always 1. As redox catalyst the same FeMoOx catalyst was used, while two different silica-supported catalysts, prepared by impregnation of silica gel, were selected as aldolization catalysts ($Cs/Zr/SiO_2$ and Na/SiO_2). $Cs/Zr/SiO_2$ catalyst generally showed better catalytic performance than Na/SiO_2. Over FeMoOx+$Cs/Zr/SiO_2$ catalysts the highest acrolein yield (67%) was obtained at 325 °C, and methanol and ethanol were almost completely converted. Further increasing of reaction temperature led to a significant decrease of the acrolein yield (7% at 350 °C). These results were obtained when a mixture of 133mg of FeMoOx and 67mg of $Cs/Zr/SiO_2$ was used. When 67mg of FeMoOx and 133mg of aldolization catalyst was used, the acrolein yield at 325 °C was 43%, and at 350 °C was still around 39 %. Considering the results obtained over a 1:1 mixture of FeMoOx and Na/SiO_2, it was observed that this combination of catalysts presents a good activity at high temperature (350 °C). The highest acrolein yield (48%) was obtained at 325 °C. And if the percentage of alcohols and oxygen in the reaction mixture increases (from 8% to 10% for each) the same acrolein yield was obtained at 350 °C. In each case (when a mixture of the two catalysts was used) total conversion of ethanol was observed, while methanol conversion drastically varied. The conversion of acetaldehyde does not always follow

the acrolein production variation; this behavior indicates that not only simple aldol condensation of acetaldehyde and formaldehyde to acrolein occurs, but that the mechanism of acrolein formation in these conditions involves some other reactions which additionally impact on acrolein production. [23]

As general conclusion the highest acrolein yields were obtained in the temperature range between 300° and 325 °C. Acrolein production increased with temperature. However for the temperatures above 325 °C acrolein yield remained constant or diminished. This could be due to the partial decomposition of the produced acrolein and other products/reactants to carbon oxides (over-oxidation reactions). For example, production of carbon oxides was reported for aldol condensation of acetaldehyde and formaldehyde due to high basicity (see Section 3.1.) Also, longer contact times and higher temperature led to increasing production of CO_x. Therefore it is expected that in the process of oxidative coupling of alcohols, owing to the presence of oxygen, carbon oxides production will be higher. Various other factors (*e.g.* ratio of MeOH:EtOH, reaction feed composition, ratio of Fe:Mo in FeMoOx catalyst…) play an important role in acrolein synthesis by oxidative coupling of alcohols. [23] Consequently, more extensive studies are necessary to understand and clarify the impact of the various factors on the reaction.

FeMoOx catalyst can be defined as the reference catalyst for this new synthesis method. FeMoOx is a redox catalyst typically employed in an industrial process of formaldehyde production by oxidation of methanol. It was reported that several factors influence the reaction efficiency such as water acting as an inhibitor, reactor type, the partial pressure of both reactants (e.g., the reaction rate increases with increasing pressure) and the methanol partial pressure (*e.g.,* in the presence of water, higher pressure causes higher reaction rate). The following mechanism for methanol oxidation to formaldehyde over FeMoOx catalyst was proposed by Pernicone: [32,96]

1) Dissociative methanol chemisorption:

$$CH_3OH + \blacksquare + O_2^- \longrightarrow (CH_3O{-}\blacksquare)^- \qquad (2.22.)$$

2) Catalyst reduction with chemisorbed formaldehyde formation:

$$(CH_3O{-}\blacksquare)^- + O_2^- \longrightarrow (CH_2O{-}\blacksquare)^{2-} + OH^- \qquad (2.23.)$$

3) Water desorption:

$$2OH^- \longleftrightarrow H_2O + O^{2-} + \blacksquare \qquad (2.24.)$$

The ability of this catalyst to directly produce a certain amount of acrolein, from methanol and ethanol, could be due to the presence of surface Lewis acidity linked to the presence of Mo^{6+} species. [23,32,96-98]

The yield to acrolein (in alcohols oxidative coupling) can be improved by addition of acidic or basic component to the FeMoOx catalyst or its modification. This will help to improve the aldol condensation between the acetaldehyde and formaldehyde, produced from methanol and ethanol. Changing the Mo:Fe ratio in the FeMoOx catalyst, doping FeMoOx catalyst with another element, and

mixing the FeMoOx catalyst with another catalyst are the strategies that can be applied for this purpose. [23,32]

Production from acetaldehyde and formaldehyde which was used as an industrial method a long time ago is not interesting anymore even if formaldehyde and acetaldehyde can be produced from biomass. Formaldehyde and acetaldehyde could not be stored and easily transported, therefore production of acrolein based on this process would require a reactor for acetaldehyde production (which is commonly by oxidation of ethylene) and in parallel a reactor for formaldehyde production (by methanol oxidation over FeMoOx catalyst) in addition to the aldolization reactor. All together the process would be very expensive. On the other hand, the process based on the oxidative coupling reaction, could be performed in a single reactor and the alcohols used like reactants are already (EtOH) or potentially (MeOH) largely produced from biomass. They can be easily transported, stored, and purchased at reasonable prices. In addition, assuming a 1:1 molar ratio of methanol/ethanol, a 70 mol% yield would be sufficient to reach an economic viability of the propylene oxidation process, taking into account the raw material cost today. The reaction is exothermic so the same reactor technology (multitubular reactors), as used for propylene oxidation or methanol oxidation to formaldehyde, can be considered, thus reducing the technology risk for the operators. Also there is a potential to use smaller reactors than for propylene oxidation, because it is known that the alcohols oxidation is achievable at lower contact times than propylene oxidation. [23,32,100]

Based on the initial positive results, and in the framework of BioMA+ project *ARKEMA, IRCELYON and UCCS* studied this new process for acrolein procuction. A PhD thesis was carried out at *UCCS* by A. Borowiec, [32] who studied the reaction in a single continuous flow quartz reactor, using 200 mg of active catalytic material. The studies were focused on adjusting the Fe:Mo ratio in the redox FeMoOx catalyst or its doping by basic elements. Also, the strategy where reference redox FeMoOx catalyst was mixed with different aldolization catalysts in a single reactor was studied. On the other hand, the PhD thesis presented in this manuscript, carried out at *IRCELYON* and *ARKEMA,* concerned the same reaction in a micropilot consisting in two consecutive continuous flow reactors using a FeMoOx catalyst (around 4g) in the oxidation reactor and different acid-base aldolization catalysts (20g) in the second reactor. The reaction was decoupled in two separate reactors because the main focus of this thesis was to study the impact of the acidity and basicity on the reaction of aldolization independently of the redox catalysts properties. This study is important in order to understand which aldolization component (with what acid/base properties) should be added to the redox FeMoOx catalyst to obtain the highest acrolein yield and optimize the process for acrolein production in a single reactor. Therefore we studied principally the impact of the acid-base properties on the gas-phase aldol condensation of acetaldehyde and formaldehyde in oxidizing conditions contrarily to previously reported researches always performed in absence of oxygen. Bibliographical research dealing with this subject is presented in the following chapter. Results and discussion are reported in chapters 6 and 7.

References

[1] Z. Peng, C. Yu, T. Cai, Q. Deng, *J. Nat. Gas Chem.* **2004**, *13*, 172-176.

[2] M. Kanno, T. Yasukawa, W. Ninomiya, K. Ooyachi, Y. Kamiya, *J.Catal.* **2010**, *273*, 1-8.

[3] F. Cavani, R. Mezzogori, A. Pigamo, F. Trifiro, E. Etienne, *Cat. Today* **2001**, *71*, 97-110.

[4] J. Guan, K. Song, H. Xu, Z. Wang, Y. Ma, F. Shang, Q. Kan, *Catal. Commun.* **2009**, *10*, 528-532.

[5] A. Tenten, H.P. Neumann, H. Exner, *US 5 583 086*, assigned to BASF, Germany.

[6] H. Engelbach, R. Krabetz, G. Duembgen, C.H. Willersinn, W. Beitelschmidt, *US 4 298 763*, assigned to BASF, Germany.

[7] H. Kasuga, E. Shiraichi, *US 2002/0198103 A1*, assigned to Nippon Shokubai CO LTD, Japan.

[8] T. Watanabe, O. Nagano, *US 2005/0032639*.

[9] T. Kurakami, T. Kojima, Y. Seo, *EP 2 011 780 B1*, assigned to Nippon Kayaku, Japan.

[10] F.G. Martin, H. Hibst, A. Tenten, *US 5 569 636,* assigned to BASF, Germany.

[11] F.G. Martin, H.P. Neumann, H. Hibst, *US 5 583 084*, assigned to BASF, Germany.

[12] A. Sudo, Y. Seo, T. Kurakami, *EP 1 629 889 B1*, assigned to Nippon Kayaku, Japan.

[13] A. Sudo, T. Kurakami, T. Kojima, S. Hayashimoto, *EP 1 867 387 B1*, assigned to Nippon Kayaku, Japan.

[14] *EP 2 436 443 A1*, assigned to Nippon Kayaku, Japan.

[15] B.N.M. Van Leeuwen, A.M. Van der Wulp, I. Duijnstee, A.J.A. Van Maris, A.J.J. Straathof, *Appl. Microbiol. Biotechnol.* **2012**, *93*, 1377-1387.

[16] L. Liu, X.P. Ye, J.J. Bozell, *ChemSusChem* **2012**, *5*, 1162-1180.

[17] S.Mourey,(*Acroléine: succès confirmés en chimie fine)* in *Info Chimie Magazine*, October **1999**, *412*, 90-96.

[18] C. García-Sancho, J.A. Cecilia, A. Moreno-Ruiz, J.M. Mérida-Robles, J. Santamaría-González, R. Moreno-Tost, P. Maireles-Torres, *Appl. Catal. B.* **2015**, *179*, 139-149.

[19] D. Arntz, A. Fischer, M. Höpp, S. Jacobi, J. Sauer, T.Ohara, T. Sato, N. Shimizu, H. Schwind, *Acrolein and Methacrolein* in *Ullmann's Encyclopedia of Industrial Chemistry*, Wiley-VCH, Weinheim

[20] W. G. Etzkorn, S. E. Pedersen, T. E. Snead, *Acrolein and Derivatives*, **2002**, http://203.199.213.48/1013/.

[21] B. Katryniok, S. Paul, M. Capron, F. Dumeignil, *ChemSusChem* **2009**, *2*, 719-730.

[22] H.Schulz, H. Wagner, *Angew. Chem.* **1950**, *62*, 105-118.

[23] L. Dubois, M. Capron, F. Dumeignil (Arkema France, Colombes), WO2014/068213A9, **2014**

[24] H. H. Szmant, *Organic Building Blocks of the Chemical Industry*, Wiley, New York, 1989.

[25] M. Ai, *Bull. Chem. Soc. Jpn.* **1991**, *64*, 1342-1345.

[26] M. Ai, *Bull. Chem. Soc. Jpn.* **1991**, *64*, 1346-1350.

[27] S. Malinowski, W.J. Palion, *React. Kinet. Catal. Lett.* **1974**, *1*, 73-78.

[28] W.J. Palion, S. Malinowski, *React. Kinet. Catal. Lett.* **1974**, *1*(4), 461-465.

[29] E. Dumitriu, V. Hulea, C. Chelaru, C. Catrinescu, D. Tichit, R. Durand, *Appl. Catal. A: Gen.* **1999**, *178*, 145-157.

[30] E. Dumitriu, V. Hulea, N. Bilba, G. Carja, A. Azzouz, *J. Mol. Catal.* **1993**, *79, 175-185.*

[31] A. Azzouz, D. Messad, D. Nistor, C. Catrinescu, A. Zvolinschi, S. Asaftei, *Appl. Catal. A: Gen.* **2003**, *241,* 1–13.

[32] A. Borowiec, PhD thesis (*Order number: 42244)*, University Lille 1 (FR), **2016**.

[33] M. Ai, *Appl. Catal.***1991**, *77,* 123-132.

[34] R. F. Howard, *Handbook of Commercial Catalysts: Heterogeneous Catalysts*, CRC Press LLC, Boca Raton, Florida, **2000**.

[35] Y. A. Saleh-Alhamed, R. R. Hudgins, P. L. Silveston, *Appl. Catal. A: Gen.* **1995**, *127*, 177-199.

[36] E. H. Xie, Q. L. Zhang, K. T. Chuang, *Appl. Catal. A: Gen.* **2001**, *220*, 215-221.

[37] H. Redlingshçfer, O. Krocher, W. Bock, K. Huthmacher, G. Emig, *Ind. Eng. Chem. Res.* **2002**, *41*, 1445-1453.

[38] W.G. Etzkorn*, Acrolein and Derivatives* in *Kirk-Othmer Encyclopedia of Chemical Technology*. **2009.**

[39] L. Chen, J. Liang, W. Weng, Y. Wang, H. Wan, J.C. Védrine, *Catal. Commun.* **2004**, *5*, 697-701.

[40] L. Chen, J. Liang, H. Lin, W. Weng, H. Wan, J.C. Védrine, *Appl.Catal. A: Gen.* **2005**, *293*, 49-55.

[41] Y.C. Kim, W. Ueda, Y. Moro-oka, *Appl.Catal.* **1991**, *70*, 175-187.

[42] X. Zhang, H. Wan, W. Weng, X. Yi, *Catal. Lett.* **2003**, *87*, 229-234.

[43] X.Zhang, H. Wan, W. Weng, *Appl.Catal. A: Gen.***2009***, 353,* 24-31.

[44] C.S. Carriço, F.T. Cruz, M.B. dos Santos, D. S. Oliveira, H.O. Pastore, H.M.C. Andrade, A.J.S. Mascarenhas, *J. Catal.* **2016**, *334*, 34-41.

[45] B. Katryniok, S. Paul, V. Bellière-Baca, P. Rey, F. Dumeignil, *Green Chem.*

2010, *12*, 2079-2098.

[46] J.L. Solomon, R.J. Madix, *J. Phys. Chem.* **1987**, *91*, 6241-6244.

[47] M. Imachi, N.W. Cant, R.L. Kuczkowski, *J. Catal.* **1982**, *75*, 404-409.

[48] G.J. Hutching, D.F. Lee, *Catal. Lett.* **1995**, *34*, 115-127.

[49] P. Vitins, K.W. Egger, *J. Chem. Soc,. Perkin Trans. 1* **1974**, 1292-1293.

[50] K. Nakagawa, Y. Teng, Z. Zhao, Y. Yamada, A. Ueda, T. Suzuki, T. Kobayashi, *Catal. Lett.* **1999**, *63*, 79-82.

[51] Z. Zhao et al. *Appl. Catal. A: Gen.* **2000**, *196*, 37-42.

[52] Z. Zhao et al. J. Catal. **2000**, *190*, 215-227.

[53] Z. Zhao, T. Kobayashi, *Appl. Catal. A: Gen.* **2001**, *207*, 139-149

[54] K. Nakagawa et al. *Catal. Lett.* **1999**, *63*, 79-82.

[55] W.C. Serjak, W.H. Day, J.M.V. Lanen, C.S. Boruff, *Appl. Environ. Microbiol.* **1953**, *2*, 14-20.

[56] E. Voisenet, *Ann. Inst. Pasteur (Paris)* **1918**, *32*, 476-510.

[57] F. B. Humphreys, *J. Inf. Dis.* **1924**, *35,* 282-290.

[58] N. *Kosaric,Z. Duvnjak, A. Farkas, H. Sahm, S. Bringer-Meyer, O. Goebel, D. Mayer, Ethanol* in *Ullmann's Encyclopedia of Industrial Chemistry,* Wiley-VCH, Weinheim, **2001**.

[59] G.G. Eremeeva, V.M. Dronkin, G.I.Gagarina*, Neftepererab. Neftakhim (Moscow)* **1979**, *16*, 19-20.

[60] K. W. Toptschijewa, S. M. Rachowskaja, I. K.Kutschkajewa *,Neftekhimiya* **1963**, *3*, 271.

[61] Renewable Fuels Association web site: http://ethanolrfa.org.

[62] E. Dahlquist (Ed.) *Biomass as Energy Source: Resources, Systems and Applications*, CRC Press (Taylor & Francis Group), London, **2013**.

[63] A.H. Rose, J.S. Harrison*, The Yeasts*, Academic Press, London, **1970**.

[64] J. *Ott, V. Gronemann, F. Pontzen, E. Fiedler, G. Grossmann, D.B. Kersebohm, G. Weiss, C. Witte, Methanol* in *Ullmann's Encyclopedia of Industrial Chemistry,* Wiley-VCH, Weinheim, **2012**.

[65] J.G. Van Bennekom, R.H. Venderbosch, H.J. Heeres, *Biomethanol from Glycerol in Biodiesel - Feedstocks, Production and Application,* **2013.** http://dx.doi.org/10.5772/53691

[66] N.S. Shamsul, S.K. Kamarudin, N.A. Rahman, N.T. Kofli, Renew. *Sustainable Energy Rev.* **2014**, *33*, 578-588.

[67] M.H. Haider, N.F. Dummer, D.W. Knight, R.L. Jenkins, M. Howard, J. Moulijn, S.H. Taylor, G.J. Hutchings, *Nat. Chem.* **2015**, *7*, 1028-1032.

[68] A.P.V. Soares, M.F. Portela, A. Kienneman, *Catal. Rev.* **2004**, *47*, 125-174.

[69] K. Weissermel, H.J. Arpe, *Industrial Organic Chemistry*, 1993.

[70] G. Alessandrini, L. Cairati, P Forzati, P.L. Villa, F. Trifiro, *J. Less Common Met.* **1977**, *54*, 373-386.

[71] N. Burriesci, F. Garbassi, M. Petrera, G. Petrini, N. Pernicone, *Solid state reactions in Fe-Mo oxide catalysts for methanol oxidation during aging in industrial plants* in *Catalyst Deactivation (Eds. B. Delmon, G.F. Froment),* Elsevier, Amsterdam, **1980.**

[72] G. Fagherazzi, N. Pernicone, *J.Catal.* **1970**, *16*, 321-325.

[73] M.R. Sun-Kou, S. Mendioroz, J.L.G. Fierro, J.M. Palacios, A. Guerrero-Ruiz, *J. Mater. Sci.* **1995**, *30*, 496-503.

[74] M. Carbucicchio, F. Trifiro, *J.Catal.* **1976**, *45*, 77-85.

[75] N. Pernicone, F. Lazzerin, G. Liberti, G. Lanzavecchia, *J. Catal.* **1969**, *302*, 293-302.

[76] G. Liberti, N. Pernicone, S. Soattini, 1972. *J.Catal.* **1972**, *27*, 52-55.

[77] J.M. Tatibouët, 1997. *Appl. Catal. A: Gen.* **1997***, 148(2)*, 213-252.

[78] W. Cheng, *J.Catal.* **1996***, 158(2),* 477-485.

[79] Y. Guan, E.J.M. Hensen, *J. Catal.* **2013**, *305*, 135-145.

[80] T. Takei, N. Iguchi, M. Haruta, *Catal. Surv. Asia* **2011**, *15(2)*, 80-88.

[81] Y. Guan, E.J.M. Hensen, *Appl. Catal. A: Gen.* **2009***, 361(1-2*), 49-56.

[82] V.I. Sobolev, K.Y. Koltunov, O.A. Simakova, A.R. Leino, D.Y. Murzin, *Appl. Catal. A: Gen.* **2012***, 433-434*, 88-95.

[83] X.M. Kong, L.L. Shen, *Catal. Commun.* **2012**, *24*, 34-37.

[84] E. Redina, A.A. Greish, I.V. Mishin, G.I. Kapustin, O.P. Tkachenko, O.A. Kirichenko, L.M. Kustov, *Catal.Today* **2014**, *241*, 246-254.

[85] H. Nair, J.E. Gatt, J.T. Miller, C.D. Baertsch, *J. Catal.* **2011***, 279(1),* 144-154.

[86] B. Mehlomakulu, T.T.N. Nguyen, P. Delichère, E. Van Steen, J.M.M. Millet, *J. Catal.* **2012**, *289*, 1-10.

[87] V. Srihari, D. Viswanath, *J. Catal.* **1976***, 43*, 43-52.

[88] B. Kilos, A.T. Bell, E. Iglesia, *J. Phys. Chem. C* **2009**, *113*, 2830-2836.

[89] I. Abdullahi, T.J. Davis, D.M. Yun, J.E. Herrera, *Appl. Catal. A: Gen.* **2014***, 469*, 8-17.

[90] R.D. Weinstein, A.R. Ferens, R.J. Orange, P. Lemaire, *Carbon* **2011**, *49(2),* 701-707.

[91] J.J. Bravo-Suárez, B. Subramaniam, R.V. Chaudhari, *Appl. Catal. A: Gen.* **2013***, 455,* 234-246.

[92] S. Veibel, J.I. Nielsen, *Tetrahedron* **1967**, *23(4*), 1723-1733.

[93] J.I. Di Cosimo, C.R. Apesteguia, M.J. L. Ginés, E. Iglesia*, J. Catal.* **2000***, 190(2),* 261-275.

[94] M.J.L. Gines, E. Iglesia, *J. Catal.* **1988***, 176(1),* 155-172.

[95] J.I. Di Cosimo, V.K. Diez, M. Xu, E. Iglesia, C.R. Apesteguia, *J. Catal.* **1998,** *178(2),* 499-510.

[96] N. Pernicone, *J. Less Common Met.* **1974**, *36*, 289-297

[97] K.A. Thavornprasert, M.Capron, L.Jalowiecki-Duhamel, O. Gardoll, M. Trentesaux, A.S. Mamede, G. Fang, J.Faye, N. Touati, H. Vezin, J.L. Dubois, J.L. Couturier, F. Dumeignil, *Appl. Catal. B* **2014***, 145*, 126-135*.*

[98] F. Trifirò, I. Pasquon, *La Chimica e l'Industria (Milan)* **1971**, *53,* 577.

[100] A.Lilić, S. Bennici, J.F. Devaux, J.L. Dubois, A. Auroux, *ChemSusChem* 2017. DOI: 10.1002/cssc.201700230.

Chapter 3.

State of the art: Catalysts acidity/basicity

3.1. Influence of acid/base properties of the catalysts on the gas-phase aldol condensation of acetaldehyde and formaldehyde.

The condensation reactions of aldehydes, as well as of ketones, are widely used in organic synthesis, mainly because they lead to C-C bonding. These reactions are typically catalyzed by bases. [1]

Acrolein can be obtained by aldol condensation of formaldehyde and acetaldehyde (Tollens reaction). [2] During the 1940s Degussa (Germany) patented acrolein production based on this reaction. The original process comprises the catalytic conversion of acetaldehyde and 30% formaldehyde in aqueous solution, stabilized with ~10% of methanol (formalin), on silica gel impregnated with 10% sodium silicate ($Na_2Si_2O_5$), at 305 °-310 °C. The main products were acrolein, water, acetaldehyde and formaldehyde, and other by-products, such as methanol, carbon dioxide and crotonaldehyde, were observed. [3] Although the industrial production of acrolein based on this reaction stopped (replaced by propylene oxidation) before the end of the 1950s, the reaction still kept the attention of several research groups since the C_1 chemicals, used as reactants, could be easily produced from biomass. [1,2,4-10] Equation 3.1. represents aldol condensation of formaldehyde and acetaldehyde and their dehydration to acrolein [2]:

$$CH_3\text{-}CHO + HCHO \rightarrow CH_2(OH)CH_2\text{-}CHO \rightarrow CH_2{=}CH\text{-}CHO + H_2O \qquad (3.1.)$$

Considering aldol condensation in gas phase the mechanism of the reaction is still not clearly described and understood. Numerous authors reported that the reaction is preferentially catalyzed on basic sites of different strength. However, a too high basicity could lead to undesired side reactions, such as over oxidation to carbon oxides and production of methanol. The importance of the presence of acidic sites and positive effect of the acid-base collaboration was, also, often reported. In those cases the production of CO_x was lower, but polymerization was more pronounced. [1,2,4-17] The aldol condensation of formaldehyde with acetaldehyde in gas phase was reported over different solid catalysts including mixed or supported oxides, [2,4-6,12,13] hydrotalcite-like materials, [1,8] zeolites [7,10,14-17] and clays[9], and the impact of basic and acidic sites was pointed out as the key factor influencing acrolein production.

Besides, various other factors, such as the type of reactor, the reaction pressure and temperature, the acetaldehyde to formaldehyde ratio, may influence this reaction. In the studies performed up to now, two types of reactors were used and the reaction was carried out in the 250 °-

500 °C temperature range, using nitrogen as carrier gas, and a mixture of acetaldehyde and 35-37% formalin (containing 8-12% of methanol) as feed. The reaction was performed at atmospheric pressure in the continuous-flow fixed bed reactor, and at 2.5 bar in the pulse type reactor. The main product was acrolein, and the presence of by-products such as CO_x, methanol, crotonaldehyde, acetone, propionaldehyde was reported. Their amount and distribution depended on the acid/base properties, as well as on other factors influencing the reaction (mainly the temperature). The optimal conditions, to perform this reaction in a continuous flow fixed bed reactor at the atmospheric pressure, were temperatures between 300° and 325 °C, and formaldehyde:acetaldehyde ratio of 2:1. For temperatures below 300 °C, acrolein production was lower, while an increased production of crotonaldehyde was observed. Higher production of acrolein was reported starting from 300 °C, while temperatures higher than 325 °C favored the production of carbon oxides (due to decomposition of acrolein), and coke. GHSV (Gas Hourly Space Velocity) should be in the 0.03-1.35 h^{-1} range for optimum results. Almost none of the studies reported for this reaction investigated the catalyst deactivation, but the coking of the catalysts could be expected. [1,2,4-10,12-17]

Considering the acid/base properties influence on the reaction mechanism, one group of authors, which studied this reaction in a pulse type reactor, reported that competition between cross- and self- aldolization reactions occurs in gas-phase, when acetaldehyde and formaldehyde are present as reactants (Scheme 3.1.). [1,7-10,14-17] Cross-aldolization is the reaction between acetaldehyde and formaldehyde to form acrolein, while self-aldolization includes condensation of two molecules of acetaldehyde to give crotonaldehyde. In gas phase formaldehyde does not self-condense. Formaldehyde acts only as carbonyl component; while acetaldehyde acts both as carbonyl and methylene component. The acid-base properties of the solid catalyst and the reaction temperature mainly influence the ratio between self- and cross-aldolization. [1,7-10,14-17]

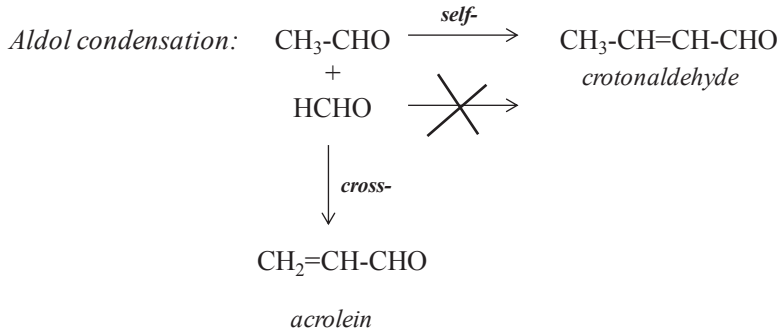

Scheme 3.1. Cross-aldol condensation of acetaldehyde and formaldehyde to form acrolein, and self-aldol condensation of two molecules of acetaldehyde to form crotonaldehyde. [1]

In addition to experimentally measured yields of crotonaldehyde, these authors also calculated the charge density, by CNDO/2 method, and explained that quite similar negative charges exist on oxygen for both aldehydes, as represented in Scheme 3.1.1. This leads to a strong competition between the adsorption of two aldehydes (Scheme 3.1.2.) on the cationic sites (acidic sites). [1]

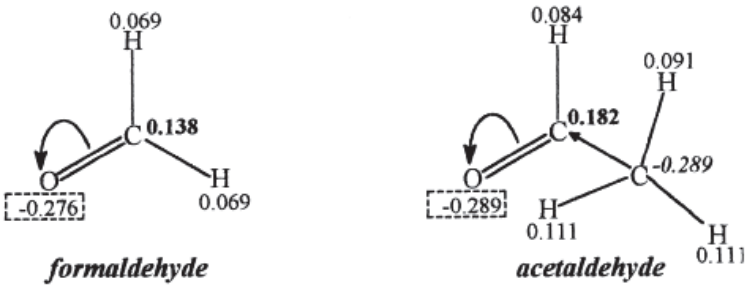

Scheme 3.1.1. Oxygen charge densities calculated and reported by Dumitriu et al. [1]

Aldol condensation proceeds by the activation of the carbonyl group on acidic sites, and the reaction substrate is the enol form of the acetaldehyde (the enolization reaction proceeds both on Brønsted and Lewis sites). The activation of acetaldehyde is favored, to some extent, thanks to its slightly higher electronic density on oxygen than for formaldehyde, and because acetaldehyde is also the substrate of reaction, the competition between cross- and self-aldolization is shifted towards self-aldolization. It was reported that the strength of the acidic sites can influence the ratio between self- and cross-aldolization, but not in a decisive manner. On weak acidic sites acetaldehyde is preferentially chemisorbed (thus crotonaldehyde formation is favored), while on strong acidic sites, an important amount of formaldehyde is chemisorbed, and, as a consequence, the amount of acrolein increases. [1]

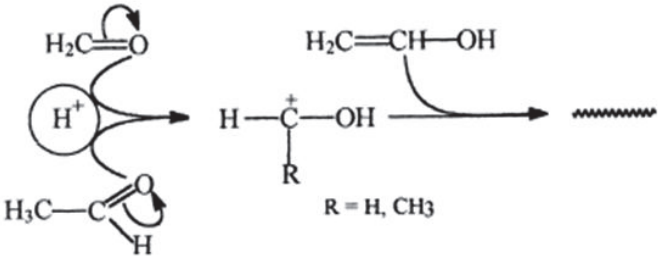

Scheme 3.1.2. Competition between acetaldehyde and formaldehyde on acidic sites. [1]

On basic sites, aldol condensation occurs by abstraction of a H-atom at the α-position of the carbonyl function of acetaldehyde to form a carbanion. The carbanion will further react with a carbonyl group (Scheme 3.1.3.). In this case, the selectivity to acrolein (the cross-aldolization product) can be better controlled. On the surfaces characterized by a high concentration of basic sites (of proper strength) the main part of acetaldehyde will be involved into the activation process (like described for acidic sites), while the formaldehyde becomes the main reaction substrate. Thus, selectivity towards acrolein would be strongly increased. [1]

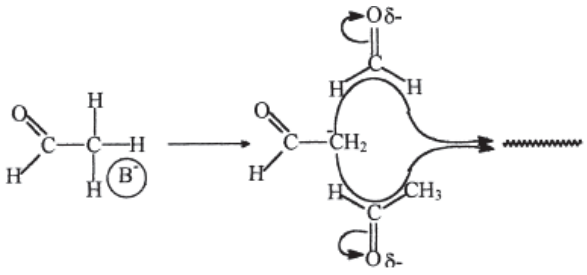

Scheme 3.1.3. Aldol condensation of acetaldehyde and formaldehyde on basic sites proposed by Dumitiu et al.[1]

The competition between the aldol condensation products (acrolein and crotonaldehyde) and the influence of the nature of the active sites, were investigated by different research groups that generally reported that the formation of acrolein is accompanied by two other side-reactions. The first is the polymerization of the produced acrolein,[1,2,6,11] and the second is the formation of methanol and carbon dioxide (exclusively from HCHO), by the following reactions (Equation 3.2.): [2,6,11]

$$2HCHO + HCOOCH_3 \rightarrow CH_3OH + HCOOH \rightarrow CH_3OH + CO_2 + H_2 \quad (3.2.)$$

Mixed and supported oxides

Aldol condensation of formaldehyde and acetaldehyde in gas phase was extensively studied on different types of mixed and supported oxides. [2,4-6,12,18]

The reaction was studied by a Polish group of scientists in the period between 1960 and 1980 on series of silica gel catalysts impregnated with alkaline ions, [4,18] and on different silica-alumina catalysts [5,12]. The best acrolein yields reported by these authors were in the 46-62 mol% range, on alkali and alkaline earth-silica catalysts. [2,18]

Malinowski and Basinski [4] reported that aldol condensation of acetaldehyde and formaldehyde produces acrolein with good yield and a minimum quantity of by-products (less than 2%), in the 200-350 °C temperature range, on basic silica-sodium oxide catalysts having different SiO_2:Na_2O ratios. These catalysts were prepared by saturating the silica gel with various quantities of sodium hydroxide-water solution. The reaction kinetics was also investigated on the basis of the results obtained in an integrating reactor at 275 and 300 °C. It was found that the reaction is accelerated by the presence of a defined amount of sodium-containing centers, probably Si-O-Na groups, while different values of the reaction rate constants were found when varying the number of these centers.

Further investigations of Malinowski and Palion [5] were performed in presence of catalytic systems constituted by mixed silica-alumina gel (Al_2O_3-SiO_2=25%-75%) and fluorine ions, in the 300-500° C temperature range. This type of surface might indeed incorporate highly acidic centers. A series of catalysts, with fluorine contents of 0.1%, 0.5%, 1%, 3%, 5%, have been prepared by saturating silica-alumina gel with aqueous solutions of hydrogen fluoride, followed by drying and calcination. Besides acrolein, by-products, like acetone and propionaldehyde and, in small quantities, methyl ethyl ketone, were obsevrved. Hydrogen, carbon monoxide, carbon dioxide and C_1- C_3 hydrocarbons were also found in the gaseous products. The maximum extent of reaction was generally observed at 350 °C. Up to 450 °C acrolein was the main reaction product. Other products were formed only in a very small amount. Above 350 °C, the amount of acrolein sharply decreases, with a simultaneous increasing in the percentage of acetone (which reaches a maximum at 400 °C). Above 400 °C, propionaldehyde started to appear, reaching the maximum production at 450 °C. Above 450 °C, methylethylketone was detected in small quantities. Considering the impact of the fluorine contents on the reaction products, the maximum acrolein yield was obtained for 0.5% and 3%

fluorine, while for the same F-loading acetone and propionaldehyde were minimized. The lowest acrolein formation corresponded to 1% fluorine content, while propionaldehyde and acetone showed the highest yields at this composition.[5]

Authors in reference [5] proposed that the surface of these catalysts contains donor, acceptor and free radical centers. Donor and acceptor centers are responsible for acrolein formation, as presented in the mechanism in Scheme 3.1.4. The maximum activity occurs when the two types of centers operate together. The ratio of acidic and basic sites (governed by the fluorine content) influences the acrolein production. Positive influence on the acrolein formation (at higher percentage of fluorine) can be due to partial hydrolysis of the Si-O-Al bond and consecutive creation of new donor and acceptor sites. It was also explained that acrolein production is affected by the simultaneous formation of acetone and methylethylketon, ascribed to a free radical mechanism (Scheme 3.1.5.). [5]

The formation of propionaldehyde (above 400 °C) may be due to the following reactions reported in Scheme 3.1.6., and consistent with the fact that, upon the flowing of formaldehyde vapors over the catalyst, CH_3OH, CO, CO_2, H_2O were observed. [5]

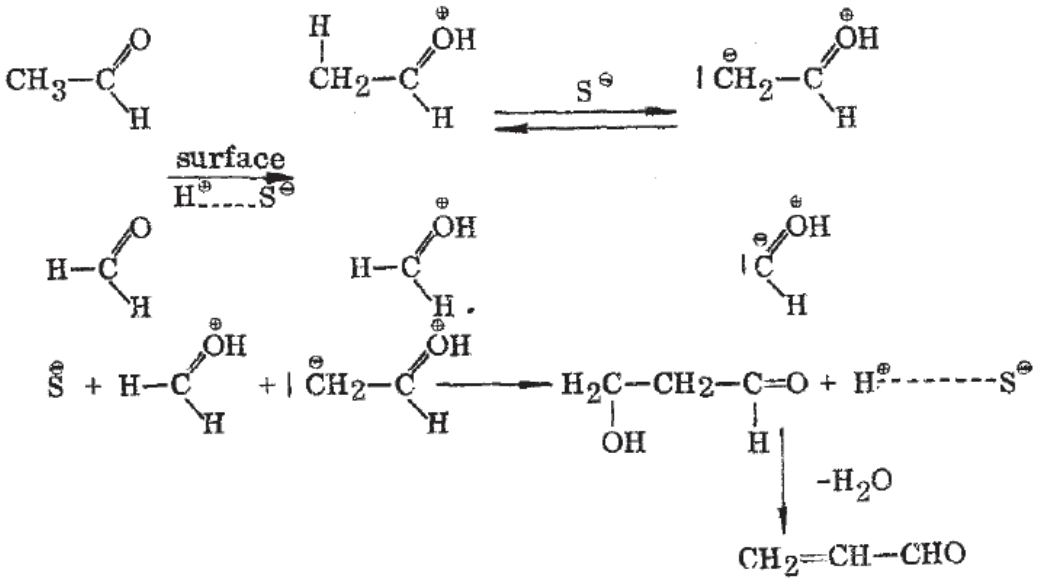

Scheme 3.1.4. Mechanism of acrolein formation proposed by Malinowski and Palion. [5]

The studies performed under the same conditions on silica, alumina and silica-alumina gels, containing 2.5%, 5%, 13%, 25% and 50% of Al_2O_3, led to production of mainly acrolein. [12]

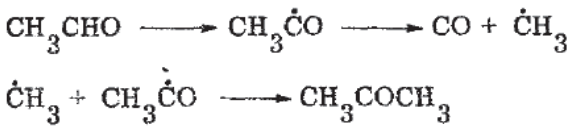

Scheme 3.1.5. Acetone formation by the two step free radical mechanism proposed by Malinowski and Palion. [5]

The same mechanism, temperature dependence, and by-products as those observed for silica-alumina catalysts (doped with fluorine ions) were also proposed (Schemes 3.1.4.-3.1.6.). [12]

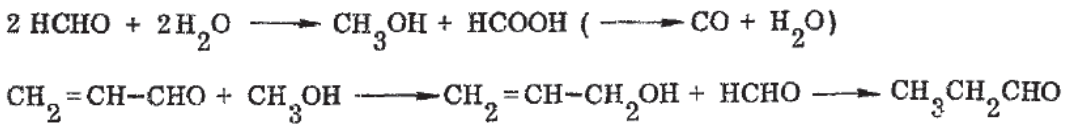

Scheme 3.1.6. Propionaldehyde formation described by Malinowski and Palion. [5]

The amount of Brønsted-type acid centers on a catalyst surface can depend on the Al_2O_3/SiO_2 ratio. The number of Brønsted centers grows with the increasing percentage of Al_2O_3, to reach a maximum at 30% Al_2O_3. At all temperatures, the highest amount of acrolein was formed when the reaction was performed on the catalyst containing 30% of Al_2O_3. The acetone maximum production was observed for catalysts containing 25% Al_2O_3 and 75% SiO_2. The formation of acrolein is ascribed to an ionic mechanism (Scheme 3.1.4.) and the Brønsted-type acid centers are responsible for its formation. The fact that the maximum activity, for both ionic (acrolein formation) and free-radical (acetone formation) reactions was noticed at the same catalyst composition, was related to the maximum number of donor centers present on the most acidic catalysts. [12]

In the beginning of 1990, vapor-phase aldol condensation of formaldehyde with acetaldehyde to form acrolein was studied in a continuous flow fixed bed reactor, at atmospheric pressure, with various basic, amphoteric or acidic oxides supported on silica gel [2] and different phosphate catalysts. [6]

All catalysts tested showed a certain activity, and the main products detected, in all cases, were acrolein, CO_2 and methanol. Generally products yields increased with temperature. The highest acrolein yields were obtained in the 280 to 320 °C temperature range. A very small amount of methyl formate was found in the products, while crotonaldehyde was not detected. In some cases, a large difference was observed between the acrolein yield and the acetaldehyde conversion. This gap was ascribed to the formation of unidentified polymers starting from acrolein (Equation 3.3.). This reaction is promoted by strong acidic sites. [2,6]

$$CH_3\text{-}CHO + HCHO \rightarrow CH_2{=}CH\text{-}CHO \rightarrow \textit{polymers} \qquad (3.3.)$$

The other side reactions generally brought to formation of CO_2 and methanol. The amount of methanol increased in parallel to that of CO_2, which indicates that these two by-products were formed from formaldehyde via the process presented in Equation 3.2. Formation of methyl formate, by dimerization of HCHO, is promoted on acid sites, while the decomposition of formic acid to CO_2 and H_2 is promoted by strong basic sites. Formation of CO_2 and methanol was relatively slow in the case of acidic catalysts. [2,6]

Silica gel catalysts showed a certain activity; the yield of acrolein reached 78 mol% with selectivity of 98 mol%. The incorporation of a basic oxide induced a strong increase in activity. No clear correlation between the electronegativity of metal ions and the activity was observed. The acrolein yield exceeded 85 mol% on Si-Li, Si-Na and Si-Mg systems. The yield was never higher than 75 mol% on Si-Cs, Si-Ba, and Si-Ca systems. [2]

The incorporation of an acidic oxide, such as P_2O_5 or B_2O_3, decreased the activity. The activity increased sharply with the incorporation of a small amount of MgO, while it decreases very fast with the addition of P_2O_5. These results suggested that the reaction is promoted by basic sites, like generally believed. It is important to notice that silica-supported MgO catalysts showed to be much more active than the unsupported ones. The combination of silica-gel with metal oxides might strongly increase the surface area, and generate new acidic sites which may also promote the reaction. These results confirmed that the proper balance of acidic and basic sites positively influences acrolein production. [2]

Relatively good performances in both activity and selectivity were obtained on Si-Zn oxide catalyst. The yield of acrolein reached 90 mol%, but the formation of CO_2 and methanol was relatively fast. The incorporation of an oxide of a heavy metal (Fe_2O_3, PbO_2, CuO) strongly promoted the formation of by-products: CO_2 and methanol (formed from HCHO). Formation of methyl formate by dimerization of HCHO is promoted by acid-base dual function, while decomposition of formic acid, to CO_2 and H_2, is promoted by very strong basic sites. [2]

Incorporation of V_2O_5 (amphoteric oxide), or an oxide of heavy metal, can enhance the catalytic activity to the level of catalysts constituted of alkali or alkaline metal (strong basic active sites). These strong active basic sites are selectively poisoned by acidic reactants (CO_2). Further reactions, especially the proton-abstraction from acetaldehyde, are promoted by very weak basic sites, deriving from V_2O_5 and amphoteric oxides (Equation 3.4.): [2]

$$CH_3CHO+OH^- \rightarrow -CH_2CHO+H_2O \qquad (3.4.)$$

To clarify the acid and base sites impact on the reaction, Ai [6] compared the catalytic performances at 320 °C on a series of single and binary oxides. The acidic single oxides (MoO_3 and WO_3) showed relatively high selectivity to acrolein, but low activities. On the other hand, V_2O_5 and amphoteric oxides (TiO_2, SnO_2, Fe_2O_3) presented high activities, but low selectivities to acrolein, accompanied by formation of CO_2 and methanol. The catalytic performance is improved by combination of V_2O_5 (or an amphoteric oxide) with an acidic oxide (MoO_3 or WO_3). The best performances were found for W-Sn and W-Fe oxide systems (with yield of acrolein up to 67 mol%).[6]

Concerning the tests performed on mixed phosphate catalysts, it was pointed out that the combination of phosphorous with an acidic oxides (MoO_3 or WO_3) drastically decreases the activity. Combination of phosphorus with certain amphoteric oxide (TiO_2, SnO_2, Fe_2O_3) strongly increases the selectivity to acrolein, while the activity gradually decreases when the phosphorous content is

increasing. The combination of phosphorous with an oxide such as Al_2O_3, ZrO_2, MgO or Bi_2O_3 is less effective. The best performances were obtained with Ni-P, Co-P, Mn-P, Fe-P, and V-P oxides. [6]

Mo-P and W-P catalysts (heteropolyanionic) which possess strong acidic sites were not active in aldol condensation, which suggests that the reaction is not promoted only by acidic sites. V_2O_5, amphoteric oxides, and oxides of heavy metals, which are considered to be more basic than MoO_3 and WO_3, because of the lower electronegativity of metal ions, show a higher catalytic activity. The activity of those oxides decreased with the incorporation of phosphorous. These observations suggest that the reaction is catalyzed by basic sites. However, similar to the studies performed with silica-supported basic oxide catalysts,[2] Ai found that the sites required to promote the acrolein formation consist of very weak basic sites (that are present in metal tungstates, molybdates, and phosphates), but not of strong basic sites. [6]

Among all silica supported and phosphate catalysts, [2,6] the best results were obtained on a Mg-Si catalyst with an atomic ratio 1:10 and on a nickel phosphate with a Ni/P ratio1:0.9. At 280 °C the yield of acrolein for Mg-Si catalyst reached 96 %, while for Ni-P yield was below 85%. However, for Ni-P the formation of CO_2 and methanol was clearly lower than that obtained for Mg-Si. This behavior is probably due to the presence of strong acidic sites on Ni-P, while silica-supported basic oxides possess mainly strong basic sites. It was proposed that the rate limiting step was different in the case of Si-Mg and Ni-P catalyst. It correspons to the protonation of HCHO by acidic sites ($HCHO+H^+ \rightarrow H_2C^+OH+H_2O$) over the Si-Mg catalyst, while over Ni-P catalyst it is connected to the proton abstraction from acetaldehyde by basic sites (Equation 3.4.). [2,6]

Summarizing the researches performed by Ai, it can be seen that the activity and selectivity of the catalysts, used in aldol condensation of formaldehyde and acetaldehyde, are driven by the balance of acidic and basic properties. The author suggested that aldol condensation is catalyzed by basic sites, but that the sites required to promote the acrolein production correspond to very weak basic sites. In addition, the presence of a certain amount of acidic sites was found positive for improving the acrolein yield. However, the catalyst activity decreased when the basic properties were strongly diminished by the incorporation of an acidic oxide. [1,2,6]

Ai also investigated acrolein formation by reaction of formaldehyde with ethanol [11], using the same catalysts as for the aldol condensation of acetaldehyde and formaldehyde.[2,6] The catalytic performances were compared at 280 °C and, once again, the main products detected were acrolein, acetaldehyde, methanol and carbon dioxide. All the catalysts were less active in this reaction than when acetaldehyde and formalin (aq. solution of formaldehyde stabilized with methanol) constitute the feed. The yield of acrolein and of by-products increased with the electronegativity of the metal ions, for a series of silica supported catalysts: Mg>Ca>Li>K. [11] Although V-P and V-Ti-P catalysts were very active in ethanol conversion, low acrolein yields were obtained, and ethane was observed as by-product. The highest yield of acrolein was obtained with Ni-P catalyst with a Ni:P atomic ratio of 3:2. The maximum yield of acrolein increased with an increase in the HCHO:EtOH ratio. The yield of acrolein reached 65 mol% for the best catalyst, when the HCHO:EtOH molar ratio was 3. Additionally,

ethanol and water mixture were fed on the best performing catalyst at the optimal conditions and it was experimentally verified that ethanol, in the absence of formaldehyde, does not dehydrate to acetaldehyde. Therefore author proposed that acetaldehyde and methanol are formed by a hydrogen transfer reaction from ethanol to HCHO. This is the first step of the process where acetaldehyde represents an intermediate compound (Equation 3.5.). Then in the second step acrolein is formed by the aldol condensation of the unreacted HCHO and the produced acetaldehyde (Equation 3.6.). [11]

$$CH_3CH_2OH + HCHO \rightarrow CH_3\text{-}CHO + CH_3OH \quad (3.5.)$$

$$CH_3CHO + HCHO \rightarrow CH_2{=}CH\text{-}CHO + H_2O \quad (3.6.)$$

The overall reaction is then defined in Equation 3.7.

$$CH_3\text{-}CH_2\text{-}OH + 2HCHO \rightarrow CH_2{=}CH\text{-}CHO + CH_3\text{-}OH + H_2O \quad (3.7.)$$

It was pointed out that over nickel phosphate (Ni-P) catalyst, the hydrogen transfer reaction (Equation 3.5.) is much more rapid than aldol condensation (Equation 3.6.). Both reactions, hydrogen transfer and aldol condensation, are generally promoted by a co-operative action of acidic and basic sites. However, the acid/base properties (required for the hydrogen transfer reaction) are not exactly the same as those required for aldol condensation. For example, silica-supported alkali metal and calcium oxides have shown to be active for aldol condensation (Eq. 3.6.), but they were inactive for the reaction of formaldehyde with ethanol (Eq. 3.5.). Probably, these catalysts are not enough acidic for promoting hydrogen transfer reactions. The silica-supported magnesium oxide showed a relatively good performance in both aldol condensation and reaction of HCHO with ethanol. On the other hand, the V-P and V-Ti-P catalysts were active for aldol condensation, but they were not working in the reaction of HCHO with ethanol. The reason is probably that the acidic properties of these catalysts are so strong that they promote the dehydration of ethanol to ethene rather than the hydrogen transfer reaction. [11]

In this latter synthesis method [11] (acrolein production from HCHO and ethanol- described by Equations 3.5.-3.7.), the amount of methanol produced was two times higher than that of the ethanol consumed. It was described that two main side reactions occur in this process. The first is the simultaneous transformation of part of the produced acetaldehyde to methanol and carbon dioxide. The second is the conversion of formaldehyde to methanol and CO_2 through a mechanism already described in the “conventional” acrolein synthesis by aldol condensation of acetaldehyde and formaldehyde [2,6], and presented in Equation 3.2.

Hydrotalcite-derived mixed oxides

Since studies of gas-phase aldol condensation of acetaldehyde and formaldehyde (using different mixed and supported oxides) showed that acrolein production is actually favored by the cooperation of acid-base sites, it is interesting to verify if Mg-Al based mixed oxide catalysts, derived

from hydrotalcite structures, could be efficient in this reaction. Their acidity and basicity can be easily tuned by varying the composition and the M^{2+}/M^{3+} ratio or the calcination temperature. [1,8,19,20]

Vapor-phase aldol condensation of formaldehyde and acetaldehyde was performed by Dumitriu and co-workers [1,8] in a pulse type microreactor at temperatures between 200°-400°C, using various oxide mixtures, obtained from hydrotalcite-like materials. These researchers also reported on the results obtained on MgO, Al_2O_3 and MgO-Al_2O_3 (prepared by mechanical mixing of MgO and Al_2O_3, Mg:Al ratio=3) catalysts.

Concerning acidity, $MgAl_3Cl$ displayed the highest number of acid sites with very high acid strength due to the presence of Cl^- anions. Similar acidities were found when CO_3^{2-} or SO_4^{2-}/CO_3^{2-} were the compensating anions for $MgAl_3$ and $MgAl_3S$, respectively, while $MgAl_2$ showed only few acidic sites when Mg/Al=2. High basic strength was evidenced for $CoAl_3$ and $NiAl_3$ catalysts. It was underlined that, due to the high specific areas, the surface density of the sites was always one order of magnitude lower than that of Mg/Al catalysts. The basicity of these samples was tentatively classified as: $MgAl_3 \cong CoAl_3 > MgAl_3S > NiAl_3 > MgAl_2 \cong MgAl_3C$. [1]

Considering MgO, Al_2O_3, and mixed MgAl and hydrotalcite derived catalysts, the typical large product distribution is shown in Figure 3.1. The main products derived from cross- and self-aldolization (acrolein and crotonaldhyde). Direct products were also methyl formate and ethyl acetate (obtained by self-dimerization of aldehydes, Tischenko reaction), and methyl acetate (obtained by cross-dimerization). Some amount of ethanol (product of the consecutive reaction) was obtained by hydrogenation of acetaldehyde (the hydrogen resulting from the decomposition of the reagents (*e.g.* HCHO->CO+H_2) and products). Methanol was already present in formaldehyde. The reaction temperature influenced the products distribution (see Figure 3.1.). [1]

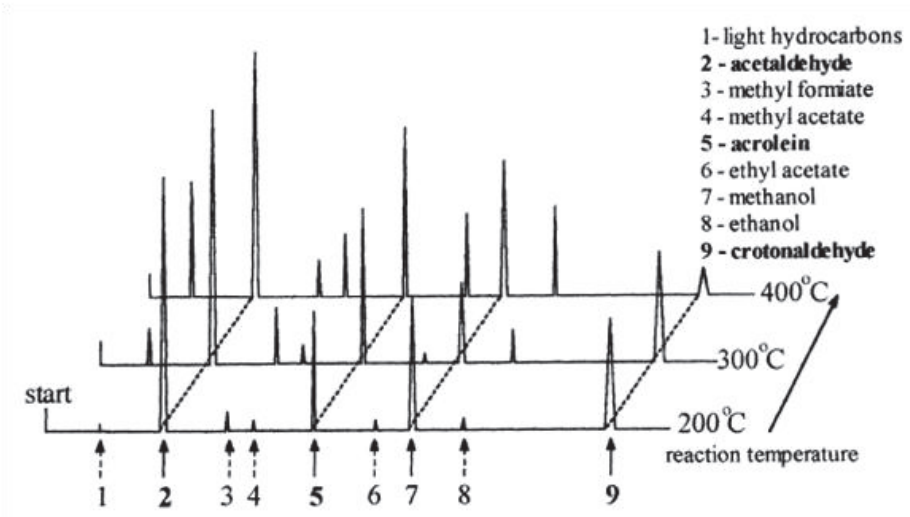

Figure 3.1. Some typical chromatograms of the organic phase for the aldol condensation of formaldehyde with acetaldehyde performed at three temperatures (200°, 300°, and 400 °C): catalyst $MgAl_3$; FA/AA=1/1.[1]

Conversion of acetaldehyde increased with the temperature, and conversions obtained over binary oxides were higher than those obtained on single oxides. Moreover, binary oxides obtained in situ, from calcinated hydrotalcite, showed almost the same activity as the physical mixture of alumina and magnesia. Alumina was more active than magnesia. These results are shown in Figure 3.1.1. Highest selectivity to aldol condensation was obtained for MgO and the lowest for Al_2O_3, due to the difference in their acid-base properties. Generally the selectivities to aldol condensation decreased as the temperature of reaction increased, for all catalysts. [1]

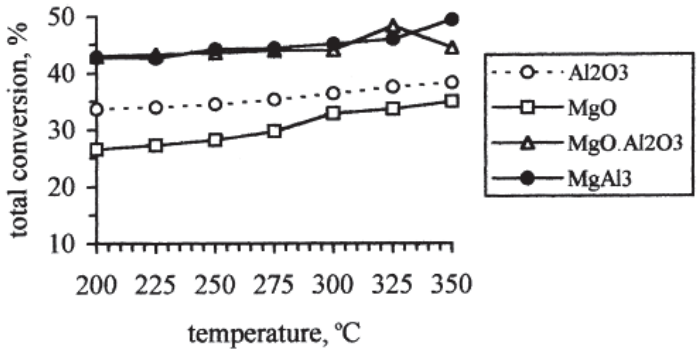

Figure 3.1.1. Effect of temperature on the total conversion of acetaldehyde: FA/AA=1/1; $T_{calination}$=450 °C. [1]

Competition between cross- and self-aldolization was influenced by the reaction temperature. Higher temperature favored acrolein production by cross-aldolization. The basicity of magnesium containing catalysts shifted the ratio between the two processes towards cross-aldolization while the acidity of alumina favored self-aldolization of acetaldehyde. The lowest selectivity to acrolein was found on alumina, while MgO and magnesium containing mixed oxides showed close selectivities to acrolein. [1]

Dimitriu et al. reported that basicity was a key factor to obtain high acrolein production. MgO and $MgAl_3$ exhibited higher selectivities to acrolein than Al_2O_3 or NiAl oxides, due to their different basicity. MgO could be considered as the most basic catalyst, with practically no acidity, while Al_2O_3 represented the most acid catalyst. The incorporation of aluminum in the brucite lattice led to a decrease of the basicity. However, $MgAl_3$ catalyst showed higher selectivities to acrolein than MgO. $MgAl_3$ presents both basic and acidic sites. Therefore Dumitriu et al proposed that aldol condensation to acrolein is strongly promoted by an acid-base sites co-operation. [1]

The basic sites of a defined strength activate acetaldehyde, by abstraction of a H-atom in α-position (Scheme 3.1.7.), while acidic sites of weak strength activate formaldehyde by an increase in the electrophilicity of the carbon atom. It is necessary that the acidic sites display a given strength to avoid the activation of the acid mechanism of aldol condensation (leading to the self-aldolization of acetaldehyde). [1]

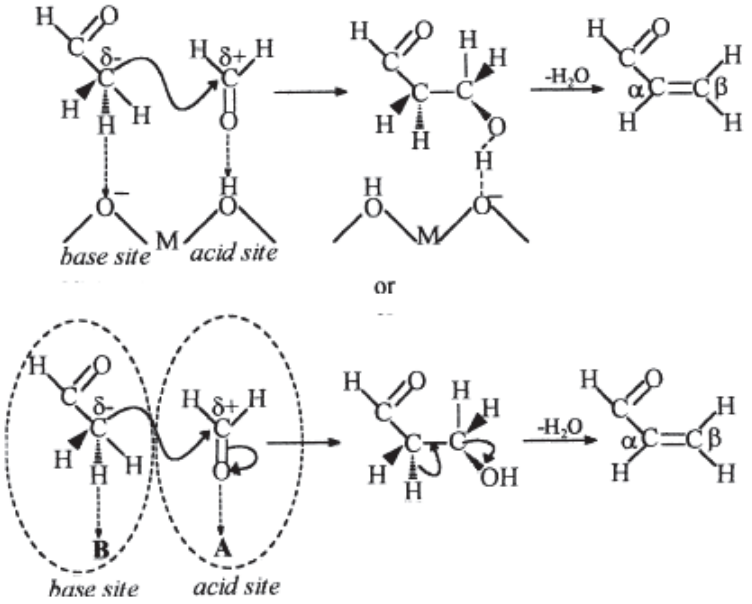

Scheme 3.1.7. The acid-base mechanism proposed by Dumitriu et al. [1]

The ratio between basic and acidic sites must have an optimum value, as well as the strength of the active sites. Incorporation of aluminum (*e.g.* $MgAl_2$), or other elements (sample CoAl or NiAl) changed the balance and thus the selectivity to acrolein strongly decreased (when acidity increased). Moreover, the nature of the compensating anions (residual Cl^- and SO_4^{2-}) increased the acidity thus resulting in a decreasing of the selectivity to acrolein. [1]

Some other factors also affect the acid/base properties of hydrotalcite-like materials and bring to different catalytic properties: different thermal treatments, Me^{2+}/Al^{3+}surface ratio, specific surface areas, etc. [1] On Mg-based catalysts it was observed that when the added metal ion presents a radius larger than that of Mg^{2+}, a distortion takes place in the lattice around the added metal ion, leading to changes in the basic properties. The addition of a metal ion with an ionic radius smaller than that of Mg^{2+} creates surface acidic sites, without any appreciable change in the amount of surface basic sites. [1,8]

Clays and Zeolites

The results obtained on clays and zeolites will not be discussed in depth since they were not used in this PhD thesis. Generally lower acrolein selectivities were obtained, especially on clays. Moreover, the preparation methods used to obtain some of the modified zeolitic materials with higher activity towards acrolein, were time demanding and therefore not interesting for industrial applications. The studies performed on these catalysts were carried out in a pulse type reactor at 2.5 bar in the 200°-400°C temperature range. [7,9,10,14-17]

As general observation, the same product distribution was reported when different types of clays and zeolites were tested as aldolization catalysts (like already reported- see Figure 3.1.). The

acrolein production took place on both type of sites, acidic and basic. Higher temperatures favored cross-aldolization reaction towards acrolein, and the ratio of acid/base sites importantly impacted the competition between cross- and self-aldolization. [7,9,10,14-17]

Azzouz et al [9] investigated the acrolein formation over montmorillonite-rich (Mt-rich) materials exchanged with Na^{+}, Cs^{+}, Mg^{2+}, Ni^{2+}, La^{3+} or UO_2^{2+} cations. The main products were acrolein and crotonaldehyde, indicating that such catalysts were active in aldol condensation. Ion-exchange modulates the catalytic activities, depending on the nature of the cation introduced, and the reaction temperature. Both the acid and base properties showed strong effects on the total conversion of acetaldehyde and on the acrolein/crotonaldehyde ratio. It was also found that cross-condensation took place exclusively over weak acidic sites. The highest cross-selectivities were obtained over Na, Cs and Mg-containing catalysts.

Dumitriu et al reported on results obtained by gas-phase aldol condensation of acetaldehyde and formaldehyde over zeolite catalysts, such as Y-faujasute, mordenite, ZSM-5 and volcanic tuff [14], and different oxides (ZnO, MgO, MoO_3, B_2O_3 and P_2O_5) deposited over ZSM-5 and Y-faujasite [7]. Oxides deposition over HZSM-5 support improved the catalytic activity, and the highest performances were obtained using a 4 wt% MgO/ZSM-5 catalyst. An excess of magnesia could hinder the pore accessibility to the reagents. The activity of such a catalyst was explained by possible cooperation between the basic MgO centers and the zeolite acidic sites. It was also observed that aldol condensation mainly occurs on medium strength sites, the strong acidic centers being mainly involved in the coking process. Unugreanu and co-authors [17] studied the acid properties of UL-ZSM-5 materials and found that acidity was improved by treatment in aqueous ammonia solutions. Catalytic properties in aldol condensation of acetaldehyde with formaldehyde were examined after this treatment. The UL-ZSM-5 were found to be less sensitive to coke deactivation than ZSM-5 of comparable Si/Al ratio, and more active than the mesostructured precursor. Various MFI type zeolites were also studied for this reaction by Dumitiru et al. [15] The samples were synthesized taking into account two factors affecting the zeolitic acidity “by synthesis”, namely the nature of the substituted heteroelement (Al, Ga, Fe, or B) and the Si/Me^{3+} ratio. It was reported that the true substitution depends on the ability of the heteroelement to be incorporated into the zeolite framework, and decreases from aluminum to boron. Generally, the acidity of the isomorphously substituted MFI catalysts was strongly influenced by the Si/Me^{3+} ratio and the structure of Me^{3+}. Both types of acidic sites, Brønsted and Lewis, were present on the surface of these catalysts. Conversions and product selectivities were influenced by the Si/Me^{3+} ratio. In aldol condensation of acetaldehyde and formaldehyde the activity of metallosilicates followed the B->Fe->Ga->Al-ZSM-5 trend. However, the selectivity for cross-aldol condensation followed the order Al->Fe->Ga->B-ZSM-5. The activity of zeolites was generally higher when strong acidic sites were present, and the selectivity towards acrolein was influenced by Lewis acid sites. [17] Cobzaru et al [16] reported results on clinoptilolite rich natural zeolites. The highest stability, activity and selectivity to acrolein have been proved on the catalysts having high number and strength of basic sites. [16] Studies performed on volcanic tuff dealuminated by acidic treatment confirmed that these types of zeolites were active as catalysts for

the aldol condensation reactions of acetaldehyde and formaldehyde, with the formation of acrolein at low temperatures (250 °C). At high temperature (over 350°C) a significant decrease of the yield of the condensation products of aldehydes was observed due to the intensification of secondary reactions with hydrocarbons formation.[10]

In conclusion for the investigation of the impact of the acid-base properties (in oxidizing conditions) we chose to test at first the group of silica-supported basic oxides (alkaline and earth alkaline metals). Thanks to the initial results, obtained on these first series of catalysts, and accordingly to the results in the literature on gas-phase aldol condensation of acetaldehyde and formaldehyde in absence of oxygen, other samples worth of interest were identified (magnesium and aluminum containing catalysts). The reaction was then performed at atmospheric pressure in a continuous flow fixed bed reactor at different temperatures and GHSVs (described in the Chapter 4: Experimental part).

Summary of the acid-base mechanism generally proposed by all researchers is given in Scheme 3.1.8. [9]

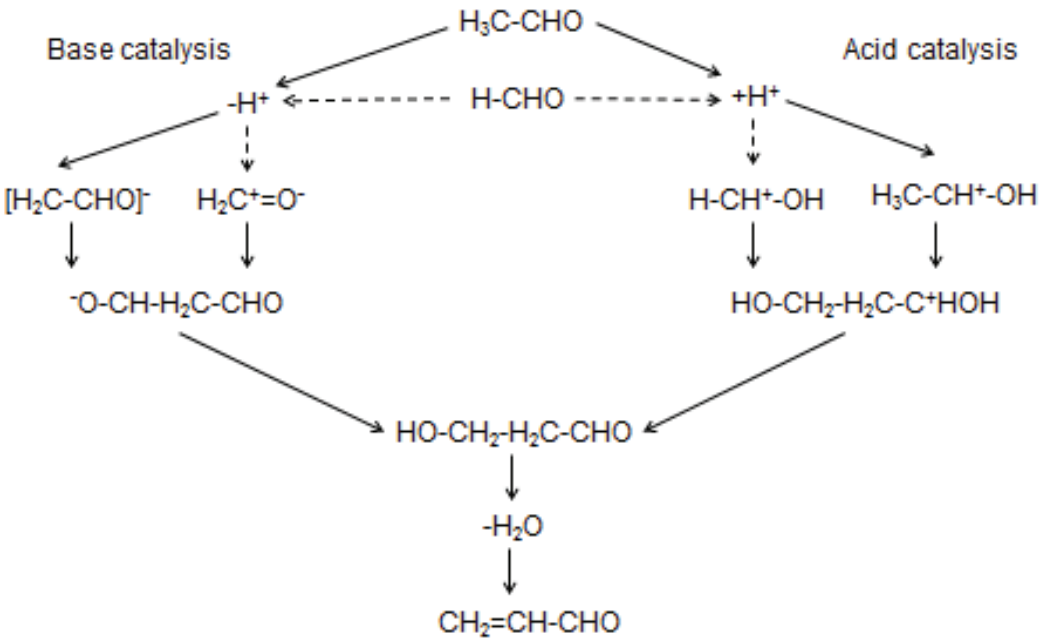

Scheme 3.1.8. Summary of the acid and base catalysis routes for acrolein production in gas-phase aldol condensation of acetaldehyde and formaldehyde. Adapted from reference 9.

As seen from the literature presented in this section, to obtain the best acrolein yield and to minimize the by-products (mostly carbon oxides, crotonaldehyde, methanol) production, it is necessary that acidity is not too strong to suppress the basic properties of the catalyst. High acrolein yield was reported when strong basic sites were present, but higher productions of CO_x and methanol were detected. If acidity was too strong, reactions of acrolein polymerization could take place. Generally acidic catalyst are active in acrolein production but always presented lower acrolein yields due to polymerization reaction or higher production of crotonaldehyde, through a process of self-aldolization

of acetaldehyde. Crotonaldehyde production was generally governed by acid/base ratio, and the strength of both sites was important. In particular, at temperatures higher than 300 °C crotonaldehyde production was not favored, while acrolein formation through cross-aldolization mechanism of acetaldehyde and formaldehyde was improved.

3.2. Acid/base properties of the catalysts investigated by gas-solid adsorption microcalorimetry coupled with volumetric line

In heterogeneous catalysis field various thermal, spectroscopic and computational methods are applied in studying the gas-solid adsorption processes mainly to determine acidic and basic properties of the catalysts. Adsorption microcalorimetry is one among the few techniques able to determine the strength of chemisorptions. Gas-solid adsorption microcalorimetry coupled with volumetric line represents the most suitable tool to determine the strength, strength distribution, and the amount of surface acid/base sites. [21] Constant effort of the researchers which are performing adsorption microcalorimetry experiments is undertaken to create unique acidity and basicity scales of the solid catalytic materials in order to facilitate distinction of solid acids and bases inspired by the pH-scales for liquid acids and bases. [22,23] However, results obtained by this technique are not enough to determine the nature of active surface acid/base sites; therefore complementary information from various spectroscopic and ab initio quantum chemistry methods are necessary. [21] Detailed explanation of this technique is given in the experimental part of this manuscript (Chapter 4, Section 4.2.7.).

Appropriate probe molecules to be used for adsorption microcalorimetry should be stable with time and with temperature. Furthermore, in the case of microporous materials, they should be small enough to readily penetrate into the intracrystalline space. The adsorbed probe at a given temperature should also have sufficient mobility to equilibrate with active sites. As calorimetry gives the total number of adsorption sites and differential heats of adsorption the values obtained depend on the nature and size of the probe molecule. [24] Besides the probe molecule, other parameters influence the results: the temperature of the sample pretreatment, the temperature of the adsorption, the specific surface area of the sample, and preparation method of the sample. [21,24,25]

Considering probing of surface basicity, the number of acidic probes able to cover a wide range of strength is rather small. The ideal probe molecule should be specific to basic sites and should not be amphoteric. For example CO_2 (pKa=6.37) is commonly chosen to characterize the basicity of solids, but it may be either adsorbed on cations or physisorbed, or may react with hydroxyls and oxide ions to form carbonate species. CO_2 is a poor donor but a good electron acceptor. Due to its acidic character, it is also frequently used to probe the basic properties of solid surfaces. The possibility that CO_2 could behave as a base and interact with Lewis acid sites should also be considered. However these sites would have to be very strong Lewis acid sites, and this particular adsorption mode of the

CO_2 molecule should be very weak and can usually be neglected. The same problems may arise when using SO_2 as an acidic probe, despite the fact that SO_2 (pKa=1.89) is more acidic than CO_2 and, thus, more likely to probe the total basicity of the surface. [24]

Usually, ammonia (pKa=9.24, proton affinity in gas phase = 857.7 kJ mol^{-1}) and pyridine (pKa=5.19, proton affinity in gas phase = 922.2 kJ mol^{-1}) are the chosen molecules to probe the overall solid acidity, since both Lewis and Brønsted acid sites retain these molecules. Trimethylamine (TMA) and triethylamine (TEA) have also been used to probe the acidity of supported oxides. However, these two molecules might not be able to equilibrate completely with the surface under typical experimental conditions. The use of substituted pyridines (2,6-dimethylpyridine) has also been considered in order to probe specifically the Brønsted sites. Ammonia is among the smallest strongly basic molecules, and its diffusion is hardly affected by a porous structure. In the light of the different possible modes of interaction of this molecule with the oxide surface, it has been found that NH_3 mostly co-ordinates to Lewis sites, but in a few cases the results were interpreted by considering the simultaneous occurrence (to a low extent) of dissociative adsorption leading to NH_2^- and OH^- surface species. Dissociative adsorption of ammonia is related to the presence of very strong acid sites of Lewis type. Some authors reported the use of strong bases as probe molecules including alkylamines, pyridines and imines. Concerning weak bases, studies of the adsorption properties of water, alcohols, thiols, olefins, aldehydes, ketones, and nitriles were performed. Acetonitrile was also reported as an interesting molecule for probing acid sites in catalysts. It is a weak base, so no protons are abstracted and actual hydroxyl groups can be observed. It also allows the investigation of both Lewis and Brønsted acidities. NO and CO were also employed as probes to identify Lewis acid sites and characterize their density and strength. [24]

The case of the simplest alcohol methanol (pKa=15) is interesting. This probe molecule is generally considered as a Brønsted acid which is able to release a H-atom and dose Brønsted basic sites. [26] But, it can as well release electron pair from oxygen and in that case behave as a Lewis base dosing Lewis acid sites. [27]

In this thesis SO_2, CO_2 ,NH_3, and methanol were employed as probe molecules to determine acidity/basicity of the catalysts and the following bibliographical research is mainly concentrated on the solids used in the present research.

3.2.1. Bulk, mixed and supported oxides

Nickel oxide (NiO) and supported nickel catalysts

Tu et al. [28] reported NH_3 and CO_2 adsorption over bulk NiO (S_{BET}=50 m^2 g^{-1}). Adsorption took place at 150 °C and samples were previously oxidized for 2h at 400 °C followed by outgassing. NiO displayed a very high initial heat of NH_3 adsorption (≈250 kJ mol^{-1}). This may be due to the coordination reaction between NH_3 and nickel cations instead of simple chemisorption of NH_3 on the

surface. The differential heats of NH_3 adsorption decreased rapidly with coverage (saturation coverage less than 1 μmol m^{-2}). It was found that NiO displayed strong basicity with an initial CO_2 adsorption heat of 145 kJ mol^{-1} and a saturation coverage of 1.5 μmol m^{-2}. [28]

Chen et al. [29] investigated the acid-base properties of reduced nickel catalysts supported on different supports (MgO, SiO_2, Al_2O_3, MgAlO and SiAlO) by NH_3 and CO_2 adsorption microcalorimetry. Before adsorption of the probe molecules, samples were outgassed for 1h at 400 °C and adsorption took place at 150 °C. The initial heat of NH_3 adsorption on Ni/MgO (S_{BET}=86 m^2 g^{-1}) was 129 kJ mol^{-1}, but rapidly decreased below 40 kJ mol^{-1} when NH_3 coverage reached 50 μmol g^{-1}. The high initial heat might be due to the adsorption of NH_3 on metallic nickel surface since MgO is a basic support. Although SiO_2 was neutral, the reduced Ni/SiO_2 (S_{BET}=373 m^2 g^{-1}) exhibited strong surface acidity with the initial heat of ammonia adsorption of around 165 kJ mol^{-1} and NH_3 coverage of about 1000 μmol g^{-1}, probably due to the formation of nickel silicate. The Ni/Al_2O_3 (S_{BET}=375 m^2 g^{-1}) displayed stronger surface acidity with an initial heat of about 175 kJ mol^{-1}. This might be due to the fact that Al_2O_3 is an acidic support and nickel aluminate was also formed in the catalyst. Ni/SiAlO (S_{BET}=351 m^2 g^{-1}) showed the strongest acidity with initial heat of about 183 kJ mol^{-1} and coverage of about 950 μmol g^{-1}. The surface acidity of Ni/MgAlO (S_{BET}=233 m^2 g^{-1}) was stronger than that of Ni/MgO, but weaker than that of Ni/Al_2O_3 according to the initial heat and coverage for the adsorption of ammonia. Actually, these catalysts can be classified into three groups in terms of their surface acidities: Ni/MgO exhibited weak surface acidity (group 1), Ni/MgAlO possessed surface acidity with intermediate strengths (group 2), and the remaining catalyst exhibited strong acidity (group 3). The initial heat and coverage were measured to be about 135 kJ mol^{-1} and 300 μmol g^{-1}, respectively, for the adsorption of CO_2 on Ni/MgO, indicating the strong basicity of this catalyst. Addition of 5% Al_2O_3 into Ni/MgO decreased the initial heat for CO_2 adsorption on Ni/MgAlO (113 kJ mol^{-1}), but increased remarkably the coverage of CO_2 from 270 to 600 μmol g^{-1} due to the increased surface area of Ni/MgAlO. Thus, the Ni/MgAlO possessed substantial amount of surface basic sites with intermediate strengths. The surface basicity of Ni/Al_2O_3 was obviously weaker than that of Ni/MgAlO since the coverage of CO_2 significantly decreased. Both Ni/SiO_2 and Ni/SiAlO possessed very weak surface basicity according to the microcalorimetric adsorption of CO_2. [29]

Ni/Al_2O_3, Ni/MgAlO and Ni/MgO catalysts (specific surface areas were 341, 244 and 86 m^2 g^{-1}, respectively) containing about 60 wt% of nickel were prepared by Hu et al, [30] and the acid-base properties of the reduced catalysts were investigated by NH_3 and CO_2 adsorption microcalorimetry ($T_{adsorption}$=150 °C). Samples were reduced 2h in H_2 at 400 °C and outgassed for 1h. The initial heat and saturation coverage for the adsorption of ammonia were measured to be 169 kJ mol^{-1} and 870 μmol g^{-1}, respectively, for Ni/Al_2O_3, significantly higher than the corresponding values (129 kJ mol^{-1} and 530 μmol g^{-1}) for Ni/MgO, indicating the stronger surface acidity of Ni/Al_2O_3 compared to Ni/MgO. The Ni/MgAlO exhibited an initial heat of 150 kJmol^{-1} and saturation coverage of 640 μmol g^{-1} for the adsorption of ammonia. Thus, the surface acidity on Ni/MgAlO was weaker than on Ni/Al_2O_3, but stronger than on Ni/MgO. The heat of NH_3 adsorption was 129 kJ mol^{-1} for the Ni/MgO catalyst, but it decreased rapidly with the increase of NH_3 coverage. The initial heat might be attributed to the

adsorption of NH_3 on the metallic nickel surfaces, since MgO is a basic support. The addition of 10% Al_2O_3 into Ni/MgO significantly increased the surface acidity in Ni/MgAlO. The initial heats for CO_2 adsorption on Ni/Al_2O_3, Ni/MgAlO and Ni/MgO were 94, 112 and 134 kJ mol^{-1}, respectively. Both the initial heat and uptake for CO_2 adsorption were significantly higher on Ni/MgO than on Ni/Al_2O_3 although the surface area of Ni/MgO was much lower than that of Ni/Al_2O_3, indicating the significantly stronger surface basicity on Ni/MgO than on Ni/Al_2O_3. The addition of about 10% Al_2O_3 into Ni/MgO decreased the initial heat for CO_2 adsorption on Ni/MgAlO, but increased remarkably the uptake of CO_2 (from 270 to 560 µmol g^{-1}). Thus, the Ni/MgAlO possessed substantial amount of surface basic sites with intermediate strengths. [30]

60%Ni/Al_2O_3-B (S_{BET}=301 m^2 g^{-1}) and 60%Ni/MgO-B (S_{BET}=152 m^2 g^{-1}) were prepared by a coprecipitation method with a n-butanol drying process by Zhao et al. [31] A commercial catalyst Ni/Al_2O_3 (S_{BET}=191 m^2 g^{-1}) was studied as comparison and NH_3 and CO_2 adsorption microcalorimetry was performed at 150 °C on samples reduced in H_2 at 450 °C for 2 h followed by degassing at the same temperature for 1 h. Initial heats for the adsorption of NH_3 were measured to be about 178 and 106 kJ mol^{-1}, respectively, for Ni/Al_2O_3-B and Ni/Al_2O_3, although the saturation coverage of NH_3 was almost the same (800 µmol g^{-1}) for the two catalysts. Thus, the surface acidity of Ni/Al_2O_3-B was stronger than that of Ni/Al_2O_3. Although the initial heat of NH_3 on Ni/MgO-B was not low (120 kJ mol^{-1}), the differential heat was decreased abruptly with the increase of coverage of NH_3, indicating the weak surface acidity on Ni/MgO-B. On the other hand, the Ni/Al_2O_3-B and Ni/Al_2O_3 possessed quite weak surface basicity, with initial heat of about 76 kJ mol^{-1}, while Ni/MgO-B presented a strong surface basicity, with initial heat of about 118 kJ mol^{-1}, and coverage of about 322 µmol g^{-1}, for the adsorption of CO_2. [31]

Bulk and supported molybdenum oxides (MoO_3)

Auroux and Gervasini [32,33] investigated the acid-base properties of a MoO_3 sample (S_{BET}=33.5 m^2 g^{-1}) by NH_3 and CO_2 adsorption calorimetry. NH_3 adsorption was performed at 150 °C. Initial heat of ammonia adsorption was around 30 kJ mol^{-1}. Curve Q_{diff} *vs.* NH_3 coverage was characteristic for heterogeneous distribution of acid sites. Surface NH_3 coverage reached 7 µmol m^{-2}. This sample did not adsorb CO_2 at room temperature indicating the absence of basicity.

Six different molybdenum oxide catalysts supported on niobium oxide (MoO_3/Nb_2O_5) were prepared by Jin et al [34] using incipient wetness impregnation method. The chemical composition of the catalysts was: 0, 3, 5 and 8 wt% of MoO_3. NH_3 adsortpion was performed at 100 °C on the samples previously outgassed at 400 °C. The initial heat at low coverage was rather high (120-140 kJ mol^{-1}), which corresponds to strong acidity. The amount of strong sites was rather low and corresponded to about 0.1 µmol g^{-1} or 3.10 $^{-3}$ µmol m^{-2}. Pure Nb_2O_5 support exhibited very low acidity with a maximum adsorption heat around 80 kJ mol^{-1}. The number of strong acid sites increased with the Mo content.

Bulk and supported iron (III) oxides (Fe_2O_3)

Fe_2O_3 sample with S_{BET}= 46 m^2 g^{-1} was pretreated in oxygen flow for 2h at 400 °C, outgassed for 2h, and then NH_3 and CO_2 adsorption calorimetry at 150 °C was performed. Considering CO_2 adsorption Fe_2O_3 exhibited initial heat of about 120 kJ mol^{-1} and a saturation coverage of 1.2 µmol m^{-2}. The initial heat and coverage for the adsorption of NH_3 were 110 kJ mol^{-1} and 3.5 µmol m^{-2}, respectively. [28]

Cardona-Martinez and Dumesic [35] performed the adsorption and desorption of pyridine at 200 °C by microcalorimetry to obtain the number and strength of Lewis acid sites on Fe_2O_3/SiO_2 and FeO/SiO_2 catalysts (0.52 wt% of Fe in both samples, S_{BET}≈400 m^2 g^{-1}). Before analysis the samples were reduced in hydrogen flow for 4h at 400 °C, then degassed and finally oxidized in oxygen flow at 200 °C for 4h. The initial differential heats of pyridine adsorption calculated from the initial slopes of the integral heat plots, were 210 and 180 kJ mol^{-1}, respectively, for Fe^{3+}/SiO_2 and Fe^{2+}/SiO_2 (Figure 3.2.1.). The reduced form of iron oxide presented considerably fewer and weaker acid sites than the oxidized form. Both the integral and differential heat curves for Fe^{2+}/SiO_2 remained below those of Fe^{3+}/SiO_2, in the studied range of coverage. The curves (Q_{diff} *vs.* coverage) continuously decreased for both samples, indicating the presence of a heterogeneous acid strength distribution. The acid strength distribution curve for divalent iron shows a high concentration of sites at 135 kJ mol^{-1} and no sites with energy higher than 181 kJ mol^{-1}. Trivalent iron showed a large concentration of sites (about 208 kJ mol^{-1}) and a low concentration of sites with intermediate strength. [35]

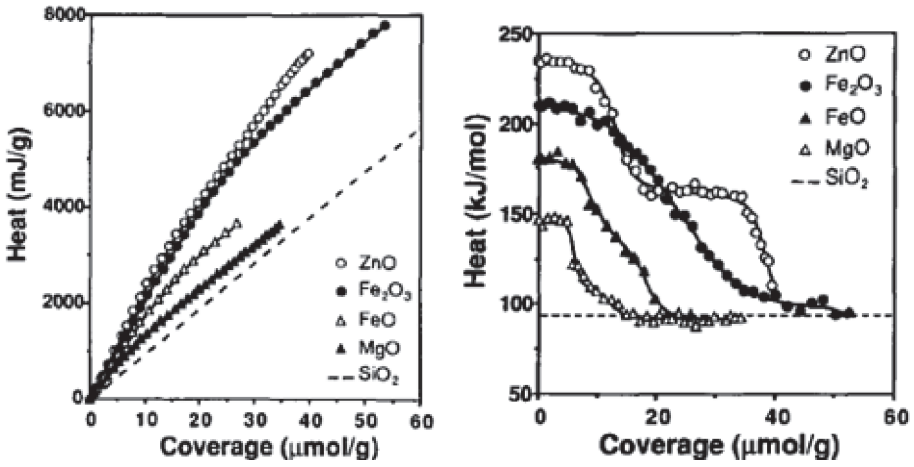

Figure 3.2.1. Integral heats of pyridine adsorption (left) and differential heats of adsorption (right) for silica-supported oxides that showed only Lewis acidity. [35]

Rossi et al. [36,37] reported results of water, n-butylamine (BA) and hexafluoroisopropanol (HFIP) adsorption microcalorimetry at room temperature, for α-Fe_2O_3 samples (S_{BET} of samples around 14 m^2 g^{-1}) prepared by decomposition of α-FeOOH at different temperatures (400 °, 700 °, and 1100 °C). They concluded that the nature of the active surface sites on the haematite samples is not modified by thermal treatment. In all cases, acidic sites strongly interacted with the basic probe BA, and basic sites of medium strength, as revealed by the interaction with HFIP, were present. The

adsorption of water was also similar for the three samples. The nature of the adsorption sites for water and BA was also unchanged by heat treatment at 1100°C, while the nature of the adsorption sites for HFIP was modified. However, the number of available sites was reported to increase significantly in the order 400 °C < 700 °C < 1100°C. Results are shown in the Figure 3.2.2. [36,37]

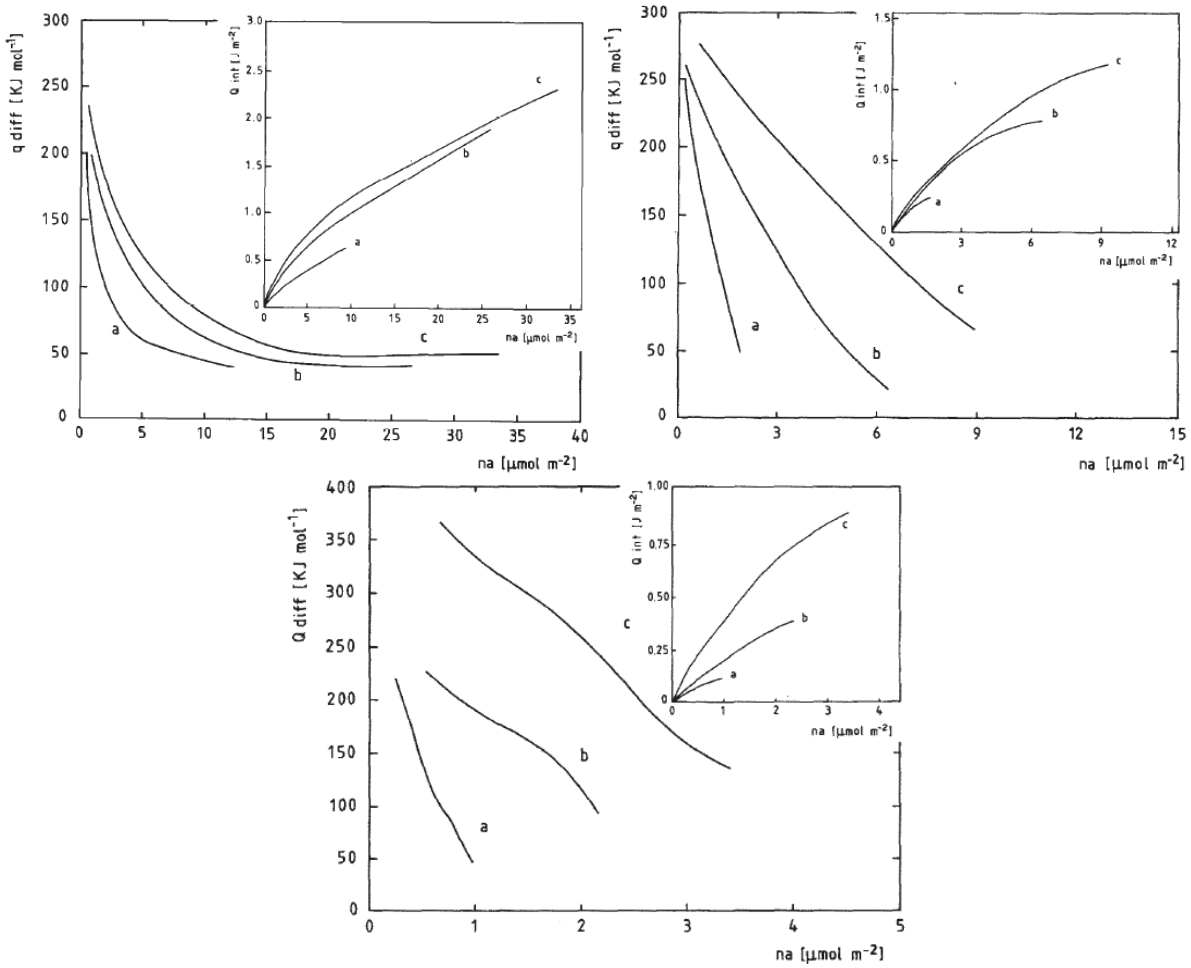

Figure 3.2.2. Plots of the differential (q_{diff}) and integral (Q_{int}; in the inset) adsorption heats against amount of water (top-left), n-butylamine (top-right), and hexafluoroisopropanol (down) adsorbed on α-Fe_2O_3 samples prepared by decomposition of α-FeOOH at 400°C (a), 700°C (b) and 1100°C (c). [36]

Bulk and supported vanadium oxides (V_2O_5 and V_2O_4)

Generally acid/base properties of bulk and supported vanadium oxides were widely characterized by adsorption microcalorimetry. Bulk V_2O_5 is reported as acidic oxide, however the tuning of the acidity and basicity is governed by the preparation method, [38] and by the choice of the support [32,39-45]

Acid-base properties of V_2O_5 samples prepared by two different methods were investigated by Xue et al. [38] V_2O_5 (S_{BET}= 7 m^2 g^{-1}) was prepared by calcination of NH_4VO_3, while mesoporous VO_x-673 (S_{BET}= 182 m^2 g^{-1}) was prepared by dissolution of V_2O_5 in aqueous solution of H_2O_2, followed by the evaporation and drying. Both samples were outgassed at 400 °C during 1h before NH_3 and CO_2 adsorption microcalorimetry (at 150 °C). V_2O_5 exhibited surface acidic sites with initial heat of about 95

kJ mol^{-1} and coverage of about 115 µmol g^{-1}, while VO_x-673 displayed initial heat of 135 kJ mol^{-1} and coverage of 650 µmol g^{-1}, for ammonia adsorption. VO_x-673 exhibited much stronger surface acidity than the conventional V_2O_5. V_2O_5 did not adsorb any CO_2, while VO_x-673 adsorbed 22 µmol g^{-1} CO_2, with initial heat of 64 kJ mol^{-1}. The weak surface basicity of VO_x-673 might be due to the reduced surface, containing mainly V^{4+} and V^{3+}. Results are shown in Figure 3.2.3. [38]

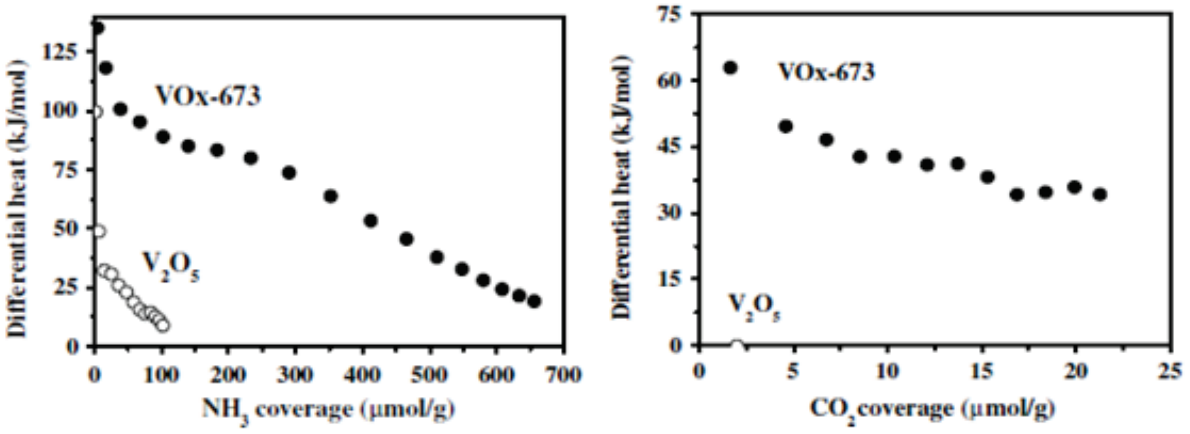

Figure 3.2.3. Differential heats *vs.* coverage for NH_3 (left) and CO_2 (right) adsorption at 150°C on V_2O_5 and VO_x-673. [38]

Le Bars et al. [39,40] studied acidic features of V_2O_5/SiO_2 catalysts by ammonia and pyridine adsorption microcalorimetry. Different samples were prepared using various synthesis methods and having V_2O_5 loadings from 1-20 wt%. As standard activation, the catalysts were heated overnight under oxygen at 400 °C, and then evacuated at the same temperature for 2 h. Adsorption was performed at 80 °C. Ammonia uptakes and enthalpies of adsorption revealed that both number and strength of the acid sites increased with vanadium content. Bulk oxide presented a much lower specific surface area (13 m^2 g^{-1}) than the V_2O_5/SiO_2 catalysts (173 to 300 m^2 g^{-1}). Initial enthalpy of ammonia adsorption of 67 kJ mol^{-1} on bulk vanadium pentoxide was reported. Higher values of initial enthalpy of ammonia adsorption have been measured for the V_2O_5/SiO_2 catalysts (78 to 124 kJ mol^{-1}), except for the 0.7 and 1.1 wt% V_2O_5/SiO_2 samples, which showed weak acidity. Ammonia adsorption on pure silica is characterized by a plateau at 35 kJ mol^{-1}. New surface sites are formed by deposition of vanadium on silica, with the presence of higher acid strength than pure silica and bulk vanadium pentoxide. [39,40]

Due to its lower basicity (pKa= 5.5), pyridine is a more selective probe molecule than ammonia (pKa= 9.25) and can therefore be applied to more finely describe the acidic features of a catalytic surface. In the domain of high acidic strength, two V_2O_5/SiO_2 catalysts (10 and 19.1 wt% V_2O_5) have been studied by pyridine adsorption. Three acid site strength groups were identified: one with adsorption enthalpies above 125 kJ mol^{-1}, a second with sites of strength between 125 and 100 kJ mol^{-1}, and a third of weak sites in the 100-70 kJ mol^{-1} range. These groups respectively represent 10, 25 and 65% of the overall pyridine uptake. [40]

Same authors [44] then investigated NH_3, pyridine and SO_2 adsorption on V_2O_5/Al_2O_3 catalysts (V_2O_5 loadings from 1 to 20 wt%) using microcalorimetry, and diffuse reflectance IR spectroscopy

(DRIFT). For V_2O_5 content below 10 wt%, the vanadium cations were well dispersed over alumina as vanadate compounds. Such vanadate species developed Brønsted and Lewis-type acidity, as shown by a DRIFT spectroscopy study of pyridine adsorption, but did not exhibit a basic character. Sulphur dioxide adsorption allowed to differentiate the vanadate layer from free alumina. Ammonia and sulphur dioxide adsorptions showed that at low vanadium coverage, a large part of the vanadate layer was bound to acid-base pairs of alumina. Vanadium pentoxide crystallites were detected below monolayer coverage, but did not contribute to the development of the acidic surface character. At low vanadium coverage (< 3 wt% V_2O_5), the acidic character of the V_2O_5/γ-Al_2O_3 catalysts is ascribed to vanadium-free alumina. Initial heats of ammonia adsorption of around 200 kJ mol^{-1} or higher were measured for V_2O_5/γ-Al_2O_3, then the acidic sites diminished in amount and strength for vanadium oxide content below 2.9 wt%. For higher vanadium contents the acidic features increased in amount and strength, while new weak acid sites appeared for the 9.8 and 20.8 wt% V_2O_5/γ-Al_2O_3 catalysts. The increase of the acidic character that was observed for the 2.9-9.8 wt% V_2O_5/γ-Al_2O_3 catalysts can be attributed to the formation of a vanadate layer. This layer was not a vanadium pentoxide network because vanadium pentoxide is known to be much less acidic than bare alumina. Ammonia adsorption study showed that the overall acidic features of the V_2O_5/γ-Al_2O_3 catalysts were provided by the uncovered part of alumina, and by the growth of a layer of a vanadate compound over the support. Such a vanadate layer appears to exhibit stronger acidity than alumina, while vanadium pentoxide crystallites hardly exhibit acidic properties. The vanadate layer exhibits a strong Brønsted-type acidity for vanadium contents higher than 3 wt% V_2O_5, as revealed by pyridine adsorption followed by DRIFT spectroscopy. The basic features of the $V_2O_5/\ \gamma$-Al_2O_3 catalysts were studied by sulphur dioxide adsorption. Figure 3.2.4. shows the differential enthalpies for sulphur dioxide adsorption on V_2O_5/γ-Al_2O_3 catalysts and on pure y-alumina. The sulphur dioxide adsorption of the catalysts rapidly decreased with the vanadium content. Sulphur dioxide can chemisorb on basic oxygen anions O^{2-} and on basic hydroxyl groups. Such adsorption modes lead to the formation of sulphites and hydrogenosulphites, respectively. Sulphur dioxide was not chemisorbed on bulk vanadium pentoxide (neither on vanadate species), therefore this probe can be considered (on V_2O_5/γ-Al_2O_3 catalysts) as selective for the titration of basic sites of vanadium-free alumina. [44]

Auroux and Gervasini [32] reported results of NH_3 and CO_2 adsorption microcalorimetry on V_2O_5 supported on silica (S_{BET}=271 $m^2\ g^{-1}$). The sample did not adsorb CO_2 at room temperature. Adsorption of NH_3 was performed at 150 °C and initial differential heat around 30 kJ mol^{-1} was measured, while surface coverage reached around 2 µmol g^{-1}.

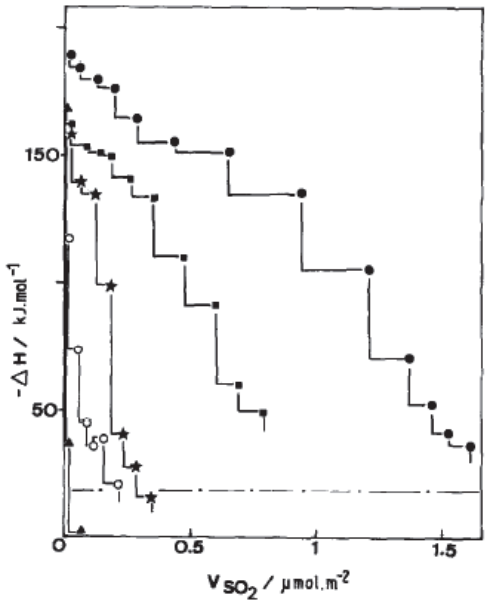

Figure 3.2.4. Differential enthalpy of sulphur dioxide adsorption at 80 °C as a function of the probe uptake on V_2O_5/y- Al_2O_3 catalysts: (▪) 1.1 wt.% V_2O_5; (*) 2.9 wt.% V_2O_5; (○) 5.2 wt.% V_2O_5; (▲) 9.8 wt.-% V_2O_5; and on (●) pure y-alumina. [44]

Alumina-, silica-, and titania-supported vanadium oxide systems with V_2O_5 loadings ranging from 3 to 12 wt% (corresponding to 0.02–0.09 V/(Al,Si,Ti) atomic ratios) were prepared by Gervasini et al. [41] and characterized by ammonia adsorption microcalorimetry. Previously to adsorption, the samples were activated in air for 12 h and then outgassed at 400 °C. Adsorption was performed at 80 °C. Table 3.2.1. summarizes the main results obtained and Figure 3.2.4. shows the plots of the differential heats of NH_3 adsorption as a function of coverage for the series of alumina, silica, and titania catalysts and the respective supports.

Table 3.2.1. Catalyst acidity evaluated by calorimetric/volumetric measurements of NH_3 adsorption. [41]

Catalyst	$V_{NH_3,tot}$ [a] (µmol/m^2)	$V_{NH_3,irr}$ [b] (µmol/m^2)	Q_{int} [c] (J/m^2)
Al_2O_3	2.486	1.476	0.309
VA-A4	2.185	1.228	0.229
VA-I5	2.182	1.171	0.205
SiO_2	0.220	0.092	0.003
VS-A6	0.735	0.094	0.057
VS-A9	0.923	0.120	0.074
VS-A12	1.295	0.175	0.107
VS-I6	0.456	0.068	0.031
VS-I10	0.632	0.137	0.044
TiO_2	5.126	3.120	0.530
VT-A3	3.593	2.275	0.343
VT-I6	4.061	2.422	0.347

[a] Adsorbed amount under an equilibrium pressure of 27 Pa.
[b] Irreversibly adsorbed volume at 27 Pa (number of strong sites).
[c] Integral heat of adsorption at 27 Pa.

The number of acid sites (both the total population, $VNH_{3,tot}$, and that of strong sites, VNH_{3irr}) decreased when V_2O_5 was deposited on alumina and titania. The acid sites were created when V_2O_5 phase was deposited on silica. Both the number and strength of the acid sites of the silica-supported

catalysts, increased with the vanadia loading, independently of the preparation method. Comparing catalysts at similar V_2O_5 loadings prepared by ALD (atomic layer deposition) and impregnation (VS-A6 with VS-I6 and VS-A12 with VS-I10), it appears that the ALD preparation brings to a V_2O_5 phase with a higher number of acid sites and a stronger surface acidity, than that prepared by impregnation. This indicates a better dispersion of the vanadia centers and a stronger interaction with the support leading to highly acidic Lewis sites. [41]

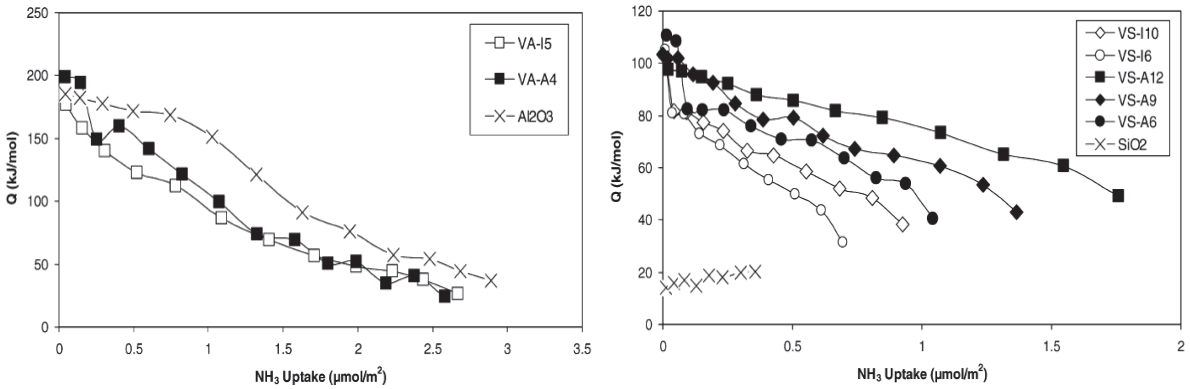

Figure 3.2.4. Differential heats of ammonia adsorption over the alumina support (left) and silica support (right) and the corresponding vanadia catalysts prepared by ALD (filled symbols) and impregnation (open symbols) methods. [41]

Similar results to the latter described research [41], were reported by Keranen and co-authors which prepared V_2O_5 catalysts supported on SiO_2 (around 4 wt% of V_2O_5) and Al_2O_3 (around 5 wt% of V_2O_5) by impregnation and ALD (atomic layer deposition) methods. [42,43] The same type of acidic sites, Lewis and Brønsted, were present in all the catalysts, and those prepared by ALD showed stronger acidity. These authors [42,43] explained that bulk V_2O_5 possesses both surface Lewis and Brønsted acidity, whereas in dehydrated conditions no Lewis acid sites are present on SiO_2 surface, while only Lewis acid sites are present on Al_2O_3 surface. Coating the bare support with a vanadium oxide layer creates new Brønsted acid sites at higher loadings and affects the number of Lewis acid sites.

NH_3 adsorption of V_2O_5 catalysts supported on niobium phosphate (NbP) with V_2O_5 loadings from 5 to 25 wt% were investigated by Sun et al. [45] Samples were outgassed overnight at 350 °C and ammonia adsorption took place at 150 °C. The vanadium and niobium elements in V_2O_5/NbP catalysts were present in the +5 oxidization state as observed from XPS. The results from XRD and LRS showed that V_2O_5 was well dispersed on the surface of NbP. Addition of V_2O_5 to NbP decreased both the initial heat and the coverage of NH_3. The surface acidity decreased with the increase of V_2O_5 loading. Figure 3.2.5. shows curves Q_{diff} *vs.* ammonia coverage. Both the number of the total population of acid sites (VNH_{3tot}) and that of strong sites (VNH_{3irr}) decreased with increasing V_2O_5 content. The results could be connected also with the decrease in surface area. The proportion of strong acid sites decreased while that of weak acid sites increased. The heat of NH_3 adsorption

gradually decreased with increasing NH_3 coverage revealing heterogeneous strength distributions of NbP and V_2O_5/NbP samples.[45]

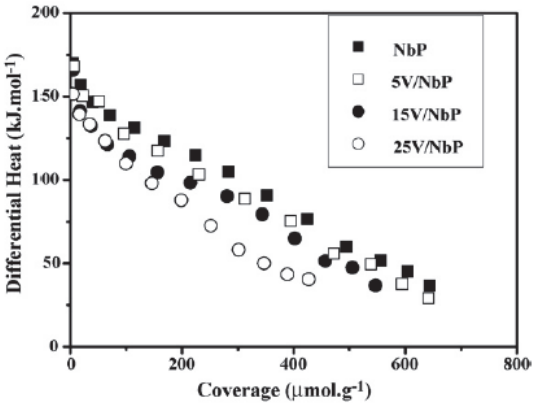

Figure 3.2.5. Differential heats *vs.* coverage for NH_3 adsorption over NbP and V_2O_5/NbP catalysts. [45]

Zhao and co-authors largely studied the acid-base surface properties of different V_2O_5/TiO_2 and $V_2O_5/TiO_2–SO_4^{2-}$ catalysts. [46-47] Catalysts containing 5, 15 and 25 wt% of V_2O_5 were prepared by successive incipient wetness impregnation and the effect of doping with SO_4^{2-} was studied. [47] The Raman spectra revealed the formation of crystalline V_2O_5 particles when the vanadia coverage was higher than 15 wt%. Redox cycles revealed that the monomeric vanadia species were easier to reduce, but more difficult to oxidize than the polymeric and crystalline species. The supported vanadia species were found to be composed of stoichiometric V_2O_4 and V_2O_5, as shown by XPS. The acidity of the catalysts was determined by ammonia adsorption microcalorimetry. Table 3.2.2. presents the initial heats of adsorption (denoted by Q_{init}) and the amount of ammonia adsorbed under an equilibrium pressure of 27 Pa. [47]

Table 3.2.2. Ammonia adsorption data from microcalorimetry measurements at 150 °C. [47]

Sample	V_{tot}[a] (27 Pa) (µmol g^{-1})	V_{tot}[a] (27 Pa) (µmol m^{-2})	V_{irr}[b] (µmol g^{-1})	V_{irr}[b] (µmol m^{-2})	Q_{init}[c] (kJ mol^{-1})
5VTi	498	2.5	291	1.5	194
5VTiS	486	2.8	316	1.8	219
15VTi	483	2.3	275	1.3	210
15VTiS	514	2.9	335	1.9	231
25VTi	425	2.6	213	1.3	220
25VTiS	406	3.0	243	1.8	145
TiO_2	517	2.5	279	1.3	210

[a] Total amount of NH_3 retained as determined at 27 Pa of equilibrium pressure.
[b] "Irreversible" amount of NH_3 retained as determined from the difference between the amounts adsorbed in the first and second adsorptions at 27 Pa.
[c] Heat evolved from the first NH_3 dose.

The initial heat of ammonia adsorption on TiO_2 was found to be about 210 kJ mol^{-1}, suggesting that the TiO_2 support used in this work was strongly acidic. The addition of V_2O_5 did not change significantly the initial heat, while the addition of SO_4^{2-} slightly increased it. Additionally, the amount of irreversibly absorbed ammonia (V_{irr}), corresponding to strong chemisorption, decreased with increasing V_2O_5 content, due to the decreasing of surface area. Nevertheless, the number and the density of strong acid sites increased with SO_4^{2-} addition. [47]

Cobalt supported on different oxides

Adsorption microcalorimetry of NH_3 and CO_2 was used to probe the surface acid-base properties of higly loaded Co/SiO_2 catalysts by Chen and Shen. [48] Adsorption of ammonia was performed at 150 °C on the catalysts reduced and evacuated at 500 °C. The initial heat and uptake were measured to be about 90 kJ mol^{-1} and 650 µmol g^{-1}, respectively, for the adsorption of NH_3 on the $60\%Co/SiO_2$, indicating that the catalyst possessed significant amount of surface acid sites, probably connected to the presence of cobalt silicate. The initial heat and uptake were measured to be about 83 kJ mol^{-1} and 508 µmol g^{-1}, respectively, for the adsorption of NH_3 on the $80\%Co/SiO_2$. The surface acidity was stronger on $60\%Co/SiO_2$ than on $80\%Co/SiO_2$, probably due to the higher amount of cobalt silicate in $80\%Co/SiO_2$. Results of CO_2 adsorption on the reduced catalysts have shoved low uptakes, and no heat was measured, indicating that the Co/SiO_2 samples essentially did not possess any surface basicity. [48]

Chen et al. [49] reported results of NH_3 and CO_2 adsorption microcalorimetry at 150 °C for highly loaded cobalt catalysts (80 wt%) on different supports (SiO_2, Al_2O_3, ZrO_2 and MgO). The initial heat and uptake were around 120 kJ mol^{-1} and 604 µmol g^{-1}, for NH_3 adsorption on the $80\%Co/Al_2O_3$, indicating strong surface acidity with high quantity of acidic sites. The initial heats were about 110 and 83 kJ mol^{-1} for the adsorption of NH_3 on $80\%Co/ZrO_2$ and $80\%Co/SiO_2$ with corresponding uptakes of about 347 and 504 µmol g^{-1}, respectively. Thus, the surface acidities were weaker on $80\%Co/ZrO_2$ and $80\%Co/SiO_2$, as compared to that of $80\%Co/Al_2O_3$. The initial heat and uptake were measured to be about 131 kJ mol^{-1} and 406 µmol g^{-1}, respectively, for the adsorption of CO_2 on the 80%Co/MgO, indicating that this catalyst possessed strong surface basicity with abundant basic sites. The initial heat and uptake were measured to be about 82 kJ mol^{-1} and 42 µmol g^{-1}, respectively, for the adsorption of CO_2 on $80\%Co/ZrO_2$. $80\%Co/ZrO_2$ presented much weaker surface basicity than 80%Co/MgO. Weak surface basicity was also measured for $80\%Co/Al_2O_3$ since the initial heat and uptake were only about 32 kJ mol^{-1} and 25 µmol g^{-1}, respectively, for the adsorption of CO_2 on this catalyst. The surface basicity was absent on the $80\%Co/SiO_2$. [49]

Zirconia containing oxides (ZrO_2)

Zirconia belongs to the group of amphoteric oxides, whose acid–base properties are easily adjusted by making mixtures with other oxides. [50] Bolis et al. [51] used CO adsorption calorimetry at room temperature as a probe for (strong) Lewis acidity at the surface of monoclinic and tetragonal ZrO_2 (S_{BET}=85 m^2 g^{-1}), sulfated-ZrO_2 (S_{BET}=85 m^2 g^{-1}) and HfO_2 (S_{BET}=48 m^2g^{-1}). For both, m- ZrO_2 and HfO_2, outgassed at 400 °C the initial heat of adsorption was around 60 kJ mol^{-1}. t-ZrO_2 and sulfated-ZrO_2 were pretreated at 450°C (this temperature was chosen in order to reach a high dehydroxylation degree, but avoiding the sulfate decomposition that in vacuum starts at T≥550 °C). The overall population of CO sites is lower for the sulfated sample, as expected, because sulfates occupy structural positions that belong to Zr^{4+} cations in the pure sample. The initial heat of adsorption of CO on sulfated-t-ZrO_2 was higher than that of pure t-ZrO_2. The value of initial differential heat was >80 kJ

mol^{-1} for the sulfated sample and ≈70 kJ mol^{-1} for t-ZrO_2. The Q_{diff} curve of the sulfated sample was higher than that of the pure sample for all the coverage range examined. However the two curves approached at higher coverages, indicating that the main difference between the two samples was the presence of very few strong Lewis sites on sulfated-t-ZrO_2. [51]

Acidity and basicity of commercial ZrO_2 (S_{BET}=63.3 m^2 g^{-1}) was investigated by NH_3 and CO_2 adsorption microcalorimetry by Auroux and Gervasini. [32,33] At 150 °C, the differential heats curves of ammonia adsorption *vs.* coverage continuously decreased (Q_{init}=180 kJ mol^{-1}) due to the presence of Lewis acid sites of various strengths. CO_2 adsorption was realized at room temperature. Initial heat of CO_2 adsorption was 125 $kJmol^{-1}$, and a plateau in the domain of medium-strength sites (around 75 kJ mol^{-1}) was observed.

NH_3 adsorption calorimetry on SiO_2-ZrO_2 (S_{BET}= 596 m^2 g^{-1}) containing 14.3 wt% of ZrO_2 was performed at 80 °C after outgassing the sample at 400 °C during 16h. Gervasini and al. [52] individuated a first plateau in the 150–140 kJ mol^{-1} region, and a second one around 90 kJ mol^{-1}.

Stosić et al. [50,53] reported NH_3 and SO_2 adsorption microcalorimetry for different zirconia containing catalysts. Samples were pretreated in vacuum at 300 °C while adsorption was realized at 150 °C. Specific surface areas of catalysts were around 50 m^2 g^{-1}. Figure 3.2.6. summarizes the microcalorimetry results. All the investigated materials showed energetic heterogeneity of both acidic and basic active sites. Among the investigated samples, WO_3-ZrO_2 and HPW/WO_3-ZrO_2 showed prominent acidic character. The other solid materials adsorbed significant amounts of both SO_2 and NH_3, which is a clear indication of their amphoteric nature. Mixing of lanthania and ceria with ZrO_2 decreases the acidic character, while the distribution of basic sites is only slightly affected. The addition of WO_3 and WO_3-HPW to zirconia significantly decreases the amount of adsorbed SO_2 and the corresponding heats of adsorption. [50]

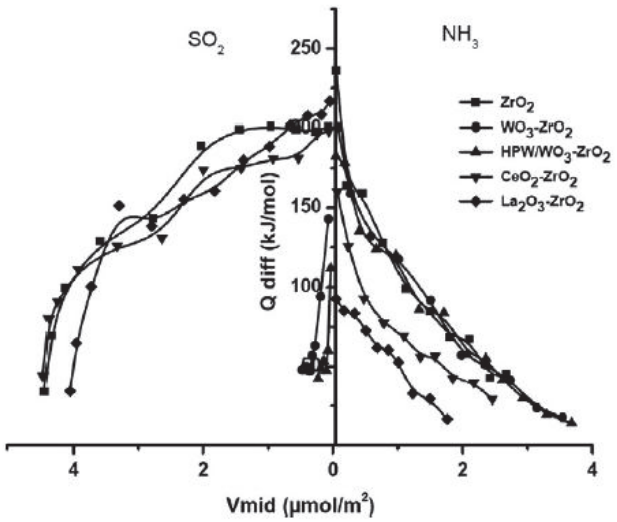

Figure 3.2.6. Differential heats of NH_3 and SO_2 adsorption as a function of surface coverage. [50]

Silica (SiO_2)

SiO_2 used in the synthesis of the catalysts presented in this thesis is obtained by evaporation of colloidal silica solution. In the literature different ways of synthesis are presented and largely studied by adsorption microcalorimetry. Silica is commonly used as catalyst support. Generally, silica possesses low acidity and basicity, but it might slightly differ due to the preparation method. [32,33,52,54] Acid-base properties of silica are easily tuned by addition of other elements. [55]

Auroux and Védrine [54] investigated the acidic and basic properties of precipitated silica (S_{BET}=180 m^2 g^{-1}) and fumed silica (S_{BET}=200 m^2 g^{-1}) using CO_2 and NH_3 adsorption. Fumed silica presented few weak acidic and basic sites. NH_3 adsorption at 23 °C (samples outgassed at 50 °C) revealed that precipitated silica displays more acidic sites (initial Q_{diff} around 85 kJ mol^{-1}) than fumed silica (initial Q_{diff} around 57 kJ mol^{-1}). This is probably due to traces of acidic impurities deriving from the preparation method. CO_2 adsorption performed at room temperature on precipitated silica (outgassed at 500 °C) showed the presence of only few basic sites.

Gervasini et al. [52] performed microcalorimetric measurements of NH_3 adsorption at 80 °C on SiO_2 (S_{BET}= 387 m^2 g^{-1}) previously outgassed at 400 °C for 16 h. Silica did not exhibit any acidity. Commercial SiO_2 (S_{BET}=117 m^2 g^{-1}) pretreated in the same way presented only very weak and very few acid sites (NH_3 adsorption performed at 150 °C). [32,33]

Masuda et al. [56] also reported similar results after measuring the differential heats of NH_3 adsorption on silica (S_{BET}=380 m^2 g^{-1}). Sample was outgassed 5h in vacuum at 400 °C, and adsorption of ammonia was performed at 25 °C. Ammonia adsorbed on silica was easily desorbed by evacuation at 25 °C indicating the presence of mainly hydrogen bonding and Van der Waals interactions.

Gervasini et al. [55] showed the influence of the addition of small amount of various elements (Li^+, Ca^{2+}, Nd^{3+}, Ni^{2+}, Zr^{4+}, SO_4^{2-}) on silica. The elements differed in electronegativity (Li<Nd<Zr<Ca<Ni<S) and in ionic radius (S<Li<Ni<Zr<Nd<Ca). Ni^{2+}, Nd^{3+}, and Zr^{4+} increased the acidity of silica surface, while Ca^{2+}, Nd^{3+}, and SO_4^{2-} increased the basicity. As observed in Table 3.2.3. the Q_{init} values do not always correspond to the common statement that the addition of a basic additive corresponds to a decrease of the acidity and vice-versa. Therefore, other parameters such as the average electronegativities of the cations and the effective charge of the oxygen atoms of the secondary oxide must be considered. For example, the general tendency is an increase of the initial heat of adsorption of SO_2 (higher basicity) when the average electronegativity decreases or when the oxygen charge increases. The opposite behavior was observed for the initial heats of NH_3 adsorption. Q_{init} of NH_3 adsorption increased when the oxygen charge decreased and when the average electronegativity increased. [55]

Adsorption of NH_3, pyridine, TEA (triethylamine) and TMA (trimethylamine) on SiO_2 was investigated by microcalorimetry and values of integral heats as a function of coverage are shown in Figure 3.2.7. [57] The strength of the basic probe molecules increases in the order NH_3<pyridine<TMA<TEA. Initial differential heat of NH_3 adsorption was around 70 kJ mol^{-1}, and like in

the other researches reported decreased linearly with coverage. Results of pyridine adsorption on silica at 200 °C revealed that the silica surface presented sites of homogeneous energy with differential heats of adsorption around 95 kJ mol^{-1}, while initial differential heat of TMA adsorption was 109 kJ mol^{-1}. TEA was adsorbed at 150 and 200 °C to test the effect of adsorption temperature on the acid strength distribution. The obtained differential heat was the same at both adsorption temperatures within experimental error, 112 kJ mol^{-1}. [57]

Table 3.2.3. Characteristics and acidity-basicity data of the samples. [55]

Sample	Surface area ($m^2.g^{-1}$)	Coverage[a]	NH_3 Q_{init} kJ.mol^{-1}	NH_3 V_{irrev} µmol.g^{-1}	NH_3 Q_{int} J.g^{-1}	SO_2 Q_{init} kJ.mol^{-1}	SO_2 V_{irrev} µmol.g^{-1}	SO_2 Q_{int} J.g^{-1}
SiO_2	310	/	83	37.7	1.5	58	2.8	0.1
Li^+	280	0.46	52	44.8	1.5	85	4.5	0.4
Ca^{2+}	241	0.55	54	37.4	1.3	142	12.5	1.5
Nd^{3+}	300	0.46	93	45.0	2.3	135	9.3	0.9
Ni^{2+}	307	0.70	99	44.6	2.6	99	2.8	0.2
Zr^{4+}	311	0.75	146	60.6	6.1	94	6.5	0.5
SO_4^{2-}	276	0.36	46	41.4	1.2	102	3.0	0.2

[a] Coverage in M^+ % of surface area

Auroux et al. [58] measured acidity of commercial SiO_2 (S_{BET}=280 m^2 g^{-1}) using pyridine adsorption microcalorimetry. Sample pretreated overnight in vacuo at 400 °C had initial differential heat of pyridine adsorption (150°C) around 90 kJ mol^{-1} and plateau around 50 kJ mol^{-1} on the curve Q_{diff} *vs.*coverage.

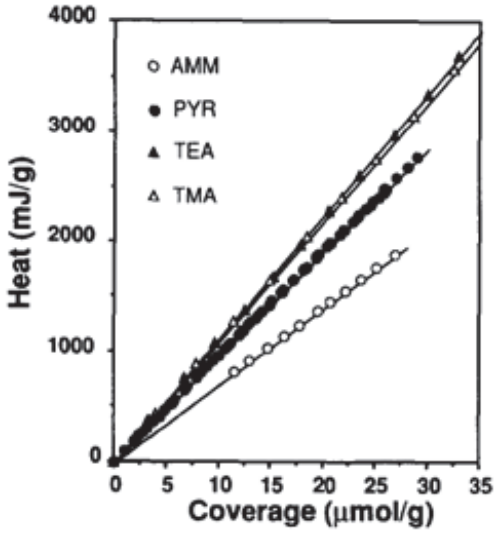

Figure 3.2.7. Integral heat of basic molecule adsorption on silica: ○- ammonia adsorbed at 150 °C, ●- pyridine adsorbed at 200 °C, ▲- TEA adsorbed at 200 °C, △- TMA adsorbed at 150 °C. [57]

Pyridine adsorption calorimetry on SiO_2 (S_{BET}= 400 m^2 g^{-1}) and SiO_2 doped with oxides of different cations (Ga^{3+}, Zn^{2+}, Al^{3+}, Fe^3, Fe^{2+}, Mg^2, Sc^{3+}) was reported by Cardona-Martinez and Dumesic. [57,59] All the samples (except for Fe) were pre-treated by oxidation in flowing oxygen at

450 °C for 4 h followed by evacuation for 2 h at the treatment temperature. Depositing metal oxides on silica increases the acidity and acid strength of the catalyst. In Figures 3.2.1. and 3.2.8. results for the samples supported on SiO_2 are shown.

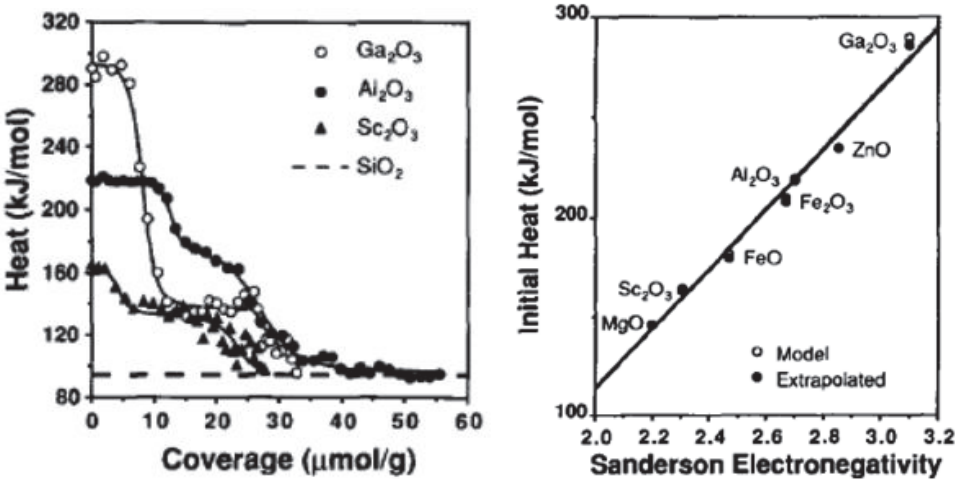

Figure 3.2.8. Differential heats of pyridine adsorption on silica-supported oxides that showed both Lewis and Brønsted acidty (left). Initial differential heats of pyridine adsorption as a function of Sanderson electronegativity of the doped cation (right). [57]

Methanol adsorption microcalorimetry at 27 °C on silica (380 m^2 g^{-1}) was studied by Natal-Santiago and Dumesic. [60] Sample was pretreated for 2h in vacuum at 327 °C. Methanol adsorbed molecularly on silica via formation of hydrogen bonds, with initial heat of interaction of 78 kJ mol^{-1}. As the methanol coverage increased, the heat of adsorption decreased monotonically until a coverage of ≈250 μmol g^{-1}. At higher coverages, the heat of adsorption was nearly constant at 60 kJ mol^{-1}. Similar results were also reported by Bolis and co-authors. [61]

Alumina (Al_2O_3)

Aluminum oxide is a typical amphoteric oxide. Adsorption of NH_3 and CO_2 on η-Al_2O_3 (240 m^2 g^{-1}) and γ-Al_2O_3 (200 m^2 g^{-1}) was investigated by Auroux and Védrine. [54] The presence of both acidic (related to Al^{3+} ions) and basic (related to O^{2-} ions) sites was observed. η-Al_2O_3 presented almost the double of strong acid sites than γ-Al_2O_3, which is presumably due to the fact that η-Al_2O_3 exhibits more surface Al ions (*i.e.* more Lewis sites). Initial differential heat of ammonia adsorption at 150 °C for η-Al_2O_3 (outgassed overnight at 400 °C) was around 140 kJ mol^{-1} and and the curve was characterized by a plateau, while γ-Al_2O_3 (outgassed overnight at 350 °C) that showed similar initial differential heat presented a continuously decreasing curve. Initial heat of CO_2 adsorption at RT for η-Al_2O_3 (outgassed overnight at 500 °C) was around 120 kJ mol^{-1}. [54]

Gervasini and co-workers [52] investigated acidity of Al_2O_3 (S_{BET}= 244 m^2 g^{-1}) using NH_3 adsorption microcalorimetry. The sample was outgassed at 400 °C for 16 h, and the adsorption of NH_3 performed at 80 °C. Initial heat for the alumina at very low NH_3 coverage was very high (270 kJ mol^{-1}).

A continuously decreasing curve was observed (without a clearly detectable plateau) in the whole range of the heats measured. This behaviour is typical for highly heterogeneous surfaces.

Shen et al. [20] measured heats of adsorption of NH_3 on commercial γ-Al_2O_3. Measurements were carried out at 150 °C. γ-Al_2O_3 sample was calcined in situ for 4h before adsorption and then evacuated for 2h at 400 °C. Initial differential heat of adsorption was ≈135 kJ mol. γ-Al_2O_3 (S_{BET}= 347 m^2 g^{-1}) activated in a different way possessed acid sites with differential heats from about 165 to 60 kJ mol^{-1}. [19] Adsorption of CO_2 on the same sample showed a small number of basic sites. The initial heat of adsorption was about 155 kJ mol^{-1}, and the heat decreased significantly with CO_2 coverage.

Gervasini et al [55] reported on the influence of adding small amount of various additives (Li^+, Ca^{2+}, Nd^{3+}, Ni^{2+}, Zr^{4+}, SO_4^{2-}) on Al_2O_3. The additives differed in electronegativity (Li<Nd<Zr<Ca<Ni<S) and in ionic radius (S<Li<Ni<Zr<Nd<Ca). As a general point of view, number and strength of acidic and basic sites have been modified by the various additives, but no clear correlation was found between the properties of additives and the acidity and basicity of alumina. The initial heat of adsorption was the most disturbed parameter by the additive. The values of Q_{init} of NH_3 adsorption significantly increased by addition of Zr^{3+} and SO_4^{2-} ions on alumina surface. Addition of Nd^{3+} increased the value of Q_{init} of SO_2 by almost 90 kJ mol^{-1}, but the number of strong basic sites remained similar to pure alumina. [55]

Auroux et al. [58] reported pyridine adsorption microcalorimetry on commercial γ-Al_2O_3 (S_{BET}= 180 m^2 g^{-1}). Adsorption was performed at 150 °C after outgassing the sample overnight at 400 °C. Initial differential heat of adsorption was around 280 kJ mol^{-1}, and the curve of differential heats of adsorption as a function of coverage decreased continuously.

Bolis et al. [51] investigated CO adsorption at room temperature γ-Al_2O_3 (S_{BET}= 186 m^2 g^{-1}) and δ,θ-Al_2O_3 (S_{BET}= 120 m^2 g^{-1}). γ-Al_2O_3 outgassed at 400 °C had initial differential heat of adsorption of 40 kJ mol^{-1}. The heat felt down to exceptionally low values ≈10 kJ mol^{-1} at high coverage. When γ-Al_2O_3 and δ,θ-Al_2O_3 were outgassed at 500 °C it was evidenced that increasing the pretreatment temperature increased CO adsorption due to creation of higher amounts of strong Lewis acidic sites. For both γ and δ,θ-Al_2O_3, the initial heat of adsorption was around 60 kJ mol^{-1}, when pretreated at 500 °C.

Microcalorimetry and FT-IR studies of methanol adsorption on alumina were reported by few researchers. [62,63] At very low coverages, methanol molecules are coordinated to the strongest Lewis sites, and then easily transformed into bridged methoxy species. With increasing coverage, another form, irreversibly adsorbed at room temperature, but desorbed by evacuation at 100-200 °C, became predominant: undissociated methanol strongly hydrogen bonded on a cation-anion couple with a strong basic character. Finally, at high coverages, a reversible form of hydrogen bonded to basic sites was detected. [62]

Busca and co-authors [62] reported results of room temperature methanol adsorption microcalorimetry on different δ-Al_2O_3 samples previously evacuated at 500 °C (773K) and 100 °C (373 K) and labeled A-773 and A-373, respectively. The curve for the differential adsorption heats, q_{diff} (see

Figure 3.2.9.), shows a step-by-step decreasing of the adsorption heats with coverage. Each step was interpreted as indicative of the successive formation of different adsorbed species. A first strongly exothermic step (step I, q_{diff} = 220-140 kJ mol^{-1}) was followed by a second step (step II), identified by a plateau in the q_{diff} curve, near 110-100 kJ mol^{-1}. A third step was characterized by q_{diff} values of about 70 kJ mol^{-1} (step III). Further enhancement of methanol pressure resulted in the evolution of heats similar to that of methanol condensation (39.2 kJ mol^{-1}), probably connected with multilayer adsorption. On A-773 a second run of measurements has also been performed after saturation with methanol at RT and thorough evacuation at RT. During such a second adsorption run a very limited strongly exothermic step was observed and q_{dlff} curve readily felt to values of 80 and then 60 kJ mol^{-1}. These values correspond roughly to those typical of step III and confirmed that such a step was due to relatively strong reversible adsorption. Calorimetric measurements on A 373 (where water is both undissociatively and dissociatively chemisorbed) showed that sites responsible for steps I and II are at least partially poisoned, indicating a competitive adsorption of water and methanol at RT. However, the total amount of adsorbed methanol was only slightly less on A-373 than on A-773, indicating that adsorbed water may act as an adsorption site for methanol. The q_{diff} curve (Figure 3.2.9.) of A-373 felt rapidly, after a limited strongly exothermic step, and gave values below 100 kJ mol^{-1}, forming a plateau near 70 kJ mol^{-1}. The similarity of this q_{dlff} value to that corresponding to step III on A-773 suggests that in both cases hydrogen bondings may play a predominant role. [62]

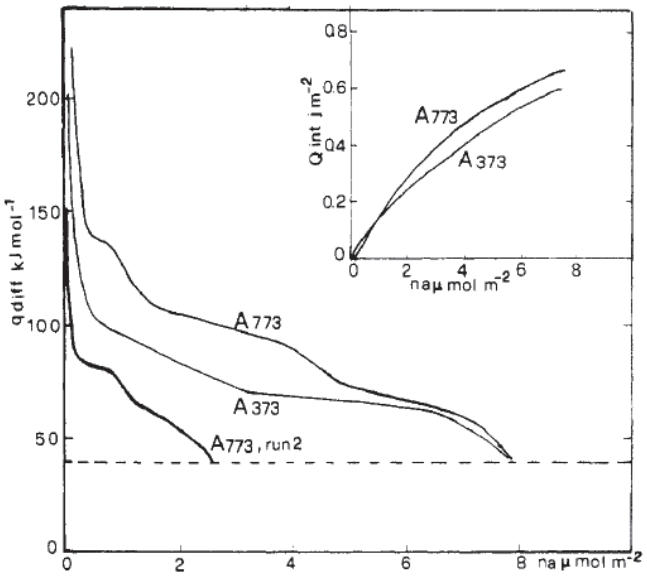

Figure 3.2.9. Integral (in the insert) and differential heats of methanol adsorption on alumina. Broken line: condensation heat of methanol. [62]

Magnesia (MgO) and other alkaline and alkaline earth metal oxides

Magnesia is a typical basic oxide largely studied by adsorption calorimetry, and mostly CO_2 was used as a probe. [19,20,54,64,65] Auroux and Vedrine [54] presented microcalorimetric experiments on MgO (S_{BET}=200 m^2 g^{-1}) where they have found strong and numerous basic sites. CO_2 adsorption at room temperature (sample outgassed at 400 °C) confirmed strong basic character of

MgO representing numerous basic sites and a plateau of differential heats of adsorption at around 110 kJ mol^{-1}. NH_3 adsorption performed at 150 °C revealed only presence of some very weak acid sites. CO_2 and NH_3 adsorption under the same conditions was performed on MgO sample (S_{BET}=197 m^2 g^{-1}) by Auroux and Gervasini. [32,33] Initial differential heat of CO_2 adsorption was around 110 kJ mol^{-1}. A short plateau on the curve of differential heats *vs.* coverage was observed, then the curve decreaseed gradually till 10 kJ mol^{-1} at 2 µmol m^{-2}. Initial differential heat of NH_3 adsorption was around 14 kJ mol^{-1} and remained constant till 4 µmol m^{-2} of coverage which is characteristic of physisorption. [32,33]

Shen and co-workers [19,20] measured the heats of adsorption of CO_2 on MgO. Measurements were carried out at 150 °C. MgO sample (S_{BET}≈ 250 m^2 g^{-1}), which was also calcined in situ before adsorption for 4h and then evacuated for 2h at 400 °C, had initial differential heat of adsorption ≈160 kJ mol^{-1}. [20] Another MgO sample (S_{BET}= 199 m^2 g^{-1}) which was pretreated in a different way, possessed basic sites with differential heats of adsorption around 170 kJ mol^{-1}. For this sample differential heat of NH_3 adsorption was also measured and reported to be very low (≈55 kJ mol^{-1}), as expected. [19]

León et al. [64] studied CO_2 adsorption of differently synthetized MgO oxides. All samples were outgassed overnight at 350 °C and adsorption of CO_2 was performed at 50 °C. From the distribution of basic sites, heterogeneity of the strength of the basic sites was observed. These sites can be separated in three groups accordingly to their strength: strong (Q> 150 kJ mol^{-1}), medium (120 kJ mol^{-1}< Q<150 kJ mol^{-1}) and weak (Q<90 kJ mol^{-1}). In particular, CO_2 adsorption calorimetry data permitted to attribute the increase of basic sites mainly to the increase of the surface area. Specific surface areas for MgO (I), MgO (II), hsMgO (I) and hsMgO (II) were 26, 70, 87 and 221 m^2 g^{-1}, respectively. Results are shown in Figure 3.2.10.[64]

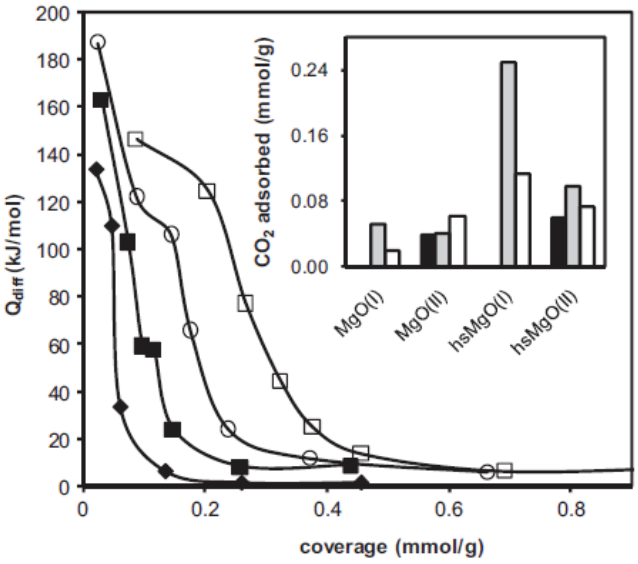

Figure 3.2.10. Differential heats of CO_2 adsorption vs. coverage at 50 °C on: MgO(I) (♦), MgO(II) (■), hsMgO(I) (□), and hsMgO(II) (○). Distribution of interaction strengths of carbon dioxide adsorption on the samples: 210 > Q >150 kJ mol^{-1} (black); 150 > Q > 90 kJ mol^{-1} (grey); 90 > Q > 30 kJ mol^{-1} (white). [64]

Gervasini et al. [55] investigated acidic and basic properties of MgO by NH_3 and SO_2 adsorption calorimetry. The temperatures of adsorption and activation are not reported. Influence of adding small amount of various additives (Li^+, Ca^{2+}, Nd^{3+}, Ni^{2+}, Zr^{4+}, SO_4^{2-}) was shown. In particular, addition of Li^+, Ca^{2+}, Nd^{3+}, Ni^{2+} increased the basicity of magnesia surface. The number of basic sites became nearly the double when Ca^{2+} or Ni^{2+} were added to pure MgO. Li^+ and Nd^{3+} additives caused a less pronounced increase of the number of basic sites on the same magnesia. Authors observed general tendency: an increase of the initial heat of adsorption of SO_2 (more basicity) when the average electronegativity decreased or when the oxygen charge increased. On the other hand the initial heat of NH_3 adsorption increased, when the oxygen charge decreased and when the average electronegativity increased. [55]

As shown before magnesia has strong and numerous basic sites but almost no acid sites [19,54,64]. When magnesia is added to silica, acidity is generated. [56] This acidity is found to be exclusively of the Lewis type. [35] Cardona-Martinez and Dumesic [35] performed adsorption of pyridine (200 °C) on a MgO/SiO_2 sample (0.23 wt% of Mg, S_{BET}≈400 m^2 g^{-1}) pretreated in oxygen flow at 450 °C for 4h, and then outgassed. Creation of new acid sites was confirmed. The initial differential heat of pyridine adsorption was 146 kJ mol^{-1}. The differential heat decreased continuously indicating that the surface was heterogeneous. NH_3 adsorption microcalorimetry on silica-magnesia (20.5 wt% of MgO; S_{BET}= 450 m^2 g^{-1}) was performed by Masuda et al. [56] Adsorption of ammonia took place at 25 °C and the sample was pretreated in vacuum for 5h at 400 °C. The heat of NH_3 adsorption on silica-magnesia was about 109 kJ mol^{-1}, and then decreased gradually to 54 kJ mol^{-1}.

Both Lewis and Brønsted basic properties of magnesium oxide were, respectively, studied by Pighini et al. [65] by adsorption calorimetry of CO_2 and methanol at RT. Different samples were investigated: MgO-commercial (MgO-c, S_{BET}=82 m^2 g^{-1}), MgO-synthesized by sol-gel method (MgO-sg, S_{BET}=145 m^2 g^{-1}), and MgO-precipitated (MgO-p, S_{BET}=100 m^2 g^{-1}). The influence of small amounts of alkaline (Na^+ and Li^+) and alkaline-earth (Ca^{2+}) cations was also studied. Considering CO_2 adsorption all curves (Q_{diff}=f(θ)) showed a plateau of homogeneous sites around 100 kJ mol^{-1}, that corresponds to middle strength basic sites of a homogeneous surface. Among all the samples MgO-c displayed the strongest basicity with an experimental initial differential heat of adsorption of 165 kJ mol^{-1}, followed by MgO-p (Q_{diff}=118 kJ mol^{-1}), and MgO-sg (Q_{diff}=112 kJ mol^{-1}). For doped magnesia samples, the initial heat of adsorption was lower (100 kJ mol^{-1}). The influence of cation added to MgO impacted more the amount of Lewis sites than the value of initial heat of adsorption. Na-MgO and Li-MgO presented the double of basic sites than MgO-p. In the case of Ca-MgO the number of basic sites was three times higher than that of MgO-p (5.1 µmol m^{-2} *vs.* 1.7 µmol m^{-2}). The initial adsorption heats of methanol showed similar values for undoped magnesia (120 kJ mol^{-1}) while the corresponding values for doped magnesia samples were reduced by 15 kJ mol^{-1}. The amount of Brønsted basic sites also increased by doping MgO. The cation influence was more pronounced in methanol adsorption experiments than in CO_2 adsorption. However in both cases, the adsorption heat values decreased in the following order: Ca^{2+}>Na^+>Li^+. [65]

Auroux and Gervasini [32,33] investigated NH_3 and CO_2 adsorption on commercial CaO (S_{BET}=45 m^2 g^{-1}). NH_3 adsorption was performed at 150 °C and very low differential heats of adsorption (around 4 kJ mol^{-1}) were measured indicating the absence of acidic sites. CO_2 adsorption was performed at room temperature. The differential heats curves presented a large plateau of chemisorption (around 160 kJ mol^{-1}). The infrared spectra of chemisorbed CO_2 on CaO confirmed the existence of only one type of adsorption sites corresponding to unidentate species, which are probably related to the large plateau of the differential heats. [32,33]

Bolis and co-authors studied methanol adsorption at room temperature on amorphous silica samples [61] and on the surface of Ca-modified amoprpous silica. [66] Prior to microcalorimetric experiments samples were vacuum-activated at 150 °C. IR spectroscopic and microcalorimetric experiments were performed in parallel to describe quantitatively and energetically the surface features of nanosized Ca-modified specimens (A200/Ca4 (4 mol% CaO), A200/Ca8, and A200/Ca16,) as a function of Ca loading and in comparison with the unmodified parent silica (Aerosil 200). [66] The presence of Ca species enhanced the adsorption capacity of silica, and created a complex reactivity. Ab initio simulation provided microscopic information on the energetics of coordinated CH_3OH adducts formed at the Ca sites (BE=104 kJ mol^{-1} *vs.* q_{diff} ~ 100 kJ mol^{-1}). The methoxylation of the surface, producing Si-OCH_3 and Ca-OH species (and not Ca-OCH_3 and Si-OH), occurs only at a certain coverage (30-40% of the total methanol uptake) and depends on both CH_3OH pressure and contact time. Data from both volumetric-calorimetric and IR spectroscopic experiments indicated, in good agreement with ab initio simulation results, that the overall interaction involves both chemical and physical adsorption processes which, to a large extent, occur simultaneously, the relevant energy transfers being very similar. The differential thermal response of the three Ca-modified surfaces was virtually the same (all experimental points lied on the same curve in the whole coverage interval examined), confirming that the nature of the interaction between *cus (coordinatively unsaturated)* Ca^{2+} ions and CH_3OH depends only little on Ca loading. The q_{diff} values for the Ca-modified samples were larger than those for unmodified silica due to the creation of new sites with more specific interaction than plain H-bonding. A rather strong interaction occured in the early stages of the process on the Ca-modified samples ($q0$ ~ 100 kJ mol^{-1}). This value, significantly larger than that obtained for pure silica (A200) ($q0$ ~ 70 kJ mol^{-1}), is compatible with either a strong CH_3OH coordination onto *cus* Ca^{2+} ions acting as Lewis acid sites, or with moderately exothermic reactive phenomena or, most likely, with a combination of the two. All q_{diff} plots were typical of highly heterogeneous surfaces. The heat values progressively decreased with increasing coverage and tend to values that (as often observed with H-bonding adsorption processes) are even lower than the latent heat of methanol liquefaction (qL =38 kJ mol^{-1}). [66]

Mg/Al oxides derived from hydrotalcite-like compounds

Mg/Al hydrotalcite-like compounds consist of brucite-like layers containing octahedrally coordinated bivalent (Mg^{2+}) and trivalent (Al^{3+}) cations, as well as interlayer anions (such as CO_3^{2-}, and

OH^-) and water. After calcination, these compounds lose interlayer anions and water to form mixed Mg/Al oxides that can be used as catalysts, precursors of catalysts and catalyst supports. [19,20] These compounds are generally acknowledged to have dominantly basic character, however their acid/base properties are influenced, and easily tuned, by the choice of calcination temperature [20], variation of Mg/Al ratio [8,19,67-69], or by adding other cations such as Fe^{3+} [70], Ni^{2+}, Cu^{2+} [71,72], or K^+ [1,73] to the Mg/Al hydrotalcite structure.

Shen end co-authors [19] studied the surface acid/base properties of hydrotalcite-derived MgAl oxides with Mg/Al molar ratios ranging from 3 to 12 using NH_3 and CO_2 adsorption (150 °C) microcalorimetry. All MgAl oxides were calcined at 500 °C and exhibited moderate acidity and basicity. Curves of differential heats as function of ammonia and CO_2 coverage are shown in the Figure 3.2.11. These materials did not possess acid and base sites with differential heats higher than 120 and 150 kJ mol^{-1}, respectively, for NH_3 and CO_2 adsorption. The number and strength of the acid sites were considerably lower than for γ-Al_2O_3, but higher than for MgO. The number and strength of the basic sites for calcined hydrotalcites were lower than for MgO, but higher than for γ-Al_2O_3. Infrared spectroscopy revealed that the acid sites on calcined hydrotalcites are mainly Lewis acid sites, while the basic sites are oxygen anions. [19]

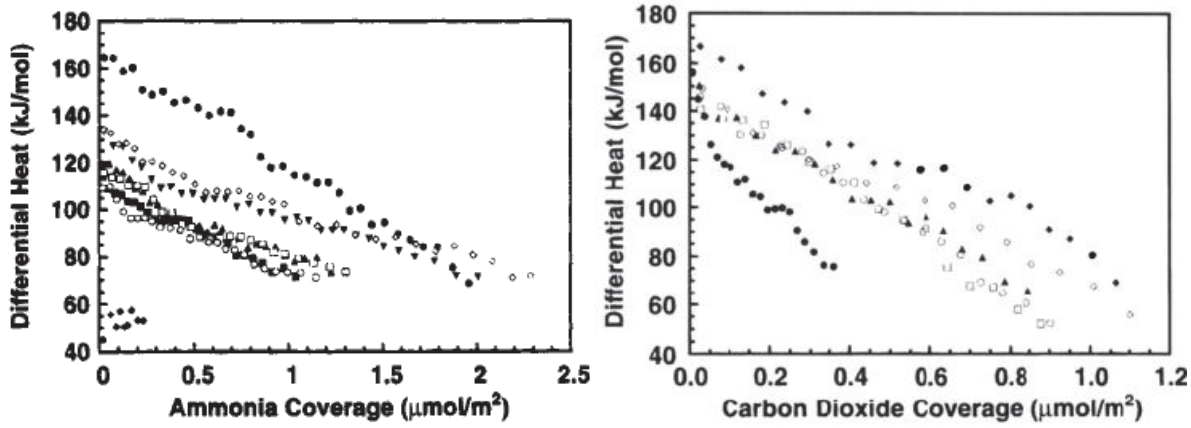

Figure 3.2.11. Differential heat *vs.* coverage for NH_3 adsorption (left) and CO_2 (right) at 150 °C on synthesized: γ-Al_2O_3 (●), 0.33 Mg/Al (▼), 3Mg/Al (■), 7Mg/Al (▲), 7Mg/Al* (□), 12Mg/Al (○), MgO (♦), and 10%MgO/γ-Al_2O_3 (◊) samples. [19]

The same authors [20] reported on NH_3 and CO_2 adsorption at 150 °C on MgAlO binary oxides (Mg/Al molar ratio is 3) derived (calcined at 400 °C, 600 °C and 800 °C) from the hydrotalcite precursor. γ-Al_2O_3 and MgO oxides were used as references. Microcalorimetric adsorptions of CO_2 and NH_3 showed that the basicity follows the order: MgO > $Mg/Al_{600\ °C}$ > $Mg/Al_{800\ °C}$ > $Mg/Al_{400\ °C}$, while the acidity of these samples decreases in the order: γ-Al_2O_3 > $Mg/Al_{400\ °C}$ > $Mg/Al_{600\ °C}$ ≈ $Mg/Al_{800\ °C}$. With the increase of calcination temperature, the surface area of the MgAlO sample decreased from 194 to 115m^2 g^{-1}, while that of MgO decreased from 254 to 38 m^2 g^{-1}. Surface acid/base sites of the calcined hydrotalcite samples were mainly of Lewis type. [20]

The studies presented by Shen et al [19,20] are also in agreement with the microcalorimetric study performed by Hulea et al which reported CO_2 adsorption on hydrotalcite-derived Mg-Al oxides with Mg/Al ratios 2 and 3, and calcined at different temperatures. [1,8]

Prescott et al [67] studied acid/base properties of Mg/Al oxides derived after calcination (550 °C) of commercial hydrotalcites with different Mg/Al ratio (0.6, 1.4, 2.2, 3.0) by CO_2 adsorption microcalorimety at 40 °C. Samples were pretreated under vacuum overnight at 400 °C. Samples were labeled CHT 0.6, 1.4, 2.2, and 3.0 and their BET surface areas: 257, 201, 114 and 203 $m^2\ g^{-1}$, respectively. MgO (S_{BET}=75 $m^2\ g^{-1}$) and alumina (S_{BET}=234 $m^2\ g^{-1}$) were used as reference catalysts. The differential heats of CO_2 adsorption as a function of CO_2 uptake are shown in Figure 3.2.12. All the samples showed initial values of heat of adsorption between 130 and 155 kJ mol^{-1}. The CHT samples have more basic sites than MgO and Al_2O_3. This applies, in particular, to the increase in the number of weak base sites on CHT samples (in agreement with the FTIR results). CHT3.0 exhibited the highest number of weak basic sites. The fast and continuous decrease in the adsorption heats (and the very broad carbonate bands in the FTIR spectra after CO_2 adsorption) indicates a wide distribution of site strength, particularly for the CHT samples. The total uptake of irreversible (chemisorbed) CO_2 decreased in the following order at a differential heat value of 50 kJ mol^{-1}: CHT3.0 > CHT1.4 > CHT2.2 > CHT0.6 > MgO > Al_2O_3. With respect to MgO, this order differed from that observed by CO_2-FTIR. This could be due to the different conditions applied; the microcalorimetric measurements were performed at 40 °C and do not distinguish between Brønsted and Lewis base sites. The FTIR measurements, on the other hand, only characterize Lewis base sites (measurement after evacuation at 150 °C). [67]

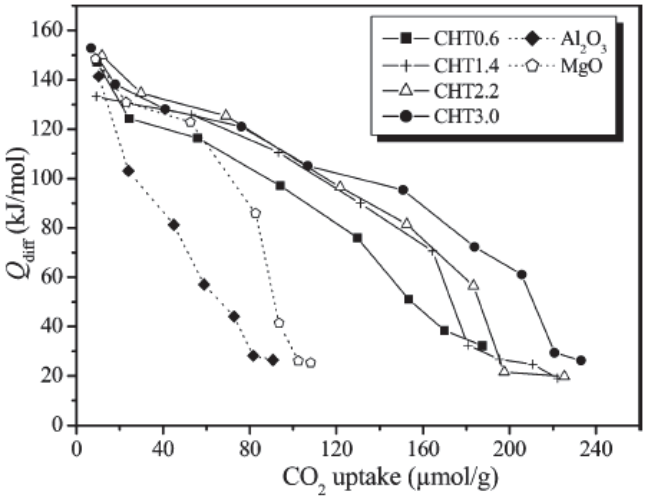

Figure 3.2.12. Differential heats of CO_2 adsorption at 40 °C as a function of uptake. [67]

Recently Stošić et al [69] reported results of SO_2 and NH_3 adsorption microcalorimetry on Mg/Al oxides prepared from hydrotalcite precursors with Mg/Al ratio varying from 2 to 7. Adsorption temperature was 150 °C and the samples were pretreated by heating overnight under vacuum at 300 °C. Table 3.2.4. summarizes composition, surface areas of the samples , and data obtained after microcalorimetric experiments. By increasing the Mg/Al ratio from 2 to 3, the adsorbed amount of SO_2

significantly increased. This amount remained almost constant for Mg/Al ratio of 4 and 5 then decreased with further increase of this ratio. Ammonia adsorption was the highest on the sample with Mg/Al=3. The amount of basic sites is significantly higher when compared to acidic sites for all materials, indicating their predominant basic character. [69]

Table 3.2.4. Mg and Al contents, S_{BET} surface areas and vi_{rrev} and v_{total} calculated from adsorption isotherms of SO_2 and NH_3 probe molecules. [69]

Sample name	Mg (mol%)	Al (mol%)	Experimental Mg/Al ratio	S_{BET} (m^2/g)	S_{BET} (m^2/g)	SO_2 amount adsorbed		NH_3 amount adsorbed		Ratio of strong basic to strong acidic sites
				Before calcination	After calcination	V_{total}[a] (μmol/g)	V_{irrev}[b] (μmol/g)	V_{total}[a] (μmol/g)	V_{irrev}[b] (μmol/g)	V_{irrev}(μmolSO_2/g)/V_{irrev} (μmolNH_3/g)
Mg/Al = 2	62.47	37.52	1.66	27	72	198.3	191.7	23.4	14.4	13.77
Mg/Al = 3	67.05	32.95	2.03	31	145	606.2	587.5	116.1	57.2	10.60
Mg/Al = 4	81.05	18.94	4.27	32	138	608.5	589.9	58.9	26.1	23.31
Mg/Al = 5	83.12	16.88	4.92	32	128	662.4	649.6	82.3	22.9	28.92
Mg/Al = 6	87.85	12.14	7.24	29	99	335.2	321.8	15.3	8.3	40.38
Mg/Al = 7	89.70	10.29	8.71	30	96	272.5	261.1	16.3	8.0	34.06

[a] Amount of NH_3 or SO_2 adsorbed under an equilibrium pressure of 0.2 Torr (27 Pa).
[b] Amount of chemisorbed NH_3 or SO_2 under an equilibrium pressure of 0.2 Torr (27 Pa).

Various oxides

$Bi_3FeMo_2O_{12}$ (2.3 m^2 g^{-1}) catalyst outgassed overnight at 450 °C presented only few weak acid sites using NH_3 adsorption at 150 °C. [54]

The acidic and basic properties for V_2O_5-P_2O_5 catalysts prepared by six different methods were reported by Ai. [74] Specific surface areas of the samples were lower than 25 m^2 g^{-1}. The acidity (number of acidic sites) per unit of the surface area of the catalysts, as determined by the amount of NH_3 irreversibly adsorbed at a pressure of about 300 mmHg and 200 °C is plotted as a function of the phosphorus content (Figure 3.2.13.). The acidity increased with the phosphorus content up to about P/V=1.6. Since the amount of SO_2 irreversibly adsorbed on the V_2O_5-P_2O_5 catalysts is too small to be measured, the amount of SO_2 reversibly adsorbed at 20°C was used as an index of the basicity. The basicity per surface area unit is also plotted in Figure 3.2.13.

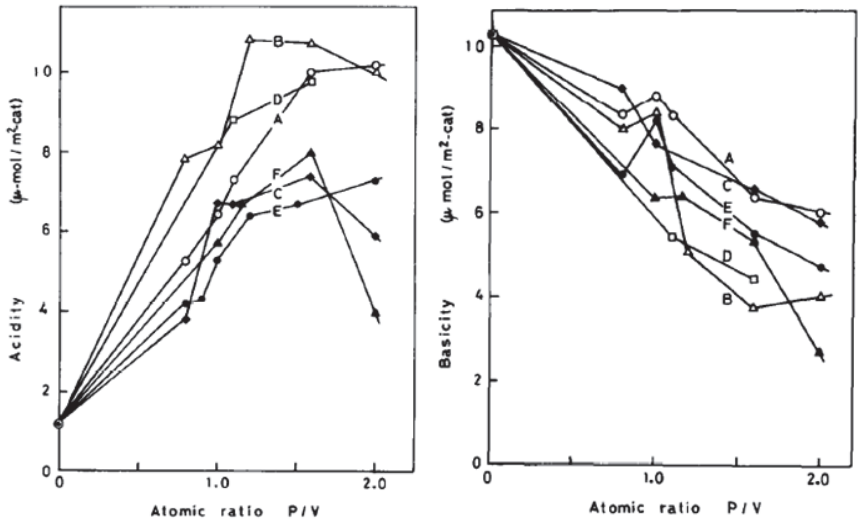

Figure 3.2.13. Acidity (left) and basicity (right) per surface unit as function of different V/P ratios of the V_2O_5-P_2O_5 catalysts. A-F refers to different routes of synthesis. [74]

The tuning of Nb_2O_5 surface acidity was successfully obtained by K^+, Ba^{2+}, and Nd^{3+} doping as reported by Gervasini et al. [75] Three series of doped samples with different amounts of each metal ion on niobic acid (2–15 atoms nm^{-2}, 1–10 atoms nm^{-2}, and 1–6 atoms nm^{-2} for K, Ba, and Nd, respectively) were prepared and characterized by convetional NH_3 adsorption in a volumetric-calorimetric apparatus. Adsorption was carried out at 80 °C, and samples were pretreated under vacuum overnight at 400 °C. Table 3.2.5. summarizes the results obtained from NH_3 adsorption on Nb_2O_5 (NBO) and on the K-, Ba-, and Nd-NBO samples series. The amount of acid sites regularly decreased with increasing K concentration, reaching an acidity decrease of 88% with the highest amount of K addition. A lighter acidity decrease was obtained by Ba-doping. The amount of acid sites of the Ba-series samples decreased with Ba addition up to 54% for the sample with the highest Ba-concentration (Ba10/NBO). The same behavior was observed by doping NBO with Nd. The surface acid strength decreased with the dopant concentration following the order: K>>Ba>Nd. The Q_{int} and Q_{av} values of the Ba and Nd doped samples not much lower than those of NBO, justifying the creation of new Lewis acid sites on the Ba and Nd samples. The three dopants interact with the NBO surface acid sites in different ways. The K-species might act like an ionic exchanger species with the Brønsted acid sites, while the Ba and Nd species might interact with larger portions of the NBO surface, and in particular with the Lewis acid sites. [75]

Table 3.2.5. Intrinsic acidity of the K-, Ba-, and Nd-doped NBO samples and pristine NBO (Nb_2O_5) obtained by NH_3 adsorption from volumetric–calorimetric analysis. [75]

Sample code	Q_{int} ($J\ g^{-1}$)	Q_{av} ($kJ\ mol^{-1}$)	Total acid sites[a] ($\mu mol\ g^{-1}$)	Total acid sites ($\mu mol\ m^{-2}$)
NBO	28	111	250	2.44
K2/NBO	11	89	120 (52%)[b]	1.36
K6/NBO	4.7	66.5	71 (72%)	1.08
K10/NBO	2.3	55	41 (84%)	0.73
K15/NBO	1.0	33	29 (88%)	0.63
Ba1/NBO	22	99	224 (10%)	2.70
Ba2/NBO	17	96	179 (28%)	2.60
Ba4/NBO	17	94	184 (26%)	2.92
Ba6/NBO	14	91.5	155 (38%)	2.87
Ba10/NBO	9.3	81	115 (54%)	2.36
Nd1/NBO	25	103	239 (4%)	3.09
Nd2/NBO	22	102	211 (16%)	2.75
Nd3/NBO	23	99	228 (9%)	3.03
Nd6/NBO	19	86	219 (12%)	3.25

[a] Determined from the adsorption NH_3 isotherm at the intersection point between the straight lines of the low-pressure part and the asymptotic part.
[b] Decrease in the number of acid sites of each doped sample in comparison with that of NBO, in percent.

3.2.2. Bulk and supported Keggin type heteropolyacids

Heteropolyacids (HPAs), due to their unique physicochemical properties, are widely used as homogeneous and heterogeneous acid and oxidation catalysts. Keggin-type HPAs ($H_{8-x}X^xM^{VI}_{12}O_{40}$,

$H_{8-x+n}X_xM^{VI}_{12-n}V^V_n O_{40}$, where X = Si^{IV}, Ge^{IV}, P^V, As^V; M = Mo^{VI}, W^V) are in particular used as catalysts. Their significantly higher Brønsted acidity than the acidity of traditional mineral acid catalysts, is of great importance for catalysis. Numerous spectroscopic, thermal and calorimetric techniques, as well as computational modelization, were used to quantify their acidity. Nowadays, more than 100 heteropolyacids of different compositions and structures are known, but only the Keggin-structure HPAs are well described, in respect to their physicochemical and catalytic properties. [76-78] In this work four Keggin-type heteropolyacids: 12-tungstophosphoric acid ($H_3PW_{12}O_4$-HPW), 12-tungstosilicic acid ($H_4SiW_{12}O_{40}$-HSiW), 12-molybdophosphoric acid ($H_3PMo_{12}O_{40}$-HPMo), and 12-molybdosilicic acid ($H_4SiMo_{12}O_{40}$-HSiMo) were investigated. Moreover, HPW and HSiW supported on silica (labeled HPW/SiO_2 and HSiW/SiO_2, respectively) were synthesized and characterized. HPAs without Keggin-type structure are thermally less stable and therefore cannot be employed for reactions performed at temperatures higher than 150 °C. [76]

The strength and the number of acid centers of the heteropolyanions can be tuned by the structure and composition, extent of hydration, type of support, thermal pretreatment, etc. Considering adsorption microcalorimetry, mostly NH_3 and pyridine were employed as probe molecules to test acidity of heteropolyanions and their salts. According to the results reported, the acidity of HPAs decreases with increasing the anion charge. For the Keggin HPAs, W-HPAs are stronger acids than Mo-HPAs. In general (in terms of Q_{diff}-values) the acidity was reported to decrease in the order HPW>HSiW>HPMo>HSiMo, and with the increasing of the pretreatment temperature (due to decomposition of Keggin structure, which is responsible of the strong acidity). [76-78] Decomposition of the Keggin structure occurs at lower temperatures for molybdenum-containing heteropolyacids. However, after thermal treatment, the Keggin unit can be regenerated in presence of water vapor, and therefore the strong acidity reestablished. [76-79] It was reported that Keggin-type HPW, HSiW, HPMo, and HSiMo decompose at 465, 445, 375, and 350 °C, respectively. [77,80] Bulk HPAs are characterized by low specific surface areas (usually lower than 5 $m^2\ g^{-1}$), therefore supported HPA catalysts are important for application in heterogeneous catalysis. [76]

Liu-Cai et al [81] reported study of unsupported and carbon supported heteropolyacids ($H_3PW_{12}O_{40}$-HPW12, $H_4SiW_{12}O_{40}$-HSiW12, $H_5BW_{12}O_{40}$-HBW12, and $H_{19}B_3W_{39}O_{131}$-HB3W39) pretreated under vacuum overnight at 150 °C by ammonia adsorption microcalorimetry (T_{ads}=150 °C). Plots of the differential sorption heat versus ammonia uptake for the bulk heteropolyacids are shown in Figure 3.2.14. The three samples HPW12, HSiW12, HBW12, in which the anions have the same Keggin structure, showed a very homogeneous distribution of acid sites with the presence of a plateau between 200 kJ mol^{-1} (for HPW12) and 170 kJ mol^{-1} (for HBW12). The acid strength appeared to be rather homogeneous for these three samples, in contrast with the behavior of $H_{19}B_3W_{39}O_{131}$ whose differential heat curve shows a continuous decrease. Moreover, the differential heat was very weak for HB3W39 (Dawson structure), even at low coverage. So the strong acidity of four bulk samples was classified to decrease in the order of HPW12> HSiW12> HBW12>> HB3W39. [81]

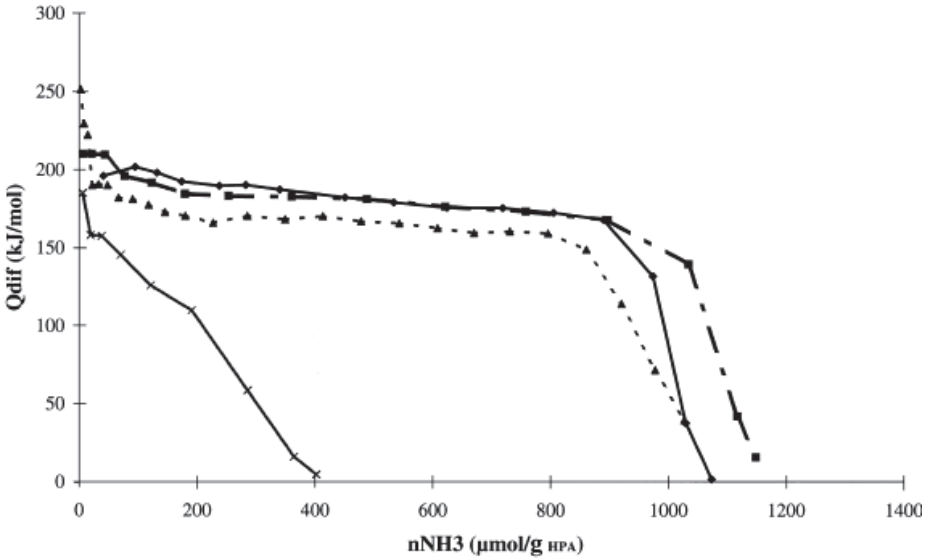

Figure 3.2.14. Differential adsorption heats *vs.* adsorbed amount of ammonia for the bulk heteropolyacids: (♦)HPW12, (■)HSiW12 (▲)HBW12 and (x) HB3W39. [81]

Considering the maximal amount of adsorbed ammonia the authors reported that it does not always correspond to the stoichiometry of the salt. The quantity of acid sites for HPW12 sample determined from data of sorption calorimetry (≈1050 µmol g^{-1} HPA) was in agreement with the theoretical value calculated from the chemical composition (≈1041 µmol g^{-1} HPA). The stoichiometric salt $(NH_4)_3PW_{12}O_{40}$ was formed. However, HSiW12 does not take up the stoichiometric quantity of ammonia (≈1200 µmol g^{-1} HPA, being equivalent to 3.46 H^+ per heteropolyanion), and this amount was considerably smaller for HBW12 (≈1100 µmol g^{-1} HPA being 3.15 H^+ per heteropolyanion. So, the higher the negative charge of heteropolyanions, the greater was the deviation from the theoretical ammonia adsorption. The following explanation was proposed: after a pretreatment at 150 °C overnight, the bonding strength between oxygen atoms and protons was probably enhanced, when the negative charge increased from 3 to 5. At the same time, interactions between the molecules $H_nXW_{12}O_{40}$ in the anhydrous solid were insured by hydrogen bonds and the number of these bonds likely increased with the negative charge of the heteropolyanion. Consequently, the migration of ammonia in the bulk of heteropolyacids became more difficult and deviation from the theoretical ammonia uptake was observed in $H_4SiW_{12}O_{40}$, and became more important with $H_5BW_{12}O_{40}$. The $H_{21}B_3W_{39}O_{132}$ sample adsorbed only ≈400 µmol g^{-1} whereas the theoretical value was 2249 µmol g^{-1}. Such a great difference was explained by its much higher negative charge and specific crystalline structure. Due to the much more compact structure of this sample ammonia did not enter into the bulk and probably reacted only with the protons on the surface and into the few near-surface layers. [81]

The acidity of the carbon supported HPW12 (S_{BET}=200 m^2 g^{-1}), HSiW12 (S_{BET}=260 m^2 g^{-1}) and HBW12 (S_{BET}=380 m^2 g^{-1}), was slightly reduced, while that of $H_{21}B_3W_{39}O_{132}$ was enhanced, compared with the corresponding bulk samples. However, characteristic large plateaus disappeared and heterogeneity in acidity was observed when the heteropolyacids were grafted on carbon support. This behavior could be related to the heterogeneity of adsorption sites on the carbon surface. [81]

Bardin et al [82] studied the acidity and its effects on the reactivity of Keggin-type heteropolycompounds using catalytic test probe reactions, microcalorimetry of ammonia sorption, and density functional quantum chemical calculations. Commercial phosphotungstic (PW), phosphomolybdic (PMo), silicotungstic (SiW), and silicomolybdic (SiMo) acids, and cesium salt ($Cs_2HPW_{12}O_{40}$) were used as model compounds. Generally, results from NH_3 adsorption microcalorimetry (T_{ads}=100 °C) showed that Q_{diff} on tungsten-based heteropolyacids was approximately 40 kJ mol^{-1} higher than the corresponding Q_{diff} obtained on molybdenum-based heteropolyacids (samples pretreated at 200 °C). Residual waters of hydration significantly affected the adsorption enthalpies. Quantum chemical calculations revealed that the most energetically favorable site of the acidic proton is a bridging oxygen atom in the anhydrous heteropolyacid. Calculations on structurally optimized small metal oxide clusters, as well as the complete Keggin unit, were used to determine the proton affinities by DFT methods. Regardless of cluster size, the proton affinity of a tungsten cluster was always lower than that of an analogous molybdenum cluster of about 20-40 kJ mol^{-1}. Small differences in the heat of NH_3 adsorption for PW and SiW were reported. However, PW had a slightly higher heat of ammonia sorption, while SiW displayed a greater uptake of ammonia (since SiW has a greater proton density). $Cs_2HPW_{12}O_{40}$ and PW had similar initial differential heats of NH_3 adsorption, but the total uptake was much lower on $Cs_2HPW_{12}O_{40}$, due to the partial replacement of acidic protons with Cs ions. [82]

These authors [82] also investigated the effect of the pretreatment conditions on the heats of ammonia adsorption (Figure 3.2.15.). PW sample pretreated at 200 °C (473 K) had higher heats of ammonia adsorption than the same sample pretreated at 300 °C (573 K). Figure 3.2.14. also compares the heats of ammonia adsorption over PW and PMo. For samples pretreated at 200 °C, the heat of ammonia sorption was about 70 kJ mol^{-1} higher for PW. PMo evidently decomposed after treatment at 300 °C since the total uptake decreased dramatically. [82]

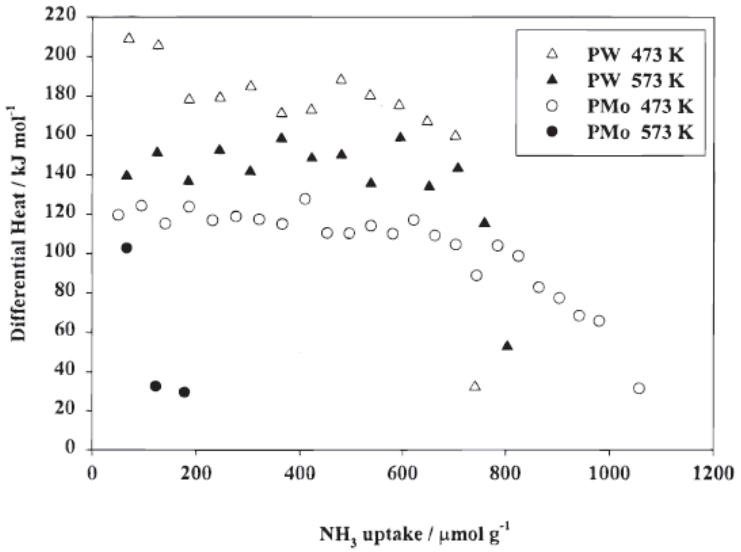

Figure 3.2.15. Comparison of differential heats of NH_3 adsorption *vs*. uptake at 100 °C for PW and PMo samples pretreated at 200 °C (473 K) and 300 °C (573 K). [82]

Microcalorimetric study of NH_3 (T_{ads}=150 °C) and SO_2 (T_{ads}=80 °C) adsorption on 12-tungstophosphoric acid (WPA) and on its alkaline earth salts (labeled as BeHWPA, MgHWPA, CaHWPA, SrHWPA, SrHWPA, BaHWPA) was reported by Damjanović et al. [83] Prior to probe molecule adsorption samples were pretreated overnight at 300 °C under vacuum. SO_2 was not adsorbed on any of the samples investigated. In Figure 3.2.16. differential heats of ammonia as a function of coverage for different alkaline earth salts and parent acid are shown. As a result of substitution of two protons with one alkaline earth cation, a decrease of both the total number of acid sites and the number of the strongest acid sites characterized by differential heats higher then 150 kJ mol^{-1}, compared to the values found in the case of initial 12 tungstophosphoric acid (WPA), was observed. While all protons seemed accessible for ammonia in Mg, Ca and Ba salts, in the case of Sr salt less then stoichiometric ammonia sorption was detected, which can be explained by the steric effect of these divalent cations. [83]

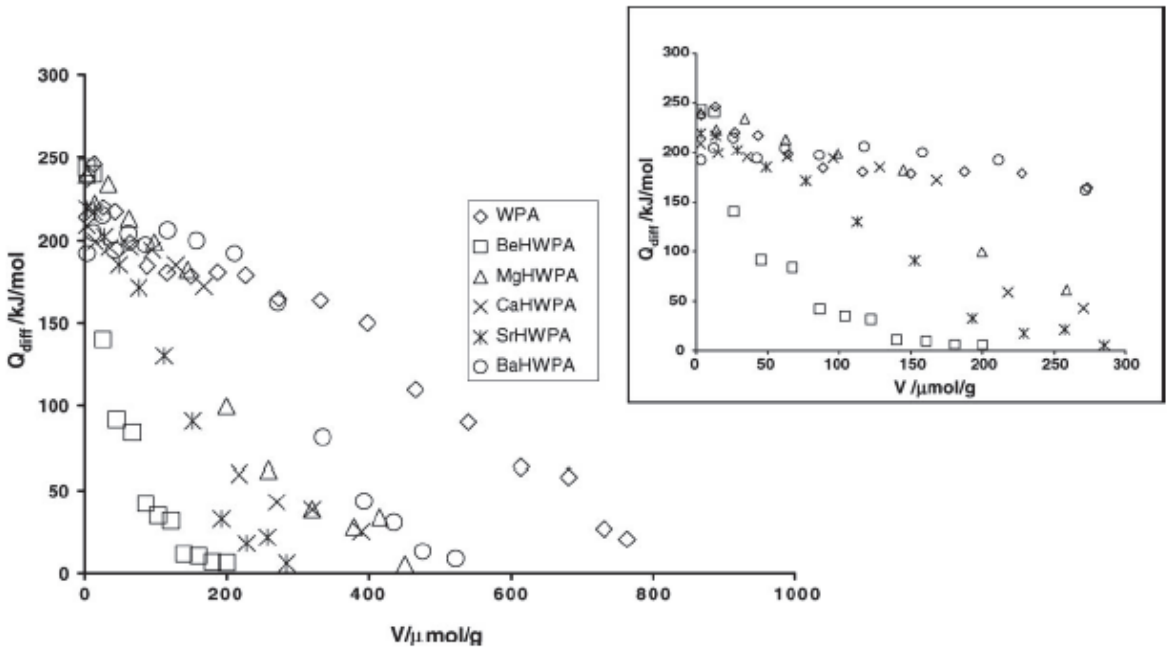

Figure 3.2.16..Differential heats of ammonia as a function of coverage for the different alkaline earth salts and parent acid. Inset shows expanded differential heat curves. [83]

Phosphomolybdic acid ($H_3PMo_{12}O_{40}$) along with niobium ($NbPMo_{12}O_{40}$), pyridine ($PMo_{12}O_{40}$pyr) and niobium/pyridine ($NbPMo_{12}O_{40}$pyr) exchanged phosphomolybdic acid compounds were prepared by Bommineni and co-authors [84], and characterized using ammonia adsorption calorimetry at room temperature. Samples were pretreated at 420 °C under vacuum. Ammonia adsorption microcalorimetry results are shown in Figure 3.2.17. The initial heat of adsorption for the $H_3PMo_{12}O_{40}$ parent catalyst was around 80 kJ mol^{-1} and decreased almost linearly to 0 kJ mol^{-1} with a total ammonia uptake of approximately 130 μmol g^{-1}. Incorporation of niobium, pyridine, or both, to the parent catalyst increased the number of adsorption sites and the initial heat of adsorption (from about 40 kJ mol^{-1} to 120 kJ mol^{-1}). From an initial value of 120 kJ mol^{-1}, the $PMo_{12}O_{40}$pyr heat of adsorption

decreased to ~50 kJ mol^{-1} beyond 300 µmol g^{-1} uptake. Similarly, the $NbPMo_{12}O_{40}$ heat curve decreased to a fairly constant 60 kJ mol^{-1} beyond 200 µmol g^{-1} uptake. Finally, both niobium and pyridine resulted in a heat of adsorption of ~80 kJ mol^{-1} beyond 200 µmol g^{-1} uptake. After the initial 50 µmol g^{-1} uptake, the catalyst with both niobium and pyridine typically had an ammonia adsorption strength ~10 kJ mol^{-1} stronger than the catalysts containing either Nb or pyridine. [84]

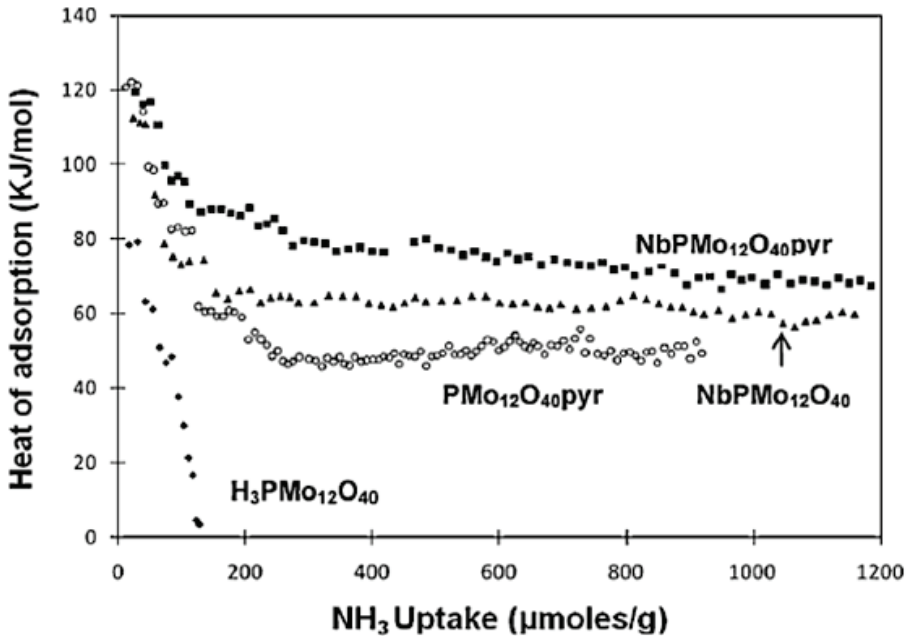

Figure 3.2.17. NH_3 uptake and heat of adsorption of the catalysts activated at 420 °C. [84]

The results of HPA acidity measurement by microcalorimetry of NH_3 adsorption were reported by Shikata et al [85] on different heteropolyanions including, among others, $H_3PW_{12}O_{40}$, $H_4SiW_{12}O_{40}$, and $H_6P_2W_{18}O_{62}$. The acid strength decreased in order: $H_3PW_{12}O_{40}$>$H_4SiW_{12}O_{40}$>$H_6P_2W_{18}O_{62}$. An interesting fact was, as observed by Timofeeva [76], that the acid strength of $H_6P_2W_{18}O_{62}$ was almost unchanged when supported on SiO_2. The acidic strength of 20% $H_6P_2W_{18}O_{62}/SiO_2$ and 20%$H_3PW_{12}O_{40}/SiO_2$ were closer. [85] This result was surprising because when $H_6P_2W_18O_{62}$ was supported on SiO_2 or carbon, the strength of the acidic centers decreased due to strong interaction with the support. Such result was probably caused by the high temperature of pre-activation of $H_6P_2W_{18}O_{62}/SiO_2$ (200 °C under vacuum), which results in isomerization and partial degradation of $H_6P_2W_{18}O_{62}$. [76,85]

Stošić and co-authors [53] reported on NH_3 and SO_2 microcalorimetric studies on HPW/TiO_2 (10wt% of HPW; S_{BET}=40 m^2 g^{-1}) and HPW/WO_3-ZrO_2 (4 wt% of HPW; S_{BET}=45 m^2 g^{-1}). Temperature of adsorption was 150 °C and the samples were pretreated overnight under vacuum at 300 °C. Considering SO_2 adsorption, relatively low amount of probe molecule was adsorbed, and HPW/TiO_2 had slightly more basic character than HPW/ WO_3-ZrO_2. For HPW/WO_3-ZrO_2 the total amount of acidic sites was only 0.13 µmol m^{-2} , while the amount of strong basic sites was 0.09 µmol m^{-2}. For HPW/TiO_2 V_{total} and V_{irrev} were 0.20 and 0.15 µmol m^{-2}, respectively. These samples showed relatively

strong acidity and the total amount of acidic sites determined was 2.73 and 2.61 μmol m^{-2} for HPW/WO_3-ZrO_2 and HPW/TiO_2, respectively . HPW/TiO_2 possessed more strong acidic sites (1.85 μmol m^{-2}) than HPW/WO_3-ZrO_2 (1.41 μmol m^{-2}). [53]

References

[1] E. Dumitriu, V. Hulea, C. Chelaru, C. Catrinescu, D. Tichit, R. Durand, *Appl. Catal. A: Gen.* **1999**, *178*, 145-157.

[2] M. Ai, *Bull. Chem. Soc. Jpn.* **1991**, *64*, 1342-1345.

[3] H.Schulz, H. Wagner, *Angew. Chem.* **1950**, *62*, 105-118.

[4] S. Malinowski, S. Basinski, *J. Catal.* **1963**, *2*, 203-207.

[5] S. Malinowski, W.J. Palion, *React. Kinet. Catal. Lett.* **1974**, *1*, 73-78.

[6] M. Ai, *Bull. Chem. Soc. Jpn.* **1991**, *64*, 1346-1350.

[7] E. Dumitriu, V. Hulea, N. Bilba, G. Carja, A. Azzouz, *J. Mol. Catal.* **1993**, *79, 175-185.*

[8] V. Hulea, D. Tichit. C. Catrinescu, E. Dumitriu, *An. Stiint. Univ. Al. I. Cuza Iasi* **1997**, *5*, 185-192.

[9] A. Azzouz, D. Messad, D. Nistor, C. Catrinescu, A. Zvolinschi, S. Asaftei, *Appl. Catal. A: Gen.* **2003**, *241,* 1–13.

[10] E. Dumitriu, C. Cobzaru, V. Hulea, S. Oprea, *Rev. Chim. (Bucharest, Romania)* **2010**, *61(4)*, 400-403.

[11] M. Ai, *Appl. Catal.***1991**, *77,* 123-132.

[12] W.J. Palion, S. Malinowski, *React. Kinet. Catal. Lett.* **1974**, *1*(4), 461-465.

[13] Patent CN 102600827 A *(Priority date 08/01/2011)*.

[14] E. Dumitriu, N. Bilba, M. Lupascu, A. Azzouz, V. Hulea, G. Cirje, D. Nibou, *J. Catal.* **1994**, *147,* 133-139.

[15] E. Dumitriu, V. Hulea, I. Fechete, A. Auroux, J. F. Lacaze, C. Guimon*, Microporous Mesoporous Mater.* **2001**, *43*, 341-359.

[16] C. Cobzaru, S. Oprea, E. Dumitriu, V. Hulea, *Appl. Catal. A: Gen.* **2008**, *351*, 253–258.

[17] A. Ungureanu, S. Royer, T.V. Hoang, D. Trong On, E. Dumitriu, S. Kaliaguine, *Microporous Mesoporous Mater.* **2005**, *84*, 283–296.

[18] S. Malinowski, H. Jablczynska-Jedrzejewska, S. Basinski, S. Benbenek, *Chim. Ind. (Paris)*, **1961**, *85*, 885.

[19] J. Shen, J.M. Kobe, Y. Chen, J.A. Dumesic, *Langmuir* **1994**, *10*, 3902-3908.

[20] J. Shen, M. Tu, C. Hu, *J. Solid State Chem.* **1998**, *137*, 295-301.

[21] *Calorimetry and Thermal Methods in Catalysis* (Ed.: A. Auroux), Springer, Berlin, **2013**.

[22] Lj. Damjanović, A. Auroux, Chapter 11: *Heterogeneous Catalysis on Solids* in *Handbook of Thermal Analysis and Calorimetry* ,Vol. 5: Recent Advances, Techniques and Applications (Eds.: M.E. Brown, P.K. Gallagher), Elsevier, Amsterdam, **2008**.

[23] A. Auroux, *Top. Catal.* **2002**, *19,* 205-213.

[24] S. Bennici, A. Auroux, *Thermal Analysis and Calorimetric Methods* in *Metal Oxide Catalysis,* Vol.1(Eds.: S. David Jackson, J.S.J. Hargreaves), Wiley-VCH Verlag GmbH & Co. KGaA, Weinheim, **2009**.

[25] A. Auroux, *Top. Catal.* **1997**, *4*, 71-98.

[26] H. Petitjean, K. Tarasov, F. Delbecq, P. Sautet, J.M. Krafft, P. Bazin, M.C. Paganini, E. Giamello, M. Che, H. Lauron-Pernot, G. Costentin, *J. Phys. Chem. C* **2010**, *114*, 3008-3016.

[27] V. Bolis, C. Busco, V. Aina, C. Morterra, P. Ugliengo, *J. Phys. Chem. C* **2008**, *112*, 16879-16892.

[28] M. Tu, J. Shen, Y. Chen, *Thermochim. Acta* **1997**, *302*, 117-124.

[29] H. Chen, M. Xue, S. Hu, J. Shen, *Chem. Eng.J.* **2012**, *181-182*, 677-684.

[30] S. Hu, M. Xue, H. Chen, J. Shen, *Chem. Eng. J.* **2001**, *162*, 371-379.

[31] J. Zhao, M. Xue, Y. Huang, J. Shen, *Catal. Commun.* **2011**, *16*, 30-34.

[32] A. Auroux, A. Gervasini, *J. Phys. Chem.* **1990**, *94*, 6371-6379.

[33] A. Gervasini, A. Auroux, *J. Therm. Anal.* **1991**, *37*, 1737-1744.

[34] Y.S. Jin, A. Ouquir, A. Auroux, J.C. Védrine, *Molybdena on Niobium Oxide Catalysts : Preparation and Characterization* in *Structure and Reactivity of Surfaces* (Eds.: C. Morterra, A. Zecchina, G. Costa), Elsevier, Amsterdam, 1989.

[35] N. Cardona-Martinez, J.A. Dumesic, *J.Catal.* **1991**, *127*, 706-718.

[36] P.F. Rossi, G. Caracciolo, G. Busca, *Colloids Surf.* **1988**, 32, 75-85.

[37] P.F. Rossi, G. Busca, V. Lorenzelli, M. Lion, J.C. Lavalley, *J. Catal* **1988**, *109*, 378-386.

[38] M.Xue, H. Chen, J. Ge, J.Shen, *Microporous Mesoporous Mater.* **2010***, 131,* 37-44*.*

[39] J. Le Bars, A. Auroux, J.C. Védrine, M. Baerns, *Microcalorimetric studies of the oxidative dehydrogenation of ethane over vanadium pentoxide catalysts* in *New Developments in Selective Oxidation by Heterogeneous Catalysis*: Studies in Surface Science *arid Catalysis,* Vol. 12, (Eds.: P. Ruiz, B. Delmon), Elsevier, Amsterdam, **1992**.

[40] J. Le Bars, J.C. Védrine, A. Auroux, S. Trautmann, M. Baerns, Appl. *Catal. A: Gen.* **1992***, 88,* 179-195.

[41] A. Gervasini, P. Carniti, J. Keränen, L. Niinistö, A. Auroux, *Catal. Today* **2004**, *96*, 187-194.

[42] J. Keränen, A. Auroux, S. Ek-Härkönen, L. Niinistö, *Thermochim. Acta*, **2001**, *379*, 233-239.

[43] J. Keränen, A. Auroux, S. Ek, L. Niinistö, *Appl. Catal., A : Gen.* **2002**, *228*, 213-225.

[44] J. Le Bars, J.C. Védrine, A. Auroux, S. Trautmann, M. Baerns, *Appl. Catal., A: Gen.* **1994**, *119,* 341-354.

[45] Q.Sun, D. Fang, S. Wang, J. Shen, A. Auroux, *Appl. Catal., A: Gen.* **2007***, 327,* 218-225.

[46] H. Zhao, S. Bennici, J. Shen, A. Auroux, *J. Mol. Catal. A: Chem.* **2009**, *309*, 28-34.

[47] H. Zhao, S. Bennici, J. Cai, J. Shen, A. Auroux, *Cat. Today* **2010***, 152,* 70-77.

[48] L. Chen, J. Shen, *Chin. J. Catal.* **2012**, *33,* 621-628.

[49] H. Chen, M. Xue, S. Hu, J. Shen, *Chem. Eng. J.* **2012**, *181-182*, 677-684.

[50] D. Stošić, S. Bennici, J.L. Couturier, J.L. Dubois, A. Auroux, *Catal. Commun.* **2012**, *17*, 23-28.

[51] V. Bolis, G. Cerrato, G. Magnacca, C. Morterra, *Thermochim. Acta* **1988**, *312*, 63-77.

[52] A. Gervasini, P. Carniti, A. Auroux, *Thermochim. Acta* **2005**, *434*, 42-49.

[53] D. Stošić, S. Bennici, S. Sirotin, P. Stelmachowski, J.-L. Couturier, J-L. Dubois, A. Travertb, A. Auroux, *Catal. Toda*y **2014**, *226*, 167-175.

[54] A. Auroux, J.C. Védrine in *Catalysis by Acids and Bases* (Eds.: B. Imelik, C. Naccache, G. Coudurier, Y.B. Taarit, J.C. Védrine), Elsevier, Amsterdam, **1985**, 311-318.

[55] A. Gervasini, G. Bellussi, J. Fenyvesi, A. Auroux, in *New Frontiers in Catalysis* (Eds.: Guczi L *et al.*), Elsevier, Amsterdam, **1993**.

[56] T. Masuda, H. Taniguchi, K. Tsutsumi, H. Takahashi, *Bull. Chem. Soc. Jpn.* **1978**, *51*, 1965-1969

[57] N. Cardona-Martinez, J.A. Dumesic, *J. Catal.* **1991**, *128*, 23-33.

[58] A. Auroux, R. Monaci, E. Rombi, V. Solinas, A. Sorrentino, E. Santacesaria, *Thermochim. Acta*. **2001**, *379*, 227-231.

[59] N. Cardona-Martinez, J.A. Dumesic, *J. Catal.* **1990**, *125*, 427-444.

[60] M.A. Natal-Santiago, J.A. Dumesic, *J. Catal.* **1998**, *175*, 252-268.

[61] V. Bolis, A. Cavenago, B. Fubini, *Langmuir* **1997**, *13*, 895-902.

[62] G. Busca, P.F. Rossi, V. Lorenzelli, M. Benaissa, J. Travert, J.C. Lavalley, *J. Phys. Chem.* **1985**, *89*, 5433-5439.

[63] M. Benaissa, O. Saur, J.C. Lavalley, *Materials Chemistry* **1982**, *7*, 699-714.

[64] M. León, L. Faba, E. Díaz, S. Bennici, A.Vega, S. Ordóñez, A. Auroux, *Appl. Catal. B.* **2014**, *147*, 796-804.

[65] C. Pighini, T. Belin, J. Mijoin, P. Magnoux, G. Costentin, H. Lauron-Pernot, *Appl. Surf. Sci.* **2011**, *257*, 6952-6962.

[66] V. Bolis, C. Busco, V. Aina, C. Morterra, P. Ugliengo, *J. Phys. Chem. C* **2008**, *112*, 16879-16892.

[67] H.A. Prescott, Z.J. Li, E. Kemnitz, A. Trunschke, J. Deutsch, H. Lieske, A. Auroux, J. Catal. **2005**, *234*, 119-130.

[68] F. Hosoglu, PhD thesis, University Lille 1 (FR), **2012**.

[69] D. Stošić, F. Hosoglu, S. Bennici, A. Travert, M. Capron, F. Dumeignil, J.L. Couturier, J.L. Dubois, A. Auroux, *Catal. Comm.* **2017**, *89*, 14-18.

[70] M. León, E. Díaz, A. Vega, S. Ordóñez, A. Auroux, *Appl. Catal. B.* **2011**, *102*, 590-599.

[71] S. Casenave, H. Martinez, C. Guimon, A. Auroux, V. Hulea, A. Cordoneau, E. Dumitriu, *Thermochim. Acta*, **2001**, *379,* 85-93.

[72] L. Dussault, J.C. Dupin, E. Dumitriu, A. Auroux, C. Guimon, *Thermochim. Acta*, **2005**, *434*, 93-99.

[73] D. Meloni, R. Monaci, M. G. Cutrufello, E. Rombi, I. Ferino, *J. Therm. Anal. Calorim.* **2015**, *119*, 1023-1036.

[74] M. Ai, *J. Catal* **1986**, *100*, 336-344.

[75] A. Gervasini, P. Carniti, M. Marzo, A. Auroux, *J. Catal* **2012**, *296*, 143-155.

[76] M.N. Timofeeva, *Appl. Catal., A: Gen.* **2003**, *256*, 19-35.

[77] I.V. Kozhevnikov, *Chem. Rev.* **1998**, *98*, 171-198.

[78] J.B. Moffat, *Metal-Oxygen Clusters: The Surface and Catalytic Properties of Heteropoly Oxometalates*, Kluwer Academic Publishers, New York, **2002**.

[79] F. Cavani, R. Mezzogori, A. Pigamo, F. Trifiro, E. Etienne, *Cat. Today* **2001**, *71*, 97-110.

[80] G.I. Kapustin, T.R. Brueva, A.L. Klyachko, M.N. Timofeeva, S.M. Kulikov, I.V. Kozhevnikov, *Kinet. Katal.* **1990**, *31*, 1017.

[81] F.X. Liu-Cai, B. Sahut, E. Fayadi, A. Auroux, G. Hervé, *Appl. Catal., A : Gen.* **1999**, *185*, 75-83.

[82] B.B. Bardin, S.V. Bordawekar, M. Neurock, R.J. Davis, *J. Phys. Chem. B* **1998**, *102,* 10817-10825.

[83] Lj. Damjanović, V. Rakić, U.B. Mioč, A. Auroux, *Thermochim. Acta* **2005**, *434*, 81-87.

[84] S. Bommineni, M.D. Skoglund, A.R. Morris, E.J. Doskocil, J.H. Holles*, Appl. Catal., A : Gen.* **2013**, *467*, 202-210.

[85] S. Shikata, T. Okuhara, M. Misono, *J. Mol. Catal. A: Chem.* **1995***, 100*, 49.

Chapter 4.

Experimental part

This chapter describes the preparation methods of catalytic materials and experimental techniques used during the PhD experiments. Emphasis is given on the gas-solid adsorption microcalorimetry technique, the main technique used during catalytic materials investigation.

4.1. Catalyst preparation

The catalysts used in this work are divided in two major groups: the catalysts used for isobutene oxidation, and the catalysts used in the process of acrolein synthesis.

4.1.1. Catalysts involved in isobutene oxidation

4.1.1.1. Bulk oxides

Nickel oxide (NiO) was synthesized by precipitation method. Ammonium hydroxide solution (14.5 M; Sigma-Aldrich) was added dropwise to 0.6 M $Ni(NO_3)_2 \cdot 6H_2O$ (Sigma-Aldrich) aqueous solution at room temperature until pH 9. The obtained light green precipitate $Ni(OH)_2$ was separated and washed with 1:1 ratio water-ethanol solution several times. It was then dried in an oven at 110 °C overnight and finally calcined at 500 °C for 5h in air flow. [1,2]

Bismuth oxide (Bi_2O_3) was prepared via precipitation method using bismuth trinitrate pentahydrate (Sigma-Aldrich) as precursor and sodium hydroxide (CHIMIE-PLUS Laboratoires) as precipitating agent. $Bi(NO_3)_3 \cdot 5H_2O$ was dissolved in concentrated nitric acid (15.9 M; Sigma-Aldrich) to prepare a 0.1 M solution. NaOH (1 M) was added dropwise in the Bi-containing solution under continuous stirring until pH=12. The obtained precipitate was aged in distilled water for 1h and then washed with distilled water several times. The solid was then dried overnight at 110 °C and calcined at 450 °C for 5h in air. [3]

For preparation of molybdenum oxide (MoO_3) a precipitation method was applied using ammonium molybdate tetrahydrate (Sigma-Aldrich) and hydrochloric acid (Sigma-Aldrich). A 4 M HCl solution was added to a $(NH_4)_6Mo_7O_{24} \cdot 4H_2O$ aqueous solution (0.1 M) until pH reached the 1.8 value. Then the white precipitate obtained was added to 50 ml of water and magnetically stirred. The obtained homogeneous mixture was then placed into a Teflon lined autoclave for 8h. When the

hydrothermal treatment was completed, the white solid powder obtained was centrifuged and rinsed with distilled water until chloride ions were completely removed (checked with silver ions). The powder was dried during 4h and finally calcined in air flow at 500 °C for 5h. [4-6]

Iron (III) oxide (Fe_2O_3) was precipitated by adding dropwise a 1 M solution of NaOH (CHIMIE-PLUS Laboratoires) to a 0.625 M solution of $FeCl_3 \cdot 6H_2O$ (Sigma-Aldrich) under continuous stirring and until pH=5 at room temperature. The obtained precipitate was aged in a Teflon lined autoclave during 3 days at 90 °C, then calcined in air at 400 °C for 4h. [7]

V_2O_5 and V_2O_4 oxides were purchased from Sigma-Aldrich.

4.1.1.2. Bulk heteropolyacids

12-tungstophosphoric acid ($H_3PW_{12}O_4$-HPW; Sigma-Aldrich), 12-tungstosilicic acid ($H_4SiW_{12}O_{40}$-HSiW; Sigma-Aldrich), 12-molybdophosphoric acid ($H_3PMo_{12}O_{40}$-HPMo; Alfa Aesar), and 12-molybdosilicic acid ($H_4SiMo_{12}O_{40}$-HSiMo; Strem) were used as bulk Keggin-type samples.

4.1.2. Catalysts involved in acrolein synthesis

4.1.2.1. Basic oxides supported on silica and alumina

Na_2O/SiO_2 (3.8 wt% of Na), K_2O/SiO_2 (5.2 wt% of K), CaO/SiO_2 (5.6 wt% of Ca), MgO/SiO_2 (3.7 wt% of Mg) catalysts were prepared by mixing the aqueous solutions of NaOH (VWR Chemicals), KOH (VWR Chemicals), $Ca(NO_3)_2 \cdot 4H_2O$ (Fluka), and $Mg(NO_3)_2 \cdot 6H_2O$ (Sigma-Aldrich), respectively, with colloidal silica Ludox TMA (Sigma-Aldrich) and evaporation in a rotavapor during 3h (50 °C, 1mbar). The salt solutions were prepared in order to obtain a theoretical bulk metal/silicon molar ratio of 0.1. The dried powders were calcined at 500 °C in N_2 atmosphere for 4h and labeled: Na/Si, K/Si, Ca/Si, Mg/Si for the catalysts, and SiO_2 for the bare support.

In order to prepare the MgO/Al_2O_3 (Mg/Al molar ratio 0.1) sample, commercial Al_2O_3 (Saint-Gobain NorPro) was impregnated by $Mg(NO_3)_2 \cdot 6H_2O$ (Sigma-Aldrich) in aqueous solution. The obtained wet powder was then dried in a rotavapor and calcined under air-flow at 550 °C for 8 h. Commercial MgO (Sigma-Aldrich) was calcined at 550 °C in air-flow for 8 h, while commercial Al_2O_3 (Saint-Gobain NorPro) was calcined for 6 h under air at 550 °C.

4.1.2.2. Mixed Mg/Al oxides (CHTs)

CHT samples with various Mg/Al molar ratios were obtained from the calcination of different commercial fresh Pural catalysts. CHT Mg/Al 0.06 catalyst was obtained by calcining commercial fresh catalyst Pural MG 5 (Sasol, Hydrotalcite, 4.3 wt% MgO and 95.7 wt% Al_2O_3) in air atmosphere at 550 °C for 8 h. Pural MG 20 (Sasol, Hydrotalcite, 18.7 wt% MgO and 81.3 wt% Al_2O_3) was calcined in the same conditions to give CHT Mg/Al 0.3 catalyst. CHT Mg/Al 0.5 and CHT Mg/Al 3 catalysts were obtained from commercial fresh catalyst Pural MG 30 (Sasol, Hydrotalcite, 28.8 wt% MgO and 71.2 wt% Al_2O_3) and Pural MG 70 (Sasol, Hydrotalcite, 68.8 wt% MgO and 31.7 wt% Al_2O_3), respectively.

4.1.2.3. Silica-supported heteropolyacids

10 wt% HPW/SiO_2 and 10 wt% HSiW/SiO_2 catalysts were prepared by wet impregnation method. Aqueous solutions of $H_3PW_{12}O_4$ (HPW) and $H_4SiW_{12}O_{40}$ (HSiW) (Sigma-Aldrich) were mixed with silica from evaporated colloidal solution (Ludox TMA, Sigma-Aldrich) and dried in a rotary evaporator during 3h (50 °C, 1mbar). The dried powders were calcined at 350 °C in air atmosphere for 4h and labeled: HPW/SiO_2 and HSiW/SiO_2. The calcination temperature was chosen in order to preserve the Keggin structure of heteropolyacids.

4.1.2.4. Various catalysts

NbP commercial catalyst (CBMM) was calcined in air atmosphere (450 °C) during 6h. Commercial ZrO_2 (4.3 wt% SiO_2, 17 wt% HfO_2, Saint-Gobain NorPro) has been used in this study as received. Commercial $FeMoO_x$ catalyst was used, while the other FeMo-like catalysts were synthesized in *UCCS Lille*.

4.1.3. List of catalytic materials

Table 4.1.3.1. Bulk single and mixed oxides used in this work.

Catalyst	Composition (wt%)	Preparation method	Precursors	Calcination temp.[a] (°C)	Chapter
NiO	-	Precipitation	$Ni(NO_3)_2{\cdot}6H_2O$, NH_4OH	500	V
Bi_2O_3	-	Precipitation	$Bi(NO_3)_3{\cdot}5H_2O$, NaOH	450	V
MoO_3	-	Precipitation	$(NH_4)_6Mo_7O_{24}{\cdot}4H_2O$, HCl	500	V
Fe_2O_3	-	Precipitation	$FeCl_3{\cdot}6H_2O$, NaOH	400	V
V_2O_5	-	Commercial, Sigma-Aldrich	-	-	V
V_2O_4	-	Commercial, Sigma-Aldrich	-	-	V
SiO_2	-	Evaporated from colloidal silica Ludox TMA	Ludox TMA (Sigma-Aldrich)	500	VI
Al_2O_3	-	Commercial, Saint-Gobain NorPro	-	550	VII
MgO	-	Commercial, Sigma-Aldrich	-	550	VII
ZrO_2	78 wt% ZrO_2, 4.3 wt% SiO_2, 17 wt% HfO_2	Commercial, Saint-Gobain NorPro	-	-	VII
NbP	49.1 wt% Nb, 10.6 wt% P, 1.6wt% K	Commercial, CBMM	-	450	VII
$FeMoO_x$	Confidential	Commercial catalyst	-	-	VI

[a] All catalysts were calcined in air.

Table 4.1.3.2. Mixed Mg/Al oxides derived from hydrotalcites (CHTs).

Catalyst	Composition (wt%)	Preparation method	Precursors	Calcination temp.[a] (°C)	Chapter
CHT Mg/Al 0.06	2.6 wt% Mg, 46.1 wt% Al	Thermal decomposition of commercial hydrotalcite	Pural MG 5 (Sasol) 4.3 wt% MgO, 95.7 wt% Al_2O_3	550	VII
CHT Mg/Al 0.3	9.4 wt% Mg, 39.5 wt% Al	Thermal decomposition of commercial hydrotalcite	Pural MG 20 (Sasol) 18.7 wt% MgO, 81.3 wt% Al_2O_3	550	VII
CHT Mg/Al 0.5	14.2 wt% Mg, 30.9 wt% Al	Thermal decomposition of commercial hydrotalcite	Pural MG 30 (Sasol) 28.8 wt% MgO, 71.2 wt% Al_2O_3	550	VII
CHT Mg/Al 3	33.3 wt% Mg, 16.0 wt% Al	Thermal decomposition of commercial hydrotalcite	Pural MG 70 (Sasol) 68.8 wt% MgO, 31.7 wt% Al_2O_3	550	VII

[a]All catalysts were calcined in air.

Table 4.1.3.3. Bulk and silica-supported heteropolyacids.

Catalyst	Preparation method	Precursors	Calcination temp.[a] (°C)	Chapter
HPW	Commercial $H_3PW_{12}O_4$ (Sigma-Aldrich)	-	-	V
HSiW	Commercial $H_4SiW_{12}O_{40}$ (Sigma-Aldrich)	-	-	V
HPMo	Commercial $H_3PMo_{12}O_{40}$ (Alfa Aesar)	-	-	V
HSiMo	Commercial $H_4SiMo_{12}O_{40}$ (Strem)	-	-	V
HPW/SiO_2	Impregnation	$H_3PW_{12}O_4$, SiO_2-evaporated from Ludox TMA (Sigma-Aldrich)	350	VII
$HSiW/SiO_2$	Impregnation	$H_4SiW_{12}O_{40}$, SiO_2-evaporated from Ludox TMA (Sigma-Aldrich)	350	VII

[a]All catalysts were calcined in air.

Table 4.1.3.4. Silica and alumina-supported basic oxides.

Catalyst	Composition (wt%)	Preparation method	Precursors	Calcination temp.[a] (°C)	Chapter
Na/Si	3.8 wt% Na	Impregnation	NaOH (VWR Chemicals), SiO_2 evaporated from Ludox TMA (Sigma-Aldrich)	500	VI
K/Si	5.2 wt% K	Impregnation	KOH (VWR Chemicals), SiO_2 evaporated from Ludox TMA (Sigma-Aldrich)	500	VI
Ca/Si	5.6 wt% Ca	Impregnation	$Ca(NO_3)_2{\cdot}4H_2O$ (Fluka), SiO_2 evaporated from Ludox TMA (Sigma-Aldrich)	500	VI
Mg/Si	3.7 wt% Mg	Impregnation	$Mg(NO_3)_2{\cdot}6H_2O$ (Sigma-Aldrich), SiO_2 evaporated from Ludox TMA (Sigma-Aldrich)	500	VI
MgO/Al_2O_3	3.9 wt% Mg, 45.4 wt% Al	Impregnation	$Mg(NO_3)_2{\cdot}6H_2O$ (Sigma-Aldrich), Al_2O_3 (Saint-Gobain NorPro)	550	VII

[a]All samples were calcined in air.

4.2. Characterization of the catalysts

Different techniques were used to characterize the physico-chemical properties of the catalytic materials used in this thesis.

4.2.1. X-ray diffraction (XRD)

X-ray diffraction is a non-destructive method for the structural characterization of powders which allows the identification of bulk phases, crystallographic structures, and estimation of the rate of crystallinity of the solid and atomic spacing. The crystalline substances act as three-dimensional diffraction gratings for X-ray wavelengths similar to the spacing of planes in a crystal lattice.

X-ray diffraction is based on constructive interferences of monochromatic X-rays sent on a crystalline sample. These X-rays are generated by a cathode ray tube, filtered to produce monochromatic radiation, collimated to concentrate, and directed towards the sample. The interaction of the incident rays with the sample produces constructive interferences (and a diffracted ray) when conditions satisfy Bragg's Law:

$$n\lambda = 2d_{hkl} \sin \theta$$

where the integer n is the order of the diffracted beam, λ is the wavelength of the incident X-ray beam, d is the distance between adjacent planes of atoms (the d-spacings), and θ is the angle of incidence of the X-ray beam. [8] Figure 4.2.1. presents the X-ray diffraction from a set of planes. This law relates the wavelength of electromagnetic radiation to the diffraction angle and the lattice spacing in a crystalline sample. The diffracted X-rays are then detected, processed and counted. By scanning the sample through a range of 2θ angles, all possible diffraction directions of the lattice should be attained due to the random orientation of the powdered material. Conversion of the diffraction peaks to d-spacings allows identification of the mineral because each mineral has a set of unique d-spacings. Typically, this is achieved by comparison of d-spacings with standard reference patterns.

All diffraction methods are based on generation of X-rays in an X-ray tube. These X-rays are directed at the sample, and the diffracted rays are collected. A key component of all diffraction is the angle between the incident and diffracted rays. Powder and single crystal diffraction vary in instrumentation beyond this. [9]

XRD patterns were recorded at the *IRCELYON XRD Analysis Service* on a Bruker D8 ADVANCE A25 diffractometer at room temperature using Cu Kα radiation (0.154 nm) from 4 to 80° in 0.02° steps with 0.5 s per step. Phase identification was performed using DiffracSuite Eva software (Bruker) and the ICDD-PDF4+ database.

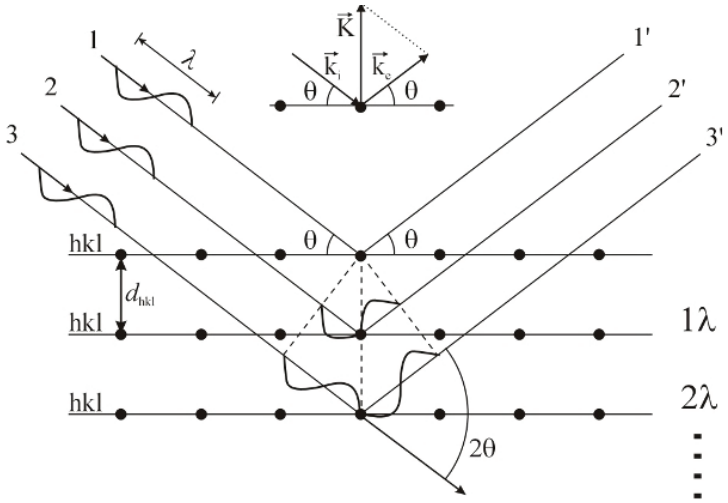

Figure 4.2.1. Diffraction from a set of planes. [10]

4.2.2. Chemical analysis (ICP-OES)

Chemical analyses of all the elements present in the various catalysts were performed by *IRCELYON Textural and Chemical Analysis Servic*e by using inductively coupled plasma-optical emission spectroscopy (ICP–OES) with an ACTIVA spectrometer from Horiba JOBIN YVON. Each measurement was made twice to avoid errors. The measurements were made after dissolution of the sample powder in a mixture of the appropriate acids for the analysis of desired element and injection of the solution into the spectrometer. Excited atoms and ions produced from each element emit a characteristic radiation whose intensity is measured. This intensity is then correlated to the amount of each element. Figure 4.2.2. represents the principle of ICP-OES analysis. The amount of carbon was determined after measuring thermal conductivity of the catalysts at *ISA (Institut des Sciences Analytiques de Lyon).*

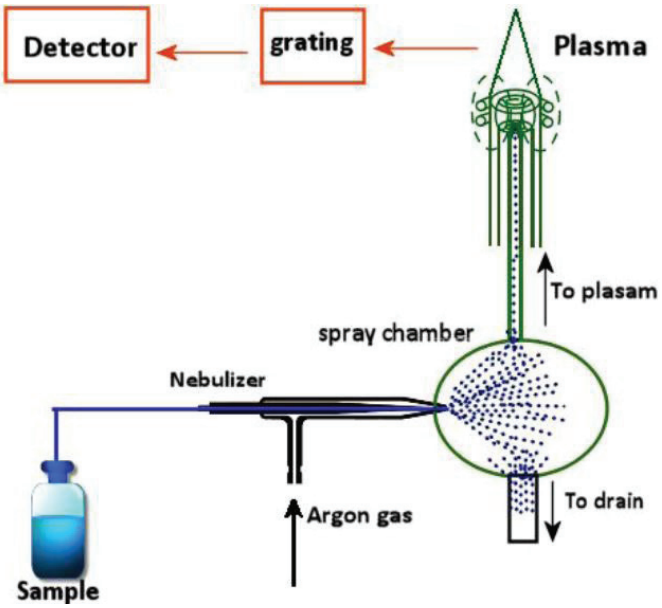

Figure 4.2.2. Diagram of sample introduction to ICP-OES. [11]

4.2.3. Thermal analysis techniques

Different thermal analysis techniques were applied including simple thermogravimetric analysis (TG) and simultaneous thermogravimetric and differential thermal analyses coupled with mass spectrometer (TG-DTA-MS).

Thermogravimetric Analysis (TGA) or Thermogravimetry (TG) is defined as a technique in which the mass of the sample is recorded versus time or temperature while the temperature of the sample is programmed, in a controlled atmosphere. The instrument is called a thermogravimetric analyzer (TGA) or a thermobalance.

Two different types of transformation can occur:

- Transformation with a mass loss: dehydration, dehydroxylation, evaporation, decomposition, desorption, pyrolysis,…
- Transformation with a mass gain: adsorption, hydration, reaction,...

Figure 4.2.3. shows a classical mass loss with the determination of the derivative curve (DTG). [12]

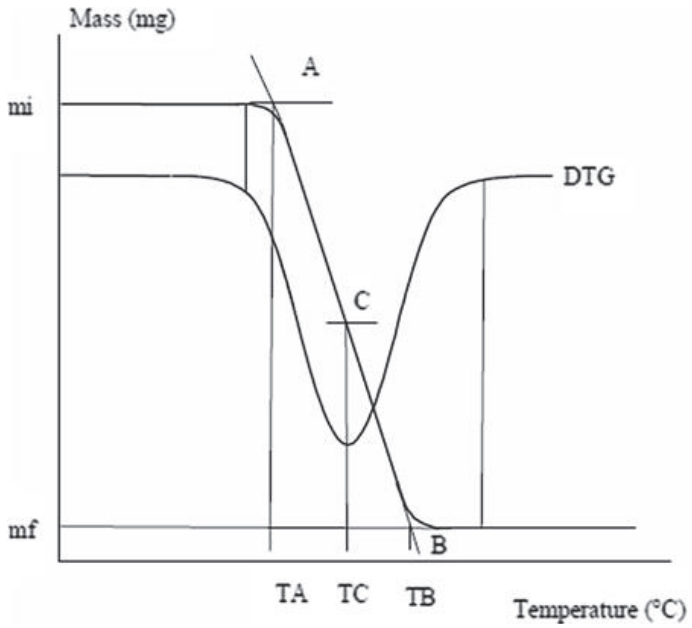

Figure 4.2.3. A TG mass loss curve with the derivative curve (DTG). [12]

The TGA technique provides information on the mass variations that occur within the sample, but most of the time, if the composition of the sample is unknown, the interpretation of the data is not easy. This is why the TGA technique is mostly used combined with other techniques such as DTA. The TG-DTA or TG-DSC combination allows obtaining the simultaneous TGA and DTA or DSC measurements on the same sample (Fig. 4.2.3.1.). The heat effects are correlated with the mass variations. The DTA or DSC signal gives also information on heat effects not correlated with mass variation (melting, phase transitions,…)

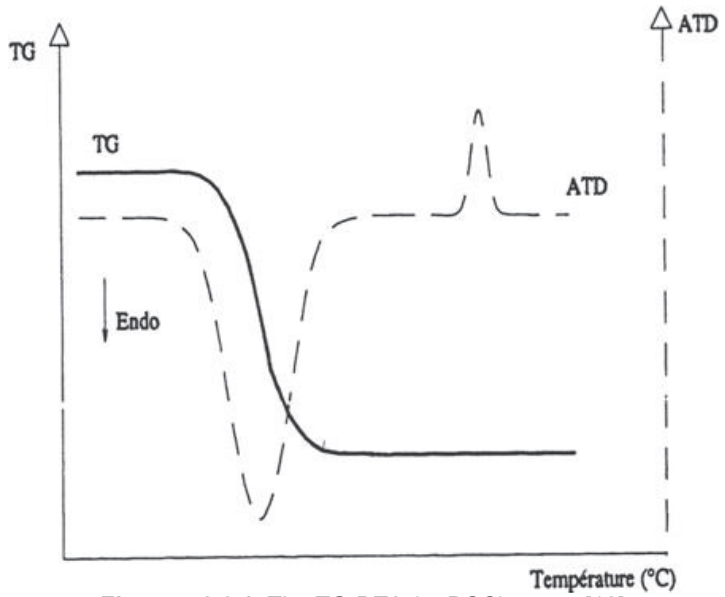

Figure 4.2.3.1. The TG-DTA (or DSC) curve. [12]

Evolved Gas Analysis (EGA) is defined as a technique of determining the nature and amount of volatile products formed during thermal analysis. The TGA technique only informs on the variation of sample mass, but hardly on the mechanisms linked to the decomposition or the reaction. The idea behind the TGA coupling is to analyze the vapors emitted by the sample during the test. In this work we used TGA-MS: the TG gives the mass loss of sample and can be connected online to a mass spectroscopy detector to determine the nature of volatile products emitted by the sample during a thermogravimetric experiment. [12]

The thermogravimetric (TG) analyses were performed on a SETARAM LABSYS instrument in the RT-900 °C temperature range, on ~40 mg of sample, with a heating rate of 5 °C min $^{-1}$, under air flow. This technique was used to determine the optimal temperature of calcination for the preparation of the catalytic materials, to verify their thermal stability and to determine the right temperature of pretreatment of the different samples previously to other characterization methods. Simultaneous thermogravimetric and differential thermal analyses (TG-DTA) of the samples were conducted on a SETARAM SETSYS Evolution 12 thermoanalyzer coupled via a heated (*ca*. 150 °C) capillary with a Pfeiffer OmniStar quadrupole mass spectrometer (MS). For TG-DTA-MS studies, samples (40-50 mg located in Pt-based open crucibles) were heated from RT to 700 °C at a constant rate of 10 °C min^{-1} under a flowing gas (50 cm^3 min^{-1} STP) of argon.

4.2.4. BET surface area and pore size determination

Specific surface area of a solid represents the total surface area per unit mass of the sample. The general principle of solid catalyst surface area measurements is based on physical adsorption and capillary condensation to obtain information about the surface area and porosity of porous materials.

Physical adsorption phenomena occur due to very low Van der Waals forces between nitrogen adsorbed molecule and membrane solid material (in powder form).

This information (adsorbed gas volume) is sufficient to determine specific surface area of solid material by Brunauer-Emmett-Teller (BET) method. S_{BET} can be calculated from the relation:

$$S_{BET} = \frac{V_m . N . S}{V_M . m_S} \quad (m^2/g)$$

Where:

• Vm: adsorbed gas volume in (cm^3);

• N: Avogadro's number = 6.023 10^{23} molecules;

• S: surface covered by one adsorbed molecule;

S = 16.2 10^{-20} m^2 $molecule^{-1}$ in case of nitrogen;

• V_M: molar volume of nitrogen in (cm^3);

• m_S: mass of solid material (g).

Specific surface areas were determined by low temperature nitrogen adsorption performed at -196 °C, on a Micromeritics ASAP 2020 apparatus (Figure 4.2.4.), after pretreatment performed for 3 h under vacuum at 200 °C, for the bulk and silica-supported heteropolyacids, or 350 °C for the other samples. For calculation of the pore volume and pore size distribution BJH (Barrett-Joyner-Halenda) method was applied. Besides, for some samples the full N_2 adsorption/desorption isotherms were performed.

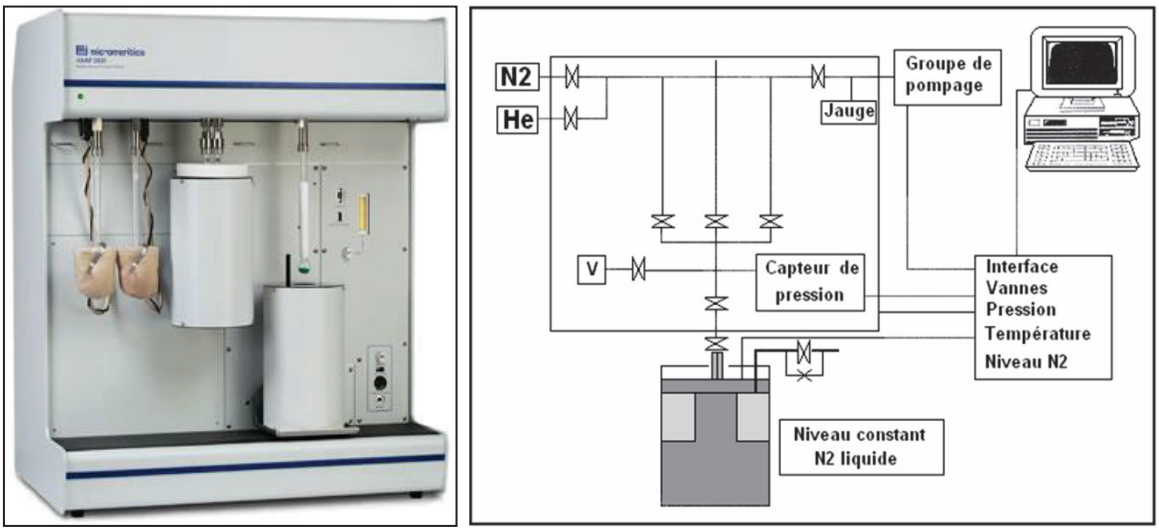

Figure 4.2.4. Micromeritics ASAP 2020 system used by the *IRCELYON Textural and Chemical Analysis Service* for S_{BET} and porosity measurements.

4.2.5. X-ray photoelectron spectroscopy

X-ray photoelectron spectroscopy (XPS) is a technique for analyzing the surface chemistry of a material. XPS can provide the elemental composition, empirical formula, chemical state and electronic state of the elements within a material. XPS spectra are obtained by irradiating a solid surface with a beam of X-rays while simultaneously measuring the kinetic energy and electrons that are emitted from the top 1-10 nm of the material being analyzed. A photoelectron spectrum is recorded by counting ejected electrons over a range of electron kinetic energies. Peaks appear in the spectrum from atoms emitting electrons of a particular characteristic energy. The energies and intensities of the photoelectron peaks enable identification and quantification of all surface elements (except hydrogen). A surface layer is defined as being up to three atomic layers thick (~1 nm), depending upon the material. Layers up to approximately 10 nm are considered ultra-thin films, and layers up to approximately 1 μm are thin films. The surface represents a discontinuity between one phase and another and, therefore, the physical and chemical properties of the surface are different from those of the bulk material. These differences mostly affect the top atomic layer of the material. In the bulk of the material, an atom is surrounded on all sides in a regular manner by atoms composing that material. Because a surface atom is not surrounded by atoms on all sides, it has bonding potential, which makes the surface atom more reactive than atoms in the bulk.

When an atom or molecule absorbs an X-ray photon, an electron can be ejected. The kinetic energy (KE) of the electron depends upon the photon energy (hv) and the binding energy (BE) of the electron (*i.e.* the energy required to remove the electron from the surface). By measuring the kinetic energy of the emitted electrons, it is possible to determine which elements are on the surface, their chemical states and the binding energy of the electron. The binding energy depends upon a number of factors, including the followings:

- The element from which the electron is emitted.
- The orbital from which the electron is ejected
- The chemical environment of the atom from which the electron was emitted.

XPS is a quantitative technique because the cross-section for the emission of a photoelectron is not dependent upon the chemical environment of the atom. [13]

The X-ray photoelectron spectra (XPS) were acquired *(IRCELYON XPS Analysis Service)* by using a KRATOS Axis Ultra DLD spectrometer equipped with a hemispherical electron analyzer and an Al anode (Al Kα =1486.6 eV) powered at 150 W, a pass energy of 20 eV, and a hybrid lens mode. The detection area analyzed was 700 μm × 300 μm. Charge neutralization was required for all samples. The peaks were referenced to the C–(C, H) components of the C 1s band at 284.6 eV. Shirley background subtraction and peak fitting to theoretical Gaussian– Lorentzian functions were performed using an XPS processing program (Vision 2.2.6 KRATOS). The residual pressure in the spectrometer chamber was 5×10^{-9} mbar during data acquisition.

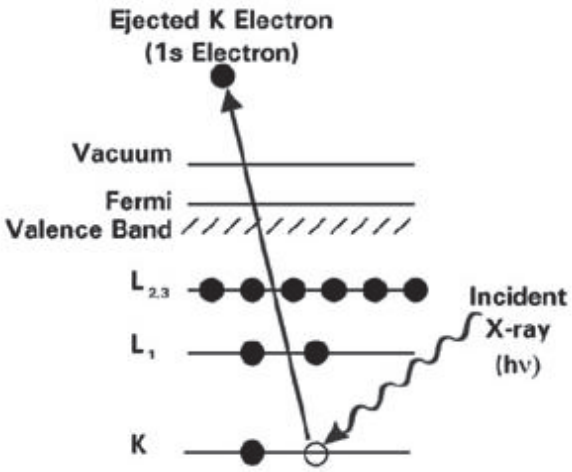

Figure 4.2.5. The photoemission process involved in XPS surface analysis. The dots represent electrons and the bars represent energy levels within the material being analyzed. The equation governing the process is: KE=hv-BE. [13]

4.2.6. ^{27}Al MAS NMR

Nuclear Magnetic Resonance (NMR) spectroscopy is an analytical chemistry technique used for determining the content and purity of a sample as well as its molecular structure. For example, NMR can quantitatively analyze mixtures containing known compounds. For unknown compounds, NMR can either be used to match against spectral libraries or to infer the basic structure directly. A variety of NMR techniques are available.

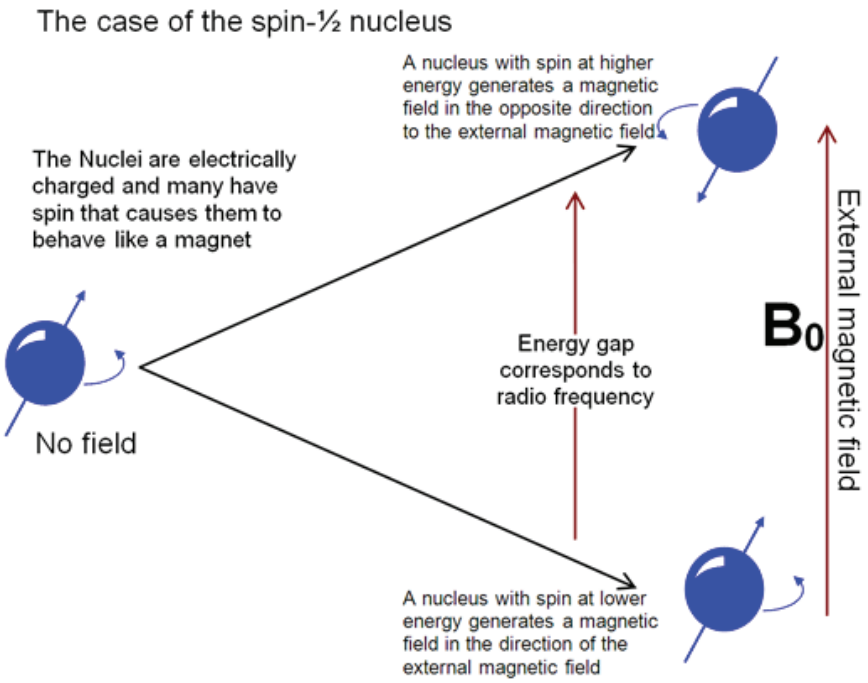

Figure 4.2.6. The basis of NMR. [14]

The principle behind NMR is that many nuclei have spin and all nuclei are electrically charged. If an external magnetic field is applied, an energy transfer is possible between the base energy to a higher energy level (generally a single energy gap). The energy transfer takes place at a wavelength that corresponds to radio frequencies and when the spin returns to its base level, energy is emitted at the same frequency. The signal that matches this transfer is measured in many ways and processed in order to yield an NMR spectrum for the nucleus concerned. Figure 4.2.6. shows the basis of NMR (it relates to spin-½ nuclei that include the most commonly used NMR nucleus, proton-^{1}H as well as many other nuclei such as ^{13}C, ^{15}N and ^{31}P). Many nuclei such as deuterium (^{2}H) or aluminum (^{27}Al) have a higher spin and are therefore quadrupolar and although they yield NMR spectra their energy diagram and some of their properties are different. [14]

^{27}Aluminum (^{27}Al) is a high sensitivity nucleus that yields broad lines over a wide chemical shift range. ^{27}Al is a spin 5/2 nucleus and is therefore quadrupolar. As a result, the signal width increases with asymmetry of the environment with somewhat broad lines in symmetrical environments (Figure 4.2.6.1.) but very broad lines in asymmetric ones. The main use of aluminum solid state NMR is to detect the presence of aluminum and measure its relaxation rate in order to detect binding. There is always a broad signal arising from the probe in the ^{27}Al spectrum. [15] In this work ^{27}Al MAS NMR technique was used to probe the structure of Mg-Al mixed oxides and alumina. As example, Figure 2.2.6.1. shows the ^{27}Al MAS NMR spectra of one $MgAl_2O_4$ sample when different spinning speeds were used.

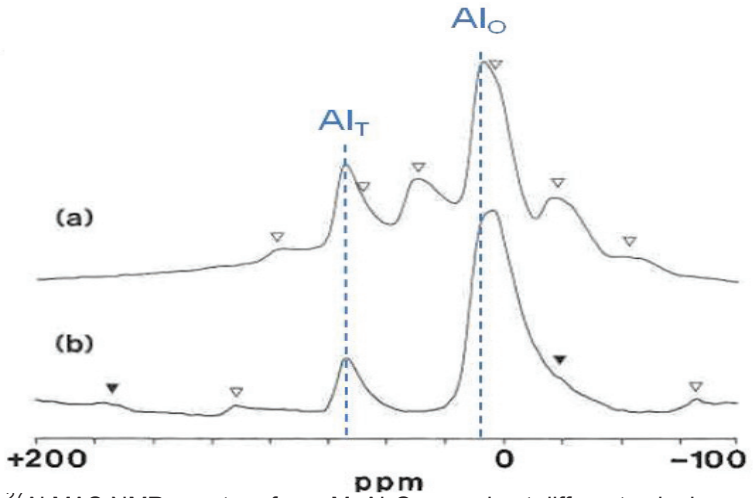

Figure 4.2.6.1. The ^{27}Al MAS NMR spectra of one $MgAl_2O_4$ sample at different spinning speeds: 3-3.5 KHz (a) and 10-11 KHz (b). Al_T and Al_O denote peaks corresponding to Al in tetrahedral and octahedral coordination, while open and solid triangles denote spinning sidebands. Adapted from ref. [16].

^{27}Al MAS NMR experiments were performed by accumulating 8192 scans on a Bruker Avance III 500WB spectrometer at a resonance frequency of 130.29 MHz with an excitation of π/12 pulses and a repetition time of 1 s. A commercial 4-mm double H/X probe was used to perform the MAS experiments with a spinning rate of 12 KHz. The reference for the chemical shifts was an aqueous 1 M $Al(NO_3)_3$ solution.

4.2.7. Adsorption microcalorimetry coupled with volumetric line

The main technique used for the investigation of gas and vapor adsorption on the solid surfaces was adsorption microcalorimetry coupled with a volumetric line.

The main interest for using this particular technique was, primarily, the investigation of the surface acid/base properties of the fresh and used catalytic materials (studied in oxidation of bio-isobutene and acrolein synthesis). Microcalorimetric experiments were performed to study the strength of interaction between the impurities possibly present in bio-isobutene and the acid/base sites of the catalysts used in the process of bio-isobutene oxidation to methacrylic acid. Considering acrolein synthesis, this technique supplied also valuable contribution to predict the possible creation of new acid/base active sites on the working catalyst, exposed to the reaction gas mixture (containing methanol, ethanol, water vapor and other reactants such as CO_2).

For the heterogeneous catalysis processes, the study of adsorption of reactive gas probe molecules onto the surface of catalysts is crucial for better understanding the nature of gas-solid interactions and obtaining the information about the active sites. Adsorption is an exothermic process and interaction of the reactive molecule with the solid surface is characterized by heat evolved which is related to the energy of the bonds formed between the adsorbed species and the adsorbent and consequently to the nature of the bonds and the chemical reactivity of the surface. [12]

Forces governing adsorption depend on the nature of both adsorbent and adsorbate and can be distinguished in: (1) Van der Waals/London-dispersion forces, similar to the forces leading to the non-ideal behavior of gases and eventually to the formation of a liquid phase; (2) chemical (covalent) forces leading to the formation of a true chemical bond between the adsorbate and the surface atoms. In the former case the process is called physical adsorption (physisorption), in the latter case chemical adsorption (chemisorption). H–bonding interactions (3) are variably classified as responsible for either physical or chemical adsorption. In fact, H–bonding interactions originate surface complexes of variable stability according to the nature of the involved species. [12]

Physisorption is intrinsically weak, characterized by relatively small heats of adsorption, close to the enthalpy of liquefaction of the adsorptive, typically comprised in the 5−45 kJ mol^{-1} range. Chemisorption, consisting of a chemical reaction confined to the solid surface, involves rearrangement of electrons of both adsorptive molecules and surface atoms, yielding to new surface terminal groups. Chemisorption heats are generally larger than physisorption heats, and are typically comprised in the 80−400 kJ mol^{-1} range. Dissociative chemisorption is distinguished from associative chemisorption, which involves the coordination of the molecules. The enthalpy change for adsorption driven by H–bonding interactions may cover a large range of values. [12]

Adsorption microcalorimetry coupled with volumetric line is one of the very few techniques which can provide information about the strength of chemisorption phenomena. The determination of the differential heats evolved, by a suitable microcalorimeter, when the amounts of gas probe

molecules adsorbed on the catalytic surface are known represents the most suitable and accurate method to determine the number, strength and energy distribution of the adsorption sites. The effective use of this technique in heterogeneous catalysis and other fields depends on the choice of probe molecule since the nature of the probe determines which surface property is going to be investigated. To access the energetic heterogeneity of surface small doses of the probe molecule (<10 μmol g^{-1}) need to be successively added on the solid in order to progressively saturate the active sites. Corresponding heats are very low (100-1000 mJ) and require some time to be evolved (depending on the time constant of the calorimeter). Calorimeters are commercial instruments able to reliably quantify such low heats. The most commonly used are the heat-flow microcalorimeters of Tian-Calvet type. This highly sensitive heat flow calorimeter linked to a sensitive volumetric system makes possible to study the gas-solid interactions and the catalytic reactions. [12]

These kinds of measurements are one of the specialties of the research group *(IRCELYON-ATARI)* where this PhD thesis was carried-out. The scheme of the system used to conduct the gas-solid adsorption microcalorimetry is represented in Figure 4.2.7. The volumetric determination of the amount of gas adsorbed was performed in a constant volume vessel linked to a vacuum pump. The volumetric line consists of two parts: the measuring element equipped with a capacitance manometer and a cell section, which includes two cells placed inside the calorimeter. The adsorbent solid is placed in one of the cells while the other cell is kept empty (reference cell). The volume of this vessel is determined by the expansion of a known gas quantity, contained in the measuring part of the assembly, into the previously evacuated cell section. This calibration must be made with the same gas and at the same temperature as the proposed study is going to be done.

Typical experimental procedure starts by outgassing the sample at the suitable pretreatment temperature and under high vacuum in the calorimetric cell. After cooling the cell to the adsorption temperature and when the thermal equilibrium of the system is reached (flat baseline), successive doses of gaseous (or vapor) probe molecules are brought into contact with catalyst sample. The heat flow signal and the corresponding pressure change (Figure 4.2.7.) were monitored and recorded until the equilibrium was reached after injection of each dose. The volume of each dose was minimized in order to detect any change in adsorption heats evolved with increasing the coverage of the surface. The adsorption was considered complete when for a significant increase in pressure no detectable heat evolution or gas adsorption could be measured. The adsorption temperature was maintained constant during the experiment. The irreversibly chemisorbed amount (V_{irr}) was evaluated as the difference between the primary adsorption isotherm (adsorbed amount of the gas as function of the equilibrium pressure) and a secondary isotherm obtained after desorption under vacuum and consecutive readsorption of the gaseous probe at the same temperature. By subtraction of readsorption isotherm from the first adsorption isotherm the amount of strong sites could be roughly estimated (Figure 4.2.7.1-left). [12]

By analyzing the data obtained directly from adsorption calorimetry measurements (Figure 4.2.7.-right) until the full coverage is attained we can get different information about the sample

properties that can be summarized on various plots. The plots most commonly used in this study are represented in Figure 4.2.7.1.

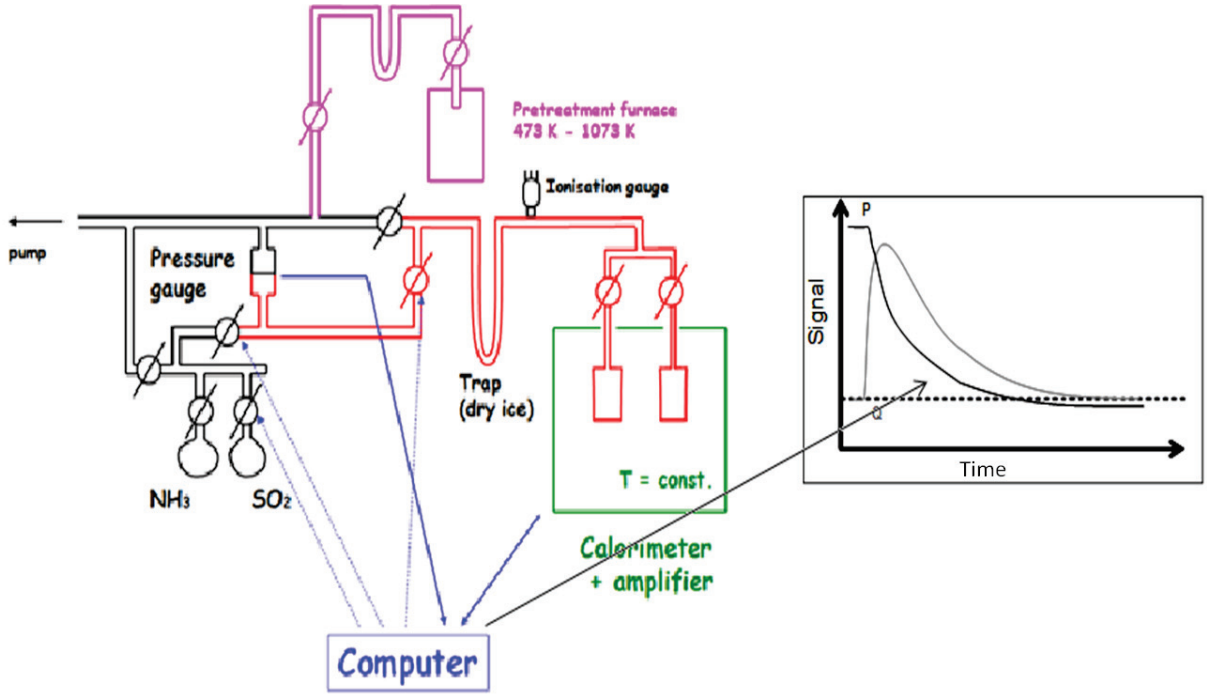

Figure 4.2.7. Scheme of gas-solid adsorption microcalorimetric-volumetric system *(IRCELYON)*, and data obtained directly from the experiments for each dose of probe molecule adsorbed (evolution of pressure and calorimetric signal) as a function of time. [12]

The volumetric isotherms (n_a=f (P)) for a cycle of adsorption, desorption by pumping at the same temperature and then readsorption are presented in Figure 4.2.7.1. The irreversibly adsorbed volume (V_{irr}), which characterizes the strong sites of the catalyst (chemisorption), can then be calculated as a difference between the total adsorbed volume (V_{tot}) and the readsorbed volume (V_{rev}, physisorption) at a given equilibrium pressure (in our case p_{eq}= 0.2 Torr (67 Pa)). These plots allow to determine the amount (number) of total, strong (chemisorption) and weak (physisorption) acid/base surface sites when adsorbing basic/acidic probes.

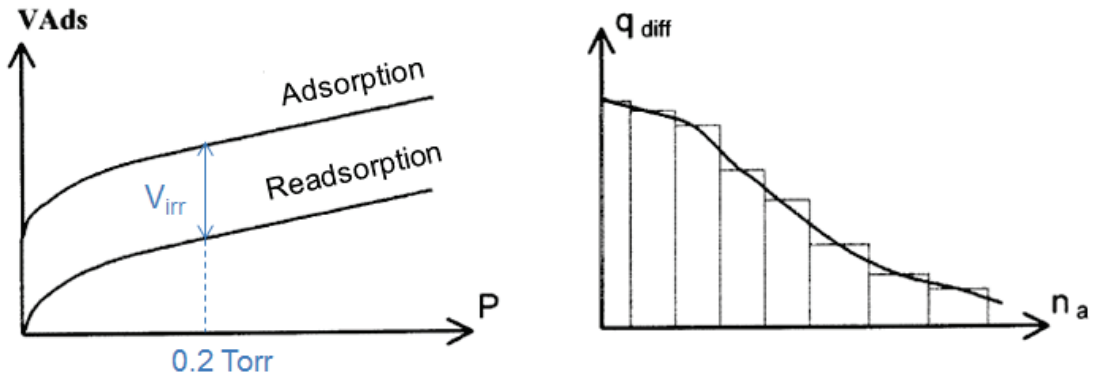

Figure 4.2.7.1. Some of the typical data obtained from volumetric-calorimetric experiments: volumetric isotherms for a cycle of adsorption and readsorption (left), and the differential heats of adsorption as a function of coverage (right). [12]

The curves of the differential heats of adsorption as a function of n_a are also widely used plots for the interpretation of the results (Figure 4.2.7.1.). Differential heat is defined as molar heat of each dose of adsorbate ($Q_{diff}=Q_{int}/dn_a$, where Q_{int} represents integral heat). The differential heat evolved from the first dose is labeled as Q_{init}-initial differential heat. The ratio of the amount of heat evolved for each increment to the number of moles adsorbed in the same period is equal to the average value for the differential enthalpy of adsorption in the interval of the adsorbed quantity. The curves Q_{diff} *vs.* coverage are rather represented as histograms. For simplification the steps of histograms are often replaced by a continuous curve connecting the centers of steps. This type of plots represents well the strength distribution of acid/base surface sites.

Results obtained by adsorption microcalorimetry are not sufficient to determine the nature of active acid/base sites and therefore complementary informations from suitable IR, MAS NMR and XPS investigations are necessary to identify these sites.

However, the variation of the differential heats of adsorption with coverage quite clearly shows energy distribution of surface active sites with respect to a given adsorbate and their varying reactivity on given adsorbents. A general representation of differential heats of adsorption as a function of probe molecule uptake presents the following features (see Figure 4.2.7.2):

a: An initial region of high heats of adsorption, representing adsorption on the strongest sites, which are usually thought to be of Lewis type. After this region the curve drops abruptly.

b: One or more regions of intermediate strength sites. Regions of constant heat in this region are attributed to sets of sites of constant strength. This is taken as an indication of discrete inhomogeneity. These features, when adsorption of base molecule on the surface of zeolite is in question, are attributed to Brønsted acid sites.

c: A region where heats decrease more or less steeply depending on the heterogeneity of the sites. In this area a bump on the curve can sometimes be observed, which indicates lateral interactions between adsorbed molecules.

d: At a high coverage heat of adsorption approaches a constant value characteristic of hydrogen bonding between the molecule and the sample or physisorption of the molecules. This constant value is depending on the nature of the probe molecule.

All regions (a, b, c, d) can be observed for certain materials (*i.e.* zeolites) presenting both Lewis and Brønsted acid sites, as probed by ammonia adsorption. For oxides presenting only Lewis acid sites, the regions a, c and d are observed.

This kind of representation of calorimetric data can be used to assess the uniformity–non-uniformity of the surface of the adsorbent with respect to energy, the energy of the lateral (adsorbate–adsorbate) interactions, and the structural or substructural (textural) changes that the adsorbent often undergoes as a result of interaction with the adsorbed substance. [12]

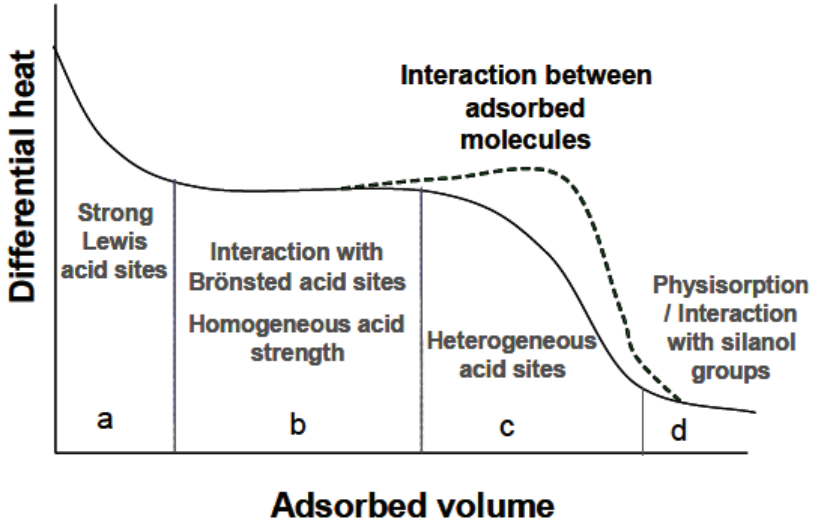

Figure 4.2.7.2. Regions in a typical curve of differential heats of adsorption versus adsorbed amount of the probe molecule. [12]

Probe molecules used in this study were NH_3, SO_2, CO_2 and methanol. When adsorption of NH_3, SO_2 and CO_2 on the catalytic materials was studied by microcalorimetry-volumetry the experiments were performed at 150 °C in a heat flow calorimeter (C80 from Setaram) linked to a conventional volumetric apparatus equipped with a Barocel capacitance manometer for pressure measurements. When methanol (MeOH) was used as a probe molecule adsorption temperature was 30 °C. The samples were pretreated in a quartz cell by heating overnight under vacuum: at 200 °C, for the bulk and silica-supported heteropolyacids, 300 °C for the FeMo-like samples, and 350 °C for the other samples. For each sample differential heats of adsorption were obtained as a function of the probe molecule coverage by repeatedly sending small doses of the gas probe onto the sample (placed in a calorimeter coupled to a volumetric line) until an equilibrium pressure of around 0.5 Torr (67 Pa) was reached. The sample was then outgassed for about 40 min at the same temperature, and a second adsorption run was performed (still at the same temperature as the first adsorption) on each sample, until equilibrium pressure of about 0.2 Torr (27 Pa) was attained. The difference between the amounts adsorbed in the first and second adsorptions at 27 Pa represents the irreversibly adsorbed amount (V_{irr}) of a respective gas, which provides an estimation of the number of strong acidic/basic sites.

4.2.8. Liquid phase adsorption calorimetry

Isothermal titration calorimetry technique can measure the heat of liquid-solid interactions. It was used to study the acid-base properties in n-decane and the adsorption capacities of bulk heteropolyacids towards phenylethylamine (PEA) in n-decane. The Scheme is given in Figure 4.2.8. The instrument is a differential heat flow calorimeter of Tian-Calvet type equipped with a preheating furnace and a stirring system. A programmable syringe pump is linked to the calorimeter by capillary

tubes. Successive pulse injections 0.3 ml of diluted solutions of probe molecule solutions (0.3M) are sent to the sample maintained at 30 °C in the calorimetric cell at 2 h time intervals. Importantly, all liquids used in this investigation are previously purged with flowing nitrogen, in order to avoid forming of air bubbles in the capillary tubes. The preheating furnace allows the injection of the probe solution at the same temperature of 30 °C as the calorimeter. The reference and measurement cells contain solvent (1.5 cm^3) and solvent with a weighted amount of the solid samples (*ca.* 50 mg), respectively. The differential system renders the heats of dilution and mixing negligible. The samples are activated ex-situ by outgassing the powders at 200 °C overnight and then transferred into the calorimeter cell. The evolved heat from the adsorption is obtained by integration of the area under the calorimetric signal, for each dose.

The adsorbed amount of probe molecule was determined by another experiment giving access to the adsorption isotherm. UV-Vis spectrometry was used for this purpose. Adsorption isotherms were carried out using 25 mg of dry sample in a closed flask containing 0.75 cm^3 of solvent and the appropriate amount of probe solution. After continuous stirring performed at constant temperature (30 °C), the two phases (solid and liquid) are separated by centrifugation (Eppendorf MinSipin, 13 400 rpm, duration of centrifugation 1.5 h). The amount of remaining probe is determined by measuring the singular absorbance of the corresponding probe molecule using a SPD-20A UV/Vis detector. Through an analytical calibration curve, each absorbance can be converted into adsorbate concentration in the solution at equilibrium. The difference between the amount of probe remaining in the solution at equilibrium and the quantity injected initially allows obtaining the amount of acid/base probe adsorbed by the solid. [17]

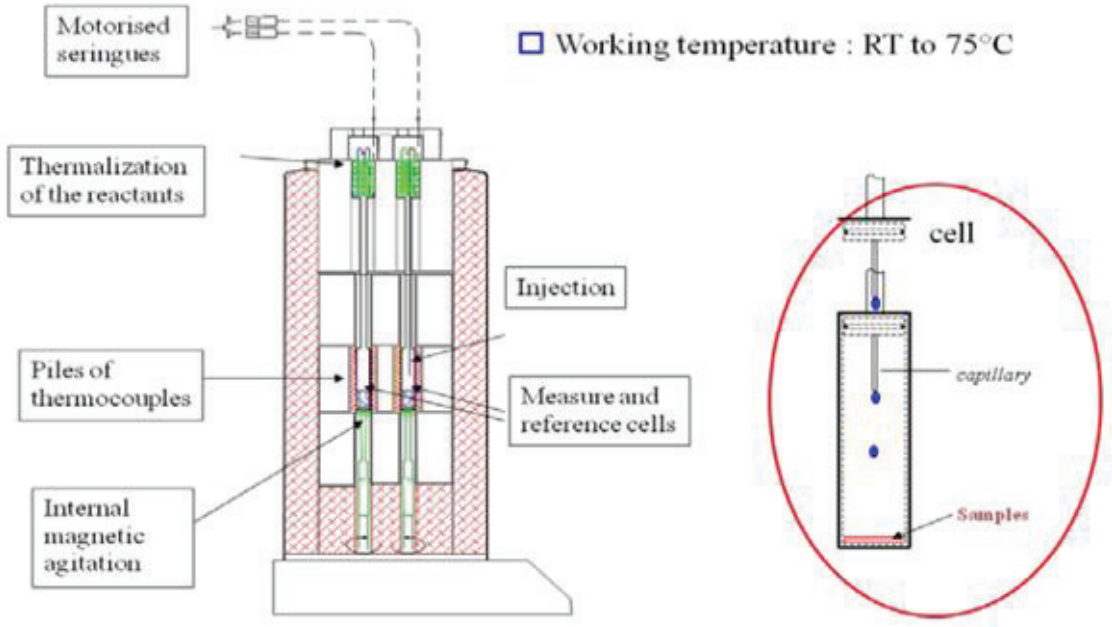

Figure 4.2.8. Schematic representation of SETARAM TITRYS calorimeter. [17]

4.3. Catalytic tests

The Micropilote used to perform the catalytic tests for acrolein synthesis was located in *ARKEMA, Centre de Recherche Rhône-Alpes, Pierre Bénite (CRRA ARKEMA).* Acrolein production was carried out with two consecutive reactors, the first used for the redox catalyst and the second for the aldolization (acid/base) catalyst. The catalytic test consists in two stainless steel continuous-flow reactors in series and working close to atmospheric pressure. The scheme of the catalytic micropilote is shown in Figure 4.3. The two vertical reactors were heated independently by two salt baths. The reaction temperature was controlled by moving a thermocouple inserted in the catalytic bed thus allowing monitoring of the temperature profile and identify the hot spots position.

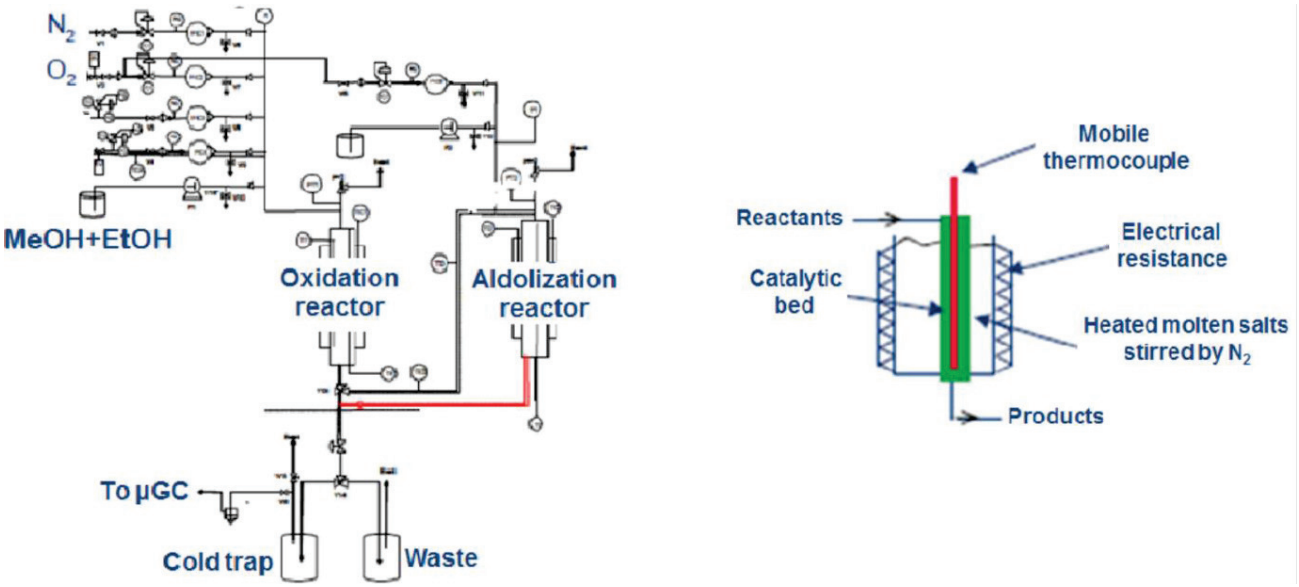

Figure 4.3. Scheme of the micropilote used for the synthesis of acrolein consisting in two consecutive reactors (left), and close view one of the interior of the reactors (right).

In the first reactor, the simultaneous ethanol and methanol (VWR Chemicals) oxidation was carried out, producing mainly acetaldehyde and formaldehyde. Hollow cylindrical-shaped pellets of the commercial FeMoOx catalyst (4g) were diluted with steatite balls (20g) and were placed into the first reactor (oxidation). The products exiting from the first reactor were directly sent to the second, where aldol condensation of acetaldehyde and formaldehyde and dehydration to acrolein were performed.

Reaction conditions in the first reactor were optimized to get the highest acetaldehyde + formaldehyde yields. Different parameters (oven temperature, gas hourly space velocity (*GHSV*), $\%O_2$, $\%N_2$, and %MeOH/EtOH) were investigated. Preliminary experiments have shown that on FeMoOx catalyst methanol reactivity was lower than ethanol reactivity. Therefore the methanol/ethanol ratio was selected to ensure to have a more appropriate formaldehyde/acetaldehyde ratio. The final chosen conditions for the first reactor were the following: MeOH/EtOH/O_2/N_2 molar ratio of 4/2/8/86, $GHSV_1$=10 000 h^{-1}, reaction temperature (T_1) of 260 °C.

In the second reactor, different aldolization catalysts (20g; particle size range 100-500µm) were tested by varying the temperature (T_2) between 250 and 360 °C and the gas hourly space velocity – (*GHSV*) between 10 000 and 5 000 h^{-1} by adjusting the feeding flow rate. The maximum reaction temperature was different for each catalyst and chosen in order to keep the ($CO+CO_2$) yield below 10 mol%. Above this threshold, the reaction becomes highly exothermic. Comparison of the catalysts was done at conversions lower than 100%.

The products exiting from the second reactor were collected in a cold trap (cooled at 0 °C by an ice bath) and the condensable products (acrolein, acetaldehyde, methanol, ethanol, crotonaldehyde and others) were quantified off-line using a gas chromatograph (column ZB-WAX plus) equipped with a FID detector. Formaldehyde could not be quantified with this analytical device. The non-condensable products (CO, CO_2, O_2, N_2) were analyzed online with a two columns micro-GC and using TCD detector. The first column filled with molecular sieves measures the CO, O_2 and N_2 concentrations, while the second column (silica plot) measures CO_2.

Conversions of the reactants: methanol, ethanol and acetaldehyde (%), carbon yield of acrolein (%), and selectivity of acrolein (%) were calculated as follows:

Conversion (%) = (Nl h^{-1} of reactant converted) / (Nl h^{-1} of reactant flowing in) x 100%;

Carbon yield of acrolein (%) = (3 x Nl h^{-1} of acrolein produced) / (Nl h^{-1} of methanol flowing in + 2x Nl h^{-1} of ethanol flowing in) x 100%.

The reaction conditions were chosen to have a MeOH/EtOH molar ratio of 2. In this case if all ethanol will be transformed into acrolein the maximum yield of acrolein could attain 75% as maximum value. Therefore a 40 % yield of acrolein would represent 53 % of the theoretical maximum (40/75).

Selectivity to acrolein (%) = (3 x Nl h^{-1} of acrolein produced) / (Nl h^{-1} of methanol reacted + 2 x Nl h^{-1} of ethanol reacted) x 100%.

References

[1] N. Sattarahmady, H. Heli, R. Dehdari Vais, *Talanta* **2014**, *119*, 207-213.

[2] A.S. Adekunle, J.A.O. Oyekunle, O.S. Oluwafemi, A.O. Joshua, W.O. Makinde, A.O. Ogunfowokan, M.A. Eleruja, E.E. Ebenso, *Int. J. Electrochem. Sci.* **2014**, *9*, 3008-3021.

[3] R. Irmawati, M.N. Noorfarizan Nasriah, Y.H. Taufiq-Yap, S.B. Abdul Hamid, *Catal. Today* **2004**, *93-95*, 701-709.

[4] J. Song, X. Wang, X. Ni, H. Zheng, Z. Zhang, M. Ji, T. Shen, X. Wang, *Mater. Res. Bull.* **2005**, *40*, 1751-1756.

[5] J. Song, X. Ni, L. Gao, H. Zheng, *Mater. Chem. Phys.* **2007**, *102*, 245-248.

[6] K. Krishnamoorthy, M. Veerapandian, K. Yun, S.J. Kim, *Colloid. Surface B* **2013**, *112*, 521-524.

[7] A. Saric, S. Music, K. Nomura, S. Popovic, *Mater. Sci. Eng. B* **1998**, *56*, 43-52.

[8] M.S. Pandian, *X-ray Diffraction Analysis: Principle, Instrument and Applications*, available at: https://www.researchgate.net/publication/260659249_X-ray_Diffraction_Analysis_Principle_Instrument_and_Applications.

[9] http://serc.carleton.edu/research_education/geochemsheets/techniques/XRD.html.

[10] https://fys.kuleuven.be/iks/nvsf/experimental-facilities/x-ray-diffraction-2013-bruker-d8-discover.

[11] http://www.chemiasoft.com/chemd/node/52.

[12] A. Auroux (Ed.), *Calorimetry and Thermal Methods in Catalysis*, Springer-Verlag Berlin and Heidelberg GmbH & Co. K, **2013**.

[13] http://xpssimplified.com/whatisxps.php.

[14] http://chem.ch.huji.ac.il/nmr/whatisnmr/whatisnmr.html.

[15] http://chem.ch.huji.ac.il/nmr/techniques/1d/row3/al.html#top.

[16] R. Millard, R. Peterson, B. Hunter, *Am. Mineral.* **1992**, *77*, 44-52.

[17] J. Cai, *PhD thesis (N° of the thesis: 11-2015)*, Université Claude Bernard Lyon 1, Lyon, France, **2015**.

Chapter 5.

The impact of bio-sourced isobutene impurities on the catalysts used for methacrylic acid production: adsorption microcalorimetry study

Abstract

The data contained in this chapter were obtained during the first year of my PhD thesis and present the study of the impact of the impurities contained in bio-isobutene on the acid/base features of industrial and model catalysts used for production of bio-methacrylic acid. The context of the present study was thoroughly described in the introduction of this manuscript (Chapter 1).

Isobutene is one of the key building-block molecules in petrochemistry used for the synthesis of various commodity products and fuels. In particular, isobutene may be converted to methacrylic acid by catalytic oxidation. Catalytic oxidation of isobutene obtained from oil to methacrylic acid is an industrial process containing two successive oxidations: isobutene to methacrolein; and methacrolein to methacrylic acid. Considering that all existing industrial production of isobutene is based on the fossil resources and that isobutene and methacrylic acid markets are still not fully satisfied, renewable resources may offer a solution. But bio-sourced isobutene might contain impurities like water vapor, CO_2, NH_3, sulfur containing compounds and other fermentation gases. In order to adjust the actual industrial process for production of bio-sourced methacrylic acid it is then crucial to investigate the impact of the impurities expected to be present in bio-isobutene on the catalysts. Adsorption calorimetry was used as the main technique to test the interaction of impurities with industrial and model catalysts.

The first stage industrial catalyst used for the isobutene to methacrolein oxidation, consists in a complex mixture of Mo, Bi, Co, Fe, Ni oxides and did not show any interaction with SO_2, CO_2 and NH_3, thus resulting to be a suitable catalyst for bio-sourced isobutene oxidation. The second stage industrial catalyst contains a mixture of oxides and Keggin-type heteropolyanions of the following elements: Mo, P, V. Analyzing the adsorption microcalorimetry results, it was observed that the second stage catalyst did not interact with acid probes (SO_2 and CO_2), but it extensively reacted with NH_3. TG-DTA-MS analysis was performed in order to identify and to investigate the stability of the NH_3 containing compounds that were formed. Thermodesorption was performed up to 600°C. The decomposition of the NH_3-containing compounds occurred in the 350-450 °C temperature region with the release of NH_3, N_2O and H_2O molecules, detected by mass-spectrometry, in the out-streaming gas. Characterizations of the 2nd stage industrial catalyst indicated that the phases responsible for this

interaction with NH_3 most probably include vanadium oxides and Mo- and P-containing heteropoly-compounds.

In order to identify which phase of the catalyst is responsible for the interaction with ammonia, model single oxides were synthesized by precipitation. Four Keggin-type commercial heteropolyacids were selected as well for studying the interaction with ammonia. Single oxides generally showed low NH_3 adsorption heats corresponding to reversible adsorption phenomena; therefore single oxides were excluded to be potentially poisoned when used for the oxidation of bio-isobutene containing impurities. On the other hand, the four heteropolyacids exhibited very strong interaction with ammonia, similar to that observed for the 2nd stage industrial catalyst. It is then confirmed that heteropoly-compound containing Mo and P are responsible for the strong interaction of ammonia with the 2nd stage industrial catalyst.

Furthermore, adsorption microcalorimetry performed on the model catalysts gave valuable contribution to the determination of the surface acid/base properties of oxides and heteropolyacids.

5.1. Introduction

Isobutene is considered as a cheap raw material for petrochemical catalytic processes for production of methacrylic acid (MAA). MAA is the main material for production of methyl methacrylate (MMA) which is an important monomer widely used for producing acrylic plastics (polymethyl methacrylate) or polymer dispersions for paints and coatings. Selective gas phase oxidation of isobutene to methacrylic acid is a well-developed two-stage industrial process performed in the 200-400 °C temperature range. The first step includes oxidation of isobutene to methacrolein (MAL), and in the second step MAL is oxidized to methacrylic acid (MAA). [1-14] As described in the introduction of this thesis synthesis of bio-isobutene from sugar by direct fermentation process has been developed by *Global Bioenergies* and is approaching the industrialization at large scale. However it is necessary to verify if the existing industrial process for petro-isobutene oxidation can be applied to bio-isobutene. Bio-isobutene produced by fermentation might contain different impurities such as water vapor, sulfur containing molecules, CO_2, NH_3 and other organic pollutants. According to numerous patents and scientific papers, the catalysts involved in the 1st stage of the process are always multicomponent Mo-Bi based oxides eventually doped with other elements as Fe, Ni, Co, Cs, K, P, Si, Cr, W. [1-3, 5-9] The 2nd stage catalysts generally consist of a mixture of oxides and Keggin-structured heteropolyacids or their salts. The elements more often cited to be present in the composition of these catalysts are Mo, V, P accompanied by As, K, Cs, Fe, Sb, Ni, Co, B, Ru, Bi, W. [1, 3, 10-14] The interaction of the various impurities with such catalysts was, at our knowledge, never reported up to now.

The aim of this work was to determine the impact of the gaseous impurities present into the bio-isobutene on the industrial and model catalysts, using adsorption microcalorimetry as main technique. The objective was to identify the phases able to interact with SO_2, CO_2 and NH_3, and to

understand the type of interaction. The bonding is characterized by the value of the differential heats (Q_{diff}) of probe molecule adsorption, and therefore Q_{diff} of probe molecule adsorption on industrial and model catalysts were compared. The catalysts were also characterized by BET, XRD, TG-DTA-MS and chemical analyses.

In addition to the study of the impurities interaction with the catalysts, performing adsorption calorimetry analysis allowed also to obtain the acid/base surface properties of the different catalysts. The data can be used to implement the acid/base scale of solid materials. [15]

5.2. Results and discussion

5.2.1. Characterization of the commercial catalysts used for the oxidation of isobutene to methacrylic acid

The chemical analysis performed on these two catalysts confirmed the dominant presence of the following elements in the 1st stage catalyst: Mo, Bi, Fe, Ni, Co; while the principal elements present in the 2nd stage catalyst were: Mo, V, P. The catalysts presented very low specific surface areas (5 and 3 $m^2 g^{-1}$ for the 1st and 2nd stage catalyst, respectively) as measured by BET method. Table 5.1. summarizes BET specific surface areas and approximate chemical composition of the industrial catalysts.

Table 5.1. BET specific surface areas and chemical composition of the 1st and 2nd stage industrial catalysts for isobutene oxidation.

Catalyst	S_{BET} ($m^2 g^{-1}$)	C. A. (wt. %)										
		Mo	Bi	Co	Fe	Ni	V	P	H	Cs	K	W
1st stage	5	10-50	1-20	1-20	1-10	1-5	traces	traces	traces	~1	traces	traces
2nd stage	3	10-50	traces	-	traces	traces	1-5	1-5	~1	-	~1	traces

Gas phase adsorption microcalorimetry was performed using CO_2, SO_2 and NH_3 as probe molecules. Pretreatment of the catalysts included outgassing overnight at 350 °C and the adsorption of the gas probe molecules on the solid catalysts was performed at 150 °C. The 1st stage catalyst did not show any interaction with any of the gas probe molecules and consequently seems to be a suitable catalyst for the oxidation of bio-isobutene to bio-methacrolein.

On the other hand, the 2nd stage catalyst did not interact with the acid probe molecules (CO_2 and SO_2), while it showed very strong interaction with ammonia, resulting in an unusual shape of the volumetric isotherms (Figure 5.1.- top) which can indicate the co-presence of chemical reaction

(between some of the phases of the catalyst and ammonia) and perhaps some reduction of the catalyst upon reaction with ammonia. The initial differential heats of NH_3 adsorption were high (between 120 and 150 kJ mol^{-1}) and the shape of the curve Q_{diff} *vs.* ammonia uptake (Figure 5.1.-bottom) revealed the heterogeneity in the catalyst composition. After addition of each successive small dose of NH_3, a very long time (30-45 minutes) was needed to reach the equilibrium before to inject the next dose (see Experimental part, Section 4.2.7.). As comparison, usually chemical/physical adsorption of such small dose of ammonia at 150 °C lasts about 15 minutes. The quantity of the sample (0.1, 0.4 or 1g) was varied in different experiments in order to complete the adsorption, desorption and readsorption steps characteristic of the experimental procedure in gas-phase adsorption microcalorimetry (described in Experimental part- Section 4.2.7.). However due to an intense adsorption of ammonia during each dose the experimental process could not be completed during one working day when the quantities of 0.4 and 1 g of the sample were used. When 0.1 g of the sample was used the full adsorption process (1^{st} isotherm) was completed. As can be seen, using 1g of catalyst led to a different shape of the isotherm which could be explained by strong diffusion problems. Moreover, the shape of the isotherms in the domain of very low pressure indicates that the adsorption can be considered as totally reversible.

Catalytic tests using standard petro-isobutene feed were performed at *ARKEMA* and the results were compared with the catalytic tests performed when 0.2 mol% of NH_3 or CH_3SH was added in the reaction feed during 100h (impurity/isobutene= 0.2 mol%). The amount of the two impurities added was much higher than that expected to be present in bio-isobutene in order to simulate long term effect of the impurities on the production process. Finally, TG-DTA-MS and XPS studies were performed on the 2^{nd} stage catalyst: fresh, after catalytic tests with addition of NH_3 and CH_3SH like impurities, and after NH_3 adsorption calorimetry analyses.

When ammonia or methyl mercaptan were present in the reaction feed no new compounds formation was detected at the exit of the first or the second stage reactors. Moreover, the catalytic performance in both reactors was not influenced during 100h in the presence of much higher amount of impurities (NH_3 and CH_3SH) than expected in bio-isobutene. XPS studies revealed that on the 2^{nd} stage catalyst nitrogen-containing compounds were deposited on the surface when ammonia was present in the feed. Chemical analysis confirmed that there was no interaction with SO_2 on both catalysts.

Figure 5.2. reports the TG and MS signals as a function of temperature obtained during TG-MS analysis of the 2^{nd} stage catalyst: fresh, after NH_3 adsorption microcalorimetry experiments, and after catalytic tests performed with the addition of ammonia in the petrochemical isobutene feed (performed at *ARKEMA*). The molecules detected by mass-spectrometry in the out-streaming gas were H_2O (from RT to 200 °C), and NH_3 and N_2O (in the 350-450 °C range). The NH_3-containing compounds formed during adsorption calorimetry or in catalytic tests were stable up to 350 °C. The decomposition performed in inert gas (Ar) involves oxygenated molecules (N_2O) with the hypothesis that NH_3 reduced the catalyst to form N_2O, as indicated by XPS analyses. The relatively low desorption temperature can explain why the catalytic activity does not decrease when the catalyst comes in contact with NH_3 in the

reaction conditions (300-400 °C). Additionally, the TG-MS and XPS analyses were performed on the HPMo heteropolyacid fresh and after adsorption of ammonia in the calorimeter, since this was the phase suspected to strongly interact with ammonia; the obtained results were indeed in agreement with the results presented for the 2nd stage catalyst. Further study consisted in ex-situ experiments for identifying the single phases of the commercial catalysts that could be responsible of the interaction with ammonia and sulfur containing compounds in bio-isobutene. For this purpose, representative model catalysts were selected and NH_3 and SO_2 gas phase adsorption microcalorimetry performed.

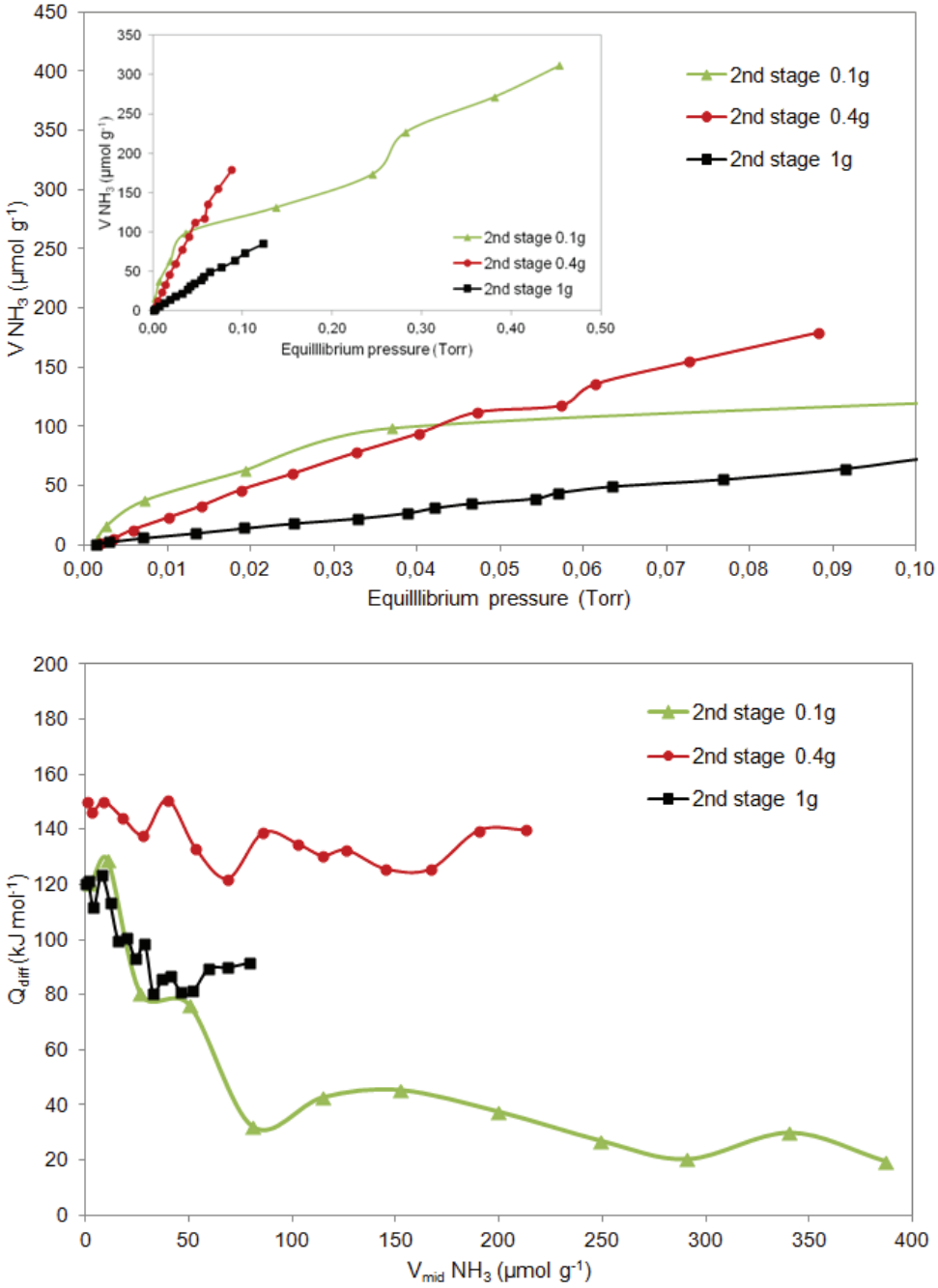

Figure 5.1. Volumetric isotherms of ammonia adsorption (top) and the curves of the differential heats (Q_{diff}) of ammonia adsorption versus coverage (bottom) for the 2nd stage industrial catalyst.

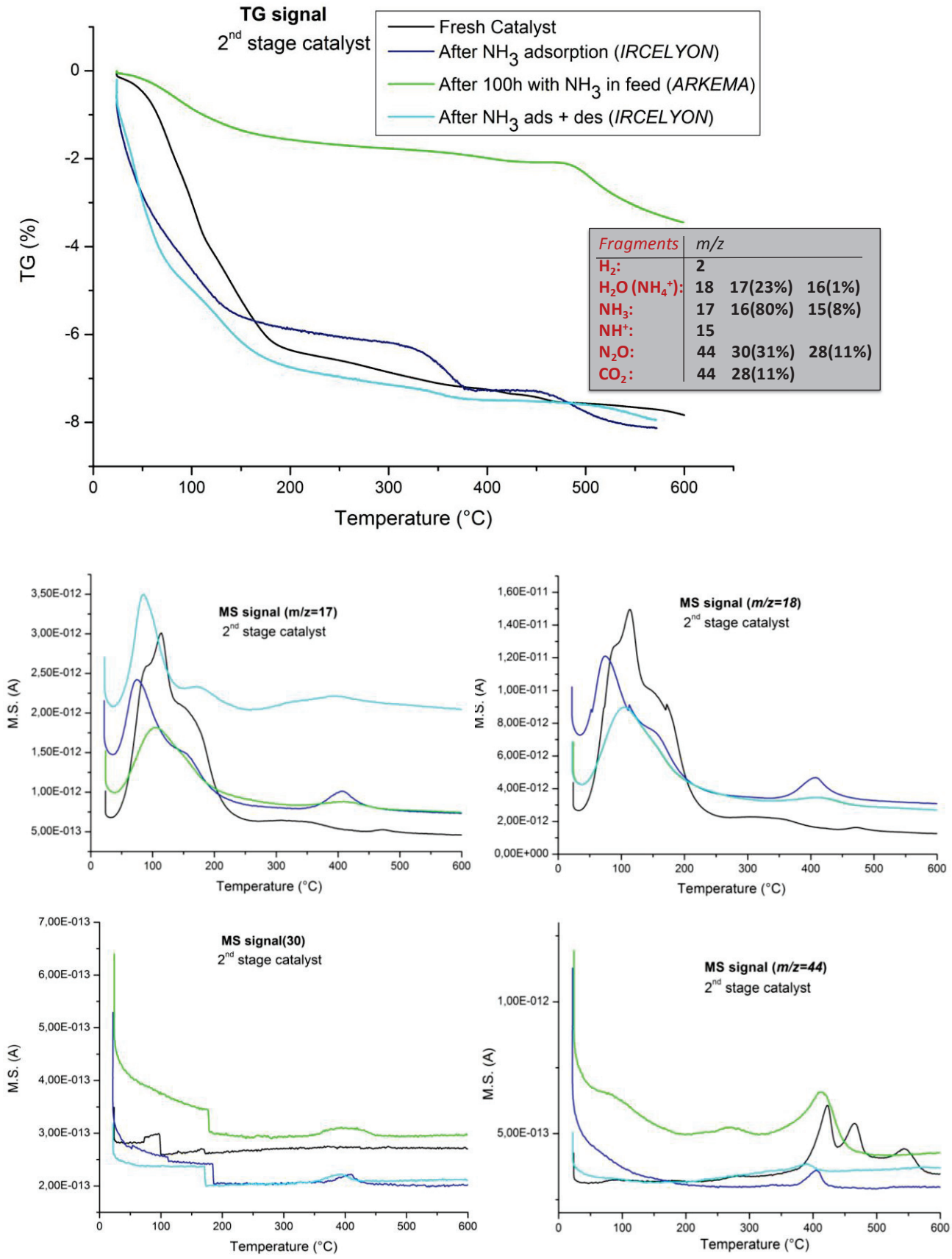

Figure 5.2. TG and MS signals as a function of temperature for the 2nd stage catalyst: fresh, after NH_3 adsorption microcalorimetry, and after catalytic tests with petrochemical isobutene in presence of ammonia.

5.2.2. Adsorption microcalorimetry performed on model catalysts

Based on the preliminary results performed on the 1st and 2nd stage industrial catalysts, single phases were identified and selected for further investigation of ammonia interaction by adsorption microcalorimetry. Results will be presented in the following sections dedicated to acid/base properties of single oxides and bulk Keggin-type heteropolyacids, respectively, and compared with the literature.

5.2.2.1. Adsorption microcalorimetry on the bulk oxides

V_2O_5, V_2O_4, MoO_3, NiO, Fe_2O_3 and Bi_2O_3 were selected as bulk oxides. V_2O_5 and V_2O_4 were purchased from Sigma-Aldrich. Specific surface areas of V_2O_5 and V_2O_4 were 4 and 9 $m^2\ g^{-1}$, respectively. MoO_3, NiO, Fe_2O_3 and Bi_2O_3 were synthesized using simple precipitation methods followed by calcination at suitable temperature (described in Experimental part of this manuscript, Section 4.1.1.1.). The structure of the synthesized single oxides was confirmed by XRD analysis. The diffractograms obtained for each of them matched with the reference XRD pattern from the ICCD-PDF4$^+$ database and are shown in figures below (Figures 5.3-5.6.). In each case the pure well crystallized phase of the desired oxide was obtained. Generally, precipitated oxides presented in this chapter were characterized by low specific surface areas (reported in Table 5.2.).

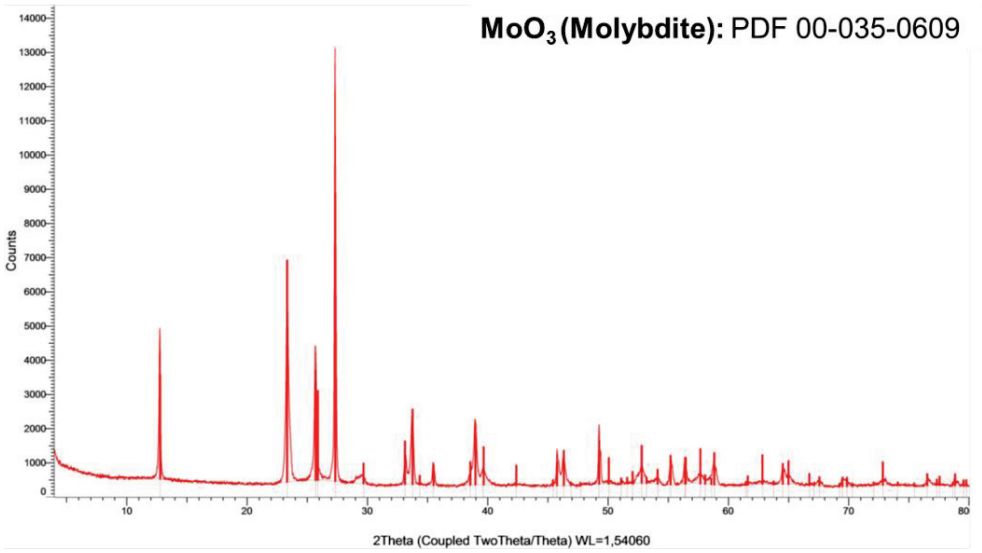

Figure 5.3. Diffractogram of the synthesized MoO_3 matched with the reference XRD pattern from ICDD-PDF4$^+$ (*Molybdite: PDF 00-035-0609*).

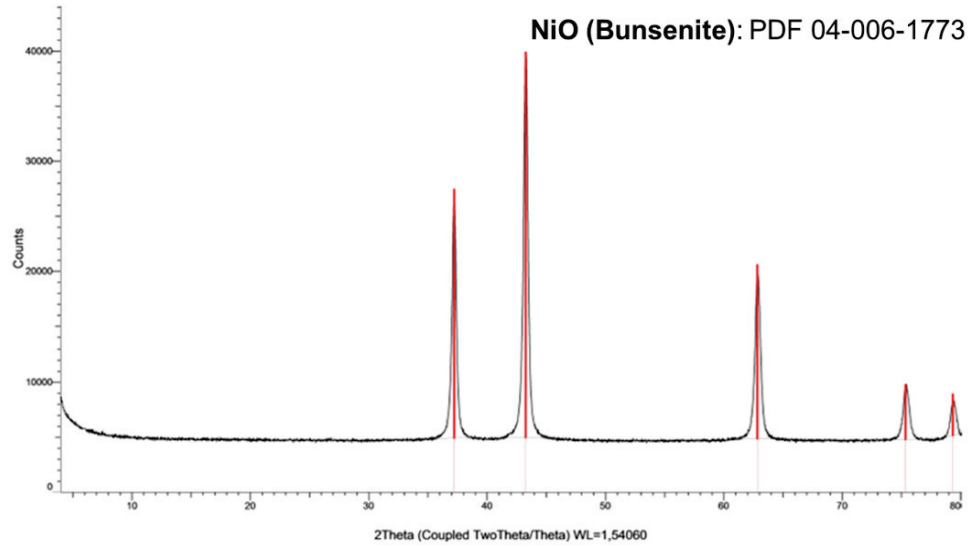

Figure 5.4. Diffractogram of the synthesized NiO matched with the reference XRD pattern from ICDD-PDF4^{+} (*Bunsenite: PDF 04-006-1773*).

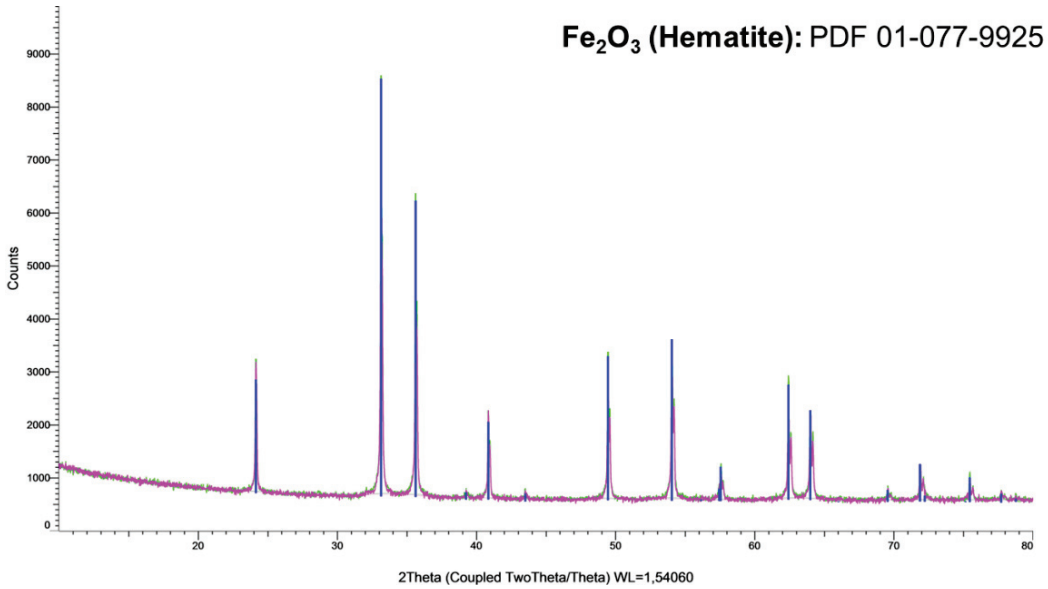

Figure 5.5. Diffractogram of the synthesized Fe_2O_3 matched with the reference XRD pattern from ICDD-PDF4^{+} (*Hematite: PDF 01-077-9925*).

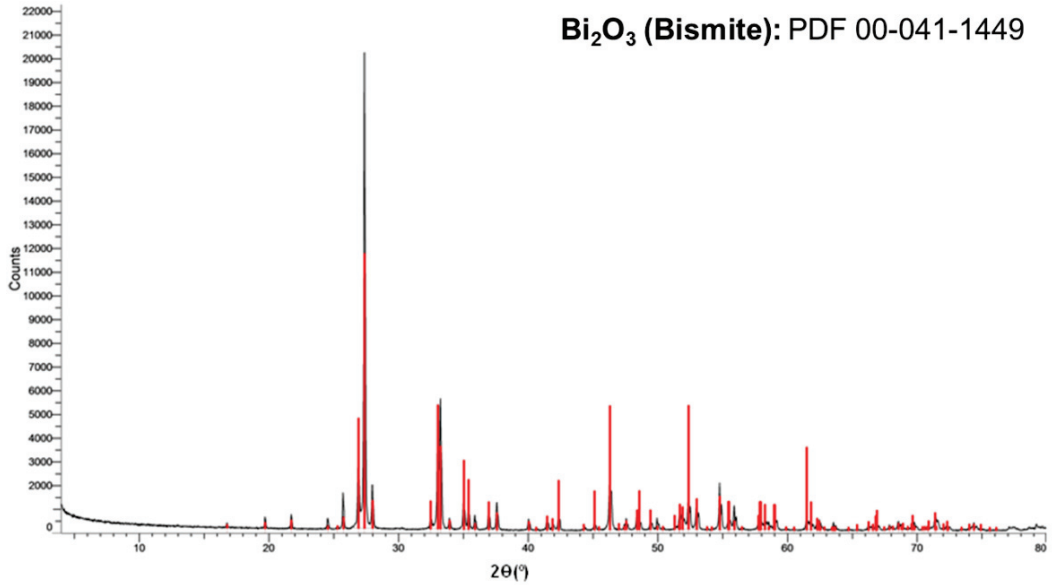

Figure 5.6. Diffractogram of the synthesized Bi_2O_3 matched with the reference XRD pattern from ICDD-PDF4$^+$ (*Bismite: PDF 00-041-1449*).

The initial values of differential heats (Q_{init}) and total amount of the probe molecules adsorbed by oxides are given in Table 5.2. Figure 5.7. represents curves of differential heats *vs.* probe molecule coverage and volumetric isotherms for NH_3 adsorption. Curves of differential heats as a function of SO_2 coverage are shown in Figure 5.8. Samples were outgassed overnight at 350 °C and probe molecule adsorption temperature was maintained at 150 °C. Although, specific surface areas of the oxides were all relatively low (below 50 $m^2\ g^{-1}$), the differences in BET values between some oxides are significant (Table 5.2.), and therefore comparison of the acid/base properties of the oxides is more suitable if specific surface areas are taken into account (µmol m^{-2}). The studies of the acid/base surface properties on these type of oxides using ammonia or sulfur dioxide adsorption microcalorimetry are not so common in the literature and not performed under the same conditions. Besides, factors like calcination temperature, BET areas, pretreatment temperature, adsorption temperature, type of probe molecule, etc; influence the acid/base properties of the solid materials under study. [16, 17]

Table 5.2. BET specific surface areas and acid/base properties of the single oxides. [a] Heat evolved after the adsorption of the first dose of the probe molecule. [b] Total amount of probe molecule adsorbed at 0.2 Torr of equilibrium pressure.

Sample	S_{BET} ($m^2\ g^{-1}$)	NH_3			SO_2		
		Q_{init}[a] (kJ mol^{-1})	V_{tot}[b] (µmol g^{-1})	V_{tot}[b] (µmol m^{-2})	Q_{init}[a] (kJ mol^{-1})	V_{tot}[b] (µmol g^{-1})	V_{tot}[b] (µmol m^{-2})
NiO	34	274	39.94	1.17	184	50.95	1.50
Fe_2O_3	12	146	36.52	3.04	162	23.18	1.93
MoO_3	3	115	9.17	3.05	-	-	-
Bi_2O_3	1	-	-	-	-	-	-
V_2O_4	9	171	24.24	2.69	-	-	-
V_2O_5	4	98	10.43	2.61	-	-	-

The highest quantity of ammonia adsorbed was observed for Fe_2O_3. The initial differential heat of NH_3 adsorption was 162 kJ mol^{-1} and values of Q_{diff} higher than 100 kJ mol^{-1} were kept until approximatively 2 µmol m^{-2} (20 µmol g^{-1}) coverage, showing the presence of strong acidic sites on the sample surface. The total ammonia coverage was 3.6 µmol m^{-2}. In the same adsorption conditions, but on Fe_2O_3 (46 m^2 g^{-1}) pretreated at higher temperature under oxygen flow, Tu et al [18] reported that ammonia coverage reached 3.5 µmol m^{-2} and that the value of Q_{init} was 110 kJ mol^{-1}. Characterization of basic properties of Fe_2O_3 (Table 5.2. and Figure 5.8.) by SO_2 adsorption confirmed the presence of strong basic sites characterized by a plateau positioned around 170 kJ mol^{-1} in the Q_{diff} *vs.* coverage curve. SO_2 total coverage reached 3.3 µmol m^{-2} (40 µmol g^{-1}). Fe_2O_3 showed amphoteric character with presence of both strong acidic and basic sites, in agreement with some previously reported research which studied adsorption of some other probe molecules by adsorption microcalorimetry to test iron oxide acid/base properties. [19-21]

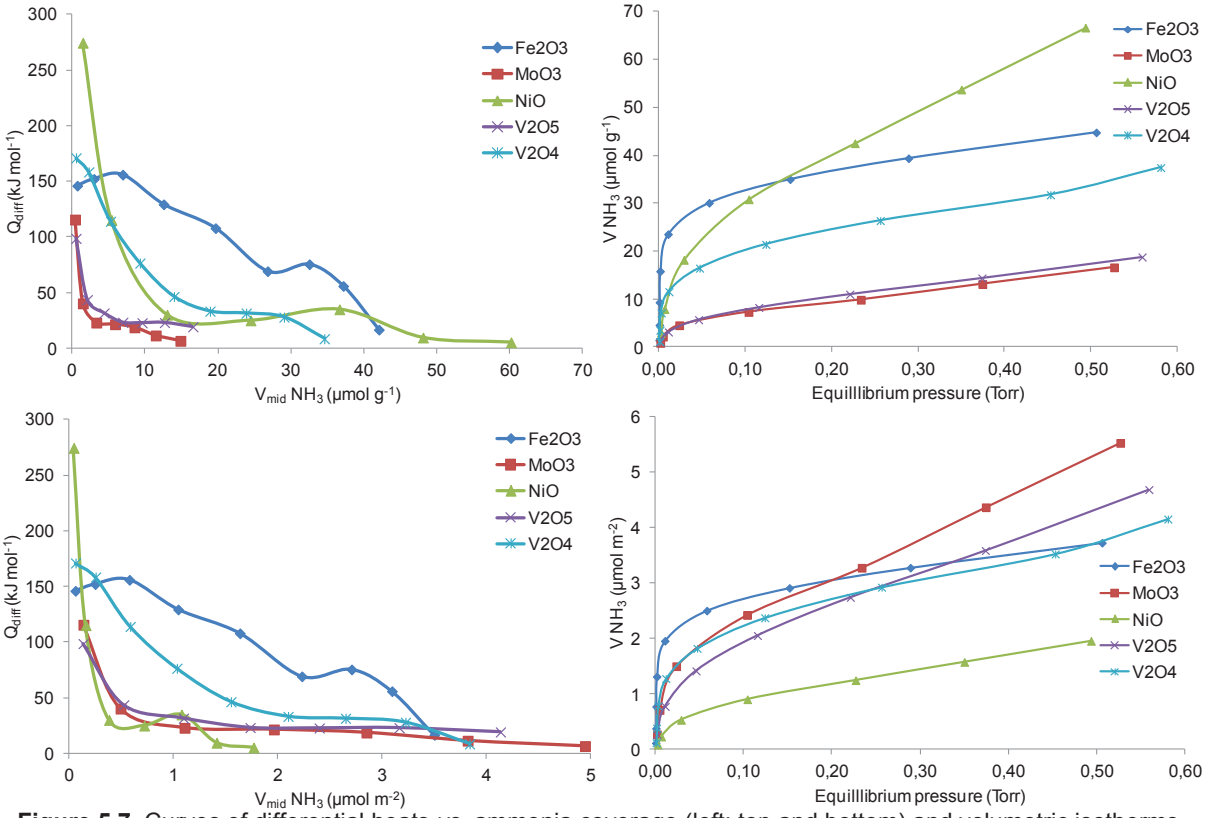

Figure 5.7. Curves of differential heats *vs.* ammonia coverage (left: top and bottom) and volumetric isotherms (right: top and bottom) for single oxides pretreated overnight under vacuum at 350 °C. Adsorption temperature was 150 °C.

NiO also showed amphoteric character. Initial heat of ammonia adsorption was very high (274 kJ mol^{-1}) but after the first dose it decreased below 50 kJ mol^{-1}, exhibiting only the presence of weak acidic sites. The results obtained are in accordance with those presented by Tu et al [18] which also reported very high initial heat of ammonia adsorption (Q_{init}≈250 kJ mol^{-1}). This behavior may be due to the formation of coordination compounds between NH_3 and nickel cations, instead of a simple

chemisorption of NH_3 on the surface. Differential heats of NH_3 adsorption decreased very quickly with coverage. Moreover, NiO displayed strong basicity (CO_2 adsorption). [18] In this thesis, NiO strong basicity was evidenced by SO_2 adsorption with an initial heat of 184 kJ mol^{-1} (and characterized by a large plateau around 130 kJ mol^{-1}) and the saturation coverage at 2.7 µmol m^{-2} (around 90 µmol g^{-1}).

All the other oxides adsorbed only NH_3. Considering V_2O_4 and V_2O_5 oxides, stronger acidity was observed for V_2O_4 which possesses some amount of strong acidic sites (Q_{init}=171 kJ mol^{-1}), while initial heat of NH_3 adsorption on V_2O_5 was lower than 100 kJ mol^{-1} and characteristic of weak acidic sites. Results obtained on vanadium oxides for acidic properties and the absence of basicity are generally in agreement with numerous researches reported on different bulk and supported vanadium oxides performed by microcalorimetry using different probe molecules. [22-29]

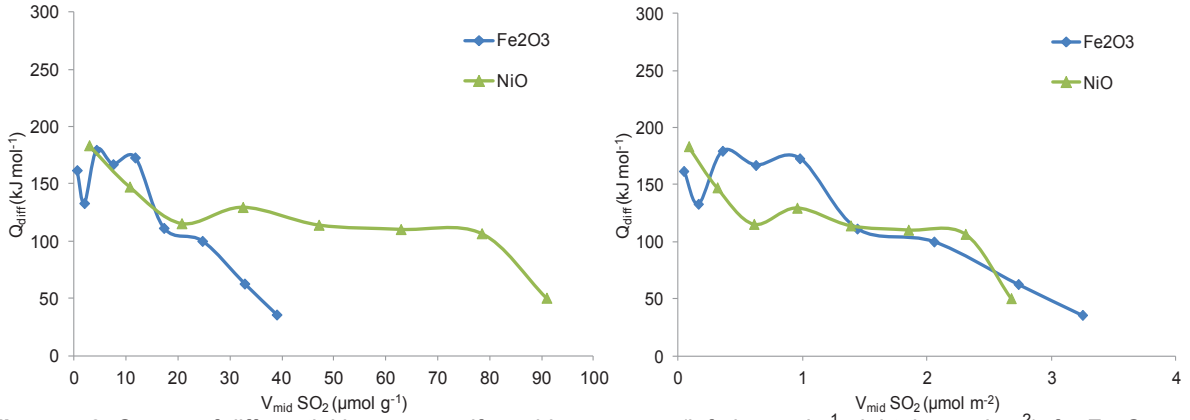

Figure 5.8. Curves of differential heats *vs.* sulfur oxide coverage (left: in µmolg^{-1}; right: in µmol m^{-2}), for Fe_2O_3 and NiO pretreated overnight under vacuum at 350 °C. Temperature of SO_2 adsorption was maintained at 150 °C.

The initial heat of ammonia adsorption on MoO_3 was 115 kJ mol^{-1}, but immediately abruptly decreased below 50 kJ mol^{-1} after the first ammonia dose. This sample showed only presence of weak acidic sites. However the total amount of ammonia adsorbed at 0.2 Torr is almost the same as that measured for Fe_2O_3 sample (both around 3 µmol m^{-2}, Table 5.2.). The results obtained for molybdenum oxide are in agreement with the results reported by Auroux and Gervasini which showed that weak acidic sites are present on the surface of this oxide (using NH_3 as probe molecule), while basic sites were not observed (absence of CO_2 adsorption). [26, 30]

Bi_2O_3 sample showed no adsorption (nor ammonia nor sulfur oxide).

5.2.2.2. Adsorption microcalorimetry on the bulk Keggin-type heteropolyacids

Heteropolyanions are polymeric oxoanions formed by the condensation of more than two different mononuclear oxoanions. Keggin-type heteropolyacids (HPAs) have especially received much

attention in the area of catalysis because their chemical properties (such as redox potential, acidity, and solubility) can be tuned by an appropriate choice of the constituent elements. They can substitute liquid acids (*i.e.* H_2SO_4) in various reactions such as oxidation, esterification, and transesterification. Moreover, they are versatile green catalysts usable in a variety of reaction media. HPAs are used in both gas-phase and liquid-phase reactions. Heteropolyacids exhibit Brønsted acidity, significantly higher compared with the acidity of traditional mineral acid catalysts. Various methods such as titration, pyridine and NH_3-TPD, adsorption microcalorimetry, spectroscopic and computational studies have been used to investigate their acid sites features. [31-37]

In this work, adsorption calorimetry in gas phase using ammonia [38] and in liquid phase using phenylethylamine (PEA) [39] has been used to characterize the acidic properties of four Keggin-type HPAs: 12-tungstophosphoric acid ($H_3PW_{12}O_{40}$, HPW), 12-tungstosilicic acid ($H_4SiW_{12}O_{40}$, HSiW), 12-molybdophosphoric acid ($H_3PMo_{12}O_{40}$, HPMo), and 12-molybdosilicic acid ($H_4SiMo_{12}O_{40}$, HSiMo).

Powder X-ray diffraction was used to confirm the crystalline structure of the heteropolyacids. As it can be observed from Figure 5.9., HPW sample shows the highest crystallinity and the 12-tungstophosphoric acid structure was confirmed, in agreement with pattern previously reported. [34, 35] HPMo and HSiMo display identical diffractograms corresponding to the XRD patterns characteristic of Keggin-structured heteropolyacids (*PDF 00-030-0317 and PDF 04-015-4751*). The lowest crystallinity was observed for HSiW acid. However, in all diffractograms there is the presence of well defined peaks in the 6-12, 17-24, and 26-30° 2θ regions.

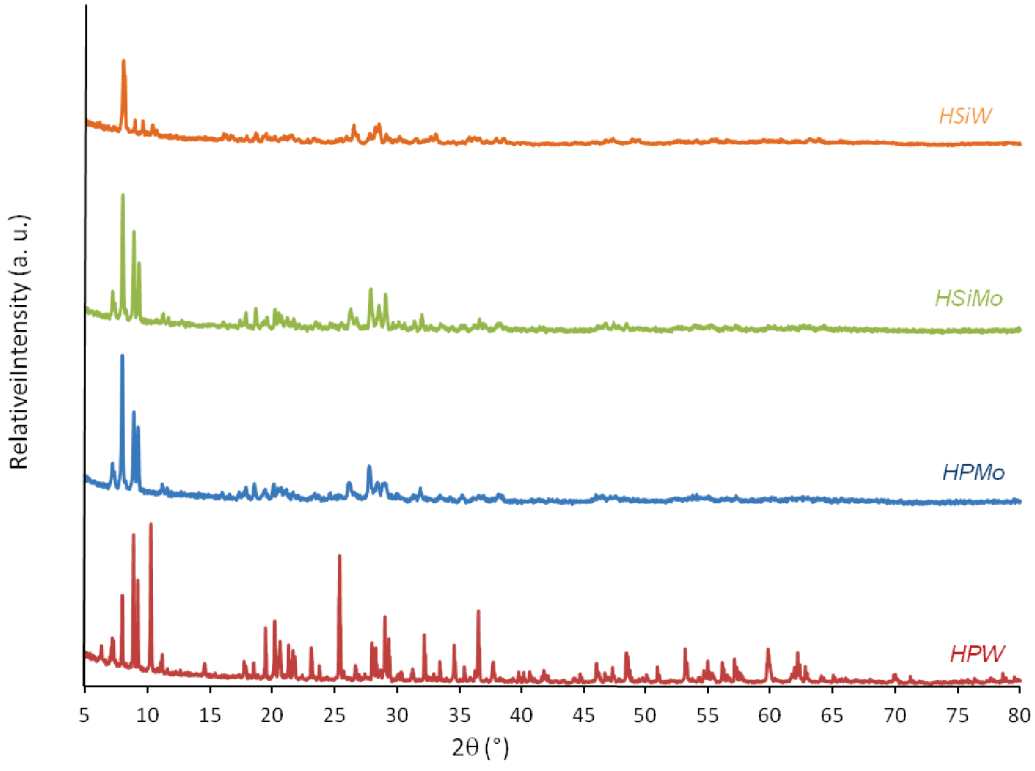

Figure 5.9. XRD patterns of heteropolyacids.

BET specific surface areas of these bulk heteropolyacids were close to 5 $m^2 g^{-1}$, as expected and previously reported. [31, 34, 36]

Adsorption microcalorimetry using ammonia as a probe molecule as well as DFT studies were relatively largely applied to determine the strength and amount of acidic sites of heteropolyacids. The most largely studied and used in heterogeneous catalysis were tungsten-containing Keggin-type heteropolyanions thanks to their higher thermal stability when compared to Mo-containing heteropolyacids. [31-37] Authors reported that the values of the initial heat of ammonia adsorption were even higher than 200 kJ mol^{-1}, while the plateaus observed on the curves Q_{diff} *vs*. coverage were located between 150 and 200 kJ mol^{-1}. Tungsten-based heteropolyacids always exhibited higher Q_{diff} values of the plateau than molybdenum-based heteropolyacids. In general, the acidity decreases in order HPW>HSiW>HPMo>HSiMo. To the other hand, heteropolyanions acidity is also significantly influenced by the pretreatment temperature prior to acidity determination, and it is reported to decrease with increasing temperature. Therefore, the choice of the appropriate pretreatment temperature is very important.

In Figure 5.10. thermal stability of the four heteropolyacids studied in this work was checked by thermogravimetric analysis, and the results obtained are in agreement with the research presented by Bardin et al. [36] The four samples lost physisorbed and hydration water up to 200 °C, leaving anhydrous Kegging units with associated protons. Further temperature increasing brought to the releasing of “protonic water” which is formed by extraction of an oxygen atom from the Keggin anion by two protons thus decomposing the heteropolyacid and resulting in a lower acidity of the material. Decomposition of the Keggin structure occurs at lower temperatures for molybdenum-containing heteropolyacids, starting from around 325 °C for HPMo and HSiMo, while HPW and HSiW were stable up to 425 °C (Figure 5.10.- top). However, it is known that after thermal treatment, the Keggin units can be regenerated in presence of water vapor and consequently the strong acidity reestablished. [4, 32] The acidity of 4 heteropolyacids was determined on samples pretreated at 200 °C before adsorption of ammonia.

Figure 5.11. displays the differential heats (Q_{diff}) curves *vs.* ammonia uptake (Figure 5.11.- top) and the volumetric isotherms (Figure 5.11.- bottom). Very high heats of ammonia adsorption were measured and high amounts of strong acidic sites were evidenced as expected. The shortest plateau on the Q_{diff} *vs.* ammonia coverage curves was observed for HPW sample, which however presented the strongest acidic sites (Q_{diff}-plateau located around 176 kJ mol^{-1} and Q_{init}=186 kJ mol^{-1}). HSiW presented a larger plateau than HPW, representative of a higher number of strong acidic sites (Q_{init}=182 kJ mol^{-1} and Q_{diff}-plateau around 155 kJ mol^{-1}). Finally, HPMo presented the largest plateau characteristic of a high number of strong acidic sites of homogeneous strength (Q_{init}=180 kJ mol^{-1} and plateau around Q_{diff}=148 kJ mol^{-1}). On the other hand, HSiMo displayed the highest value of Q_{init} (200 kJ mol^{-1}) but no clear plateau was observed and the curve of Q_{diff} *vs.* coverage continuously decreased. However, this sample adsorbed the highest amount of ammonia.

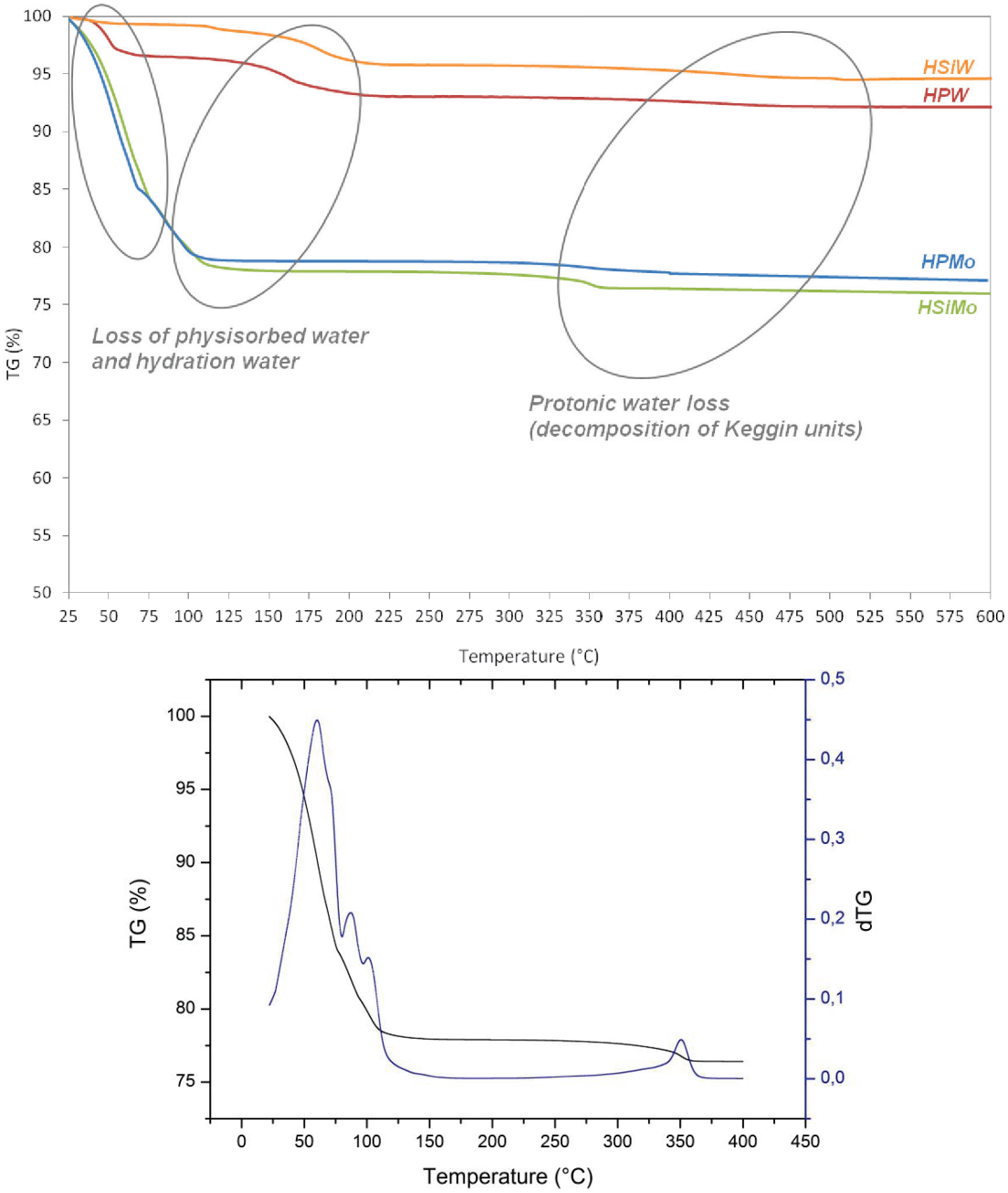

Figure 5.10. TG curves of bulk heteropolyacids (top). TG-DTA curves for HSiMo given as example (bottom).

Table 5.3. summarizes the heats evolved from the adsorption of the first dose of NH_3 (Q_{init}), the values of Q_{diff}-plateau, and the total amount of NH_3 adsorbed at 0.2 Torr of equilibrium pressure. These data were used to make a comparison among the heteropolyacids considering the strength of the acidic sites and the amount of strong acidic sites. The comparison is represented in Figure 5.12.

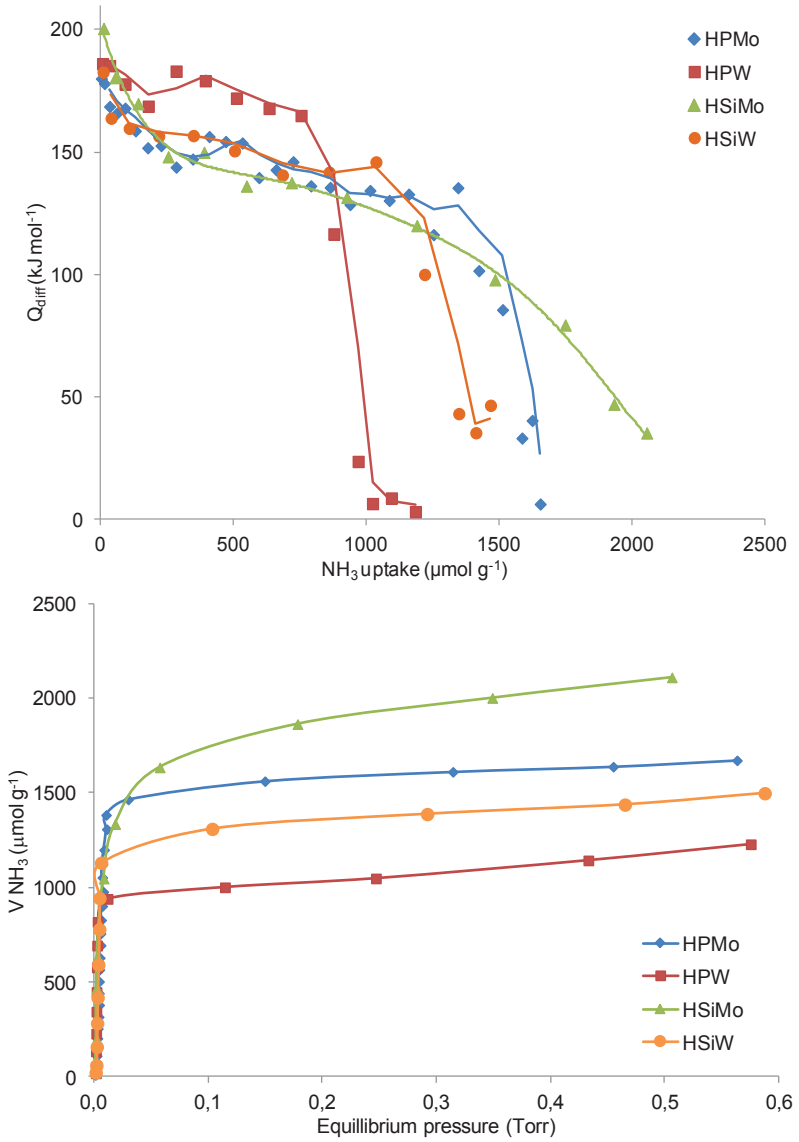

Figure 5.11. Curves of differential heats *vs.* ammonia coverage (top) and volumetric isotherms (bottom) for heteropolyacids pretreated overnight under vacuum at 200 °C. Temperature of ammonia adsorption was maintained at 150 °C.

Table 5.3. Acidic properties of bulk heteropolyacids. [a] Heat evolved after the adsorption of the first dose of ammonia. [b] Estimated value (Q_{diff}-plateau) of the plateau observed for curves Q_{diff} *vs.* coverage. [c] Total amount of ammonia adsorbed at 0.2 Torr of equilibrium pressure.

Sample	NH_3			
	Q_{init}[a] (kJ mol^{-1})	Q_{diff}-plateau (kJ mol^{-1})	V_{tot} (µmol g^{-1})	V_{tot} (µmol m^{-2})
HPW	186	176	1031.4	206.3
HPMo	180	148	1577.1	315.4
HSiW	182	155	1350.0	270.0
HSiMo	200	140	1881.5	376

As observed in Figure 5.12. the strength of acidic sites decreases in the HPW>HSiW>HPMo>HSiMo order, as already shown in the literature. [31-37] On the other hand, the amount of the ammonia adsorbed at 0.2 Torr decreases in the inverse order, which is also in

agreement with previous studies [31-37]: HSiMo>HPMo>HSiW>HPW. We can observe that, concerning the number of acid sites, $H_4SiMo_{12}O_{40}$>$H_3PMo_{12}O_{40}$ and $H_4SiW_{12}O_{40}$>$H_3PW_{12}0_{40}$ respectively, in agreement with their respective number of protons in the structure.

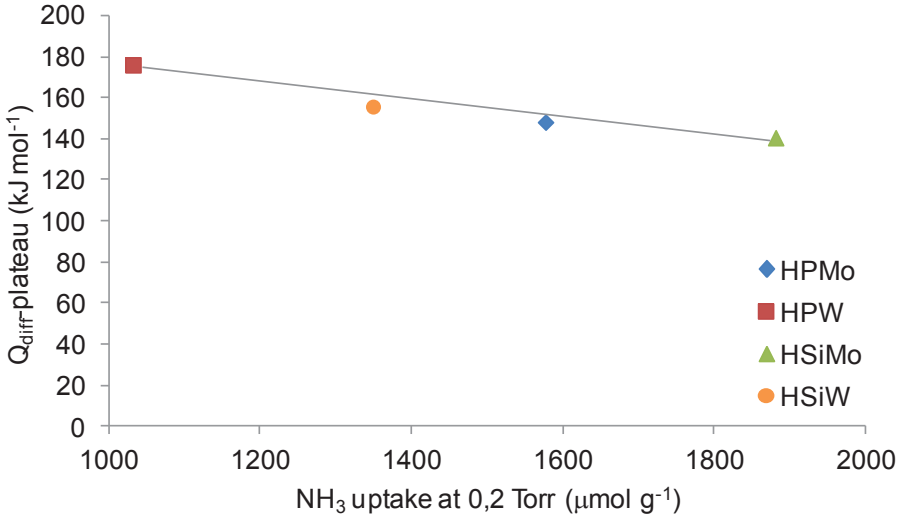

Figure 5.12. Classification of the acidity of heteropolyacids.

Additionally, gas phase NH_3 adsorption microcalorimetry performed on heteropolyacids pretreated in vacuum overnight at 350 °C was performed and the results were compared with gas-adsorpton microcalorimetry of the samples pretreated at 200 °C. Results consistent with those proposed in the literature were obtained when gas phase ammonia adsorption calorimetry was performed on the heteropolyacids pretreated at 350 °C under vacuum. [35, 36] From Figure 5.13. it can be observed that HPW still presents a well defined plateau of strong sites at Q_{diff} around 165 kJ mol^{-1} (which is about 10 kJ mol^{-1} lower than that measured for sample pretreated at 200 °C, Figure 5.11. and Table 5.3.). The acidity of HSiW was stronger affected by the higher pretreatment temperature, and even if Q_{init}=180 kJ mol^{-1} and the amount of ammonia adsorbed were very similar to that reported in Figure 5.11. and Table 5.3, the plateau completely disappeared. As expected, the acidity of molybdenum-containing heteropolyacids was strongly affected by the higher pretreatment temperature due to decomposition of the Keggin structure (Figure 5.10.), responsible for superacidity of heteropolyacids.

Moreover the acidity of the 4 heteropolyacids was also determined in liquid phase (n-decane, a non-polar and non-protic solvent) using phenylethylamine- PEA (0.3M PEA solution in n-decane). The samples were pretreated under vacuum overnight at 200 °C. The curves of differential heats *vs.* phenylethylamine (PEA) coverage are presented in Figure 5.14. PEA solution in n-decane was selected as acidity probe in liquid phase and adsorption was carried on at 30 °C. All samples show lower heats of adsorption in liquid phase than in gas phase (Figure 5.11.). The strength and the number of acid sites are apparently strongly influenced by the solvent surrounding the sample surface, in this case n-decane. The heats of adsorption in n-decane are lower than in gas phase due to the

displacement of the solvent by the basic probe, which is an endothermic phenomenon. In liquid phase the differences among the samples are smoothed. HPW, HPMo, and HSiW present very similar curves. HSiMo presents the smallest amount of strong acidic sites.

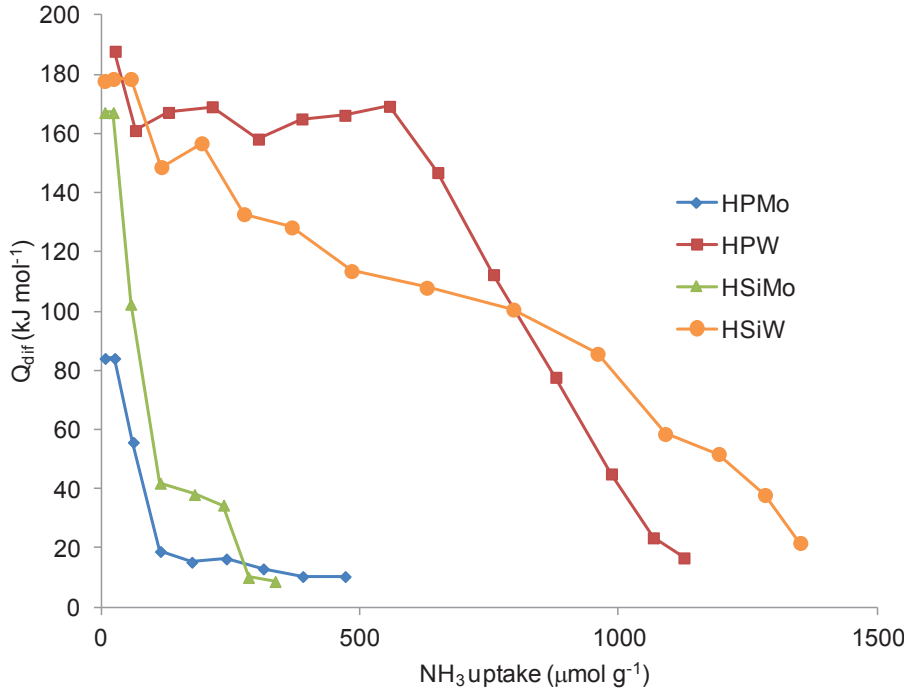

Figure 5.13. Curves of differential heats *vs.* ammonia coverage for the heteropolyacids pretreated overnight under vacuum at 350 °C. Temperature of ammonia adsorption was maintained at 150 °C.

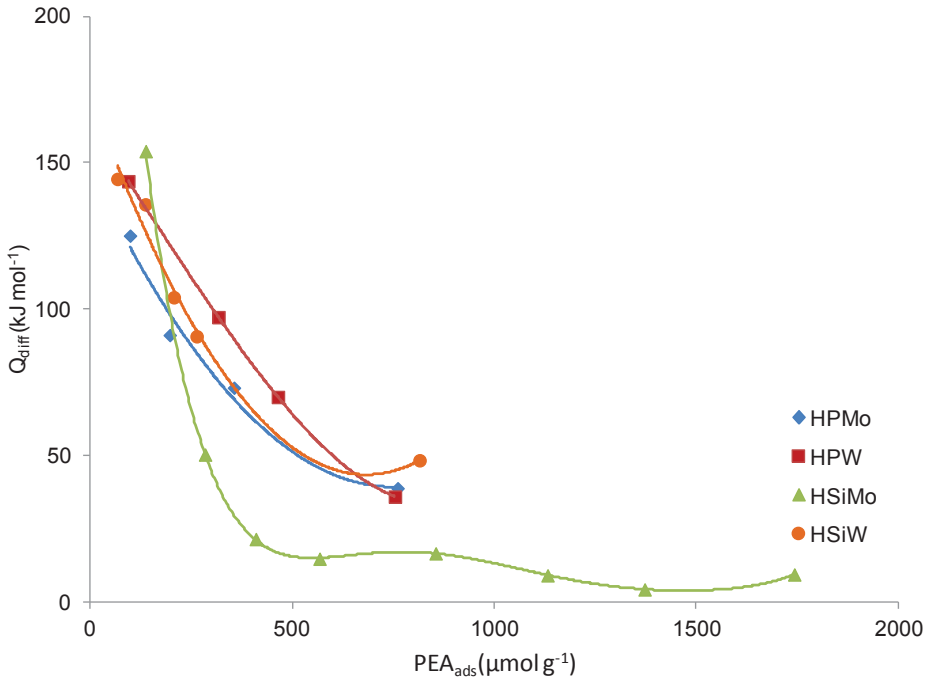

Figure 5.14. Curves of differential heats *vs.* PEA coverage for the heteropolyacids pretreated overnight under vacuum at 200 °C. Adsorption of PEA (PEA solution in n-decane) performed at 30 °C (right).

5.3. Conclusions

This chapter described the work performed with the aim to understand if industrial catalysts used in the two step gas-phase oxidation of isobutene (IBN) to methacrylic acid (MAA) can be applied for a process using bio-sourced isobutene obtained by fermentation of sugars. The impact of acid (SO_2 and CO_2) and basic (NH_3) impurities on commercial and model catalysts was investigated.

The 1st stage catalyst appears to be convenient for oxidation of IBN to methacrolein (MAL). The main phases of the catalyst do not interact with SO_2, CO_2 and NH_3. The presence of heteropolyacid compounds is thus excluded. The 2nd stage catalyst showed strong interaction with ammonia. The NH_3-containing compounds formed during adsorption calorimetry are stable up to 350-450 °C. Their decomposition in inert gas involves oxygenated molecules (N_2O) with the consequent reduction of the catalyst. The species interacting with ammonia involve molybdophosphoric acid or its vanadium containing salt. Interaction with ammonia still occurred when molybdophosphoric acid was replaced by other heteropolyacids (HPW, HSiMO, HSiW). Catalytic tests performed by *ARKEMA* (adding different impurities in the standard petro-isobutene feed) and characterization of the used catalysts confirmed that only presence of ammonia as impurity in bio-isobutene could lead to lower catalytic performances on the 2nd stage catalyst due to its reduction.

However, in this step of the project it was evidenced that the composition of bio-isobutene is very similar to that of the petro-isobutene and therefore NH_3 does not represent a significant impurity which can influence the yield of methacrylic acid or have a potential impact on the catalysts used.

Public results and information about the process of bio-isobutene production and composition of the bio-isobutene, as well as considering production of bio-methacrylic acid from bio-isobutene can be found on the official web sites and press releases of *Global Bioenergies* and *ARKEMA*.

Further work of this PhD thesis was focused exclusively on gas-phase acrolein production from methanol and ethanol mixture, and more precisely on the impact of the acid/base surface properties of the catalysts involved in the aldolization step of this process.

References

[1] J. Guan, K. Song, H. Xu, Z. Wang, Y. Ma, F. Shang, Q. Kan, *Catal. Commun.* **2009**, *10*, 528-532.

[2] M. Kanno, T. Yasukawa, W. Ninomiya, K. Ooyachi, Y. Kamiya, *J. Catal.* **2010**, *273*, 1-8.

[3] Z. Peng, C. Yu, T. Cai, Q. Deng, *J. Nat. Gas Chem.* **2004**, *13*, 172-176.

[4] F. Cavani, R. Mezzogori, A. Pigamo, F. Trifiro, E. Etienne, *Catal. Today* **2001**, *71*, 97-110.

[5] A. Tenten, H.P. Neumann, H. Exner, *US 5 583 086*, assigned to BASF, Germany.

[6] H. Engelbach, R. Krabetz, G. Duembgen, C.H. Willersinn, W. Beitelschmidt, *US 4 298 763*, assigned to BASF, Germany.

[7] H. Kasuga, E. Shiraichi, *US 2002/0198103 A1*, assigned to Nippon Shokubai CO LTD, Japan.

[8] T. Watanabe, O. Nagano, *US 2005/0032639*.

[9] T. Kurakami, T. Kojima, Y. Seo, *EP 2 011 780 B1*, assigned to Nippon Kayaku, Japan

[10] F.G. Martin, H. Hibst, A. Tenten, *US 5 569 636,* assigned to BASF, Germany.

[11] F.G. Martin, H.P. Neumann, H. Hibst, *US 5 583 084*, assigned to BASF, Germany.

[12] A. Sudo, Y. Seo, T. Kurakami, *EP 1 629 889 B1*, assigned to Nippon Kayaku, Japan.

[13] A. Sudo, T. Kurakami, T. Kojima, S. Hayashimoto, *EP 1 867 387 B1*, assigned to Nippon Kayaku, Japan.

[14] *EP 2 436 443 A1*, assigned to Nippon Kayaku, Japan.

[15] A. Auroux, *Top. Catal.* **2002**, 19, 205-213.

[16] A. Auroux (Ed.), *Calorimetry and Thermal Methods in Catalysis*, Springer- Verlag Berlin and Heidelberg GmbH & Co. K, **2013**.

[17] A. Auroux, *Top. Catal.* **1997**, *4*, 71-89.

[18] M. Tu, J.Y. Shen, Y. Chen, *Thermochim. Acta* **1997**, *302*, 117–124.

[19] P.F. Rossi, G. Caracciolo, G. Busca, *Colloids Surf.* **1988**, *32*, 75–85.

[20] P.F. Rossi, G. Busca, V. Lorenzelli, M. Lion, J.C. Lavalley, *J. Catal.* **1988**, *386*, 378–386.

[21] N.Cardona-Martinez, J. Dumesic, *J. Catal.* **1991**, *127*, 706–718.

[22] M. Xue, M. Chen, J. Ge, J. Shen, *Microporous Mesoporous Mater.* **2010**, *131*, 37–44.

[23] J. Le Bars, A. Auroux, J.C. Védrine, M. Baerns, *Stud. Surf. Sci. Catal.* **1992**, *72*, 181–189.

[24] J. Le Bars, J.C. Védrine, A. Auroux, S. Trautmann, M. Baerns, *Appl. Catal., A* **1992**, *88*, 179–195.

[25] A. Gervasini, P. Carniti, J. Keränen, L. Niinistö, A. Auroux, *Catal. Today* **2004,** *96,* 187–194.

[26] A. Auroux and A. Gervasini, *J. Phys. Chem.* **1990**, *94*, 6371-6379.

[27] J. Keränen, A. Auroux, S. Ek-Härkönen, L. Niinistö, *Thermochim. Acta*, **2001**, *379*, 233–239.

[28] J. Keränen, A. Auroux, S. Ek, L. Niinistö, *Appl. Catal., A* **2002**, *228*, 213–225.

[29] J. Le Bars, J.C. Védrine, A. Auroux, S. Trautmann, M. Baerns, *Appl. Catal., A* **1994**, *119,* 341–354.

[30] A. Gervasini, A. Auroux, *J. Catal.* **1991**, *131*, 190-198.

[31] J.B. Moffat, *Metal-Oxygen Clusters: The Surface and Catalytic Properties of Heteropoly Oxometalates*, Kluwer Academic Publishers, New York, **2002**.

[32] I. Kozhevnikov, *Chem. Rev.* **1998**, *98*, 171-198.

[33] M.N. Timofeeva, *Appl. Catal., A* **2003**, *256*, 19-35.

[34] F.X. Liu-Cai, B. Sahut, E. Fayadi, A. Auroux, G. Hervé, *Appl. Catal., A* **1999**, *185*, 75-83.

[35] Lj. Damjanović, V. Rakić, U.B. Mioč, A. Auroux, *Thermochim. Acta* **2005**, *434*, 81–87.

[36] B.B. Bardin, S.V. Bordawekar, M. Neurock, R.J. Davis, *J. Phys. Chem. B* **1998**, 102, 10817-10825.

[37] B.B. Bardin, R.J. Davis, M. Neurock, *J. Phys. Chem. B* **2000**, 102, 3556-3562.

[38] S. Bennici, A. Auroux, *Thermal analysis and calorimetric methods* in *Metal oxide catalysis* (Eds. S. J. Hargreaves and S. D. Jackson), VCH-Wiley, **2009**.

[39] A. Gervasini, P. Carniti, A. Auroux, *Thermochim. Acta* **2005**, *434*, 42-49.

Chapter 6.

Influence of Catalyst Acid/Base Properties in Acrolein Production by Oxidative Coupling of Ethanol and Methanol *(Publication I)*

Published in *ChemSusChem;*
ChemSusChem **2017***, 10,* 1916-1930. DOI: 10.1002/cssc.201700230

CHEMISTRY & SUSTAINABILITY

CHEMSUSCHEM

ENERGY & MATERIALS

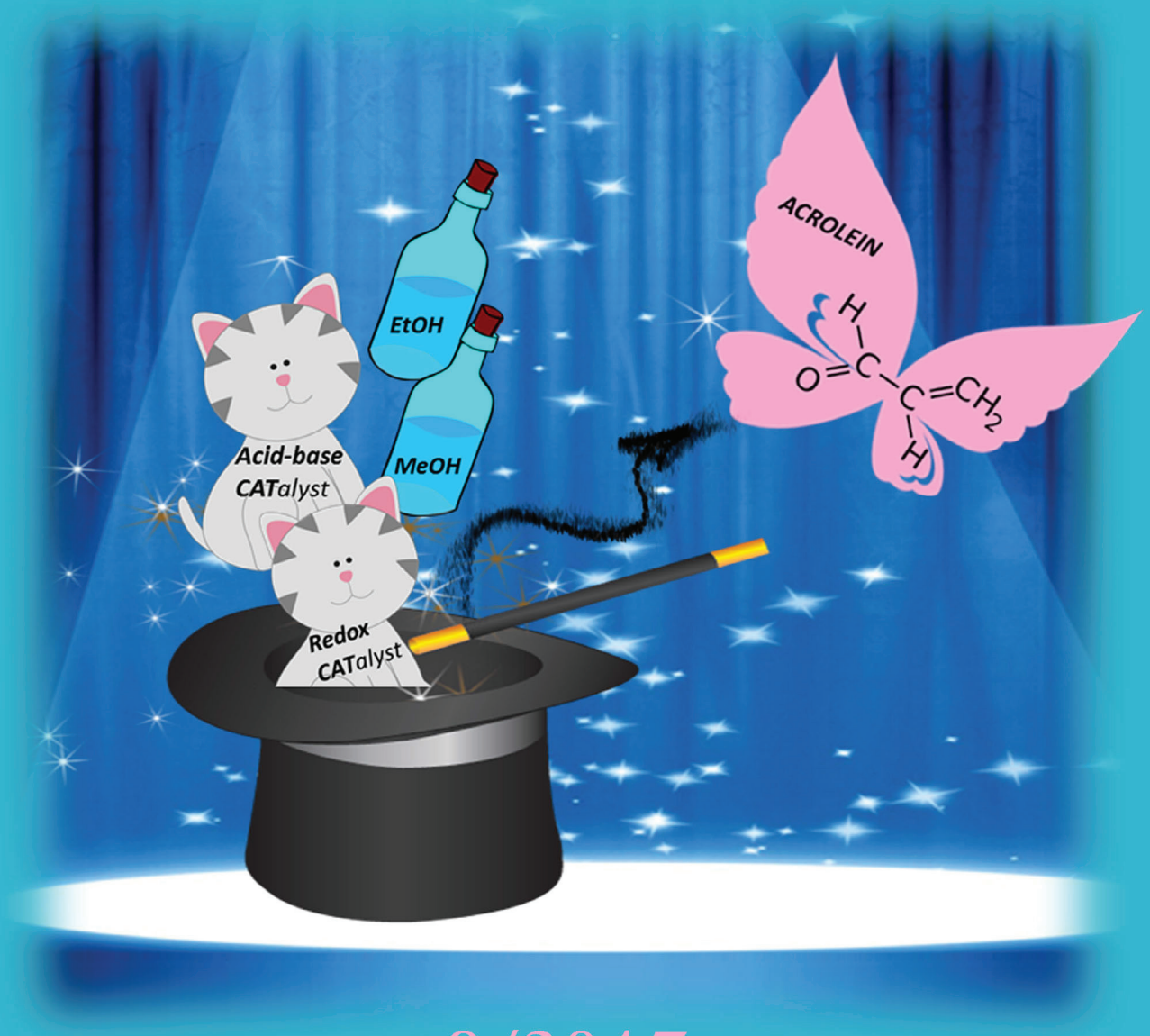

9/2017

Cover Picture:
Lilić et al.
Influence of Catalyst Acid/Base Properties in Acrolein Production by Oxidative Coupling of Ethanol and Methanol

A Journal of
ChemPubSoc Europe

WILEY-VCH

www.chemsuschem.org

COVER PICTURE

A. Lilić, S. Bennici, J.-F. Devaux, J.-L. Dubois, A. Auroux**

■■ – ■■

Influence of Catalyst Acid/Base Properties in Acrolein Production by Oxidative Coupling of Ethanol and Methanol

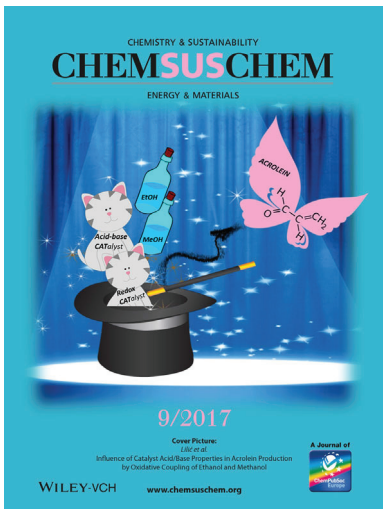

The Inside Cover picture shows the magic of acrolein direct synthesis by oxidative coupling of alcohols (OCA). The process starts by methanol and ethanol oxidation to formaldehyde and acetaldehyde, respectively, on a $FeMoO_x$ redox catalyst followed by the cross-aldolization of aldehydes and dehydration to acrolein taking place on the acid/base catalyst. The alcohols involved in this process can be biosourced; therefore, this new route to produce acrolein is even more interesting as it can replace current fossil-based production of acrolein (oxidation of propylene). In their Full Paper (DOI: 10.1002/cssc.201700230), Lilić et al. discuss the influence of the acid/base sites on the acrolein yield.

ChemPubSoc Europe

DOI: 10.1002/cssc.201700230

CHEMSUSCHEM Full Papers

VIP *Very Important Paper*

Influence of Catalyst Acid/Base Properties in Acrolein Production by Oxidative Coupling of Ethanol and Methanol

Aleksandra Lilić,[a] Simona Bennici,*[a] Jean-François Devaux,[b] Jean-Luc Dubois,[c] and Aline Auroux*[a]

Oxidative coupling of methanol and ethanol represents a new route to produce acrolein. In this work, the overall reaction was decoupled in two steps, the oxidation and the aldolization, by using two consecutive reactors to investigate the role of the acid/base properties of silica-supported oxide catalysts. The oxidation of a mixture of methanol and ethanol to formaldehyde and acetaldehyde was performed over a $FeMoO_x$ catalyst, and then the product mixture was transferred without intermediate separation to a second reactor, in which the aldol condensation and dehydration to acrolein were performed over the supported oxides. The impact of the acid/base properties on the selectivity towards acrolein was investigated under oxidizing conditions for the first time. The acid/base properties of the catalysts were investigated by NH_3-, SO_2-, and methanol-adsorption microcalorimetry. A MgO/SiO_2 catalyst was the most active in acrolein production owing to an appropriate ratio of basic to acidic sites.

Introduction

Acrolein, the simplest unsaturated aldehyde, is widely used in the chemical industry as an intermediate for the synthesis of various chemical products such as acrylic acid, methionine, biocides, and other numerous chemicals.[1–3] In the third decade of the past century, acrolein was industrially produced by aldolization of acetaldehyde and formaldehyde.[4] Later, another synthetic pathway based on propylene oxidation was applied and widely studied.[1] More recently, owing to the growing interest in more diverse raw materials and the need to decrease greenhouse-gas emissions, and to optimize the supply of the reactants, new production processes starting from renewable feedstock (glycerol, propanol, ethanol, methanol) have been considered.[5,6]

Glycerol dehydration has been proposed as a promising alternative for acrolein production.[5,7–12] The acrolein production from glycerol has numerous advantages because glycerol is now ubiquitous as a co-product of the oleochemical industry and biodiesel production. Crude glycerin is a product that is still a rather cheap source of carbon. Following the 12 principles of green chemistry,[13] glycerol dehydration based on waste can be used for on-site/on-demand production to avoid storage and transportation of a dangerous but essential chemical compound. Glycerol can be considered as a renewable compound and the dehydration is performed over acidic heterogeneous catalysts. No additional chemicals are required, the atom economy is maximized (a 3 carbon glycerol molecule affords a 3 carbon acrolein molecule and water), and no solvent except water are used. The energy efficiency is evidenced by the improved carbon foot print: CO_2 captured by plants during growth is transformed into glycerol and later acrolein, which at the end of the product life will be transformed back into CO_2. The risk of pollution can be prevented by on-time/on-site production, which also minimizes the risk of accidents. However, glycerol dehydration also has some drawbacks. Currently glycerin, as a coproduct of biodiesel or oleochemicals, is available in a ratio of 10 wt% of the oil or fat used. This means that for a large biodiesel plant of 250 kt year^{-1}, only 25 kt glycerol is produced, which will be turned into 10 kt year^{-1} acrolein assuming a yield of approximately 70 mol%. This may seem like a large amount but remains small with regard to the requirements of a world-scale plant for methionine or more particularly for acrylic acid (the standard size is now 160 kt year^{-1}). Small-scale plants mean a large contribution of the plant capital cost to the production cost in the form of depreciation, but also as maintenance, property tax, and insurance. Glycerol dehydration catalysts also tend to deactivate rather quickly (in a matter of hours or minutes for the worst catalysts and in a matter of days for the best ones).[14–16] This deactivation requires a frequent regeneration of the catalysts, which increases

[a] A. Lilić, Dr. S. Bennici, Prof. A. Auroux
IRCELYON
UMR 5256 CNRS- Université Lyon 1
2 avenue Albert Einstein, 69626- Villeurbanne cedex (France)
E-mail: simona.bennici@uha.fr
aline.auroux@ircelyon.univ-lyon1.fr

[b] Dr. J.-F. Devaux
ARKEMA
Centre de Recherche Rhône Alpes
69493 Pierre Bénite, Cedex (France)

[c] Dr. J.-L. Dubois
ARKEMA
Direction Recherche & Développement
420 Rue d'Estienne d'Orves, 92705 Colombes (France)

The ORCID identification number(s) for the author(s) of this article can be found under http://dx.doi.org/10.1002/cssc.201700230.

the capital cost of the plant because some catalyst is immobilized during the regeneration and does not contribute to the production. Moreover, glycerol dehydration is an endothermic process performed at approximately 300 °C, whereas the regeneration is exothermic (coke combustion) and performed at higher temperatures. If the process is properly balanced, with reaction and regeneration working in parallel, the heat released during regeneration can cover part of that required for the reaction. Nevertheless, additional heat will be necessary for downstream separation. Whenever refined glycerol is needed in the process, the raw material cost is increased because refined glycerol prices are in the range of 500–700 € ton^{-1}.[14–16] Although refined glycerol might be preferred in some cases, it is wise to leave some remaining water in it because pure glycerol is a highly viscous material at room temperature and would require heated storage in winter or cold weather. In contrast, aqueous glycerol has a much lower melting point, so glycerol containing 50–20 wt% water is more suitable for storage and also more easily pumped.

Therefore, there is still a need to develop an alternative process to produce acrolein or acrylic acid at lower cost, through a route that eventually would use renewable resources. Several companies and research organizations have tried to develop routes using fermentation products such as lactic acid or 3-hydroxypropionic acid to find a sugar-based route. Although these substrates have a potential as low-cost raw materials, the additional fermentation and dehydration steps increase the cost if necessary chemicals, utilities (mainly energy), and labor are considered. Consequently, these routes have not been successful yet. The plants need to be integrated, meaning that, for example, lactic acid needs to be produced on purpose for the dehydration to acrylic acid, because at the current market price of lactic acid its dehydration would otherwise not make sense from an economic point of view.

With the aim to find renewable materials that are easy to transport and transform into acrolein, thus minimizing the investment in existing plants, the oxidation of mixed alcohols (methanol and ethanol, the latter being already biobased) has recently been proposed. In 2012, Dubois et al.[6] described a process to produce acrolein by oxidative coupling of ethanol and methanol. In this process, the conversion of the alcohols to formaldehyde and acetaldehyde as well as the simultaneous condensation and dehydration of the two aldehydes to acrolein are performed in the presence of oxygen. All previous studies published so far[17a–b,18,19] concerning the aldolization route used a mixture of acetaldehyde and aqueous formaldehyde solution stabilized with methanol (Tollens process).[20] This process required a reactor for acetaldehyde production (which is commonly an oxidation of ethylene) in parallel to a reactor for formaldehyde production (either methanol oxidation over an iron-molybdate catalyst or methanol oxydehydrogenation over a silver catalyst) in addition to the aldolization reactor. Altogether, this represents a massive capital cost.

In the following process a single reactor is required, thus reducing the capital cost significantly. The oxidative coupling of alcohols (OCA) solves most of the previously mentioned issues: methanol and ethanol are widely available; ethanol is already biobased and there are more and more projects to produce biobased/renewable methanol, including from urban waste (Enerkem technology). The reaction is highly exothermic owing to the oxidation of the alcohols and, because it is performed above 200 °C, allows the recovery of useful heat for the process. Methanol and ethanol are easily transported and stored, and they can be purchased at reasonable prices. In addition, assuming a 1:1 molar ratio of methanol/ethanol, a 70 mol% yield would be sufficient to match the propylene oxidation process on raw-material-cost basis, leaving room for improvement. Because the reaction is exothermic, the same reactor technology (multitubular reactors) as for propylene oxidation (or methanol oxidation to formaldehyde) can be considered, thereby reducing the technology risk for operators. However, because the alcohol oxidation reaction is known to proceed at shorter contact times [higher gas hourly space velocity (GHSV)] than the propylene oxidation, there is a potential to have smaller reactors, thus reducing the capital cost. The direct acrolein production by gas-phase OCA is illustrated in Scheme 1. Both reaction steps can be performed in a single reactor catalyzed by iron molybdate ($FeMoO_x$),[6] but knowing that aldolization reactions are catalyzed by acids and/or bases, improved yield and selectivity towards acrolein should be obtained by boosting the aldolization reaction over acidic/basic catalysts.

$$CH_3CH_2OH + CH_3OH + O_2 \longrightarrow CH_3CHO + HCHO + 2H_2O \quad (1)$$

$$CH_3CHO + HCHO \longrightarrow CH_2(OH)CH_2CHO \longrightarrow CH_2{=}CH\text{-}CHO + H_2O \quad (2)$$

Scheme 1. Expected reaction pathway of acrolein production starting from methanol and ethanol.

Wishing to understand how to improve acrolein selectivity, we decoupled this two-step reaction in two separate consecutive reactors and investigated the impact of the acid/base properties of aldolization catalysts under oxidizing conditions in the second reactor. In the first reactor (R_1), a mixture of methanol, ethanol, nitrogen, and oxygen is introduced and the oxidation to formaldehyde and acetaldehyde proceeds over $FeMoO_x$. All products exiting from the first reactor are directly sent to the second reactor (R_2), in which the aldol condensation of the two aldehydes and further dehydration to acrolein proceeds over silica-supported oxide catalysts. The catalyst screening was performed at low conversion (< 100%). The reaction temperature was kept low enough to maintain the ($CO + CO_2$) yield below 10 mol%. To compare the different catalysts, the optimal operating conditions were identified for each catalyst by taking into account the ($CO + CO_2$) yield, reaction temperature, and contact time.

The acid/base properties of solid catalysts are known to play a key role in aldolization. The aldol condensation of formaldehyde with acetaldehyde in the gas phase was reported over different solid catalysts including mixed oxides,[17] zeolites,[19,21–23] hydrotalcites,[18] and clays,[24] and the balance between acidic and basic sites was often pointed out as the key factor driving the selectivity of the reaction. Until now, re-

searchers do not agree whether the best catalytic results are obtained over basic,[17a] acidic, or amphoteric catalysts.[17b,18–20,24] The presence of basic sites is reported to be essential to increase the activity and selectivity of the aldolization, but their strength also plays a role in eventual side reactions. In the gas phase, the acid/base properties of the catalyst drive the competition between cross-aldolization of formaldehyde and acetaldehyde to form acrolein and self-aldolization of acetaldehyde to form crotonaldehyde. Production of crotonaldehyde is limited at temperatures higher than 300 °C, and acrolein production generally increases with reaction temperature. Besides, various other factors may influence this reaction, including reactor type, reaction pressure, and acetaldehyde/formaldehyde ratio.[1–19,21–28] Owing to the complexity of the process, further research is needed to understand the role of the acidity and basicity of the catalysts in such reactions and to clarify the reaction pathway. The quantification of the acid/base-site concentration and strength on the surface of oxide catalysts is even more crucial if the reaction is performed in the presence of oxygen because it can lead to over-oxidation.

In the present study, we prepared a series of catalysts by impregnating a silica support with basic oxide (Na_2O, K_2O, MgO, CaO) precursors to perform the cross-condensation of acetaldehyde and formaldehyde to produce acrolein. The addition of different guest oxides of the first and second groups of the periodic table to the silica support allowed the modulation of acidity and basicity on the catalyst surface.[29] The acid/base properties of the involved catalysts were investigated by adsorption calorimetry with gaseous NH_3, SO_2, and methanol vapor as probe molecules. This technique allows the simultaneous determination of the number, strength, and strength distribution of the active sites.

Results and Discussion

Surface and structural characterization of the catalysts

Table 1 displays the list of catalysts investigated in this work, their specific surface area, the pore volume (V_p), the average pore diameter ($Ø_{av}$), and the results of chemical and X-ray photoelectron spectroscopy (XPS) analyses. A pronounced decrease of specific surface area was observed between the silica (144 $m^2 g^{-1}$) and the Na/Si (23 $m^2 g^{-1}$) and K/Si (31 $m^2 g^{-1}$) catalysts, whereas Ca/Si and Mg/Si maintained high specific surface areas of 90 and 108 $m^2 g^{-1}$, respectively. The N_2-adsorption isotherms are of type IV, characteristic of mesoporous solids, with an H1 hysteresis (referring to IUPAC classification) for the catalysts, and an H2 hysteresis for SiO_2 (the complete adsorption/desorption isotherms and related comments are reported in the Supporting Information). All catalysts showed metal loadings between 3 and 6 wt%, as determined by chemical analysis. It is possible to estimate the amount of metal (Na, K, Ca, and Mg) needed to obtain a monolayer coverage by assuming that 10^{19} oxygen atoms per m^2 are present on the silica surface (taking into account the average number of oxygen atoms in the hexagonal unit cell of SiO_2 and the cell parameters).[30–33] Assuming that the theoretical monolayer coverage will be obtained if all oxygen atoms on the silica surface are saturated with the metal atoms of the basic oxide and that there is no surface-area decrease of the silica support during calcination, 5.5, 9.4, 9.6, and 5.8 wt% of metal would be necessary to attain the theoretical monolayer coverage for Na/Si, K/Si, Ca/Si, and Mg/Si, respectively. Based on the chemical analysis (Table 1), the observed metal coverages were lower than required for the theoretical monolayer: 70% of the theoretical monolayer for Na/Si and Mg/Si, and 60% for K/Si and Ca/Si. Besides a higher surface area, the Mg/Si catalyst surface is more enriched in metal than the other catalysts, with a surface Mg loading of 23.8 wt% (measured by XPS). For the other catalysts, the surface concentration is very close to the bulk concentration, indicating that once deposited the metals migrate into the silica matrix; in some cases this was accompanied by crystallization and strong surface-area decrease. Na/Si displays the highest amount of carbonates on the surface, as evidenced by the XPS analysis of C 1s (Table 1 and Figure 1) that shows

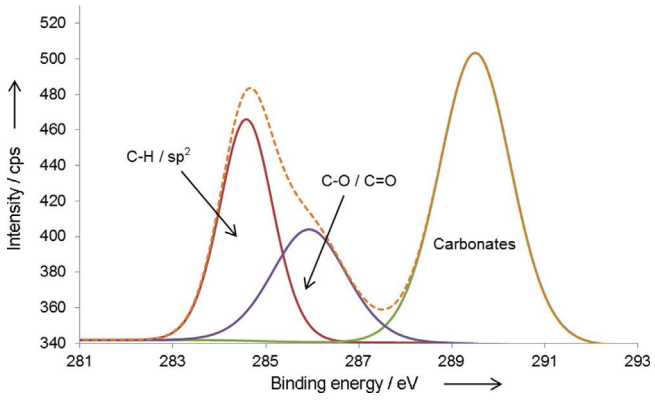

Figure 1. XPS C 1s spectra of Na/Si: overall spectrum (dotted line), specific carbon-containing surface species (solid lines).

Table 1. BET surface area, pore volume, pore diameter, chemical analysis (C.A.), and XPS analysis of the catalysts.

Sample	S_{BET} [$m^2 g^{-1}$]	V_p [$cm^3 g^{-1}$]	$Ø_{av}$ [nm]	C.A. [wt%] metal	XPS [wt%] C	Na	K	Ca	Mg	C	O	Si
SiO_2	144	0.250	6	–	–	–	–	–	–	–	–	–
Na/Si	23	0.135	24	3.8	0.4	6.1				2.8	48.1	43.0
K/Si	31	0.098	18	5.2	< 0.3	0.4	7.2			0.1	47.8	44.5
Ca/Si	90	0.242	11	5.6	< 0.3	0.6		7.5		1.2	46.7	44.1
Mg/Si	108	0.405	14	3.7	< 0.3	0.2			23.8	1.4	40.9	33.7

the carbonate contribution centered at 289.5 eV. The other three samples also show the presence of carbonates on the surface, but to a much lower extent, as reported in Table 1. With regard to the metal-oxide phases (Figure 2), only Na/Si presents X-ray patterns related to the presence of sodium silicate, whereas K/Si, Ca/Si, and Mg/Si display spectra similar to amorphous silica, thus indicating a good dispersion of the guest oxide and a small crystallite size.

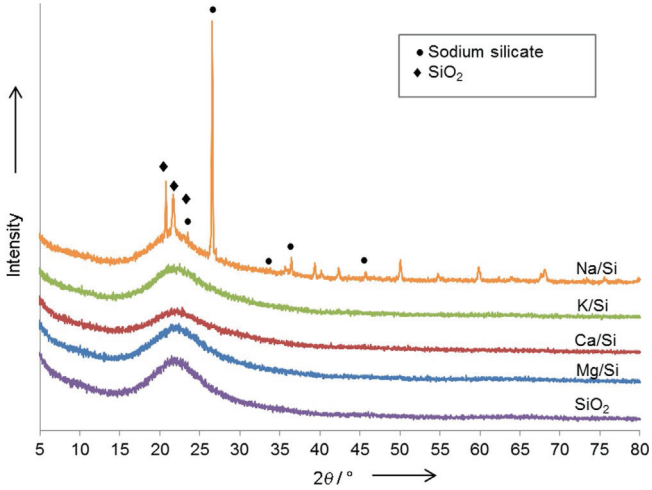

Figure 2. XRD patterns of silica support and silica-supported catalysts.

Acid/base properties of the catalysts

The number, strength, and strength distribution of acid/base sites of the investigated catalysts were measured by adsorption microcalorimetry of gas probe molecules. NH_3 was used as a basic molecule able to quantify both Lewis- (coordinately unsaturated metallic cations) and Brønsted-acidic sites (arising from terminal hydroxyl groups),[34,35] whereas SO_2 titrated basic sites consisting mostly of surface oxygen ions.[35,36] Table 2 reports the total and irreversible (chemisorbed) amounts [μmol g^{-1}] of both probe molecules adsorbed at 27 Pa equilibrium pressure and the initial heats of adsorption (Q_{init}) for the investigated catalysts. The total and irreversible basic/acidic site ratios are given in the same table. The differential heat curves versus coverage are reported in Figure 3, whereas Figure 4 displays the strength distribution of acidic and basic

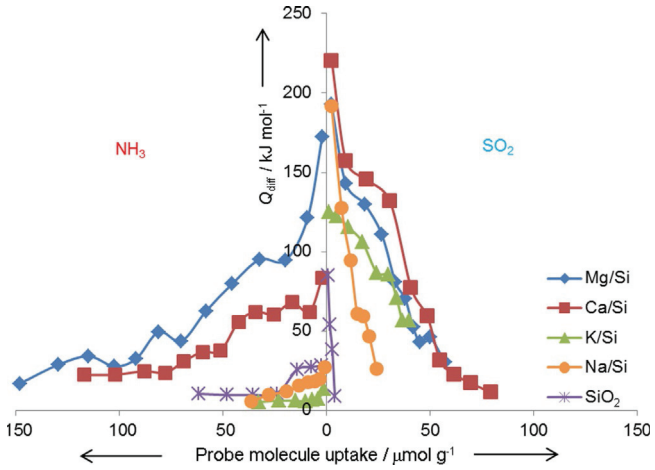

Figure 3. Differential heats of NH_3 and SO_2 adsorption as a function of surface coverage on fresh silica-supported catalysts.

sites for each catalyst. All catalysts present strength heterogeneity in both their surface acidic and basic sites, as suggested by the continuous decrease of the differential heat curves. As previously reported,[37–40,41a,42,43] the SiO_2 support does not present any basicity and only weak acidity. Deposition of basic oxides on the silica surface increases the surface basicity (Figure 3 and Table 2). Ca/Si exhibited the highest number of basic sites (V_{tot} = 61.4 μmol g^{-1}), followed by Mg/Si and K/Si (V_{tot} = 46.1 and 35.5 μmol g^{-1}), whereas Na/Si showed the lowest amount of basic sites (V_{tot} = 19.5 μmol g^{-1}). The presence of strong basic sites (characterized by Q_{diff} > 150 kJ mol^{-1}) was observed on Ca/Si, whereas Na/Si and Mg/Si contained a lower amount, and K/Si showed no presence of strong basic sites (Figure 4). An increase in basicity was observed with decreasing electronegativity of the cation deposited on the silica. That is the case for Ca/Si and Mg/Si (second group of the periodic table) as well as for K/Si and Na/Si (first group of the periodic table).[40]

The initial heats of NH_3 adsorption decrease with decreasing electronegativity, and the acidity follows the order Mg/Si > Ca/Si > Na/Si > K/Si. From NH_3 adsorption results, (Figure 3) it can be observed that impregnating the silica support with K_2O or Na_2O further decreases the acidity, whereas the deposition of MgO or CaO improves the acid properties. These results are in agreement with the investigation previously reported by Ger-

Table 2. V_{irrev} and V_{tot} calculated from adsorption isotherms of SO_2 and NH_3 obtained from microcalorimetry measurements at 150 °C.

Sample	SO_2 V_{tot}[a] [μmol g^{-1}]	V_{irrev}[b] [μmol g^{-1}]	Q_{init}[c] [kJ mol^{-1}]	NH_3 V_{tot}[a] [μmol g^{-1}]	V_{irrev}[b] [μmol g^{-1}]	Q_{init}[c] [kJ mol^{-1}]	$Base_{tot}/Acid_{tot}$[d] V_{tot}[a] [μmol SO_2 g^{-1}]/ V_{tot} [μmol NH_3 g^{-1}]	$Base_{chem}/Acid_{chem}$[e] V_{irrev}[b] [μmol SO_2 g^{-1}]/ V_{irrev} [μmol NH_3 g^{-1}]
SiO_2	2.7	1.8	85	33.8	14.2	28	0.08	0.13
Na/Si	19.5	12.6	192	17.4	7.4	27	1.12	1.70
K/Si	35.5	19.2	125	15.2	5.1	13	2.34	3.79
Ca/Si	61.4	45.8	220	76.2	28.0	84	0.81	1.63
Mg/Si	46.1	30.0	193	105.3	44.3	173	0.44	0.67

[a] Total amount of SO_2 and NH_3 adsorbed under an equilibrium pressure of 27 Pa. [b] Amount of chemisorbed SO_2 and NH_3 under an equilibrium pressure of 27 Pa. [c] Heat evolved from the first SO_2 or NH_3 dose. [d] Ratio of total basic to acidic sites. [e] Ratio of chemisorbed basic to acidic sites.

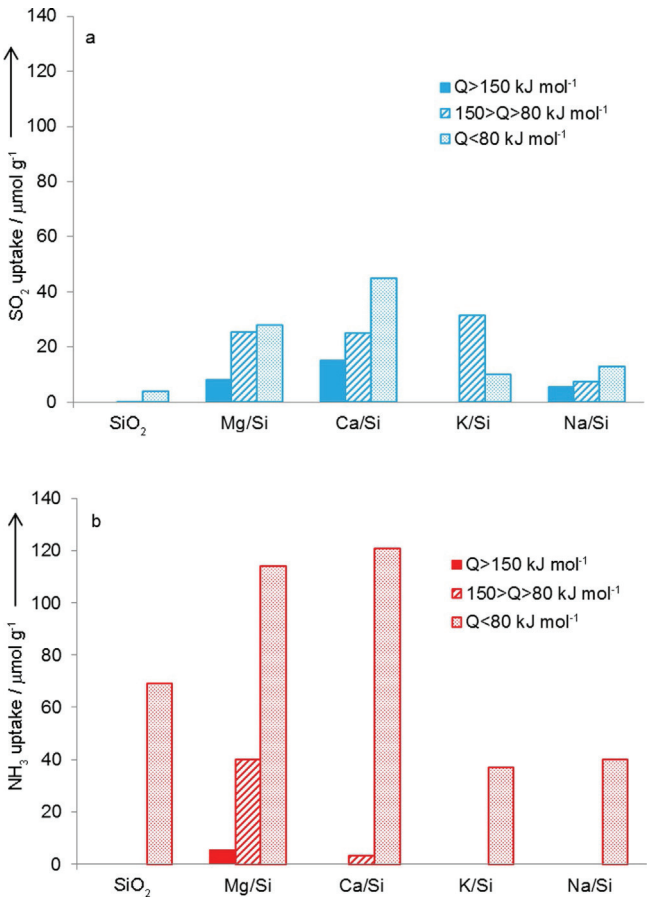

Figure 4. Strength distribution of a) basic and b) acidic sites of fresh silica-supported catalysts.

vasini et al.[40] Mg/Si presents the highest initial heat of NH_3 adsorption ($Q_{init} = 173\ kJ\,mol^{-1}$) among the tested catalysts and is the only catalyst presenting strong ($Q_{diff} > 120\ kJ\,mol^{-1}$) acid sites (Figure 4). Even if MgO is known (and expected) to be a basic oxide,[34,37,39,40,42,43] MgO can lead to the creation of acid sites upon deposition on a silica surface (exclusively of Lewis type), as previously reported.[41b,44,45] Meanwhile, the addition of CaO on the silica support gives rise only to relatively weak acid sites ($Q_{diff} < 80\ kJ\,mol^{-1}$), which are also reported to be of Lewis type.[46] The ratios of total basic/acidic sites and chemisorbed basic/acidic sites were calculated and are reported in Table 2. Mg/Si presents an amphoteric behavior with a more pronounced acidic character. For Ca/Si, which also presents an amphoteric character, the acidity is connected to the presence of a high number of weak acid sites.

Quantification of acid and basic sites was performed on the fresh catalysts. On a working catalyst, exposed to the reaction gas mixture (containing methanol, ethanol, water vapor, and other products and reactants), adsorption will occur and can affect the acid/base-site distribution. Therefore, it is of interest to characterize the acid/base surface properties using reactants as probe molecules, and methanol can be considered as a suitable probe for this purpose although it is scarcely used in adsorption microcalorimetry experiments. Some researchers investigated methanol adsorption on different oxides including MgO,[47,48] SiO_2,[49,50] and CaO supported on amorphous silica[46] by using adsorption microcalorimetry, IR spectroscopy, or computational methods. Interaction of methanol vapor with acid/base surface sites may involve not only physisorption and associative chemisorption but also dissociative chemisorption. Generally, methanol can be considered as a Brønsted acid that is able to release its H atom and dose Brønsted-basic sites.[48] Methanol can also release an electron pair from its oxygen, and in that case behaves as a Lewis base, dosing Lewis-acid sites.[35,46] For pure magnesia samples[47,48] it has been reported that undissociated methanol species are physisorbed on MgO. Further dissociative adsorption, as reported by Bensitel et al.,[47] results exclusively from methanol deprotonation. The proton (H^+) and methoxy fragment (CH_3O^-) adsorb on the O^{2-} anion and Mg^{2+} cations, respectively, creating OH^- and Mg–OCH_3^+ species.[48] Depending on the topology and defects present on the surface, stabilization of methoxy species by bridging two or more cations can occur.[47,48] On the silica surface,[49,50] dissociative adsorption of methanol on siloxane bridges leads to the creation of Si–OCH_3 and Si–OH species on the surface. Bolis et al.[46] studied associative/dissociative chemisorption of methanol vapor on the surface of Ca-modified silica (4, 8, and 16 mol% CaO) through the parallel use of IR spectroscopy and microcalorimetry experiments. The presence of Ca species on the surface enhances the adsorption with respect to the unmodified parent silica. The methoxylation of the surface, leading to Si–OCH_3 and Ca–OH species (instead of Ca–OCH_3 and Si–OH) occurs only to a limited extent (30–40% of the total methanol uptake) and depends on both methanol pressure and contact time.[46] Using calorimetry, Bolis et al.[46] evidenced that dissociative chemisorption does not exhibit a significantly more exothermic effect than associative chemisorption of molecularly adsorbed methanol ($Q_{init} \approx 100\ kJ\,mol^{-1}$).

Methanol adsorption isotherms and differential heats curves are shown in Figure 5. Mg/Si displays the highest methanol adsorption ($V_{tot} = 228\ \mu mol\,g^{-1}$) followed by Ca/Si ($V_{tot} = 187\ \mu mol\,g^{-1}$), whereas K/Si, SiO_2, and Na/Si adsorbed significantly lower quantities of methanol ($V_{tot} = 104$, 81, and 47 $\mu mol\,g^{-1}$ respectively) at an equilibrium pressure of 27 Pa. No quantitative comparison of the amounts of methanol, NH_3, and SO_2 adsorbed can be performed owing to the different adsorption temperatures (30 °C for methanol vapor, and 150 °C for NH_3 and SO_2 gas), which lead to a different distribution of the types of sites on the surface. However, it can be observed that the amount of methanol adsorbed is always higher than the sum of acidic and basic sites determined, respectively, by NH_3 and SO_2 adsorption (Figure 3). This is not surprising because methanol, through the above explained associative/dissociative chemisorption, interacts simultaneously with metallic cations (acid sites) and surface oxygen atoms (basic sites). Therefore, formation of M–OCH_3 and M–OH (M = Mg, Ca, K, Na, Si) species can be expected as previously reported.[46–50] It is evident that under dosing conditions (adsorption calorimetry measurements) both acid and base sites adsorb methanol irreversibly through the associative/dissociative mechanism, possibly creating acid–base pairs that are not present on the clean

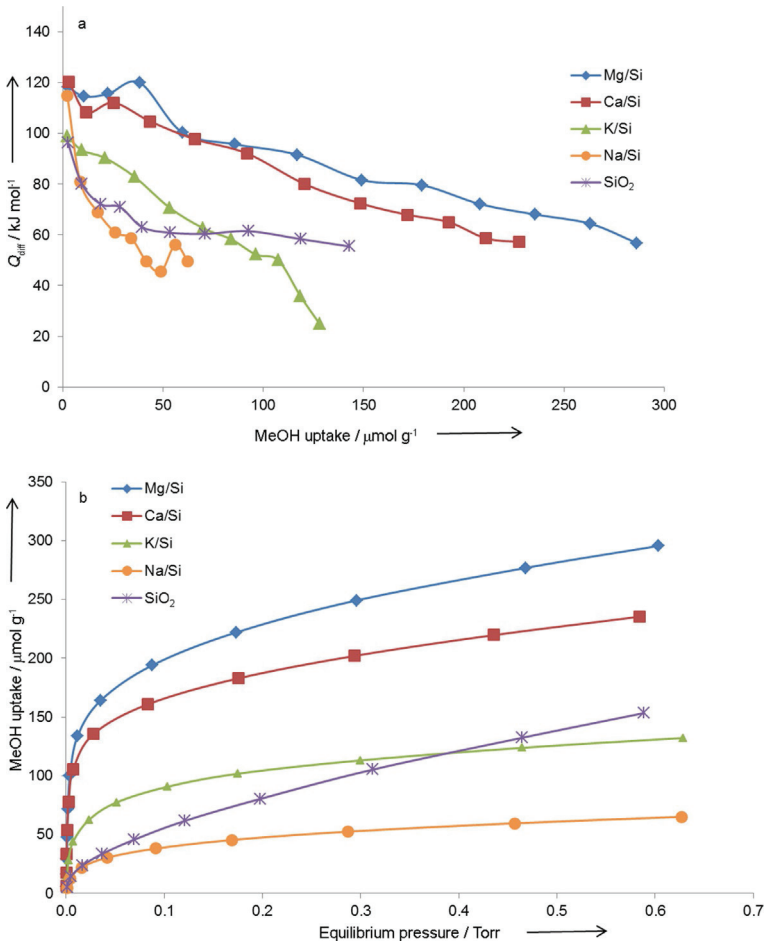

Figure 5. a) Differential heats as a function of surface coverage and b) isotherms obtained from MeOH-adsorption microcalorimetry on fresh silica-supported catalysts. 1 Torr = 133.322 Pa

catalyst surface under vacuum. The initial heats of adsorption are around 100 kJ mol^{-1} for pure silica, but they increase up to 120 kJ mol^{-1} in the presence of Mg or Ca. Similar behavior might be expected under reaction conditions in the presence of methanol (and probably water).

In addition, adsorption microcalorimetry of NH_3 and SO_2 was performed on the $FeMoO_x$ catalyst used in the redox step, showing that when oxidized (state in which the catalyst is present during acrolein production under oxidizing conditions) this catalyst does not exhibit basic sites but relatively strong acidic sites.

Catalytic tests

A way to improve the yield and selectivity to acrolein in the OCA is to add a basic catalyst to $FeMoO_x$ to facilitate the cross-aldolization of acetaldehyde and formaldehyde to acrolein. Therefore, a comparison of various aldolization catalysts (metal oxides deposited on silica) in the production of acrolein starting from a mixture of methanol and ethanol in the presence of oxygen was performed. Special care was taken to work outside the flammability limits (details are reported in the Supporting Information).

The appropriate oxidation reaction conditions in the first reactor (R_1) were selected to obtain the highest (acetaldehyde + formaldehyde) yield based on numerous catalytic tests in the presence of a commercial $FeMoO_x$ catalyst. Different parameters (furnace temperature, **GHSV**, $\%O_2$, $\%N_2$, and %MeOH/EtOH) were systematically varied to identify the optimal conditions, which were finally fixed a follows: A MeOH/EtOH/O_2/N_2 mixture in the molar ratio of 4:2:8:86, a GHSV of 10000 h^{-1} (or 5000 h^{-1}), and an oven temperature of 260 °C. For GHSV = 10000 h^{-1}, the conversion of methanol was maintained at 53 mol%, whereas the conversion of ethanol was 81 mol%. It is important to mention that under these conditions the alcohols are not fully converted in R_1 to investigate the impact of the non-reacted alcohols on the aldolization-catalyst behavior. Formaldehyde and acetaldehyde (and some amount of acrolein) were produced over the commercial $FeMoO_x$ redox catalyst in the first reactor. The acrolein yield was 7 mol% (with a selectivity of 10%), and the acetaldehyde yield was 28 mol% (42% selectivity) over the redox catalyst alone. The total yield for ($CO + CO_2$) was 3 mol%. For a GHSV of 5000 h^{-1}, the conversion of methanol was 59 mol%, and that of ethanol 89 mol%. The acrolein yield was 8 mol% (with a selectivity of 11%), and the acetaldehyde yield was 32 mol% (44% selectivity) over the

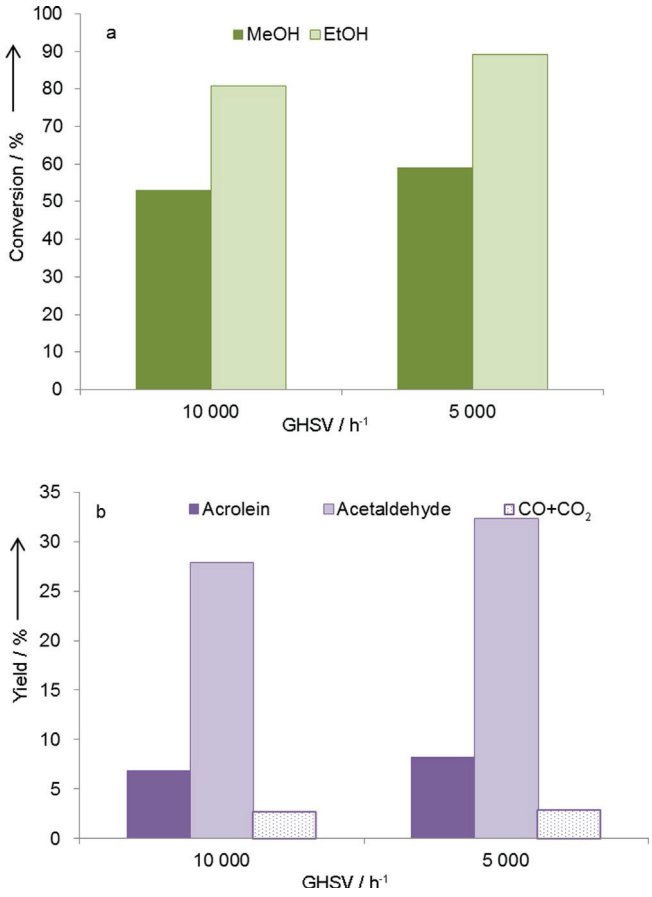

Figure 6. Catalytic performance of $FeMoO_x$ (exit R_1) at 260 °C and GHSV = 10000 or 5000 h^{-1}: a) Conversion of methanol and ethanol and b) yields of the main products of the reaction.

redox catalyst alone. The total yield for ($CO + CO_2$) remained 3 mol.%. The results are presented in Figure 6. The $FeMoO_x$ catalyst tested over 100 h did not show any deactivation. At the same time, the composition of the reaction products remained constant.

The exit-stream from the redox reactor (R_1) was then directly sent to the aldolization reactor (R_2), in which further acrolein production was performed over the silica-supported catalysts prepared as described in the Experimental Section. Two preliminary tests were conducted. The first test consisted of sending the exit-stream from the redox reactor (feed: MeOH/EtOH/O_2/N_2 = 4:2:8:86 mol%; 260 °C; GHSV = 5 000 h^{-1}) directly into the empty aldolization reactor maintained at 320 °C. It was confirmed that a homogeneous reaction does not proceed in the empty reactor (R_2). The second test consisted of feeding MeOH/EtOH/O_2/N_2 = 4:2:8:86 mol% at a GHSV of 5000 h^{-1} over $FeMoO_x$ (R_1, 260 °C) and Mg/Si (R_2, 270 °C) catalysts to verify the time needed for stabilization of acrolein production in the aldolization reactor. A stable working regime was established after 5 h, and then the acrolein yield remained nearly constant. Tests over SiO_2, Na/Si, K/Si, Ca/Si, and Mg/Si were performed in a 250–360 °C temperature range, at a GHSV of 10000 or 5000 h^{-1}. These conditions were varied for each catalyst to maintain the ($CO + CO_2$) yield below 10 mol% and to identify the optimal working conditions for each catalyst. Detailed results of the catalytic tests for each catalyst are presented in Figures 7–11.

The main products in each catalytic test were acrolein, acetaldehyde, methanol, ethanol, CO, and CO_2. Traces of diethylether, propionaldehyde, acetone, crotonaldehyde, acetic acid, acrylic acid, and others were also present. The low carbon balance (66–80 mol%) results from a missing reliable quantification of formaldehyde (one of the main products of the reaction), the production of unidentified polymers accumulating at the reactor exit,[17a] and the deposition of coke on the catalyst surface [as revealed by chemical analysis and thermogravimetric differential thermal analysis mass spectroscopy (TG-DTA-MS) of the used catalysts (see below)].

As a general trend, the increase of the reaction temperature (T_2) enhanced acetaldehyde conversion and selectivity towards acrolein but also the production of carbon oxides. Longer contact times (GHSV = 5000 h^{-1}) had a positive influence on the selectivity to acrolein but also enhanced the carbon oxide yield. Production of crotonaldehyde was not significant (yields lower than 0.3 mol% in all catalytic tests), although crotonaldehyde was expected as the product of the self-aldolization of acetaldehyde.[24,25]

Among the aldolization catalysts, Mg/Si (at 320 °C and 5000 h^{-1} GHSV) led to 35 mol% acrolein yield at 44 mol% se-

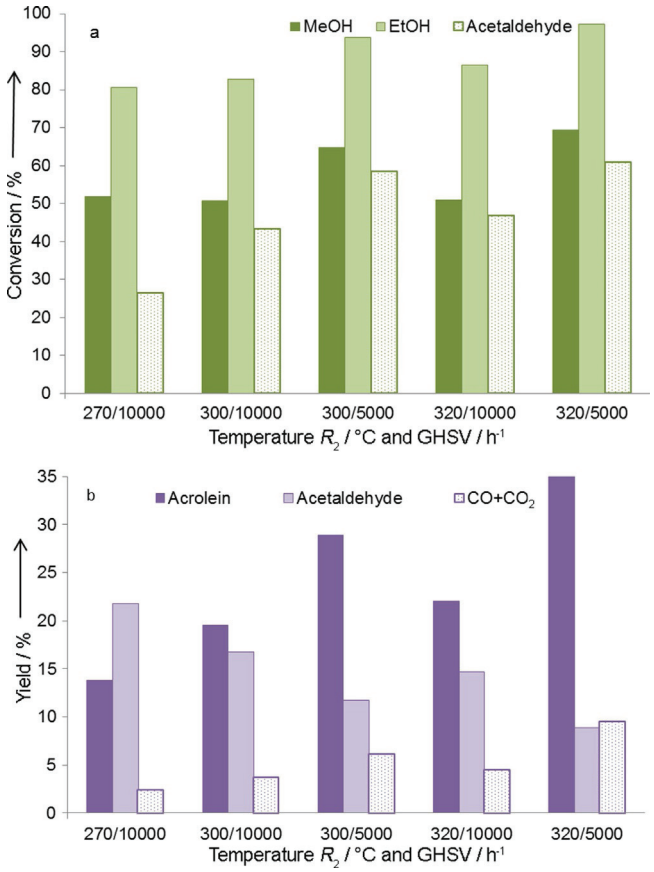

Figure 7. Catalytic performance of Mg/Si (exit $R_1 + R_2$) under different conditions: a) Conversion of methanol, ethanol and acetaldehyde and b) yields of the main products of the reaction.

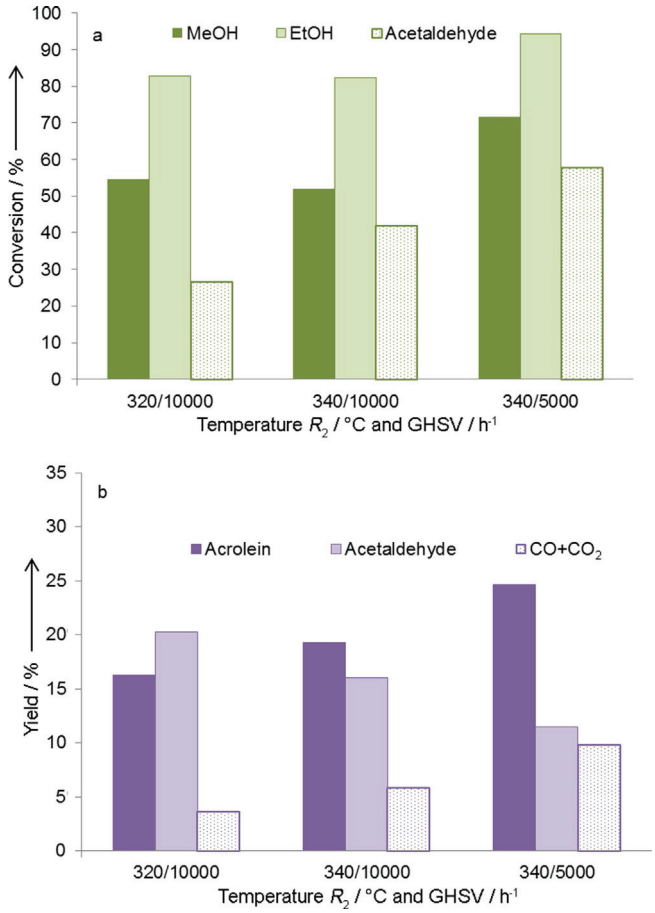

Figure 8. Catalytic performance of Na/Si (exit R_1+R_2) under different conditions: a) Conversion of methanol, ethanol and acetaldehyde and b) yields of the main products of the reaction.

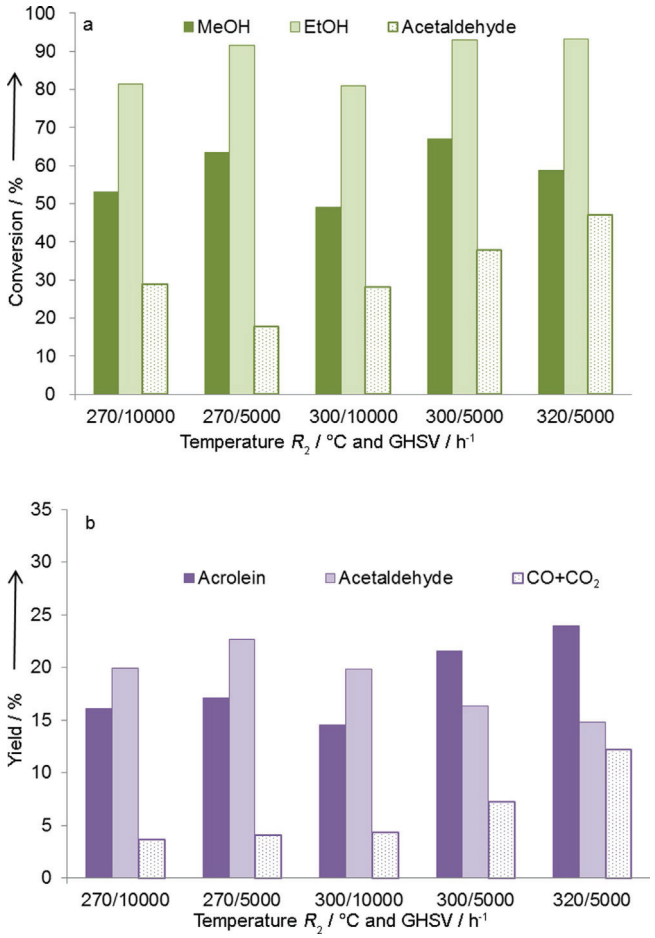

Figure 9. Catalytic performance of Ca/Si (exit R_1+R_2) under different conditions: a) Conversion of methanol, ethanol and acetaldehyde and b) yields of the main products of the reaction.

lectivity, and a ($CO+CO_2$) yield of 10 mol% (Figure 7). This represents the highest acrolein yield obtained among all tested catalysts. Na/Si (at 340 °C and 5000 h^{-1} GHSV) afforded 25 mol% acrolein yield at 30 mol% selectivity, and 10 mol% ($CO+CO_2$) yield (Figure 8). Ca/Si and K/Si (Figures 9 and 10) displayed a lower acrolein production and the highest ($CO+CO_2$) production at relatively low temperatures. At 5000 h^{-1} GHSV and 320 °C for Ca/Si and 300 °C for K/Si, the ($CO+CO_2$) yields were already higher than 10 mol%, thus limiting the possibility to further increase the reaction temperature to enhance acetaldehyde conversion and acrolein yield. With regard to the catalytic activity of the SiO_2 support (Figure 11), the maximum acrolein yield was only 15 mol% (at 360 °C and 5000 h^{-1} GHSV) but with less than 10 mol% of carbon oxide yield; this acrolein yield is quite similar to that obtained over $FeMoO_x$ alone. The catalytic performances shown by Mg/Si and Na/Si are in agreement with the trend previously presented by Ai,[17a] who worked in the absence of oxygen. The results of the catalytic tests for each catalyst at a ($CO+CO_2$) yield <10 mol% (optimal working conditions) are summarized in Figure 12.

Influence of acid/base properties on acrolein production

In the absence of oxygen, aldolization between acetaldehyde and formaldehyde is reported to be generally catalyzed by basic sites of suitable strength, but high overall basicity also promotes secondary reactions that can lead to a higher ($CO+CO_2$) yield. In addition, the presence of acid sites is also reported as beneficial for acrolein selectivity.[17a,18,23,24]

Under our reaction conditions, the presence of a defined amount of strong basic sites proved to be necessary to enhance the selectivity to acrolein (Figures 4 and 12). For Mg/Si, Ca/Si, and Na/Si, which exhibit strong basic sites ($Q_{diff}>$ 150 kJ mol^{-1}), high production of acrolein was observed. On the SiO_2 support and K/Si, there is no presence of strong basic sites, and the selectivity towards acrolein was much lower. Moreover, SiO_2 displayed a low oxidation behavior that can be related to the total absence of basicity. Figure 13 shows the acrolein yield as a function of the strong basic/strong acidic sites ratio (from Table 2), indicating that if this ratio increases, the acrolein yield decreases, and that acrolein production depends on the acid/base character of the catalyst. Mg/Si is amphoteric with overall dominant acidic character in comparison to the other catalysts, and shows the best catalytic performance.

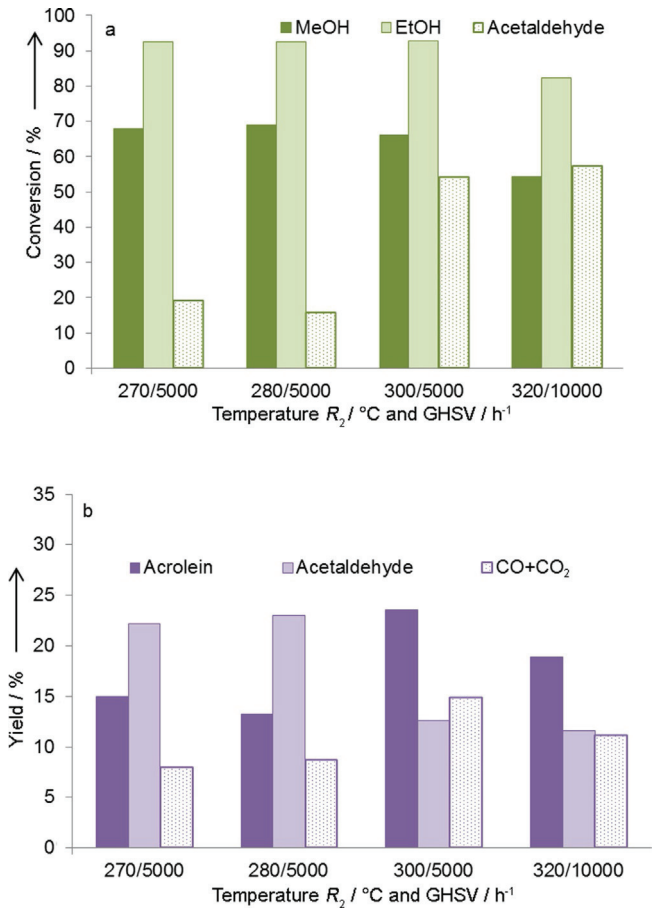

Figure 10. Catalytic performance of K/Si (exit R_1+R_2) under different conditions: a) Conversion of methanol, ethanol and acetaldehyde and b) yields of the main products of the reaction.

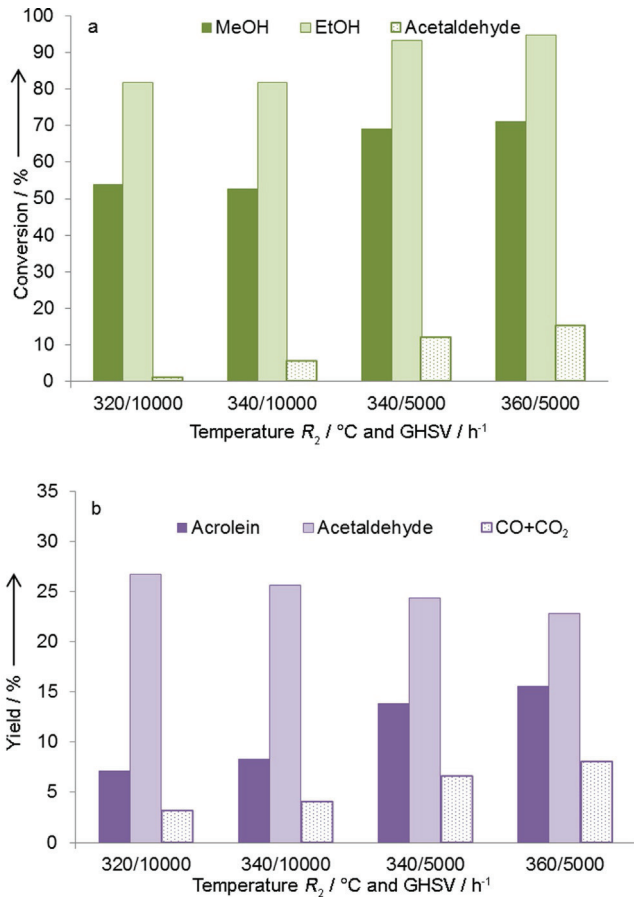

Figure 11. Catalytic performance of SiO_2 support (exit R_1+R_2) under different conditions: a) Conversion of methanol, ethanol and acetaldehyde and b) yields of the main products of the reaction.

Although Mg/Si and Ca/Si display similar basicity, there is a difference in their catalytic behavior in acrolein production. Mg/Si is the only catalyst of the series that also possesses very strong acid sites ($Q_{diff} > 150$ kJ mol^{-1}; Figure 4 and Table 2), and this additional feature seems to further improve the acrolein selectivity. Cooperation of strong basic and acidic sites seems to boost acrolein production and at the same time diminish the oxidizing character of the catalyst (expected because of the high basicity). Ca/Si, which contains strong basic sites (Figure 4) and a high overall basicity (Table 2), but mainly weak acid sites ($Q_{diff} < 80$ kJ mol^{-1}), shows higher CO and CO_2 production than Mg/Si when compared at the same temperature (320 °C) and contact time (GHSV = 5000 h^{-1}, see Figures 7b and 9b). K/Si shows low acrolein selectivity owing to a moderate number of basic sites in combination with a lack of acidity (Table 2). Na/Si, which contains very few strong basic sites and very few acidic sites (Table 2 and Figure 3), presents a relatively high selectivity towards acrolein (at 340 °C and GHSV = 5000 h^{-1}; Figure 12); this improved catalytic activity is a result of the low oxidizing ability of Na/Si, which can consequently work at higher reaction temperatures, favoring acrolein production. The relatively good catalytic performances of Na/Si might be connected to the presence of a crystalline phase of sodium silicate (detected by XRD, Figure 2) and the presence of a high amount of carbonates on the surface (detected by XPS, Table 1). These type of silicate sites can be active in aldolization, as previously reported by Ji et al.[51] Among all catalysts investigated in the present research, Mg/Si, possessing both strong acidic and basic sites, was the most active under oxidizing conditions. This observation is in agreement with previous studies performed in the absence of oxygen that report on the beneficial effect of acid/base cooperation for acrolein production.[17a,18,24]

Notably, the catalysts are modified during the reaction. For example, a working catalyst may have more or less basic sites owing to adsorption of acidic molecules (i.e., CO_2) or coke deposition. Because the catalytic activity of the catalyst might depend on the acidity/basicity after modification under working conditions, catalytic tests were performed after selectively poisoning the acidic (with NH_3) or basic (with SO_2) sites of the aldolization catalyst (Mg/Si) in the second reactor. First, a catalytic test was performed as usual with a MeOH/EtOH/O_2/N_2 molar ratio of 4:2:8:86 at a GHSV of 5000 h^{-1} (Table 3, columns 2 and 4). Then, NH_3 or SO_2 was added to the gas mixture exiting from the first reactor and sent through the aldolization catalyst bed (second reactor) overnight at 320 °C. A second catalytic test was then performed (Table 3, columns 3 and 5).

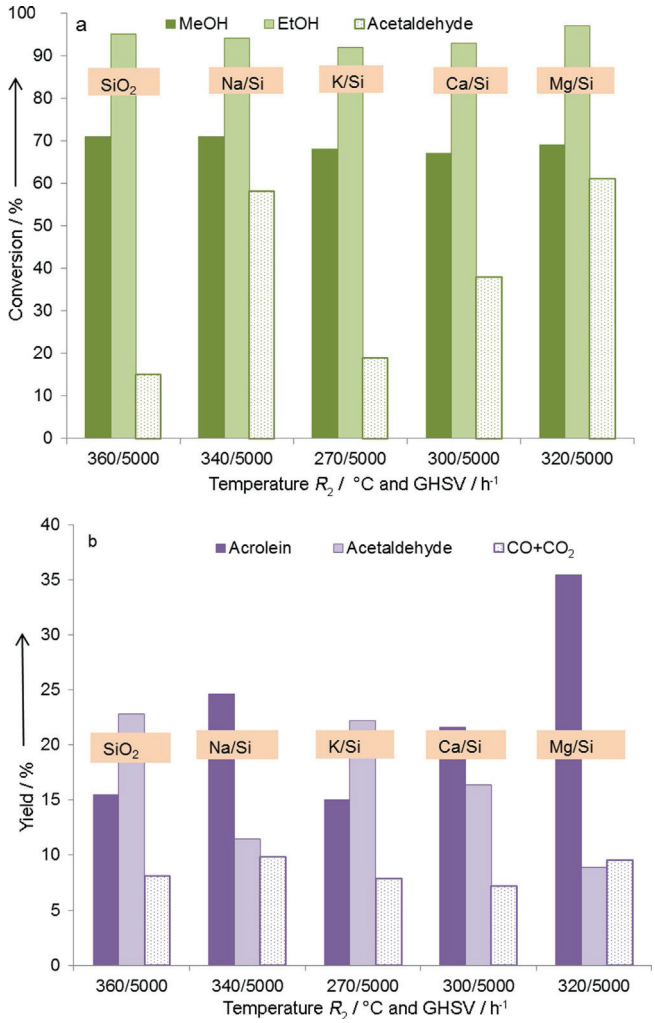

Figure 12. Comparison of catalytic tests of silica support and silica-supported catalysts under optimal conditions [with respect to ($CO+CO_2$) yield < 10%]: a) Total conversions of methanol and ethanol, and conversion of acetaldehyde in the second reactor performed under the optimal conditions for each catalyst. b) Corresponding yields of the main reaction products.

Table 3. Catalytic tests results (feed: MeOH/EtOH/O_2/N_2 = 4:2:8:86 mol%; R_1 ($FeMoO_x$, 260 °C) + R_2 (Mg/Si, 320 °C) after poisoning the basic (with SO_2) or acidic (with NH_3) sites of Mg/Si under reaction conditions.

Yield *Y* or conversion *C*	Before SO_2	After SO_2	Before NH_3	After NH_3
C MeOH [%]	69	69	72	70
C EtOH [%]	96	95	97	95
Y ($CO+CO_2$) [%]	10.1	9.6	9.5	13.4
Y acetaldehyde [%]	8	13	9	18
Y acrolein [%]	39	34	34	21
Y crotonaldehyde [%]	–	–	–	–

Acidic- or basic-site poisoning resulted in a decreased acrolein production, showing that both acid and base features are involved in the aldolization. In particular, if the acidic sites were poisoned by NH_3, the catalytic activity was strongly affected (acrolein yield decreased from 34 to 21%). The observation that Mg/Si (the only sample of the series presenting strong acid sites) is the most active catalyst matches the results obtained in this last experiment.

Mg/Si: physicochemical characterization of the used catalyst and deactivation study

Mg/Si was the most active catalyst for acrolein production under oxidizing conditions at 320 °C and GHSV = 5000 h^{-1} (35 mol% acrolein yield and 44 mol% acrolein selectivity; see Figures 7 and 12); therefore, it was chosen for stability studies over more than 100 h. The results are presented in Figure 14. Conversion of acetaldehyde decreased from 72 to 53% over 140 h.

Further physicochemical characterizations on used Mg/Si were performed. The specific surface area decreased to 85 $m^2 g^{-1}$ (108 $m^2 g^{-1}$ for the fresh catalyst), but the amorphous structure of the catalyst was preserved (XRD). The color of the catalyst after 140 h operation was dark brown, whereas the fresh catalyst was white; chemical analysis revealed the presence of 4.2 wt% carbon on the used catalyst (< 0.3 wt% on the fresh one). TG-DTA-MS analysis confirmed the results of the chemical analysis, revealing that the carbon loss after ther-

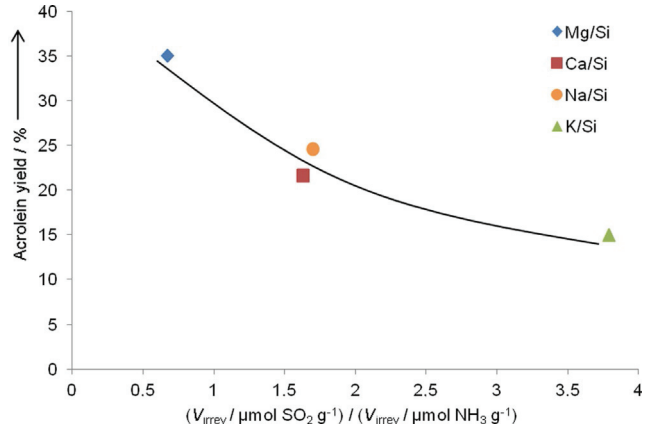

Figure 13. Acrolein yield as a function of the ratio of basic to acidic sites (V_{irrev} µmol SO_2 g^{-1}/V_{irrev} µmol NH_3 g^{-1}).

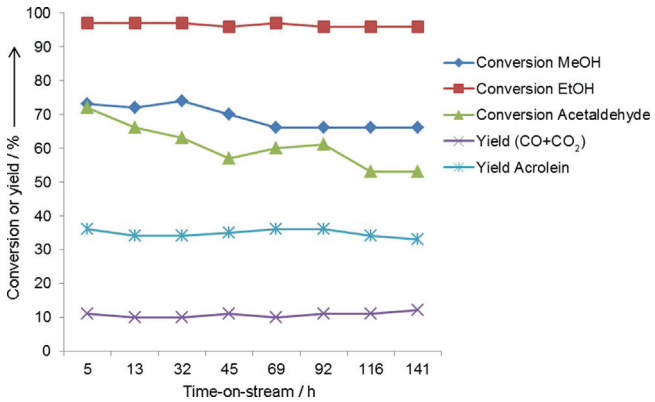

Figure 14. Catalytic activity of Mg/Si as a function of time under optimal conditions (320 °C; 5000 h^{-1}).

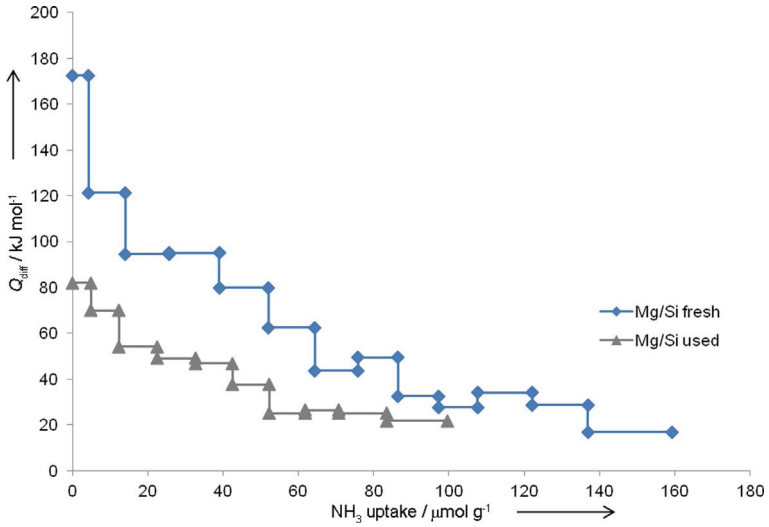

Figure 15. Differential heats of NH_3 adsorption as a function of surface coverage on fresh and used (after 140 h) Mg/Si catalysts.

mal treatment at 700 °C represented a weight loss of 4.4 wt%. Comparison of TG-DTA-MS experiments on the fresh and used Mg/Si catalysts confirmed that the weight loss on the used catalyst originated mostly from hydrocarbon species. 7.7 wt% carbon was detected on the surface of the used Mg/Si catalyst by XPS analysis (1.4 wt% on the surface of the fresh catalyst, resulting from carbonate species).

Finally, NH_3- and SO_2-adsorption microcalorimetry was performed on the used Mg/Si catalyst (after ca. 140 h). As shown in Figure 15, the number and strength of acidic sites on the used catalyst was much lower than on the fresh one (corresponding to a poisoning of ca. 38% of the total acid sites present on the fresh catalyst). However, weak acidic sites ($Q_{diff} <$ 80 kJ mol^{-1}) were still present in significant amounts on the used catalyst. In contrast, microcalorimetry measurements of SO_2 adsorption revealed that there were almost no strong nor medium-strength basic sites left on the surface of the used catalyst ($V_{tot} = 9$ µmol g^{-1} and $Q_{init} \approx 30$ kJ mol^{-1}). Therefore, it can be concluded that the majority of the basic sites were preferentially poisoned by coke deposition after 140 h reaction. This indicates that acrolein production over this catalyst probably continued owing to the presence of the remaining acidic sites.

Study of the reaction pathway

To identify whether the limited acrolein production is a result of the reversibility of the reaction (retro-aldolization), additional experiments were performed by feeding with acrolein and water (acrolein/H_2O/O_2/N_2 = 6:6:6:82 mol%). Experiments were performed both on the $FeMoO_x$ catalyst alone and on the $FeMoO_x$ and Mg/Si catalysts placed in the consecutive reactors. No significant production of acetaldehyde from acrolein could be detected, excluding the possibility of a retro-aldolization reaction. Above 300 °C, the ($CO + CO_2$) yield increased over both catalysts, showing that acrolein was partially over-oxidized. These results indicate that part of the acrolein produced in the presence of oxygen is immediately transformed to carbon oxides at such high temperature, thus limiting the possibility to obtain higher acrolein yields. Moreover, the moderate selectivities towards acrolein can also be connected with a concomitant decomposition into CO and CO_2. Polymerization of acrolein (or other reactants present in the reaction mixture) is also confirmed by the presence of coke on the used catalyst and of polymeric compounds observed at the exit tubes of the reactors.[17a]

Crotonaldehyde (product of acetaldehyde self-aldolization) was never detected in significant amounts during the various catalytic tests. By feeding crotonaldehyde and water (crotonaldehyde/H_2O/O_2/N_2 = 6:6:6:82 mol%) over $FeMoO_x$ and Mg/Si at 320 °C, the retro-aldolization of crotonaldehyde (to form acetaldehyde) could be excluded for these catalysts because no acetaldehyde was detected.

Based on the presented results, the high acrolein selectivity over Mg/Si seems to be governed by the cooperation of acidic and basic sites. Dumitriu et al.[18] proposed that on basic sites, aldol condensation occurs by the abstraction of an H atom from the α-position of the carbonyl function of the acetaldehyde, forming a carbanion that further reacts with the carbonyl group of the formaldehyde. This would mean that on the strong basic sites of Mg/Si, most of the acetaldehyde is involved in the activation process, whereas formaldehyde would act as the reaction substrate. However, the absence of crotonaldehyde in all tests performed under oxidizing conditions invalidates this mechanism. The same authors reported that high basicity of the catalyst gives rise to overproduction of CO and CO_2 owing to the presence of side reactions. This observation is in agreement with the obtained catalytic results. Other researchers[24] described that basic sites activate both acetaldehyde and formaldehyde (by creating carbanions) that further condense to acrolein.

Considering the acid-catalyzed mechanism of the aldol condensation of formaldehyde and acetaldehyde, Dumitriu et al.[18] reported that competition between the adsorption of the two

aldehydes on cationic sites can be expected owing to the similar negative charges on the oxygen atoms of both molecules. Condensation then proceeds through activation of the carbonyl group on acidic sites, followed by the reaction of the substrate (enol form of acetaldehyde). Strong acidic sites on the catalyst enable both acetaldehyde and formaldehyde chemisorption, which increases the selectivity to acrolein. On weak acid sites only adsorption of acetaldehyde is allowed, leading to crotonaldehyde production. This mechanism should be excluded in the present reaction conditions because no formation of crotonaldehyde was observed. Other studies performed in the absence of oxygen[24] described that on acid sites both acetaldehyde and formaldehyde were activated (creating two carbocations) and further reacted to form acrolein. Finally, weak acidity was proposed to be connected with the dehydration of the aldol to acrolein.

To summarize, the previously proposed acid–base catalyzed mechanisms involve the activation of acetaldehyde. Somehow, in our reaction process (performed in the presence of oxygen), no crotonaldehyde production was ever observed when methanol and ethanol were fed [(EtOH + MeOH)/O_2/N_2 = (2 + 4):8:86 mol%] over $FeMoO_x$ and silica-supported basic oxide catalysts, suggesting that the selected catalysts are not able to activate acetaldehyde in the conventional manner. This also suggests that reaction pathway to acrolein should somehow proceed through formaldehyde activation. Additional catalytic tests were then performed by feeding only ethanol (EtOH/O_2/N_2 = 6:8:86 mol%) or only methanol in the reaction mixture (MeOH/O_2/N_2 = 6:8:86 mol%) over $FeMoO_x$ and Mg/Si. The results of these experiments are summarized in Tables 4 and 5.

Tests performed by feeding ethanol/O_2/N_2 (in the absence of methanol)

Because no production of crotonaldehyde over $FeMoO_x$ catalyst in the first reactor or over the aldolization catalyst Mg/Si in the second reactor was detected when feeding ethanol and methanol, and to understand if self-aldolization can occur under oxidizing reaction conditions, ethanol (without methanol) was fed, and the crotonaldehyde concentration was measured (Table 4, columns 2 and 3).

These results lead to the conclusion that under the present reaction conditions, self-aldolization must be significantly slower than cross-aldolization because crotonaldehyde is hardly produced in the reaction. In the presence of the Mg/Si aldolization catalyst (270 °C), some crotonaldehyde was observed for the first time, suggesting that at lower temperatures self-aldolization might be expected (Table 4, column 3), in line with thermodynamic expectations. Generally, aldol condensation reactions are exothermic. For the aldol condensation of acetaldehyde and formaldehyde to afford acrolein, some authors proposed that the competitive production of crotonaldehyde (by self-aldolization of two acetaldehydes) is connected to the reaction temperature and that crotonaldehyde production significantly decreases (or even completely disappears) at temperatures higher than 300–350 °C.[18,21,52] Moreover, Scalbert et al.[53] studied the relevance of acetaldehyde self-aldolization in the process of ethanol condensation to butanol and reported that the reaction pathway involving acetaldehyde self-aldolization was irrelevant for this process in the 350–410 °C temperature range. However, when performing the catalytic test in the presence of both ethanol and methanol (as described above), the absence of crotonaldehyde cannot be caused only by the reaction temperature because the catalytic tests were performed in the 250–360 °C range. Instead, the presence of oxygen might be the key to explaining the different acetaldehyde activation behavior. The main product obtained in these experiments in the absence of methanol (as reported in Table 4) is acetaldehyde. Carbon oxides are also produced.

Over $FeMoO_x$ and MgSi, low quantities of acrolein were observed, thus indicating that some traces of formaldehyde are also formed in the process. Colmont et al.[54] previously reported that formaldehyde and CO_x were observed with acetaldehyde when a mixture of ethanol/O_2/He was fed over a FeMoLa catalyst. Probably, some $CH_3CH(OH)CH_2COH$ aldol can be produced over $FeMoO_x$ or the aldolization catalyst. It would decompose to acetone over Mg/Si, either by a ketonization through acetic acid[55] or through a direct decomposition to acetone and CO_x. The presence of acrolein (3%, Table 4) can be explained by gas-phase decomposition of ethanol to formaldehyde, which further reacts with acetaldehyde to afford acrolein. In the absence of Mg/Si (empty R_2, last column in Table 4), no formation of acrolein was observed. Instead, a higher formation of (CO + CO_2) accompanied by a decrease in acetaldehyde production was observed. In a homogeneous gas-phase, acetaldehyde decomposition to methanol and CO_2 can occur in the presence of oxygen, as previously reported by Blanchard et al.[56]

Table 4. Catalytic tests results obtained by feeding EtOH/O_2/N_2 = 6:8:86 mol% over $FeMoO_x$ and Mg/Si at a GHSV of 5000 h^{-1} and different temperatures.

Yield *Y* or conversion *C*	R_1 (260 °C) $FeMoO_x$	R_1 (260 °C) $FeMoO_x$ + R_2 (270 °C) Mg/Si	R_1 (260 °C) $FeMoO_x$ + R_2 (320 °C) empty
C EtOH [%]	92	92	94
Y (CO + CO_2) [%]	7	12	37
Y acetaldehyde [%]	65	53	18
Y acrolein [%]	1	3	0.5
Y acetone [%]	0.2	0.5	0.2
Y MeOH [%]	–	1	13
Y crotonaldehyde [%]	0.3	1.7	0.1

Tests performed by feeding methanol/O_2/N_2 (in the absence of ethanol)

Table 5 summarizes the results of catalytic tests when a MeOH/O_2/N_2 = 6:8:86 mol% mixture was introduced into the redox (R_1) and aldolization (R_2) reactors (containing $FeMoO_x$ and Mg/Si, respectively). Higher production of (CO + CO_2) and methanol was observed with increasing temperature of the aldolization reactor, owing to the probable oxidation of formaldehyde produced over $FeMoO_x$. Ai,[17a] who studied acrolein production starting from a mixture

Table 5. Catalytic tests results obtained by feeding $MeOH/O_2/N_2 = 6:8:86$ mol% over $FeMoO_x$ and Mg/Si at a GHSV of 5000 h^{-1} and different temperatures.

Yield *Y* or conversion *C*	R_1 (260 °C) $FeMoO_x$	R_1 (260 °C) $FeMoO_x$ + R_2 (270 °C) Mg/Si	R_1 (260 °C) $FeMoO_x$ + R_2 (300 °C) Mg/Si	R_1 (260 °C) $FeMoO_x$ + R_2 (320 °C) Mg/Si
C MeOH [%]	78	76	65	62
Y ($CO + CO_2$) [%]	6	12	18	25
Y acetaldehyde [%]	–	–	–	–
Y acrolein [%]	–	–	–	–
Y acetone [%]	–	–	–	–
Y EtOH [%]	–	–	–	–
Y crotonaldehyde [%]	–	–	–	–

of acetaldehyde and formaldehyde in the absence of oxygen, reported a relatively high production of carbon oxides and methanol.

Conclusions

Characterization of the catalysts by XRD, N_2 sorption, thermal and chemical analysis, X-ray photoelectron spectroscopy (XPS), and NH_3-, SO_2-, and methanol-adsorption calorimetry revealed important physicochemical characteristics that can be connected to their catalytic performance for the acrolein production under oxidizing conditions. To increase the selectivity to acrolein, the carbon oxide production must be decreased by improving the acidity of the aldolization catalyst (R_2). The balance between basic and acidic sites enhances the acrolein selectivity. Therefore, the fine tuning of the acid/base surface properties is crucial to improve the acrolein selectivity and to minimize carbon oxide production resulting from over-oxidation. The Mg/Si catalyst was the most active for production of acrolein under oxidizing conditions owing to the presence of both strong basic and acidic sites. It was experimentally confirmed that both types of sites participate in the reaction. Acrolein production diminished significantly if the acidic sites were poisoned by NH_3 flow, proving that their presence is beneficial to the acrolein yield. The main products detected in each catalytic test were acrolein, acetaldehyde, methanol, ethanol, CO, and CO_2. Crotonaldehyde was not produced during the oxidative coupling of methanol and ethanol, indicating that under the present reaction conditions the self-condensation kinetics are much slower than that of the cross-condensation reaction. As a general conclusion, although these catalysts offer promising yields of acrolein, they are still a factor of two away from what would be required for a viable process (estimated yield $\approx$70%).

Experimental Section

Catalyst preparation

Na/SiO_2 (3.8 wt% Na_2O), K/SiO_2 (5.2 wt% K_2O), Ca/SiO_2 (5.6 wt% CaO), and Mg/SiO_2 (3.7 wt% MgO) were prepared by wet impregnation. Aqueous solutions of NaOH (VWR Chemicals), KOH (VWR Chemicals), $Ca(NO_3)_2{\cdot}4H_2O$ (Fluka), and $Mg(NO_3)_2{\cdot}6H_2O$ (Sigma–Aldrich) were mixed with colloidal silica Ludox TMA (Sigma–Aldrich) and evaporated in a rotary evaporator for 3 h (50 °C, 1 mbar). The salt solutions were prepared to have a theoretical bulk metal/silicon molar ratio of 0.1. The dried powders were calcined at 500 °C in N_2 atmosphere for 4 h and labeled Na/Si, K/Si, Ca/Si, Mg/Si, and SiO_2 for the bare support.

Catalyst characterization

XRD patterns were recorded on a Bruker D8 Advance A25 diffractometer at room temperature using CuKα radiation (0.154 nm) from 4 to 80° in 0.02° steps with 0.5 s per step.

Specific surface areas were determined by low-temperature N_2 adsorption performed at −196 °C on a Micromeritics 2020 apparatus after pretreatment performed for 3 h at 350 °C under vacuum. The BET method was used to derive specific surface areas (S_{BET}) from the resulting isotherms. The Barrett–Joyner–Halenda (BJH) method applied to the desorption branch of the isotherm allowed us to obtain the pore volume and the average pore diameter.

The XPS spectra were acquired by using a KRATOS Axis Ultra DLD spectrometer equipped with a hemispherical electron analyzer and an Al anode (AlKα = 1486.6 eV) powered at 150 W, a pass energy of 20 eV, and a hybrid lens mode. The detection area analyzed was 700 μm × 300 μm. Charge neutralization was required for all samples. The peaks were referenced to the C–(C, H) components of the C 1s band at 284.6 eV. Shirley background subtraction and peak fitting to theoretical Gaussian–Lorentzian functions were performed using an XPS processing program (Vision 2.2.6 KRATOS). The residual pressure in the spectrometer chamber was 5×10^{-9} mbar during data acquisition.

Chemical analyses were performed using inductively coupled plasma optical emission spectroscopy (ICP-OES) with an ACTIVA spectrometer from Horiba JOBIN YVON. Prior to analysis, the samples were dissolved in a mixture of inorganic acids (H_2SO_4, HNO_3, and HF or $HClO_4$, HNO_3, and HF). The amount of carbon was determined after measuring thermal conductivity of the catalysts.

Simultaneous TG-DTA of the samples was conducted on a Setaram Setsys Evolution 12 thermoanalyzer coupled by a heated (ca. 150 °C) capillary with a Pfeiffer Omnistar quadrupole MS. For TG-DTA-MS studies, samples (40–50 mg located in Pt-based open crucibles) were heated from RT to 700 °C at a constant rate of 10 °C min^{-1} under Ar flow (50 cm^3 min^{-1} STP).

The acid/base properties of the catalysts were studied by adsorption microcalorimetry of NH_3 and SO_2. The experiments were performed at 150 °C in a heat-flow calorimeter (C80 from Setaram) linked to a conventional volumetric apparatus equipped with a Barocel capacitance manometer for pressure measurements. The samples were pretreated in a quartz cell by heating overnight under vacuum at 350 °C. The differential heats of adsorption were measured as a function of coverage by repeatedly sending small doses of the probe gas onto the sample until an equilibrium pressure of approximately 67 Pa was reached. The sample was then outgassed for 40 min at the same temperature, and a second adsorption run

was performed at 150 °C on each sample, until an equilibrium pressure of approximately 27 Pa was attained. The difference between the amounts adsorbed in the first and second adsorptions at 27 Pa represents the irreversibly adsorbed amount (V_{irr}) of a respective gas, which provides an estimation of the number of strong acidic/basic sites. To obtain additional information concerning the Brønsted basicity of the samples, methanol was used as probe molecule following the same procedure but at an adsorption temperature of 30 °C.

Catalytic tests

Acrolein production was performed with two consecutive reactors (R_1 and R_2), the first one being used for the redox catalyst and the second one for the aldolization (acid/base) catalyst. The setup consisted of two sequential stainless-steel continuous-flow reactors working close to atmospheric pressure. The two vertical reactors were heated independently by two salt baths. The reaction temperature was controlled by moving a thermocouple inserted in the catalytic bed, thus allowing to follow the temperature profile and to identify the hot-spot positions.

In the first reactor, the simultaneous ethanol and methanol (VWR Chemicals) oxidation was performed, producing mainly acetaldehyde and formaldehyde. A commercial $FeMoO_x$ catalyst (4 g) was diluted with steatite (20 g) and placed into the first reactor. The products exiting from the first reactor were directly sent to the second, in which aldol condensation of acetaldehyde and formaldehyde and dehydration to acrolein was performed. Reaction conditions in the first reactor were optimized to obtain the highest (acetaldehyde + formaldehyde) yield. Different parameters (oven temperature, GHSV, $\%O_2$, $\%N_2$, and %MeOH/EtOH) were investigated. Preliminary experiments showed that over $FeMoO_x$ methanol reactivity was lower than ethanol reactivity. Therefore, the methanol/ethanol ratio was selected to ensure a more appropriate formaldehyde/acetaldehyde ratio. The final chosen conditions for the first reactor were MeOH/EtOH/O_2/N_2 molar ratio = 4:2:8:86, $GHSV_1 = 10\,000\ h^{-1}$, $T_1 = 260$ °C.

In the second reactor, aldolization catalysts (20 g), prepared as described above, were tested by varying the temperature (T_2) between 250 and 360 °C and the GHSV between 10 000 and 5 000 h^{-1} by adjusting the catalyst amount. The maximum reaction temperature was different for each catalyst and chosen to keep the ($CO + CO_2$) yield below 10 mol%. Above this threshold, the reaction became highly exothermic. Comparison of the catalysts was performed at conversions lower than 100%. The products exiting from the second reactor were collected in a cold trap (cooled to 0 °C by an ice bath), and the condensable products (acrolein, acetaldehyde, methanol, ethanol, crotonaldehyde, and others) were quantified offline by GC (column ZB-WAX plus) equipped with a flame ionization detector. Formaldehyde could not be quantified with this analytical device. The non-condensable products (CO, CO_2, O_2, N_2) were analyzed online with a two-column micro-GC using thermal conductivity detector. The first column filled with molecular sieves measured the CO, O_2, and N_2 concentrations, and the second column (silica plot) measured CO_2.

Conversions (C) of the reactants methanol, ethanol, and acetaldehyde [%], the carbon yield (Y) of acrolein [%], and the selectivity (S) towards acrolein [%] were calculated as follows:

$C\,[\%] = (NL\,h^{-1}\ reactant_{converted})/(NL\,h^{-1}\ reactant_{in}) \times 100\,\%$

$Y_{acrolein}\ [\%] = (3 \times NL\,h^{-1}\ acrolein_{produced})/(NL\,h^{-1}\ MeOH_{in} + 2 \times NL\,h^{-1}\ EtOH_{in}) \times 100\,\%$

Because the reaction conditions were chosen to obtain a MeOH/EtOH molar ratio of 2, if all ethanol was transformed to acrolein the maximum yield of acrolein could reach 75% at best. Therefore, a 40% yield of acrolein would represent 40/75 = 53% of the theoretical maximum.

$S_{acrolein}\,[\%] = (3 \times NL\,h^{-1}\ acrolein_{produced})/(NL\,h^{-1}\ MeOH_{reacted} + 2 \times NL\,h^{-1}\ EtOH_{reacted}) \times 100\,\%$

To confirm the absence of crotonaldehyde and to clarify the reaction pathway, additional experiments consisting of introducing crotonaldehyde/H_2O/O_2, EtOH/O_2/N_2, or MeOH/O_2/N_2 mixtures over the $FeMoO_x$ redox catalyst and over Mg/Si, the best aldolization catalyst, were performed. As complementary investigation, the introduction of acrolein/H_2O/O_2 over $FeMoO_x$ and Mg/Si was performed to understand the possibility of further conversion of the produced acrolein. Crotonaldehyde and acrolein for these experiments were purchased from Sigma–Aldrich.

Acknowledgements

This work was supported by the French Environment and Energy Management Agency (ADEME) within the framework of the Investissements d'Avenir program ("Investment for the Future"). The authors acknowledge the scientific services of IRCELYON.

Conflict of interest

The authors declare no conflict of interest.

Keywords: acidity · alcohols · aldol reaction · basicity · calorimetry

[1] D. Arntz, A. Fischer, M. Höpp, S. Jacobi, J. Sauer, T. Ohara, T. Sato, N. Shimizu, H. Schwind, *Acrolein and Methacrolein in Ullmann's Encyclopedia of Industrial Chemistry*, Wiley-VCH, Weinheim.
[2] *Acroléine: succès confirmés en chimie fine*: S. Mourey, *Info Chim. Mag.* **1999**, *412*, 90–96.
[3] L. Liu, X.P. Ye, J.J. Bozell, *ChemSusChem* **2012**, *5*, 1162–1180.
[4] H. Schulz, H. Wagner, *Angew. Chem.* **1950**, *62*, 105–118.
[5] J. L. Dubois (Arkema France, Colombes), WO2011083225A1, **2011**.
[6] J. L. Dubois, M. Capron, F. Dumeignil (Arkema France, Colombes), WO2014/068213A9, **2014**.
[7] T. H. Kang, J. H. Choi, Y. Bang, J. Yoo, J. H. Song, W. Joe, J. S. Choi, I. K. Song, *J. Mol. Catal. A* **2015**, *396*, 282–289.
[8] A. Witsuthammakul, T. Sooknoi, *Appl. Catal. A* **2012**, *413–414*, 109–116.
[9] A. Chieregato, M. D. Soriano, F. Basile, G. Liosi, S. Zamora, P. Concepción, F. Cavani, J. M. López Nieto, *Appl. Catal. B* **2014**, *150–151*, 37–46.
[10] M. Massa, A. Andersson, E. Finocchio, G. Busca, F. Lenrick, L. Reine Wallenberg, *J. Catal.* **2013**, *297*, 93–109.
[11] D. Stošić, S. Bennici, S. Sirotin, C. Calais, J. L. Couturier, J. L. Dubois, A. Travert, A. Auroux, *Appl. Catal. A* **2012**, *447–448*, 124–134.
[12] D. Stošić, S. Bennici, J. L. Couturier, J. L. Dubois, A. Auroux, *Catal. Commun.* **2012**, *17*, 23–28.
[13] P. T. Anastas, J. C. Warner, *Green Chemistry: Theory and Practice*, Oxford University Press, New York, **1998**.
[14] M. Dalil, M. Edake, C. Sudeau, J. L. Dubois, G. S. Patience, *Appl. Catal. A* **2016**, *522*, 80–89.
[15] M. Dalil, D. Carnevali, M. Edake, A. Auroux, J. L. Dubois, G. S. Patience, *J. Mol. Catal. A* **2016**, *421*, 146–155.
[16] J. Deleplanque, J. L. Dubois, J. F. Devaux, W. Ueda, *Catal. Today* **2010**, *157*, 351–358.
[17] a) M. Ai, *Bull. Chem. Soc. Jpn.* **1991**, *64*, 1342–1345; b) M. Ai, *Bull. Chem. Soc. Jpn.* **1991**, *64*, 1346–1350; c) M. Ai, *Appl. Catal.* **1991**, *77*, 123–132.
[18] E. Dumitriu, V. Hulea, C. Chelaru, C. Catrinescu, D. Tichit, R. Durand, *Appl. Catal. A* **1999**, *178*, 145–157.
[19] E. Dumitriu, V. Hulea, I. Fechete, A. Auroux, J. F. Lacaze, C. Guimon, *Microporous Mesoporous Mater.* **2001**, *43*, 341–359.

[20] B. Tollens, P. Wigand, *Justus Liebigs Ann. Chem.* **1891**, *265*, 316 – 340.
[21] C. Cobzaru, S. Oprea, E. Dumitriu, V. Hulea, *Appl. Catal. A* **2008**, *351*, 253 – 258.
[22] A. Ungureanu, S. Royer, T. V. Hoang, D. Trong On, E. Dumitriu, S. Kaliaguine, *Microporous Mesoporous Mater.* **2005**, *84*, 283 – 296.
[23] E. Dumitriu, V. Hulea, N. Bilba, G. Carja, A. Azzouz, *J. Mol. Catal.* **1993**, *79*, 175 – 185.
[24] A. Azzouz, D. Messad, D. Nistor, C. Catrinescu, A. Zvolinschi, S. Asaftei, *Appl. Catal. A* **2003**, *241*, 1 – 13.
[25] E. Dumitriu, N. Bilba, M. Lupascu, A. Azzouz, V. Hulea, G. Cirje, D. Nibou, *J. Catal.* **1994**, *147*, 133 – 139.
[26] E. Dumitriu, C. Cobzaru, V. Hulea, S. Oprea, *Rev. Chim.* **2010**, *61*, 400 – 403.
[27] W. J. Palion, S. Malinowski, *React. Kinet. Catal. Lett.* **1974**, *1*, 461 – 465.
[28] S. Malinowski, S. Basinski, *J. Catal.* **1963**, *2*, 203 – 207.
[29] M. Calatayud, A. Ruppert, B. Weckhuysen, *Chem. Eur. J.* **2009**, *15*, 10864 – 10870.
[30] W. D. Callister, D. G. Rethwisch, *Materials Science and Engineering: An Introduction*, John Wiley & Sons, New York, **2007**.
[31] http://www.quartzpage.de/gen_struct.html.
[32] PDF 00-033-1161 (XRD pattern for quartz SiO_2) from database PDF-4$^+$ 2016 (ICDD).
[33] W. Steurer, A. Apfolter, M. Koch, T. Sarlat, E. Sondergard, W. E. Ernst, B. Holst, *24th European Conference on Surf. Sci. (ECOSS-24)* **2007**, *601*, 4407 – 4411.
[34] A. Auroux, A. Gervasini, *J. Phys. Chem.* **1990**, *94*, 6371 – 6379.
[35] *Calorimetry and Thermal Methods in Catalysis* (Ed.: A. Auroux), Springer, Berlin, **2013**.
[36] C. Guimon, A. Gervasini, A. Auroux, *J. Phys. Chem. B* **2001**, *105*, 10316 – 10325.
[37] A. Auroux, J. C. Védrine in *Catalysis by Acids and Bases* (Eds.: B. Imelik, C. Naccache, G. Coudurier, Y. B. Taarit, J. C. Védrine), Elsevier, Amsterdam, **1985**, pp. 311 – 318.
[38] A. Gervasini, P. Carniti, A. Auroux, *Thermochim. Acta* **2005**, *434*, 42 – 49.
[39] A. Gervasini, A. Auroux, *J. Catal.* **1991**, *131*, 190 – 198.
[40] A. Gervasini, G. Bellussi, J. Fenyvesi, A. Auroux in *New Frontiers in Catalysis* (Eds.: L. Guczi, F. Solymosi, P. Tétényi), Elsevier, Amsterdam, **1993**.
[41] a) N. Cardona-Martinez, J. A. Dumesic, *J. Catal.* **1991**, *128*, 23 – 33; b) N. Cardona-Martinez, J. A. Dumesic, *J. Catal.* **1991**, *127*, 706 – 718.
[42] J. Shen, M. Tu, C. Hu, *J. Solid State Chem.* **1998**, *137*, 295 – 301.
[43] J. Shen, J. M. Kobe, Y. Chen, J. A. Dumesic, *Langmuir* **1994**, *10*, 3902 – 3908.
[44] T. Masuda, H. Taniguchi, K. Tsutsumi, H. Takahashi, *Bull. Chem. Soc. Jpn.* **1978**, *51*, 1965 – 1969.
[45] J. Velasquez Ochoa, C. Bandinelli, O. Vozniuk, A. Chieregato, A. Malmusi, C. Recchi, F. Cavani, *Green Chem.* **2016**, *18*, 1653 – 1663.
[46] V. Bolis, C. Busco, V. Aina, C. Morterra, P. Ugliengo, *J. Phys. Chem. C* **2008**, *112*, 16879 – 16892.
[47] M. Bensitel, O. Saur, J. C. Lavalley, *Mater. Chem. Phys.* **1991**, *28*, 309 – 320.
[48] H. Petitjean, K. Tarasov, F. Delbecq, P. Sautet, J. M. Krafft, P. Bazin, M. C. Paganini, E. Giamello, M. Che, H. Lauron-Pernot, G. Costentin, *J. Phys. Chem. C* **2010**, *114*, 3008 – 3016.
[49] V. Bolis, A. Cavenago, B. Fubini, *Langmuir* **1997**, *13*, 895 – 902.
[50] A. G. Pelmenschikov, G. Morosi, A. Gamba, A. Zecchina, S. Bordiga, E. A. Paukshtis, *J. Phys. Chem.* **1993**, *97*, 11979 – 11986.
[51] W. Ji, Y. Chen, H. H. Kung, *Appl. Catal. A* **1997**, *161*, 93 – 104.
[52] V. Hulea, D. Tichit, C. Catrinescu, E. Dumitriu, *An. Stiint. Univ. "Al. I. Cuza" Iasi Chim.* **1997**, *5*, 185 – 192.
[53] J. Scalbert, F. Thibault-Starzyk, R. Jacquot, D. Morvan, F. Meunier, *J. Catal.* **2014**, *311*, 28 – 32.
[54] M. Colmont, G. Bucataru, A. Borowiec, M. Capron, F. Dumeignil, M. Huvé, F. Capet, F. Damay, O. Mentré, P. Roussel, *Dalton Trans.* **2015**, *44*, 14444 – 14452.
[55] J. Bussi, S. Parodi, B. Irigaray, R. Kieffer, *Appl. Catal. A* **1998**, *172*, 117 – 129.
[56] L. P. Blanchard, J. B. Farmer, C. Ouellet, *Can. J. Chem.* **1957**, *35*, 115 – 123.

Manuscript received: February 8, 2017
Revised: February 24, 2017
Accepted Article published: February 24, 2017
Final Article published: March 23, 2017

ChemSusChem (DOI: 10.1002/cssc.201700230):

Supporting Information

Influence of catalyst acid/base properties in acrolein production by oxidative coupling of ethanol and methanol

Aleksandra Lilić,[a] Simona Bennici,*[a] Jean-François Devaux,[b] Jean-Luc Dubois[c] and Aline Auroux*[a]

N_2-adsorption isotherms

All samples present isotherms of type IV (see Figures S1-S5). Hysteresis of type H1 typical of mesoporous solid materials with cylindrical pores is observed for the Na,K,Ca,Mg/SiO_2 samples. SiO_2 presents a H2 hysteresis connected to the presence of bottle-neck pores. This kind of pore shape justifies the low average pore diameter measured (6 nm). Moreover part of SiO_2 pores is not accessible to nitrogen, as shown from the relatively low total pore volume (0.250 cm^3/g) when compared to that of Mg/SiO_2 (0.405 cm^3/g). During catalyst preparation, the colloidal silica is probably modified to different extents by the interaction with the salt solutions, resulting in more accessible pores (higher average pore diameters).

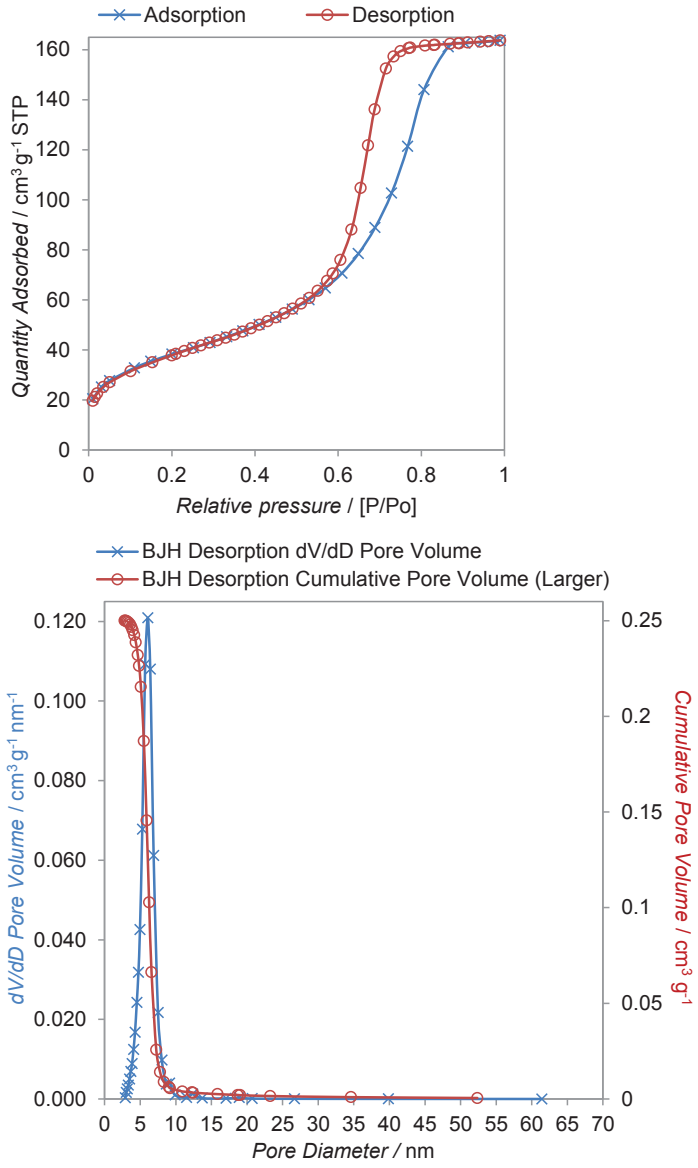

Figure S1. Nitrogen adsorption/desorption isotherms (left), and pore size distribution curves (right) for bare SiO_2.

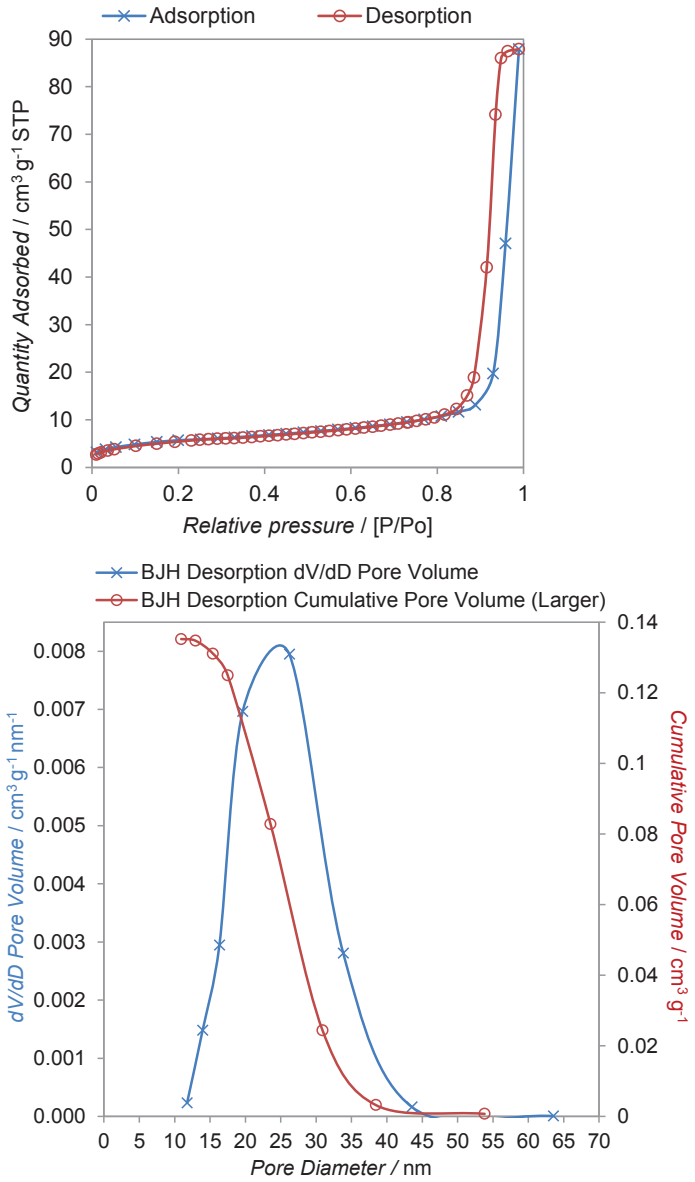

Figure S2. Nitrogen adsorption/desorption isotherms (left), and pore size distribution curves (right) for Na/Si catalyst.

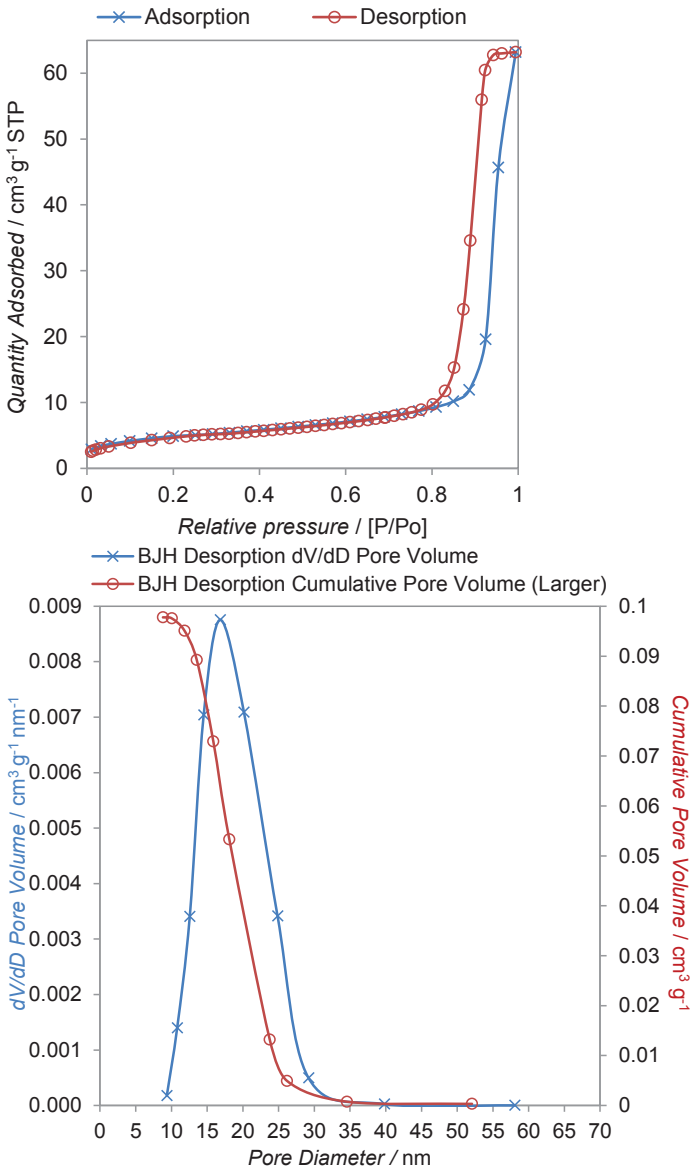

Figure S3. Nitrogen adsorption/desorption isotherms (left), and pore size distribution curves (right) for K/Si catalyst.

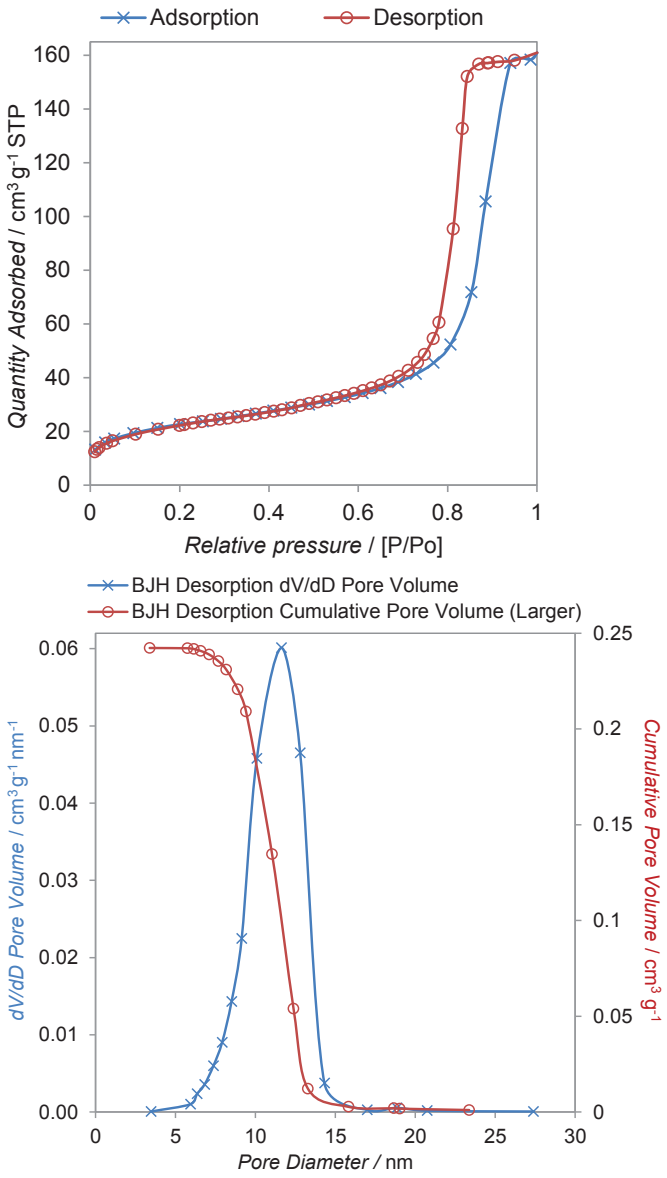

Figure S4. Nitrogen adsorption/desorption isotherms (left), and pore size distribution curves (right) for Ca/Si catalyst.

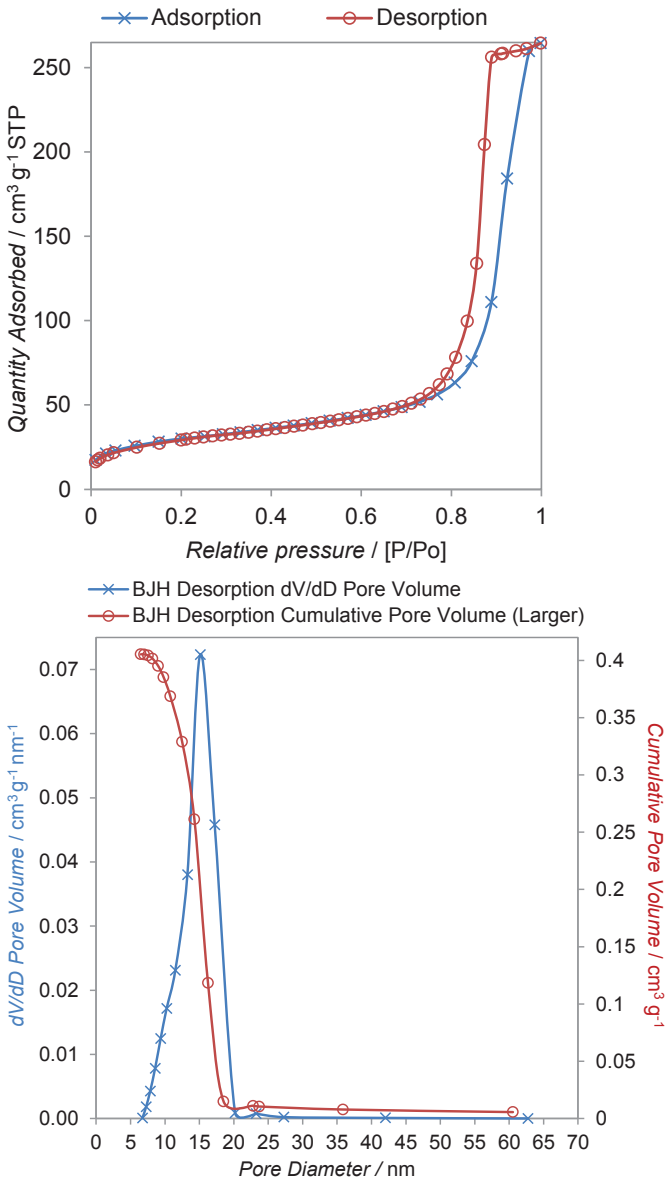

Figure S5. Nitrogen adsorption/desorption isotherms (left), and pore size distribution curves (right) for Mg/Si catalyst.

Flammability limits

For all oxidation reactions it is important to know where are the flammability limits of the reagents considered. There are tabulated data available for methanol and ethanol, in air-nitrogen mixtures.[a] However those data are quite often available are room temperature and atmospheric pressure only. It is then important to remember how those limits vary with process conditions. Usually when the temperature is increasing, the upper flammability limit (alcohol rich limit) is going to increase. UFL is also going to increase with the pressure, but in the present case since we plan to run our reactions close to the atmospheric pressure, this is not the most important parameter. The lower flammability Limit (LFL) is not as much affected by pressure and temperature. So in absence of data it can be considered as only slightly expended towards lower concentrations. In the present case, this is not our focus since the

experiments are planned in the higher concentration region, in order to maximize the productivity.

The second important fact to remind is how the limits are measured: a known amount of alcohol (at a concentration low enough to avoid condensation) is loaded in a sphere (or sometimes cylinder), then the inert gas and the oxygen while mixing all the gases. Then mixing is stopped and the mixture is ignited. To determine the limit a minimum pressure increase is defined. But when the composition is approaching the flammability limit, there are still some reactions taking place but they are taking much time and would correspond to long delays before self-ignition; or the pressure increase is not large enough. Then it means that when the composition is close to the flammability limits some gas phase reactions can take place, and would be minimized when either the composition gets away of the limits or when the residence time in those conditions is minimized. In industrial processes, the flow rates, and especially the linear velocities of gasses, are much higher than in laboratory equipment, so the residence times and gas phase reactions are reduced, but their impact might be large. Therefore reactors would be equipped with safety devices (rupture disks, sensors…) to handle these risks.

It is therefore important to know where the limits are. Of course, it would be unexpected to find tabulated data for all the compositions of methanol and ethanol mixtures that would need to be investigated. So a fair approximation can be calculated using the Le Chatelier rule: 1/UFL (mix) = x1/UFL (Methanol) + x2/UFL(Ethanol) and similar equation for the Lower Flammability Limit. In this equation, x1 and x2 represent the relative concentrations of methanol and ethanol in the alcohol mixture. Based on the data reported in the publication of Brooks and Crowl,[50] the limits were determined for several Oxygen-Nitrogen compositions, and the graph for a 50 % / 50 % mole ratio was calculated, and reported in the Figure S6.

To carry the reaction on a redox catalyst like Iron-Molybdate (FeMoOx), it is necessary to keep enough oxygen partial pressure at the exit of the reactor to avoid over reduction of the catalyst, since it is an irreversible process. Since the stoichiometry of the reaction is:

$CH_3OH + CH_3CH_2OH + O_2 \rightarrow CH_2=CH\text{-}CHO + 3\ H_2O$

It is necessary to keep an O_2/Alcohol ratio above ½ (so on the right side of the stoichiometric line in Figure S6) unless the reaction is done at partial conversion.

As the Upper Limit is shifted to the left side (higher concentration) with an increase of the temperature, the appropriate working conditions are in the range of less than 20 % alcohols, and less than 5-10 % oxygen (also to maximize the productivity).

We also want to stress here that the approximations of the flammability limits done here, do not replace the real experimental measurements that should be done once the appropriate alcohols mix composition is known.

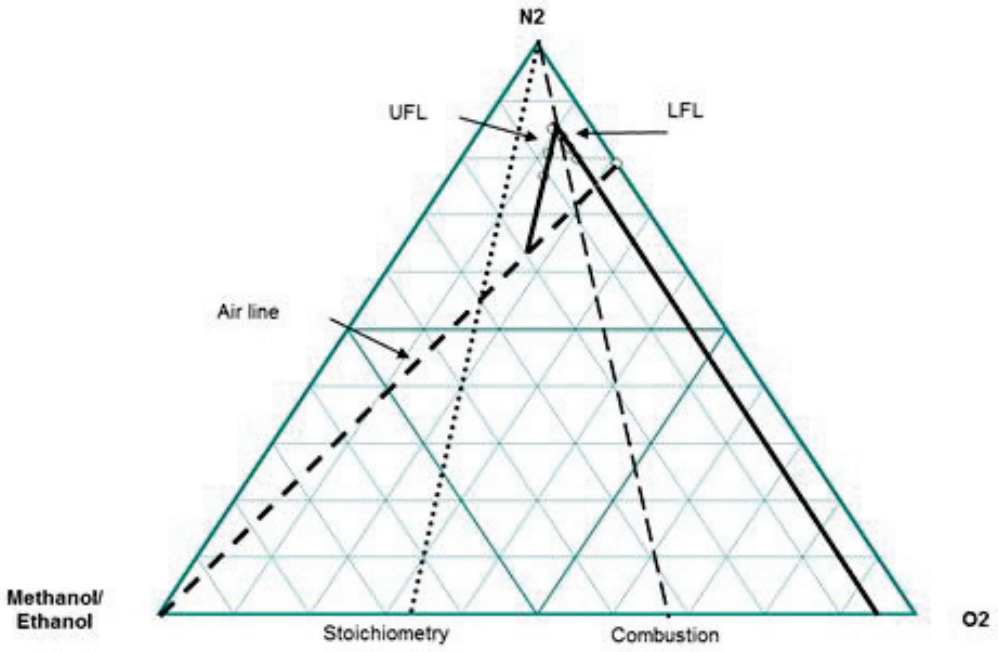

Figure S6. Flammability limits diagram at 25°C for methanol and ethanol mix=50%:50% molar ratio.

References:

[a] M.R. Brooks, D.A. Crowl, *J. Loss Prev. Process Ind.* **2007**, *20*, 144-150.

Chapter 7.

A comparative study of basic, amphoteric and acidic catalysts in the oxidative coupling of methanol and ethanol for acrolein production *(Publication II)*

Published in *ChemSusChem;*
ChemSusChem **2017**, *10*, 3459-3472. DOI: 10.1002/cssc.201701040

CHEMISTRY & SUSTAINABILITY

CHEMSUSCHEM

ENERGY & MATERIALS

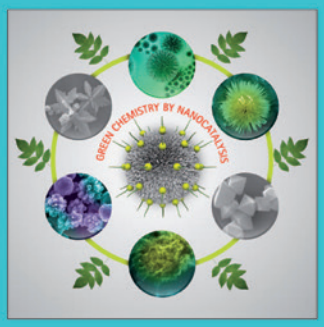

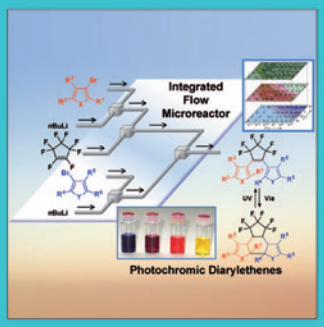

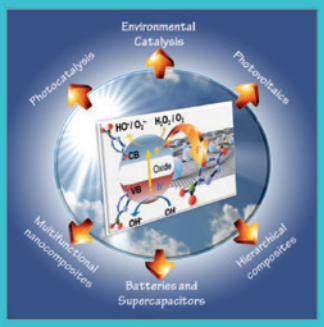

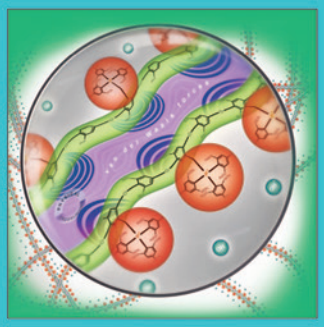

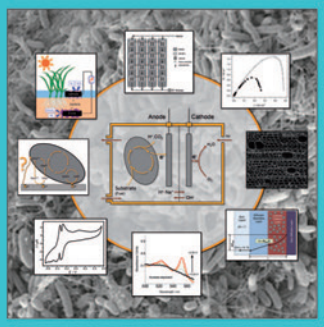

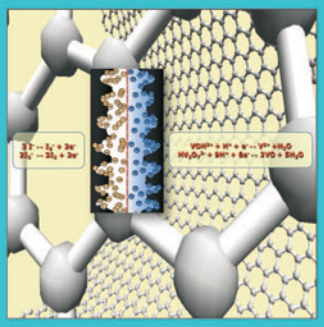

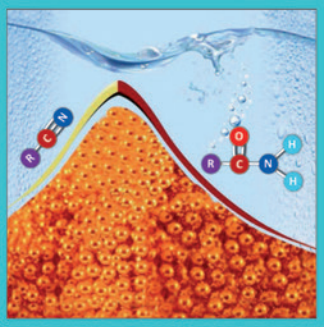

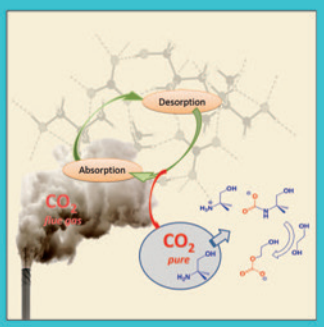

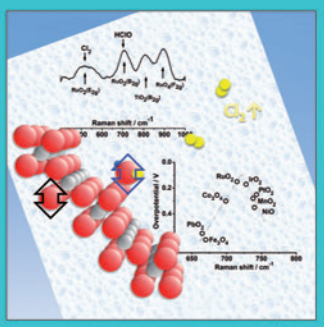

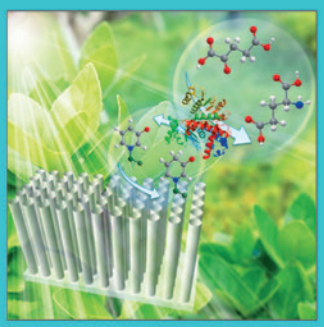

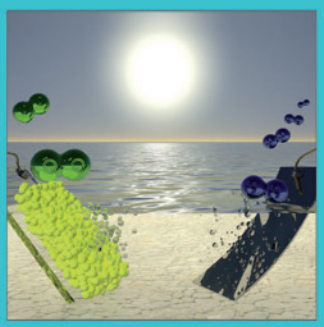

Reprint

A Journal of

ChemPubSoc Europe

WILEY-VCH

www.chemsuschem.org

ChemPubSoc Europe

DOI: 10.1002/cssc.201701040

CHEMSUSCHEM Full Papers

A Comparative Study of Basic, Amphoteric, and Acidic Catalysts in the Oxidative Coupling of Methanol and Ethanol for Acrolein Production

Aleksandra Lilić,[a] Tiantian Wei,[a] Simona Bennici,*[a] Jean-François Devaux,[b] Jean-Luc Dubois,[c] and Aline Auroux*[a]

The impact of acid/base properties (determined by adsorption microcalorimetry) of various catalysts on the cross-aldolization of acetaldehyde and formaldehyde leading to acrolein was methodically studied in oxidizing conditions starting from a mixture of methanol and ethanol. The aldol condensation and further dehydration to acrolein were carried out on catalysts presenting various acid/base properties (MgO, Mg–Al oxides, Mg/SiO_2, NbP, and heteropolyanions on silica, HPA/SiO_2). Thermodynamic calculations revealed that cross-aldolization is always favored compared with self-aldolization of acetaldehyde, which leads to crotonaldehyde formation. The presence of strong basic sites is shown to be necessary, but a too high amount drastically increases CO_x production. On strong acid sites, production of acrolein and carbon oxides (CO_x) does not increase with temperature. The optimal catalyst for this process should be amphoteric with a balanced acid/base cooperation of medium strength sites and a small amount ($< 100\ \mu mol\,g^{-1}$) of very strong basic sites ($Q_{diff} > 150\ kJ\,mol^{-1}$).

Introduction

Acrolein is an important chemical intermediate with a high degree of reactivity arising from the conjugation of the vinyl group with a carbonyl group. In the chemical industry, acrolein can be converted to a high quantity of different derivatives, such as acrylic acid, methionine, biocides, and other high added-value products. Owing to the versatile applications of acrolein, it has attracted researchers' interests since the beginning of the 20th century.[1–3]

The first industrial process for acrolein production was aldol condensation of formaldehyde and acetaldehyde.[4] This process was quickly replaced by propylene direct oxidation, which is still the dominating process in the industry to produce acrolein, using bismuth molybdate type catalysts.[1–3]

Besides the processes that have been reported and applied to the industrial production of acrolein, continuous research has been undertaken to further develop more environmentally friendly methods starting from renewable feedstocks and to optimize the cost of the production process.[1,5–12]

In this respect, alcohol oxidative coupling of methanol and ethanol has been recently proposed and extensively studied as a potential method to replace the current fossil-based production of acrolein from propylene.[6,7] In this process, which takes place in the gas phase, acrolein can be directly synthesized in a single reactor, thus minimizing the investment costs.[6,7,12]

Even if this process can be performed in a single reactor on iron molybdate ($FeMoO_x$) as a reference redox catalyst, the process occurs in two consecutive steps, which can take place at the same time (i.e., in the same reactor). The first consists of the oxidation of methanol and ethanol to produce formaldehyde and acetaldehyde, then the second step implies the aldol condensation of formaldehyde and acetaldehyde and the dehydration of the two aldehydes to acrolein in the presence of oxygen. Knowing that aldolization reactions are generally catalyzed by basic and/or acidic sites, improved yield and selectivity towards acrolein should be obtained by enhancing the cross-aldolization reaction on acid/base catalysts.[6,7,12]

The focus of the present work is to understand how the amount and strength of the acidic and/or basic sites influences the yield of acrolein produced by alcohol oxidative coupling in the gas phase. In particular, the influence of acidity/basicity will be studied in relation to the aldol condensation of acetaldehyde and formaldehyde to acrolein in oxidizing conditions. This knowledge is necessary to understand how to improve acrolein production in a single reactor by using a mixture of $FeMoO_x$ redox catalyst and an aldolization acid/base catalyst. Therefore, as reported in a previous paper,[7] the two-step reaction has been performed in two separate consecutive reactors. The impact of the acid/base properties of aldolization catalysts on acrolein production has been investigated. In the first reactor, a mixture of methanol, ethanol, nitrogen, and oxygen was

[a] Dr. A. Lilić, T. Wei, Dr. S. Bennici, Prof. A. Auroux
IRCELYON, UMR 5256 CNRS- Université Lyon 1
2 avenue Albert Einstein, 69626-Villeurbanne cedex (France)
E-mail: simona.bennici@uha.fr
aline.auroux@ircelyon.univ-lyon1.fr

[b] Dr. J.-F. Devaux
ARKEMA, Centre de Recherche Rhône Alpes
69493 Pierre Bénite, Cedex (France)

[c] Dr. J.-L. Dubois
ARKEMA, Direction Recherche & Développement
420 Rue d'Estienne d'Orves, 92705 Colombes (France)

Supporting Information and the ORCID identification number(s) for the author(s) of this article can be found under: https://doi.org/10.1002/cssc.201701040.

introduced and the oxidation to formaldehyde and acetaldehyde took place on the iron molybdate ($FeMoO_x$) catalyst. All products exiting from the first reactor were then directly sent to the second reactor where the aldol condensation of the two aldehydes and further dehydration to acrolein proceeded on different mixed or supported oxide catalysts, as well as on heteropolyacids supported on silica. Considering the aldol condensation of acetaldehyde and formaldehyde in the gas phase (in the absence of O_2), various research groups have previously shown that many factors may influence the reaction pathway, such as the type of reactor, the reaction pressure and temperature, the acetaldehyde to formaldehyde ratio, etc. These experiments were performed in most cases by co-feeding acetaldehyde and a formaldehyde solution, the latter being made of formaldehyde, water, and methanol, which stabilizes the formaldehyde. So even in this case, the aldol catalyst was contacted with water, acetaldehyde, formaldehyde, and methanol. Some variations of the ratio composition can explain some discrepancies in published results. In particular, when the self-condensation of acetaldehyde was performed, in most cases no water or methanol were present in the feed. However, the main differences in the catalytic results are connected to the surface acid/base properties of the catalysts used. It was also reported that competition between cross-condensation of acetaldehyde and formaldehyde to give acrolein and self-condensation of acetaldehyde to form crotonaldehyde can be governed by the balance between acid and base sites.[13–25] Catalytic materials from the following families were widely studied: mixed oxides,[13,14] zeolites,[16–19] hydrotalcites,[15,25] and clays.[20] It is generally acknowledged that aldol condensation can be catalyzed by either acid or base or both kinds of sites following the mechanisms shown in Scheme 1,[20] even if, up to now, the different authors do not agree on whether the best catalytic results are obtained on basic, acidic, or amphoteric catalysts. Very often the absence of measurements of both the acidity and basicity of the catalysts led to not fully justified conclusions.[13–25]

Ai[13,14] suggested that aldol condensation of formaldehyde and acetaldehyde is catalyzed by basic sites, and that weak basic centers lead to acrolein formation, whereas stronger

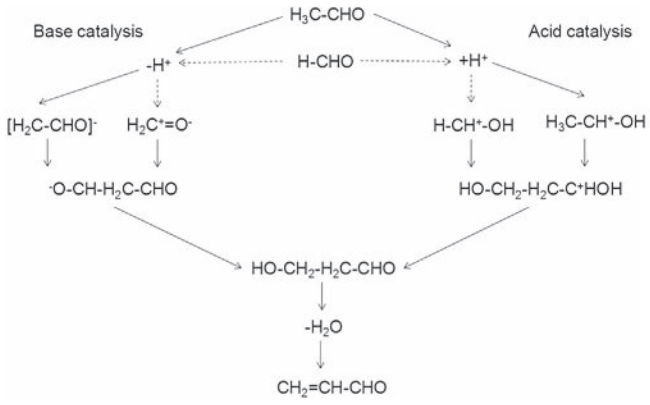

Scheme 1. Summary of basic and acidic reaction pathways proposed for cross-aldol condensation of formaldehyde and acetaldehyde. Adapted from Ref. [20].

basic sites increase production of CO_2 and methanol. On the other hand, the catalytic activity might decrease when the basicity is strongly lowered by the incorporation of an acidic oxide. Azzouz and co-authors[20] reported that basic sites are necessary for catalyzing cross-condensation as they can activate acetaldehyde by abstracting a H atom at the α-position of carbonyl. Meanwhile, weakly acidic sites can activate formaldehyde by increasing the electronegativity of the C atom. With respect to activity, acidic sites exhibit a strong influence on selectivity; the cross-selectivity seems then to be controlled by acidity rather than basicity. On the contrary, Cobzaru et al.[17] demonstrated that although both acidic and basic sites can activate the condensation reaction, the overall catalytic activity enhancement is governed by strong basic properties.

In a previous study,[7] performed in the presence of oxygen, the presence of strong basic sites ($Q_{diff} > 150\ kJ\,mol^{-1}$) was revealed to be essential for improving the acrolein production, whereas a high number of basic sites led to higher production of carbon oxides. It was stated that magnesium oxide supported on silica (amphoteric catalyst) was the most active. In this case, the acrolein yield was improved thanks to the additional presence of strong acidic sites. Acid/base cooperation created a positive impact on acrolein yield by decreasing the unwanted production of carbon oxides. Only cross-condensation of acetaldehyde and formaldehyde was observed, whereas self-condensation of acetaldehyde was not detected under the studied conditions.

Further research is needed to understand the role of acidity and basicity of the catalysts, to clarify the reaction pathway, and to understand the thermodynamic limitations.

The goal of the present research was to clarify the role of catalyst acid/base features on acrolein production by preparing samples with tuned acid/base surface properties. Solids with only acidic, basic, or amphoteric surface properties have been chosen as catalysts for the second step (aldolization) of the described process. Therefore, Mg–Al oxides, derived from commercial hydrotalcites with different Mg/Al ratios, as well as MgO supported on alumina were chosen as amphoteric catalysts. Hydrotalcite-like compounds present a layered structure with positively charged brucite-like layers and interlayers.[26,27] Calcined hydrotalcites are generally recognized as basic mixed oxides. However, they possess a certain acidity, and the basic/acidic balance of the calcined hydrotalcites can be modified by changing the chemical composition (M^{2+}/M^{3+} ratio),[28,29] the temperature of calcination,[30] or the nature of the cations in the layers.[31–33] MgO was chosen as a basic catalyst,[34,35] whereas heteropolyacids (tungstophosphoric and tungstosilic) supported on silica[36] and niobium phosphate[37] were selected for their unique acidic characters.

The acid/base properties of the involved catalysts were investigated by adsorption microcalorimetry by using gaseous ammonia and sulfur dioxide, and methanol vapor as probe molecules. This technique allows the simultaneous determination of the number, strength, and strength distribution of the acid/base sites. Other physicochemical properties were determined by using XRD, NMR, thermal and chemical analyses, and N_2-adsorption at $-196\,^{\circ}C$.

Results and Discussion

Physicochemical properties

Table 1 displays the list of the investigated catalysts, their specific surface area (S_{BET}), and results of chemical analyses. Among them, as expected, MgO (calcined commercial MgO)[38–42] presents the lowest specific surface area (53 $m^2 g^{-1}$).

Table 1. BET surface areas and chemical analysis (CA) of the calcined catalysts.

Sample	S_{BET} [$m^2 g^{-1}$]	CA [wt%]	
		Mg	Al
MgO	53	–	–
MgO/SiO_2[7]	108	3.7	–
MgO/Al_2O_3	219	3.9	45.4
CHT Mg/Al 3	201	33.3	16.0
CHT Mg/Al 0.5	251	14.2	30.9
CHT Mg/Al 0.3	279	9.4	39.5
CHT Mg/Al 0.06	255	2.6	46.1
Al_2O_3	230	–	–
ZrO_2	143	–	–
HPW/SiO_2	117	–	–
$HSiW/SiO_2$	117	–	–
NbP	98	Nb: 49.1; P: 10.6; K: 1.6	

MgO/Al_2O_3 displays a relatively high specific surface area, 219 $m^2 g^{-1}$, close to that of the alumina support (S_{BET} = 230 $m^2 g^{-1}$). For the calcined hydrotalcites (CHTs), the surface area decreased with increasing Mg content. As an exception, CHT Mg/Al 0.3 showed a higher Brunauer–Emmett–Teller (BET) surface area (279 $m^2 g^{-1}$) than CHT Mg/Al 0.06 (255 $m^2 g^{-1}$), despite a higher Mg/Al ratio. This is probably due to the difference in structure between the two samples as further discussed. The BET surface areas obtained for calcined hydrotalcites are in agreement with results previously reported.[29,43] Bulk heteropolyacids are generally characterized by very low specific surface areas. Deposition on silica increases the heteropolyacid dispersion and consequently the specific surface area, as can be observed for HPW/SiO_2 and $HSiW/SiO_2$.[36] Both samples exhibit similar specific surface areas (117 $m^2 g^{-1}$), relatively close to that of the silica support (144 $m^2 g^{-1}$). The full characterization of the silica support used in this work was already reported in a previous study.[7]

The X-ray diffraction patterns of basic and amphoteric samples are reported in Figure 1 (see Figure S1 in the Supporting Information for non-calcined hydrotalcites, HTs, used as precursors). The MgO sample presented the most sharp and intense peaks, which indicates a considerably high crystallinity in agreement with the low surface area. Meanwhile, the pattern of calcined MgO/Al_2O_3 exhibited broader peaks and lower crystallinity, accordingly to a higher specific surface area. The peaks identified on MgO/Al_2O_3 are characteristic of γ-alumina and are almost identical to those of pure Al_2O_3. In the pattern of non-calcined MgO/Al_2O_3, (precursor) peaks from both $Mg(NO_3)_2{\cdot}6H_2O$ and Al_2O_3 were observed (not shown), which indicates the successful impregnation. From Figure 1 it can be

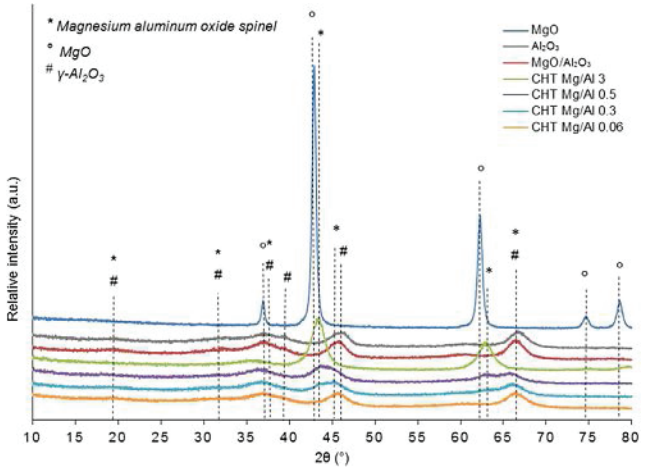

Figure 1. XRD patterns of basic and amphoteric catalysts.

observed that calcined hydrotalcites (CHTs) are poorly crystallized. Those with lower Mg/Al ratios and presenting higher surface areas exhibited broader diffraction peaks.[28] Concerning the CHT Mg/Al 3 sample, the MgO phase was observed by XRD but with a lower crystallinity than pure MgO. Moreover, it can be noticed that for CHT Mg/Al 3 the characteristic peaks of MgO and Mg_xAlO_y spinel structure overlap. For the other CHT samples richer in alumina (lower Mg/Al ratio), the characteristic pattern of the Mg–Al oxide phases can be detected, particularly for CHT Mg/Al 0.5 and 0.3. However, this pattern is very similar to that of alumina as already identified for sample Mg/Al 0.06. Indeed, for CHT samples, increasing the Mg/Al ratio leads to a decrease of the aluminium oxide pattern contribution, with concomitant enhancement of the peaks characteristic of magnesium oxide. XRD patterns for samples CHT Mg/Al 0.5 and CHT Mg/Al 3 are similar to those previously reported in the literature.[29]

Thermogravimetric/differential thermal analysis/mass spectroscopy (TG-DTA-MS) results (see the Supporting Information, Figure S3) are in agreement with the XRD results obtained for HT precursors and allow us to better understand the structure of mixed Mg/Al oxides obtained after calcination of HT precursors. Hydrotalcites calcined at 550 °C (labeled as CHTs) showed quite good thermal stabilities, with mass losses lower than 12 wt% owing to the presence of hydration water.

To confirm the identification of alumina, magnesia, and Mg–Al mixed oxide phases, ^{27}Al NMR spectra of Mg-containing catalysts were recorded (Figure 2). NMR spectroscopy is more sensitive to phase transitions than XRD and can probe the presence of structures existing in very small quantities.

At first sight, all samples show similar spectra characteristic of both alumina and Mg_xAlO_y spinel structures. Aluminium is coordinated to oxygen in mainly two configurations corresponding to a peak centered at around 8.5 ppm (attributed to octahedrally coordinated aluminium, Al_O), and a peak centered at around 65 ppm (attributed to tetrahedrally coordinated aluminium, Al_T).[28,29,43–48] Considering the alumina and MgO/Al_2O_3 samples, an additional contribution at around 35 ppm is observed and can be attributed to pentahedrally coordinated alu-

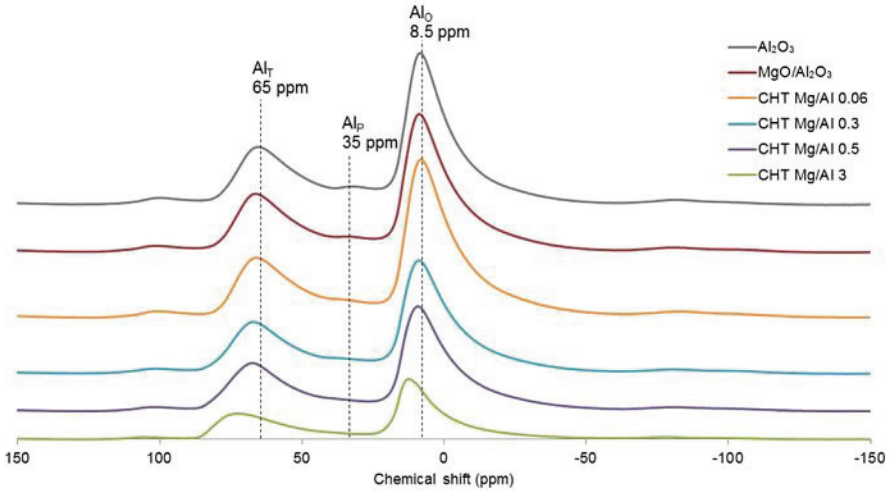

Figure 2. ^{27}Al MAS NMR spectra of amphoteric catalysts.

minium cations characteristic of the γ-alumina structure. All the other observed peaks correspond to spinning sidebands. The NMR spectra obtained for CHT samples are in agreement with those reported in previous research and correspond to the Mg_xAlO_y spinel phase for CHT Mg/Al 0.06, 0.3, and 0.5 catalysts. Diez et al.[43] showed that the chemical shift diminishes with increasing alumina content. In alumina, the Al-O polyhedron is surrounded only by Al^{3+} cations. Higher chemical shifts for both peaks, Al_O and Al_T, are observed in the ^{27}Al NMR spectrum of CHT Mg/Al 3 as part of the Mg^{2+} cations in the MgO matrix of this sample is replaced by Al^{3+} (more electronegative), as nearest neighbor cations. Based on the XRD and NMR results, and in agreement with previous reported research,[28,29,43,49] we can actually distinguish two different structures in Al-rich catalysts and Mg-rich catalysts. Alumina-rich samples (CHT Mg/Al 0.06 and 0.3) are heterogeneous oxides where Mg^{2+} and Al^{3+} cations are present in two separate phases consisting of quasi-amorphous Al_2O_3-like phase (γ-alumina) and MgO. The CHT Mg/Al 0.5 sample, defined as a transitional composition, is constituted of Mg_xAlO_y, γ-Al_2O_3, and MgO oxides. The CHT Mg/Al 3 sample forms a homogeneous hydrotalcite-like structure characteristic of Mg-rich mixed oxides, where Mg^{2+} and Al^{3+} cations are in close interaction (intimate contact) as Al^{3+} replaces Mg^{2+} cations in the MgO matrix.[28,29,43,49]

Acid/base properties

The number, strength, and strength distribution of the acid/base sites of the investigated catalysts were measured by adsorption microcalorimetry of gas probe molecules. Ammonia was used as a basic molecule, which is able to quantify both Lewis (coordinatively unsaturated metallic cations) and Brønsted acidic sites (arising from terminal hydroxyl groups),[50,51] whereas sulfur dioxide titrated basic sites consisting mostly of surface oxygen ions.[51,52] Table 2 reports the total and irreversible (chemisorbed) amounts (μmol g^{-1}) of both probe molecules adsorbed at 0.2 torr of equilibrium pressure and the ini-

Table 2. Total and chemisorbed amounts of probe molecules (V_{tot} and V_{irrev}) calculated from adsorption isotherms of SO_2 and NH_3 obtained by microcalorimetry measurements at 150 °C, and the corresponding ratios of basic to acidic sites.

Sample	SO_2		NH_3		$Base_{tot}/Acid_{tot}$[c]	$Base_{chem}/Acid_{chem}$[d]
	V_{tot} [μmol g^{-1}][a]	V_{irrev} [μmol g^{-1}][b]	V_{tot} [μmol g^{-1}][a]	V_{irrev} [μmol g^{-1}][b]	$V_{tot}(SO_2)$[a]/ $V_{tot}(NH_3)$	$V_{irrev}(SO_2)$[b]/$V_{irrev}(NH_3)$
MgO	224	201	50	26	–	–
MgO/SiO_2[7]	46	30	105	44	0.44	0.67
MgO/Al_2O_3	432	369	289	105	1.49	3.51
CHT Mg/Al 3	368	325	146	41	2.52	7.93
CHT Mg/Al 0.5	443	391	242	101	1.83	3.87
CHT Mg/Al 0.3	482	420	284	121	1.70	3.47
CHT Mg/Al 0.06	462	393	321	149	1.44	2.64
Al_2O_3	349	281	289	151	1.21	1.86
ZrO_2	222	178	211	89	1.05	2.00
HPW/SiO_2	–	–	120	57	–	–
$HSiW/SiO_2$	–	–	112	58	–	–
NbP	–	–	138	51	–	–

[a] Total amount of SO_2 and NH_3 adsorbed under an equilibrium pressure of 0.2 torr (27 Pa). [b] Amount of chemisorbed SO_2 and NH_3 under an equilibrium pressure of 0.2 torr (27 Pa). [c] Ratio of total basic to acidic sites. [d] Ratio of basic to acidic chemisorption sites.

tial heats (Q_{init}) of adsorption. The ratios of total and chemisorption basic to acidic sites are also reported in Table 2. The acid/base properties were also measured by using methanol adsorption at room temperature (Table 3, Figure 7).

Table 3. Initial differential heats (Q_{init}), V_{irrev} and V_{tot} calculated from adsorption isotherms of methanol obtained from microcalorimetry measurements at 30 °C.

Sample	MeOH		
	Q_{init} [kJ mol^{-1}][a]	V_{tot} [μmol g^{-1}][b]	V_{irrev} [μmol g^{-1}][c]
MgO	128	331	247
MgO/Al_2O_3	146	1149	912
CHT Mg/Al 3	151	944	735
CHT Mg/Al 0.5	159	1194	968
CHT Mg/Al 0.3	159	1277	1015
CHT Mg/Al 0.06	149	1318	1056
Al_2O_3	175	1148	812

[a] Heat evolved from the first methanol dose. [b] Total amount of methanol adsorbed under an equilibrium pressure of 0.2 torr (27 Pa). [c] Amount of chemisorbed methanol under an equilibrium pressure of 0.2 torr (27 Pa).

Acidic catalysts

Volumetric isotherms of NH_3 adsorption and differential heat curves versus coverage for the acidic catalysts are presented in Figure 3. The NbP catalyst showed a slightly higher total amount of ammonia adsorbed (including a higher quantity of very strong ($Q_{diff} > 150$ kJ mol^{-1}) acidic sites) than heteropolyacids supported on silica (Table 2 and Figure 3) and the obtained results are similar to those reported by Sun et al.[37] HPW and HSiW are known to exhibit very strong acidic Brønsted surface sites as previously shown by adsorption microcalorimetry.[53,54] Depositing heteropolyanions on silica (HPA/SiO_2) allows well dispersed acid catalysts to be obtained with improved specific surface areas in comparison to bulk heteropolyacids. Consequently, the differential heats of ammonia adsorption (Q_{diff}) and the amount of ammonia adsorbed (μmol g^{-1}) depend on the amount of heteropolyacid deposited on silica. The thermal stability of HPA/SiO_2 stays close to that of the parent heteropolyacid, but it is known that in the presence of water vapor, a thermally decomposed Keggin structure on the silica surface can be regenerated and therefore very strong acidity reestablished.[36] Both HPW/SiO_2 and $HSiW/SiO_2$ samples exhibited relatively close acidity to that of the NbP sample. For bulk HPW and HSiW heteropolyacids, the curves of differential heat versus coverage generally show a large plateau at Q_{diff} values higher than 150 kJ mol^{-1} (very strong acidic sites),[53,54] whereas in this study on supported heteropolyacids (10 wt% HPA/SiO_2) they continuously decreased (Figure 3), and a lower amount of ammonia was adsorbed. From Figure 3 and Table 2 it can be observed that HPW/SiO_2 adsorbed slightly more ammonia (V_{tot}) than $HSiW/SiO_2$, whereas $HSiW/SiO_2$ presented a higher amount of strong sites.

Basic and amphoteric catalysts

The volumetric isotherms of SO_2 and NH_3 adsorption on basic and amphoteric catalysts are presented in Figure 4, whereas Figure 5 displays the differential heat curves versus coverage. The strength distribution of basic and acidic sites is presented in Figure 6.

As a general trend, the differential heat curves of SO_2 adsorption (Figure 5), presented plateaus (in the 150–200 kJ mol^{-1} range) characteristic of strong basic sites of homogeneous strength. For MgO, CHT Mg/Al 3, and ZrO_2 catalysts, the curves decreased more steeply and plateaus were not observed. The acidity of the amphoteric catalysts (Figure 5) is characterized by sites with large strength spectra and an absence of well-defined plateaus.

According to the results previously reported in the literature,[34,55] magnesia possesses a large amount of basic sites and, as can be observed from the values of differential heats

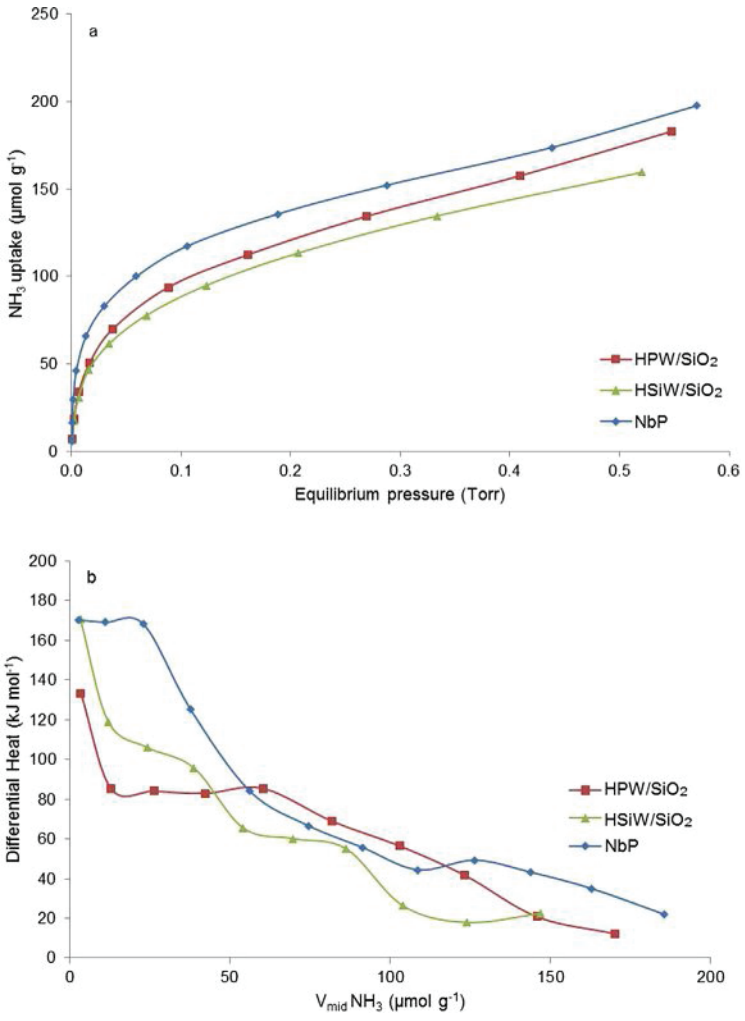

Figure 3. Volumetric isotherms (a) and differential heats versus surface coverage (b) obtained from ammonia adsorption microcalorimetry on acidic catalysts.

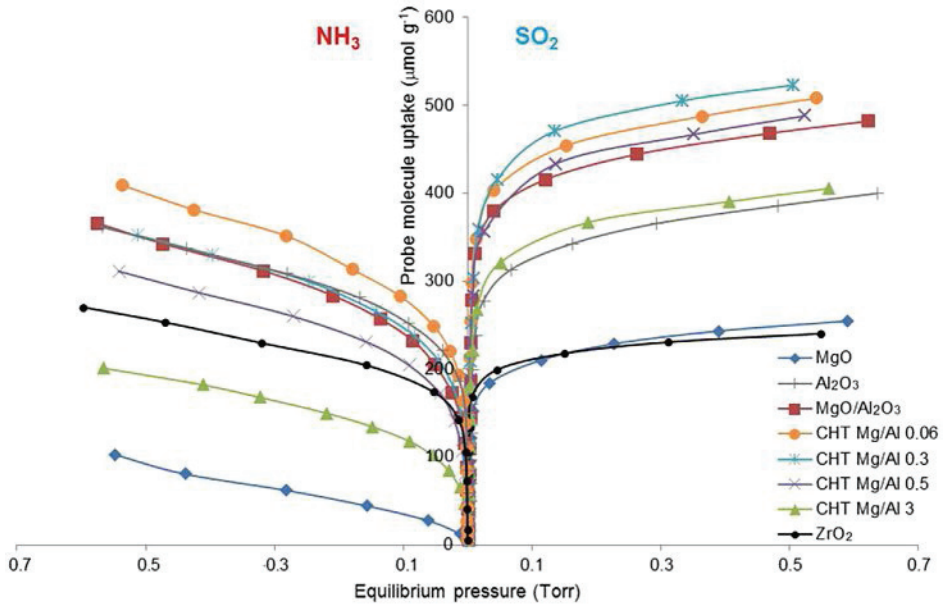

Figure 4. Volumetric isotherms of NH_3 and SO_2 adsorption on basic and amphoteric catalysts.

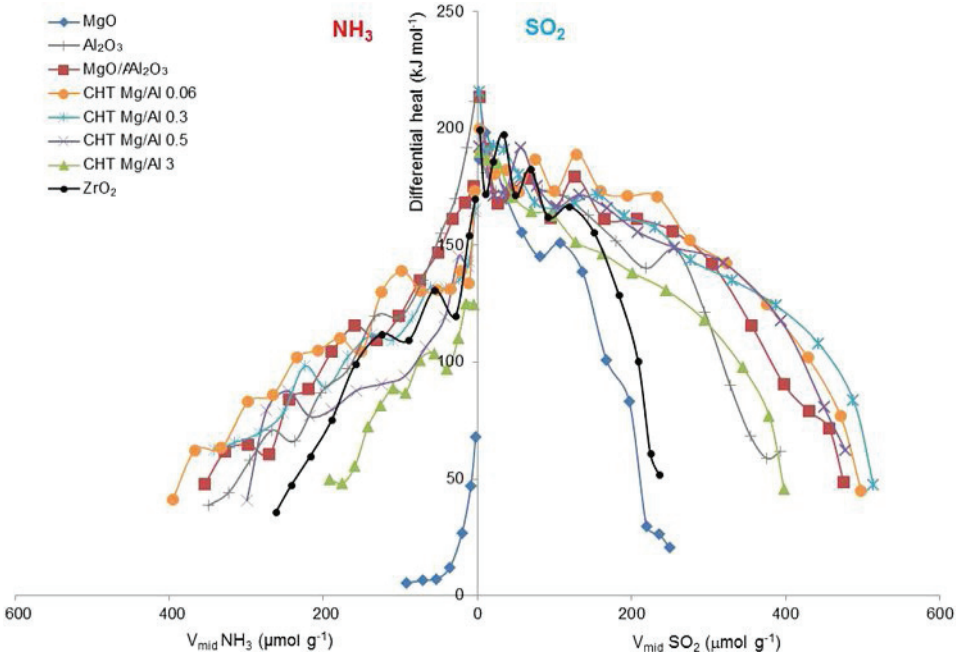

Figure 5. Differential heats NH_3 and SO_2 adsorption as a function of surface coverage on basic and amphoteric catalysts.

reported in Figure 5, is characterized by the presence of strong basic sites ($Q_{diff} > 150\ kJ\ mol^{-1}$). For the alumina sample, both acidic (related to Al^{3+} ions) and basic sites (related to O^{2-} ions) were observed.[34,55] As shown in Table 2, except for pure MgO, all magnesium-containing samples display both acidity and basicity, with the presence of strong sites, as deduced by the high values of the initial differential heats that vary in the 125–240 $kJ\ mol^{-1}$ range. The relatively lower values of adsorbed amount for pure MgO are related to the low specific surface area of this sample (corresponding to a consequential low amount of sites on the solid surface). Comparing the acid/base properties of MgO supported on alumina to those of pure MgO and bare Al_2O_3, it can be noticed (Figures 4 and 6, and Table 2) that the total amount of ammonia adsorbed (acidity) and the quantity of very strong ($Q_{diff} > 150\ kJ\ mol^{-1}$) acidic sites is almost the same for MgO/Al_2O_3 and alumina samples, whereas the basicity of MgO/Al_2O_3 is much higher than that of pure alumina. Mixed Mg/Al oxides obtained by calcination of hydrotalcites (CHTs) are generally recognized to be basic catalysts,[28] as confirmed by the present results (Figures 4–6, and Table 2). Basicity can be tuned by varying the Mg/Al ratio of the parent hydrotalcite-like material and the general trend, observed by

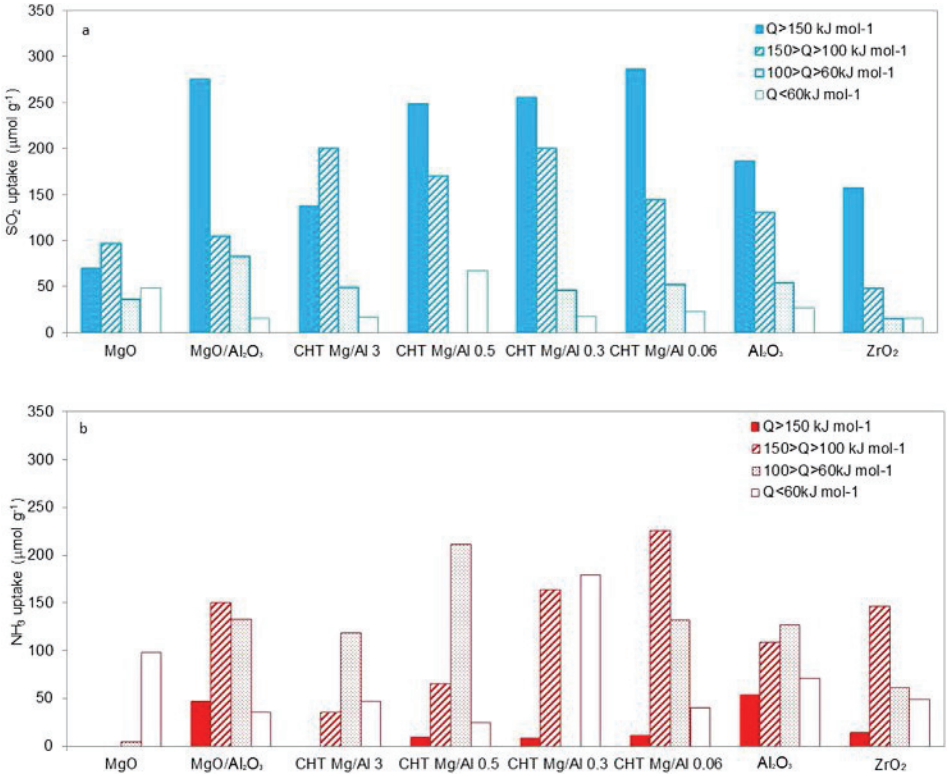

Figure 6. Strength distribution of basic (a) and acidic (b) sites of basic and amphoteric catalysts.

other research groups performing adsorption microcalorimetry measurements,[28,29,49] is that basicity generally decreases on decreasing the Mg content. However, few exceptions were reported[49,56] as the acid/base properties of mixed Mg–Al oxides also depend on their final structure, which is governed by the calcination temperature of the hydrotalcite-like precursor.[25,30] Moreover, acidity or basicity measurements can differ also depending on the type of probe molecule used, the temperature of adsorption, and the pretreatment parameters.[51,57]

The overall basic character of the CHT samples (Table 2, last two columns) decreases on decreasing the Mg/Al ratio, as previously reported.[28,29] Differently, the differential heats and amount of sulfur dioxide adsorbed on these samples (Table 2) do not follow this trend. The CHT Mg/Al 3 sample displays a lower amount and strength (Q_{diff}) of basic sites than the other CHT samples (Figures 4–6, and Table 2). This behavior can be due to the different structures and specific surface areas of the CHT samples as explained before in the "Physicochemical properties" section. CHT Mg/Al 0.06 and 0.3 represent the so-called "alumina-rich Mg–Al oxides",[43] which display a non-homogeneous structure, mostly consisting of alumina oxide accompanied by small amounts of MgO phase, whereas the non-homogeneous structure of the CHT Mg/Al 0.5 sample is characterized by the co-existence of Mg_xAlO_y, MgO, and Al_2O_3 oxides. Their structure can be roughly approximated to the structure of MgO supported on alumina. Indeed, they generally show acidity and basicity features more similar to MgO/Al_2O_3 than to CHT Mg/Al 3 (Figures 4–6). The CHT Mg/Al 3 sample presents a homogeneous Mg_xAlO_y hydrotalcite-like structure, as described in the "Physicochemical properties" section,[29,43] where Al^{3+} cations are incorporated into the structure of the MgO matrix and therefore Mg^{2+} cations are in intimate contact with Al^{3+} cations. The electronegativity of aluminium is higher than that of magnesium and, when aluminium cations are introduced into the MgO structure, the resulting basicity of this sample is lower[25,43,55] than for the CHT Mg/Al 0.06, 0.3, and 0.5 samples. For these samples, the Mg^{2+} and Al^{3+} cations are not in intimate contact but separated into two different phases (alumina-like and MgO oxides). In general, the acidity decreases as the content of magnesia increases, and CHT Mg/Al 0.06 shows the highest number of acid sites.[28]

Additionally, the acidity and basicity of ZrO_2, which also belongs to the group of amphoteric oxides the acid/base properties of which can be easily tuned by introduction of other oxides, were investigated (Figures 4–6). The sample exhibited lower amounts of basic and acidic sites than magnesium-containing amphoteric catalysts, but with similar strength. The ZrO_2 acid/base properties were in agreement with those previously reported.[9,50]

It is worth our interest to characterize the acid/base surface properties by using some of the reactants as probe molecules, and methanol can be considered as a suitable probe for this purpose.[7,35,39,40,58,59] Only a few studies have reported microcalorimetric adsorption of methanol on magnesia[35,39,40] and alumina,[58,60] however, this is a suitable experimental technique to study the strength of methanol interaction with a solid surface.

Researchers who have investigated the adsorption of methanol on magnesium oxide surfaces by adsorption microcalorim-

etry, IR spectroscopy, or computational methods agree that the interaction of methanol vapor involves physisorption and associative/dissociative chemisorption.[35,39,40] Undissociated methanol species can be physisorbed on the Mg^{2+} cations and O^{2-} anions of the MgO surface. The differential heats of this interaction are reported to be around 60 kJ mol^{-1}, whereas a strong associative chemisorption of methanol is characterized by differential heats in the 90–125 kJ mol^{-1} range.[40] This last type of interaction involves coordinatively adsorbed methanol molecules. Further dissociative adsorption results exclusively from methanol deprotonation.[35,39,40] The proton (H^+) and methoxy fragment (CH_3O^-) adsorb on the O^{2-} anion and Mg^{2+} cations, respectively, creating hydroxy (OH^-) and methoxy (Mg-OCH_3^+) species. Depending on the topology and defects present on the surface, the interaction of these two species through hydrogen bonding can take place, as well as the stabilization of methoxy species by bridging two or more magnesium cations. Dissociative chemisorption is characterized by differential heats ranging between 150 and 230 kJ mol^{-1}.[40]

Aluminium oxide is an amphoteric oxide and possesses much stronger Lewis acid sites (Al^{3+}) than MgO (which is a basic oxide) therefore acid/base pairs (Al^{3+}/O^{2-}) are characteristic for the alumina surface.[39,58,60] However, the new active species which can be created on the aluminium oxide surface after methanol adsorption are very similar to those created on MgO.[35,39,40,58]

As reported by Busca et al.,[58] physisorption of methanol through hydrogen bonding on oxygen atoms of alumina is characterized by differential heats of around 70 kJ mol^{-1}. Differential heats in the range between 100 and 110 kJ mol^{-1} are characteristic for so-called "true" coordinative interactions, where the methanol molecule is coordinatively bonded to the Al^{3+} cation and the O^{2-} anion of the alumina surface through its oxygen atoms and by hydrogen-bond donor interaction, respectively. Differential heats between 140 and 220 kJ mol^{-1} were attributed to the associative/dissociative chemisorption characteristic of the presence of strong Lewis acid sites (Al^{3+}). Undissociated methanol molecules are strongly coordinated on the strong Lewis acid sites (Al^{3+} cations) and can be easily transformed into bridging methoxy species and OH groups on the alumina surface. Methoxy (M-OCH_3) and hydroxyl (OH) species created at the surface of MgO and Al_2O_3, as well as coordinatively adsorbed methanol, might act as adsorption sites on the metal oxide surface.

The MeOH vapor adsorption isotherms and differential heats are displayed in Figure 7, whereas Table 3 presents the amount of methanol adsorbed at 0.2 torr. All samples present large amounts of methanol adsorbed. The highest MeOH uptake measured at 0.2 torr reached 1318 μmol g^{-1} for the CHT Mg/Al 0.06 sample. A decreasing tendency of MeOH adsorption was observed as the Mg/Al ratio increased. The initial differential heats for the calcined hydrotalcites were around 150–160 kJ mol^{-1}, whereas the initial heat of methanol adsorption on MgO was much lower (128 kJ mol^{-1}). The highest initial heat value was observed for alumina (175 kJ mol^{-1}). The present results are in agreement with those previously reported for methanol adsorption on magnesia and alumina surfaces.[35,39,40,58]

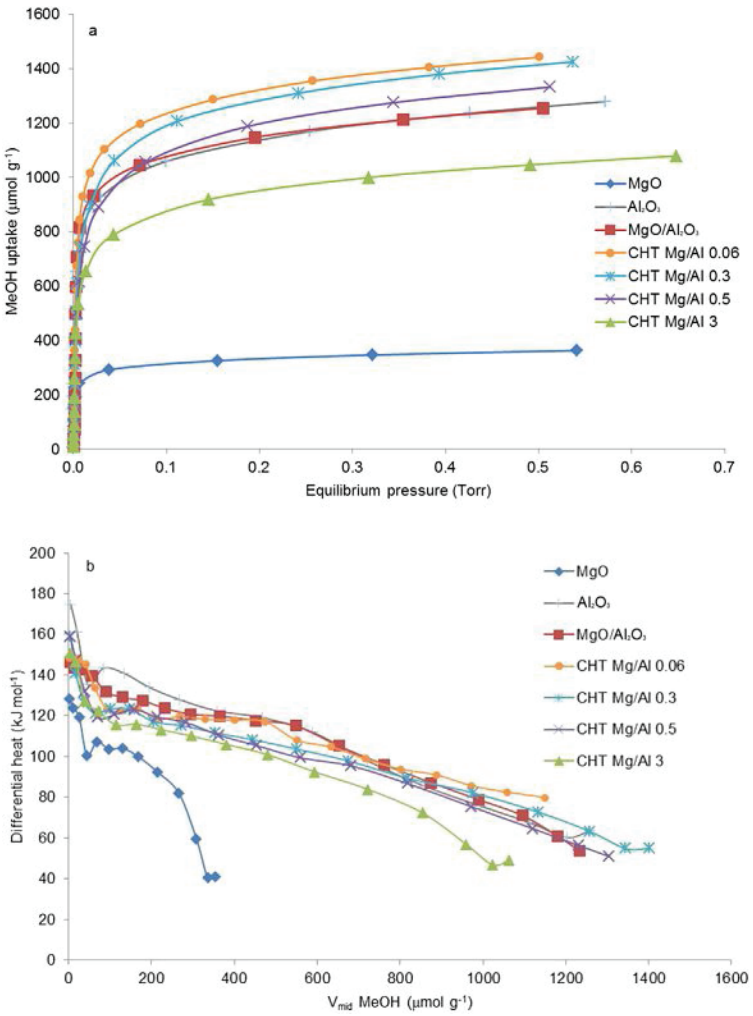

Figure 7. Volumetric isotherms (a) and differential heats versus surface coverage (b) obtained from methanol adsorption microcalorimetry on basic and amphoteric catalysts.

Comparison of our Q_{diff} values (Figure 7) and previously reported results allow us to estimate which species are created on the catalyst surface after methanol adsorption.[40,58] The MgO sample presented a short plateau (at 100 kJ mol^{-1}), on the curve Q_{diff} versus coverage, and it can be expected that only coordinative bonding of methanol molecules occurs at the MgO surface.[40] Differently, for all other amphoteric samples, co-existence of associatively and dissociatively formed species can be expected as indicated by the shape of the curves Q_{diff} versus coverage and the values of differential heats.[40,58] The samples consisting of dominantly alumina phase, such as Al_2O_3, MgO/Al_2O_3, and CHT Mg/Al 0.06, presented very similar shapes of the curves (Q_{diff} vs. coverage) and

values of differential heats are similar to those previously reported by Busca and co-authors for pure alumina.[58] Values of the differential heats higher than 140 kJ mol^{-1} indicate the simultaneous presence of dissociatively created bridged methoxy species and undissociated strongly coordinated methanol molecules on the strong Lewis acid sites (Al^{3+}). Long plateaus in the 110–130 kJ mol^{-1} range are attributed to the so-called "true" coordinative interaction between methanol and acid/base pairs (Al^{3+}/O^{2-}). For the CHT samples containing a higher amount of magnesia phase, these plateaus (110–130 kJ mol^{-1}) are shorter, but the presence of bridged methoxy species and strongly coordinated methanol on the alumina acid cations is also very probable ($Q_{diff} > 140$ kJ mol^{-1}). These results suggest that the creation of new acid/base sites on the surface of pure MgO does not occur after methanol adsorption, whereas on the surface of amphoteric catalysts (especially those with higher alumina content) new acid/base sites consisting of methoxy and hydroxy groups are created on the alumina surface. In previous studies, the experiments performed by Ai and other authors[13–25] were done with solutions of formaldehyde/water and methanol (formalin) and acetaldehyde; therefore methanol was already present in the stream.

Methanol vapor titrated the acid/base pairs on the catalyst surface in dosing conditions (adsorption calorimetry measurements) and new active sites might be created on the clean catalyst surface under vacuum. Similar behavior might be expected in reaction conditions in the presence of methanol (and other reactants or products). These new created and potentially active sites might play an important role.

Catalytic tests and influence of surface acid/base features on the catalytic activity

For all oxidation reactions, it is important to know where are the flammability limits of the reagents considered; they are reported in a previous work.[7]

Formaldehyde and acetaldehyde (and some amount of acrolein) were produced on the redox $FeMoO_x$ commercial catalyst placed in the first reactor (R_1) fed with methanol and ethanol. At gas hourly space velocity (GHSV) = 10 000 h^{-1}, the conversion of methanol was equal to 61 mol%, whereas the conversion of ethanol was 86 mol%. In these reaction conditions, alcohols are not fully converted, so the impact of the non-reacted alcohols on the aldolization catalysts behavior must be also taken into account. The acrolein yield was 8 mol% (with a selectivity of 11%) and acetaldehyde yield was 27 mol% (selectivity of 37%) on the redox catalyst alone. The total yield for ($CO + CO_2$) was 3 mol%. At GHSV = 5000 h^{-1}, the conversion of methanol increased to 78 mol% and that of ethanol to 95 mol%. The acrolein yield was 12 mol% (with a selectivity of 14%) and the acetaldehyde yield was 27 mol% (with a selectivity of 31%) on the redox catalyst alone, whereas the total yield for ($CO + CO_2$) measured 4 mol%.

The exit stream of the redox reactor (R_1) was then directly sent into the aldolization reactor (R_2) where further acrolein production was performed on the different aldolization catalysts prepared as described in the Experimental Section. The catalytic tests were performed in the 250–320 °C temperature range, and at GHSV = 10 000 or 5000 h^{-1}. The investigated conditions were chosen for each catalyst to maintain the ($CO + CO_2$) yield below 10 mol%, to identify the optimal working conditions. The main products detected in each catalytic test were acrolein, acetaldehyde, methanol, ethanol, CO, and CO_2. Traces of diethyl ether, propionaldehyde, acetone, acetic acid, acrylic acid, etc., were also present. The low carbon balance (in the 66–80 mol% range) is due to the lack of reliable quantification of formaldehyde (one of the main products of the reaction), to the production of unidentified polymers accumulating at the reactor exit,[13] and to the deposition of coke on the catalyst surface.[7]

No production of crotonaldehyde was observed, contrarily to what was reported by some other research groups observing crotonaldehyde as the product of self-aldolization of acetaldehyde (in their case in the absence of O_2 and added water).[15–22,25] However, as we already reported,[7] in oxidizing conditions only cross-condensation of acetaldehyde and formaldehyde takes place, whereas self-condensation to crotonaldehyde does not occur. In addition, when ethanol is oxidized on iron molybdate, either alone or in combination with an aldolization catalyst, no or very low crotonaldehyde production is observed, whereas the acetaldehyde yield is high. Together with acetaldehyde formation, water is also produced. It is also coproduced when methanol is oxidized to formaldehyde. The thermodynamics of the reactions of acrolein formation from acetaldehyde and formaldehyde and crotonaldehyde formation from acetaldehyde were examined. Figure 8 represents the equilibrium conversions as a function of temperature in both cases: acrolein or crotonaldehyde formation. Thermodynamic data were provided from ProSim software, which uses the enriched DIPPR database from the AIChE (American Institute of Chemical Engineers, see the Supporting Information). In the temperature range between 150 and 400 °C, crotonaldehyde formation is never favored compared to acrolein. Then, when the reaction proceeds from the alcohols, the partial pressure of water vapor is even higher owing to the alcohol oxidation to the aldehydes, which further inhibits the self-aldolization reaction.

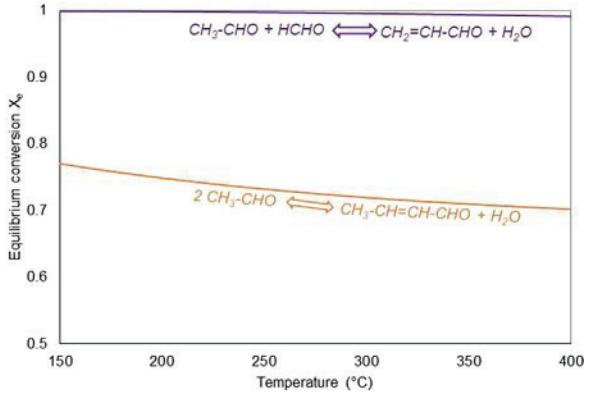

Figure 8. Acetaldehyde and formaldehyde equilibrium conversion as a function of temperature.

The main goal of the present research was to identify a catalyst (or a couple of catalysts) presenting both redox and acid/base properties that is able to perform the reaction in oxidizing conditions in a single reactor as explained by Dubois and co-workers.[6,7,12] The best results obtained on FeMo-like catalysts in terms of acrolein yield were performed at temperatures slightly higher than 300 °C, preferably between 300 and 325 °C. For this reason, the aldolization catalyst that will be chosen to boost the $FeMoO_x$ performances should function and remain stable at temperatures higher than 300 °C. Developing an industrial process using two consecutive reactors was also described as an alternative, more costly solution. In this case, the redox and the aldolization catalysts could operate at different temperatures.[6,7,12]

In the absence of oxygen, the aldolization reaction between acetaldehyde and formaldehyde is reported to be generally catalyzed by basic active sites of proper strength, but high overall basicity also promotes secondary reactions, which can lead to higher ($CO+CO_2$) yields. In addition, the presence of acid sites is also reported to be beneficial for acrolein selectivity.[13,15,19,21] Recently, the impact of the catalyst acid/base properties on the reaction carried out in the presence of oxygen has been studied on silica-supported basic oxides.[7] The presence of strong basic sites ($Q_{diff} > 150$ kJ mol^{-1}) was proved to be necessary to enhance the acrolein yield. Moreover, the paper reported that increasing the amount of basic sites seems to increase the carbon oxides production, and that a higher amount of relatively strong ($Q_{diff} > 100$ kJ mol^{-1}) acidic sites has a positive influence on enhancing the acrolein yield and to limit the production of ($CO+CO_2$). However, further investigations are still needed to identify the optimal strength and amount of basic sites for improved acrolein and reduced carbon oxides production at higher temperatures. It is, also, important to clarify the respective influence of only acidic or only basic sites on acrolein production and on ($CO+CO_2$) yield. This information will provide additional understanding of how the optimal aldolization catalyst should be designed. For this purpose, adsorption microcalorimetry is a very powerful and adapted tool, which allows us to determine the amount and the strength of the surface acidic or basic sites and therefore to correlate the acid/base surface properties to the catalytic activity.

For all catalysts (basic, amphoteric, and acidic) tested in the present work and in previous research,[7] acrolein production is enhanced at temperatures higher than 300 °C. Higher contact time (GHSV = 5000 h^{-1}) improves acrolein yield, too. On the other hand, increasing the temperature and contact time leads to higher production of carbon oxides. High temperature (in the presence of oxygen) leads to decomposition of the products (acrolein, acetaldehyde, formaldehyde). The decomposition to ($CO+CO_2$) becomes more important than acrolein production starting from 320 °C, therefore there is no interest to increase the process temperature as the acrolein produced gradually transforms to carbon oxides.[7] As a consequence, the optimal temperature for this reaction has been identified as being between 300 and 320 °C.[6,12]

The values of ethanol and methanol conversions remained close to those measured at the exit of the first reactor for all samples, even if tested at different temperatures and contact times. Acetaldehyde conversion increased with temperature and contact time.

Catalytic activity of acidic catalysts

The three acidic catalysts (HPW/SiO_2, $HSiW/SiO_2$, and NbP) displayed similar catalytic behavior and the catalytic tests performed on HPW/SiO_2 are reported in the Supporting Information (Figure S4) as examples. From Figure 9 it is possible to compare the strength distribution of acidic sites and the catalytic activities at 270 °C/5000 h^{-1} for the three acidic catalysts. As observed, a higher quantity of strong acidic sites ($Q_{diff} >$ 150 kJ mol^{-1}) does not improve the acrolein yield, but also does not significantly increase the ($CO+CO_2$) production.[7] Finally, it can be observed that a certain amount of acrolein is always produced on the relatively strong ($Q_{diff} > 100$ kJ mol^{-1}) acidic sites, but does not increase with the temperature. Acidic sites seem not to have any influence on the increased production of carbon oxides in this process.

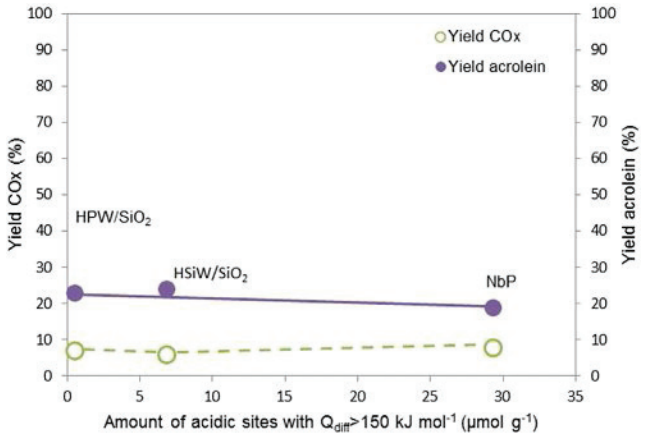

Figure 9. Correlation between acrolein and carbon oxides yield and the amount of strong ($Q_{diff} > 150$ kJ mol^{-1}) acidic sites for acidic catalysts (270 °C/5000 h^{-1}).

Catalytic activity of basic and amphoteric catalysts

Catalytic tests results for basic and amphoteric catalysts at different temperatures (T_2) and contact times (GHSV) are shown and fully discussed in the Supporting Information (Figures S5–10). In Figure 10 correlations between acrolein and ($CO+CO_2$) yields and the amount of strong basic sites are reported for the experiments performed at 300 °C/10 000 h^{-1}. This comparison allows us to observe how the presence of strong ($Q_{diff} >$ 150 kJ mol^{-1}) basic sites influence the acrolein and ($CO+CO_2$) production for basic and amphoteric catalysts. As already explained, the amphoteric catalysts tested in this work present high basicity and a generally dominant basic character (Table 2, Figures 4–6) thus resulting in very high amounts of

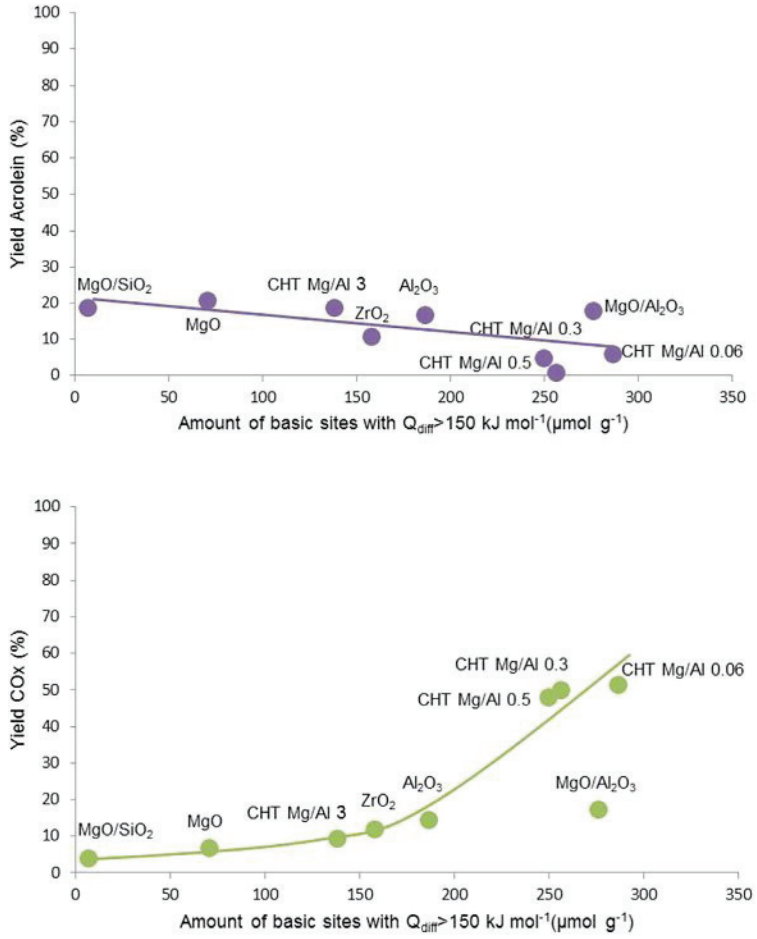

Figure 10. Correlations between acrolein and carbon oxides yield (300 °C/10 000 h^{-1}) and the amount of strong (Q_{diff} > 150 kJ mol^{-1}) basic sites for basic and amphoteric catalysts.

($CO + CO_2$) produced. The basic features of the CHT samples decrease with Mg/Al ratio (Table 2). It was previously reported that high basicity generally is necessary to give increased production of acrolein, but can cause a rise of the side reactions resulting in increased carbon oxides production. As observed from the catalytic tests, for some catalysts an enormous amount of ($CO + CO_2$) was produced. Clearly, the increase of CO_x production (around 50 mol%) on CHT catalysts is connected with the increase of the amount of strong basic sites (Q_{diff} > 150 kJ mol^{-1}). Indeed, the CHT Mg/Al 3 catalyst (which showed the lowest amount of strong basic sites) presents the lowest yield of carbon oxides (9.5 mol%), and the highest yield of acrolein (19 mol%). The amount of strong basic sites is much higher for the other CHT samples, thus leading to a very high ($CO + CO_2$) yield (around 50%). Even if MgO/Al_2O_3 possesses a very similar amount of strong basic sites like Al-rich CHT Mg/Al catalysts, its catalytic performance at 300 °C/10 000 h^{-1} is completely different. The MgO/Al_2O_3 catalyst presents a significantly lower carbon oxides yield (17.5%) and consequently higher acrolein production (18%) than CHT Mg/Al oxides. This different behavior can be connected to the higher amount of strong acidic sites on MgO/Al_2O_3 and is in agreement with our previous research.[7] The MgO catalyst, which presents the lowest amount of strong basic sites (below 100 µmol g^{-1}), displays, also, the lowest carbon oxides production. These results prove that the high quantity of basic sites increases ($CO + CO_2$) production. Comparison of the acid/base properties of the catalysts and their performance in optimal conditions (carbon oxides yield below 10%) confirms that MgO is the best performing sample (acrolein yield of 28% at 270 °C and 300 °C), thanks to its proper quantity of strong basic sites.

The catalytic performances of the basic and amphoteric catalysts depend on the amount of strong basic sites (Q_{diff} > 150 kJ mol^{-1}). To have a good acrolein yield and a minimal carbon oxides production, it is crucial that the amount of strong basic sites remains lower than 100 µmol g^{-1}. Additional presence of strong acidic sites in sufficient amount positively influences the catalytic activity by decreasing the carbon oxides production.

Once tested, the various aldolization catalysts presenting a wide range of acidic and basic properties, MgO-containing materials were identified to be the most promising aldolization catalysts for this process.[7] The acid/base properties of MgO/SiO_2, MgO, and MgO/Al_2O_3 catalysts are compared in Figure 11. MgO is a completely basic catalyst, whereas MgO/SiO_2 and MgO/Al_2O_3 are amphoteric catalysts. MgO/SiO_2 is characterized by a similar amount of basic and acidic sites with a slightly dominant acidic character.[7] On the other hand, the MgO/Al_2O_3 catalyst has a much higher number of acidic and especially strong basic sites compared with MgO/SiO_2 and displays a dominant basic character.

Owing to its high basicity, even at 300 °C, MgO/Al_2O_3 produced remarkably higher amounts of carbon oxides compared with MgO and MgO/SiO_2 (Table 4). At 320 °C, only MgO/SiO_2 presented good catalytic activity, yielding 35 mol% of acrolein and CO_x in 10 mol%. Comparing the catalytic per-

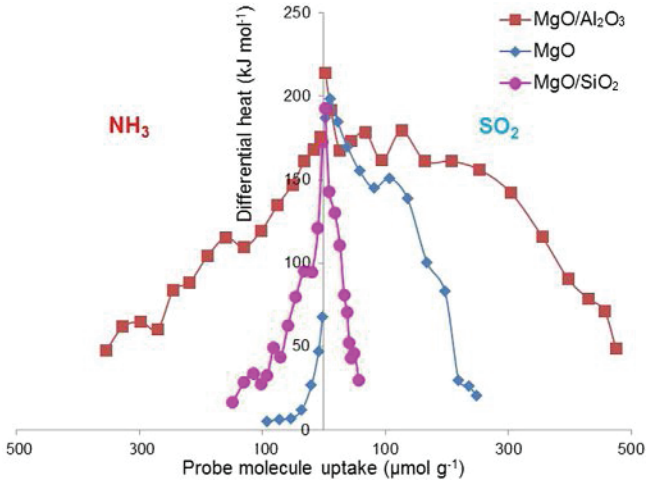

Figure 11. Differential heats of NH_3 and SO_2 adsorption versus coverage for MgO/SiO_2, MgO, and MgO/Al_2O_3 samples.

Table 4. Comparison of catalytic tests results by using a methanol and ethanol mixture (feed: (MeOH + EtOH)/O_2/N_2 = (4 + 2):8:86 mol%) on $FeMoO_x$ (R_1) + MgO/SiO_2, MgO, and MgO/Al_2O_3 (R_2) catalysts. Optimal conditions = carbon oxides yield below 10 mol%.

Conditions: T [°C]/GHSV [h^{-1}]	300 °C/10 000 h^{-1}		320 °C/5000 h^{-1}		Optimal conditions
Yield [mol%]	acrolein	CO_x	acrolein	CO_x	acrolein
MgO/SiO_2[7]	19	4	35	10	35
MgO	21	7	22	17	28
MgO/Al_2O_3	18	17.5	17	36	22

formances of these three Mg-containing catalysts, MgO supported on silica is the best aldolization catalyst to be used in a single reactor process together with the $FeMoO_x$ redox catalyst. Pure MgO could be considered as well as a good choice, whereas MgO/Al_2O_3 appears not to be suitable for this purpose.

These results confirm that CO_x production increases with the amount of strong basic sites and that additional presence of strong acidic sites has a positive influence to limit ($CO + CO_2$) production. Strong basic sites should be present in an amount lower than 100 μmol g^{-1} to avoid the over-oxidation impact caused by a too high basicity. If the amount of basic and acidic sites is similar, the acrolein yield is higher and carbon oxides production limited. In addition, the acrolein yield decreases when the catalyst presents a strong basic character.

Figure 12 gives evidence of the relationship that exists between the strong acid/base properties of samples and their yield of CO_x. The more basic the catalysts, the more carbon oxides produced, which confirms that the presence of a too high amount of basic sites is detrimental to acrolein production. The amount of carbon deposited on the surface (as verified by TG-DTA-MS) after 48 h of reaction is about 8 wt% for samples CHT Mg/Al and MgO/Al_2O_3 whereas only 4.3 wt% for MgO and 2.3 wt% for HPW/SiO_2, thus confirming again the negative effect of a high basicity.

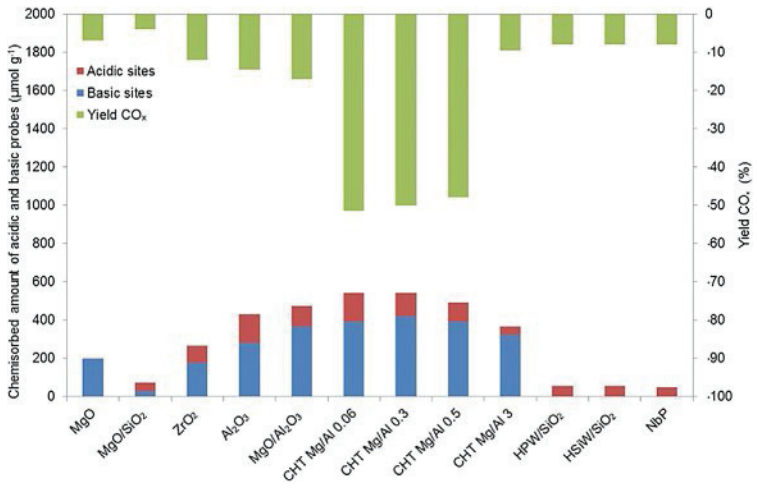

Figure 12. Correlation between acid/base properties of catalysts as determined by adsorption calorimetry and CO_x yield (300 °C, GHSV = 10 000 h^{-1}).

Conclusions

Characterization of the aldolization catalysts by NH_3, SO_2, and methanol adsorption calorimetry provided the amount, strength, and strength distribution of acid and base sites on the catalysts surfaces.

It was found that aldol-condensation of acetaldehyde and formaldehyde to acrolein in the presence of oxygen takes place on both basic and acidic sites. On strong basic sites, acrolein production increases with temperature, but at the same time, a high amount of strong basic sites leads to higher production of carbon oxides. On strong acidic sites, the production of acrolein and ($CO + CO_2$) does not increase by increasing the temperature and the amount of acidic sites. Coexistence of strong basic and strong acidic sites in similar amounts (preferably with a strong basic sites to strong acidic sites ratio close to 1) seems to be the best surface configuration for maximizing the acrolein production, in oxidizing reaction conditions. On amphoteric catalysts with a sufficient amount of strong acidic sites, acrolein production is enhanced and carbon oxides production is limited, thus allowing the catalyst to work at higher temperatures.

Among the MgO-based catalysts, MgO/SiO_2 is confirmed to be the best catalyst, followed by MgO. Both present the proper amount of strong basic sites, < 100 μmol g^{-1}. The catalytic performance of magnesia is improved when deposited on a silica support,[7] thanks to the creation of new acidic sites, in addition to the basicity originating from magnesia. Finally, magnesium oxide supported on alumina showed lower catalytic activity than pure magnesia and silica-supported magnesia, because the amount of strong basic sites was much higher than that of strong acidic sites, thus strongly enhancing carbon oxides production.

Experimental Section

Catalyst preparation

CHT (calcined hydrotalcites) samples with various Mg/Al molar ratios were obtained from the calcination of different commercial hydrotalcite-like fresh Pural catalysts (Sasol). CHT Mg/Al0.06 catalyst was obtained by calcining commercial fresh catalyst Pural MG 5 (4.3 wt% MgO and 95.7 wt% Al_2O_3) in air atmosphere at 550 °C for 8 h. Pural MG 20 (18.7 wt% MgO and 81.3 wt% Al_2O_3) was calcined in the same conditions to give CHT Mg/Al0.3 catalyst. CHT Mg/Al0.5 and CHT Mg/Al3 catalysts were obtained from commercial fresh catalyst Pural MG 30 (28.8 wt% MgO and 71.2 wt% Al_2O_3) and Pural MG 70 (68.8 wt% MgO and 31.7 wt% Al_2O_3), respectively. To prepare the MgO/Al_2O_3 (Mg/Al = 1:10 mol) sample, commercial Al_2O_3 (Saint-Gobain NorPro) was impregnated with $Mg(NO_3)_2 \cdot 6H_2O$ (Sigma–Aldrich) in aqueous solution. The obtained wet powder was then dried in a rotavapor and calcined under air-flow at 550 °C for 8 h. MgO (Sigma–Aldrich) was calcined at 550 °C in air-flow for 8 h, whereas Al_2O_3 (Saint-Gobain NorPro) was calcined for 6 h under air at 550 °C. NbP (CBMM) was calcined in air atmosphere (450 °C) for 6 h. ZrO_2 (Saint-Gobain

NorPro, 4.3 wt% SiO_2, 17 wt% HfO_2) has been used in this study. HPW/SiO_2 (10 wt%) and $HSiW/SiO_2$ (10 wt%) catalysts were prepared by the wet impregnation method. Aqueous solutions of heteropolyacids (Sigma–Aldrich) were mixed with silica obtained by evaporating a colloidal solution Ludox TMA (Sigma–Aldrich) and the mixture was further evaporated in a rotary evaporator for 3 h (50 °C, 1 mbar). The dried powders were calcined at 350 °C in air atmosphere for 4 h and labeled: HPW/SiO_2 and $HSiW/SiO_2$. The calcination temperature was chosen to preserve the Keggin structure of the heteropolyacids.

Catalyst characterization

XRD patterns were recorded by using CuK_α radiation (0.154 nm) at room temperature with a Bruker D8 Advance A25 diffractometer from 4° to 80° 2θ in 0.02° steps with 0.5 s per step. Specific surface areas were determined by nitrogen adsorption at −196 °C with a Micromeritics ASAP 2020 apparatus. The samples were pre-treated for 3 h at 200 (HPAs supported on silica) or 300 °C (other samples) under vacuum, prior to nitrogen adsorption. The BET method was used to determine specific surface areas (S_{BET}). Simultaneous thermogravimetric and differential thermal analyses (TG-DTA) of the samples were conducted with a SETARAM SETSYS Evolution 12 thermoanalyzer coupled via a heated (ca. 150 °C) capillary with a Pfeiffer OmniStar quadrupole mass spectrometer (MS). For TG-DTA-MS studies, samples (40–50 mg located in Pt-based open crucibles) were heated from room temperature to 750 °C at a constant rate of 5 °C min^{-1} under a flowing gas (50 $cm^3 min^{-1}$ STP) of air. Chemical analyses were performed by using inductively coupled plasma optical emission spectroscopy (ICP-OES) with an ACTIVA spectrometer from Horiba JOBIN YVON. Prior to analysis, the samples were dissolved in a mixture of inorganic acids H_2SO_4, HNO_3, and HF. The amount of carbon and nitrogen was determined after measuring the thermal conductivity of the catalysts. ^{27}Al MAS NMR experiments were performed by accumulating 8192 scans with a Bruker Avance III 500WB spectrometer at a resonance frequency of 130.29 MHz with an excitation of $\pi/12$ pulses and a repetition time of 1 s. A commercial 4 mm double H/X probe was used to perform the MAS experiments with a spinning rate of 12 kHz. The reference for the chemical shifts was an aqueous 1 M $Al(NO_3)_3$ solution. The acid/base properties of the catalysts were studied by adsorption microcalorimetry of NH_3, SO_2, and methanol. The technique and the applied experimental conditions were the same as previously described in Ref. [7].

Catalytic tests

Acrolein production was carried out in a two consecutive reactors system; the first reactor (R_1) was filled with the redox $FeMoO_x$ catalyst, whereas the second (R_2) was filled with the aldolization (acid/base) catalyst. The catalytic test set-up, consisting of two stainless-steel continuous-flow reactors placed in series and working close to atmospheric pressure, was previously described, as well as the equations applied for conversions, yields, and selectivities calculations.[7] The reaction conditions in the first reactor were optimized to get the highest acetaldehyde and formaldehyde yields. The final chosen conditions were the following: $MeOH/EtOH/O_2/N_2$ molar ratio of 4:2:8:86, GHSV = 10 000 h^{-1}, reaction temperature (T_1) of 260 °C. GHSV was calculated as the total flow rate divided by the catalyst volume. In the second reactor (R_2), the aldolization catalysts (20 g) were tested at temperature (T_2) between 250 °C and 320 °C and the gas hourly space velocity (GHSV) between 10 000 and 5000 h^{-1} by adjusting the feeding flow rate. All catalysts were sieved and only the particles in the 100–500 μm diameter range were selected for catalytic tests. The maximum reaction temperature was different for each catalyst and chosen to keep the ($CO + CO_2$) yield below 10 mol%. Above this threshold, the reaction becomes highly exothermic. Comparison of the catalysts was done at conversions lower than 100%.

Acknowledgments

This work was supported by the French Environment and Energy Management Agency (ADEME) within the framework of the "Investissements d'Avenir" program ("Investment for the Future"). The authors acknowledge the scientific services of IRCELYON. Special acknowledgment goes to Carole Mutschler and Prof. Pascal Fongarland from the Laboratoire de Génie des Procédés Catalytiques (LGPC, Lyon, France) for their precious help with the thermodynamic calculations.

Conflict of interest

The authors declare no conflict of interest.

Keywords: acidity · alcohols · aldol reaction · basicity · calorimetry

[1] L. Liu, X. P. Ye, J. J. Bozell, *ChemSusChem* **2012**, *5*, 1162 – 1180.
[2] *Acrolein and Methacrolein*, D. Arntz, A. Fischer, M. Höpp, S. Jacobi, J. Sauer, T. Ohara, T. Sato, N. Shimizu, H. Schwind in *Ullmann's Encyclopedia of Industrial Chemistry*, Wiley-VCH, Weinheim, **2012**.
[3] a) S. Mourey, *Info Chim. Mag.* **1999**, *412*, 90 – 96; b) http://www.industrie.com/chimie/.
[4] H. Schulz, H. Wagner, *Angew. Chem.* **1950**, *62*, 105 – 118.
[5] L. Dubois (Arkema France, Colombes), WO2011083225A1, **2011**.
[6] L. Dubois, M. Capron, F. Dumeignil (Arkema France, Colombes), WO2014/068213A9, **2014**.
[7] A. Lilić, S. Bennici, J. F. Devaux, J. L. Dubois, A. Auroux, *ChemSusChem* **2017**, *10*, 1916 – 1930.
[8] T. H. Kang, J. H. Choi, Y. Bang, J. Yoo, J. H. Song, W. Joe, J. S. Choi, I. K. Song, *J. Mol. Catal. A* **2015**, *396*, 282 – 289.
[9] D. Stošić, S. Bennici, J. L. Couturier, J. L. Dubois, A. Auroux, *Catal. Commun.* **2012**, *17*, 23 – 28.
[10] M. Dalil, M. Edake, C. Sudeau, J. L. Dubois, G. S. Patience, *Appl. Catal. A* **2016**, *522*, 80 – 89.
[11] J. Deleplanque, J. L. Dubois, J. F. Devaux, W. Ueda, *Catal. Today* **2010**, *157*, 351 – 358.
[12] A. Borowiec, J. F. Devaux, J. L. Dubois, L. Jouenne, M. Bigan, P. Simon, M. Trentesaux, J. Faye, M. Capron, F. Y. Dumeignil, *Green Chemistry* **2017**, *19*, 2666 – 2674.
[13] M. Ai, *Bull. Chem. Soc. Jpn.* **1991**, *64*, 1342 – 1345.
[14] M. Ai, *Bull. Chem. Soc. Jpn.* **1991**, *64*, 1346 – 1350.
[15] E. Dumitriu, V. Hulea, C. Chelaru, C. Catrinescu, D. Tichit, R. Durand, *Appl. Catal. A* **1999**, *178*, 145 – 157.
[16] E. Dumitriu, V. Hulea, I. Fechete, A. Auroux, J. F. Lacaze, C. Guimon, *Microporous Mesoporous Mater.* **2001**, *43*, 341 – 359.
[17] C. Cobzaru, S. Oprea, E. Dumitriu, V. Hulea, *Appl. Catal. A* **2008**, *351*, 253 – 258.
[18] A. Ungureanu, S. Royer, T. V. Hoang, D. Trong On, E. Dumitriu, S. Kaliaguine, *Microporous Mesoporous Mater.* **2005**, *84*, 283 – 296.
[19] E. Dumitriu, V. Hulea, N. Bilba, G. Carja, A. Azzouz, *J. Mol. Catal.* **1993**, *79*, 175 – 185.
[20] A. Azzouz, D. Messad, D. Nistor, C. Catrinescu, A. Zvolinschi, S. Asaftei, *Appl. Catal. A* **2003**, *241*, 1 – 13.
[21] E. Dumitriu, N. Bilba, M. Lupascu, A. Azzouz, V. Hulea, G. Cirje, D. Nibou, *J. Catal.* **1994**, *147*, 133 – 139.

[22] E. Dumitriu, C. Cobzaru, V. Hulea, S. Oprea, *Rev. Chim.* **2010**, *61*, 400 – 403.
[23] W. J. Palion, S. Malinowski, *React. Kinet. Catal. Lett.* **1974**, *1*, 461 – 465.
[24] S. Malinowski, S. Basinski, *J. Catal.* **1963**, *2*, 203 – 207.
[25] V. Hulea, D. Tichit, C. Catrinescu, E. Dumitriu, *An. Stiint. Univ. "Al. I. Cuza" Iasi Chim.* **1997**, *5*, 185 – 192.
[26] F. Cavani, F. Trifiro, A. Vaccari, *Catal. Today* **1991**, *11*, 173 – 301.
[27] R. Salomão, M. O. C. Villas Bôas, V. C. Pandolfelli, *Ceram. Int.* **2011**, *37*, 1393 – 1399.
[28] J. Shen, J. M. Kobe, Y. Chen, J. A. Dumesic, *Langmuir* **1994**, *10*, 3902 – 3908.
[29] H. A. Prescott, Z. J. Li, E. Kemnitz, A. Trunschke, J. Deutsch, H. Lieske, A. Auroux, *J. Catal.* **2005**, *234*, 119 – 130.
[30] J. Shen, M. Tu, C. Hu, *J. Solid State Chem.* **1998**, *137*, 295 – 301.
[31] S. Casenave, H. Martinez, C. Guimon, A. Auroux, V. Hulea, A. Cordoneau, E. Dumitriu, *Thermochim. Acta* **2001**, *379*, 85 – 93.
[32] M. Tu, J. Shen, Y. Chen, *Thermochim. Acta* **1997**, *302*, 117 – 124.
[33] L. Dussault, J. C. Dupin, E. Dumitriu, A. Auroux, C. Guimon, *Thermochim. Acta* **2005**, *434*, 93 – 99.
[34] A. Auroux, J. C. Védrine in *Catalysis by Acids and Bases* (Eds.: B. Imelik, C. Naccache, G. Coudurier, Y. B. Taarit, J. C. Védrine), Elsevier, Amsterdam, **1985**, pp. 311 – 318.
[35] H. Petitjean, K. Tarasov, F. Delbecq, P. Sautet, J. M. Krafft, P. Bazin, M. C. Paganini, E. Giamello, M. Che, H. Lauron-Pernot, G. Costentin, *J. Phys. Chem. C* **2010**, *114*, 3008 – 3016.
[36] I. Kozhevnikov, *Chem. Rev.* **1998**, *98*, 171 – 198.
[37] Q. Sun, A. Auroux, J. Shen, *J. Catal.* **2006**, *244*, 1 – 9.
[38] M. León, L. Faba, E. Díaz, S. Bennici, A. Vega, S. Ordónez, A. Auroux, *Appl. Catal. B* **2014**, *147*, 590 – 599.
[39] M. Bensitel, O. Saur, J. C. Lavalley, *Mater. Chem. Phys.* **1991**, *28*, 309 – 320.
[40] C. Pighini, T. Belin, J. Mijoin, P. Magnoux, G. Costentin, H. Lauron-Pernot, *Appl. Surf. Sci.* **2011**, *257*, 6952 – 6962.
[41] J. K. Bartley, C. Xu, R. Lloyd, D. I. Enache, D. W. Knight, G. J. Hutchings, *Appl. Catal. B* **2012**, *128*, 31 – 38.
[42] V. V. Chesnokov, A. F. Bedilo, D. S. Heroux, I. V. Mishakov, K. J. Klabunde, *J. Catal.* **2003**, *218*, 438 – 446.
[43] V. K. Díez, C. R. Apesteguia, J. I. Di Cosimo, *J. Catal.* **2003**, *215*, 220 – 233.
[44] A. L. McKenzie, C. T. Fishel, R. J. Davis, *J. Catal.* **1992**, *138*, 547 – 561.
[45] W. T. Reichle, S. Y. Kang, D. S. Everhardt, *J. Catal.* **1986**, *101*, 352 – 359.
[46] A. Corma, V. Fornés, F. Rey, *J. Catal.* **1994**, *148*, 205 – 212.
[47] R. L. Millard, R. C. Peterson, B. K. Hunter, *Am. Mineral.* **1992**, *77*, 44 – 52.
[48] B. J. Wood, R. J. Kirkpatrick, B. Montez, *Am. Mineral.* **1986**, *71*, 999 – 1006.
[49] F. Hosoglu, PhD Thesis (defended 30/10/2012), University Lille , France, **2012**.
[50] A. Auroux, A. Gervasini, *J. Phys. Chem.* **1990**, *94*, 6371 – 6379.
[51] *Calorimetry and Thermal Methods in Catalysis* (Ed.: A. Auroux), Springer, Heidelberg, **2013**.
[52] C. Guimon, A. Gervasini, A. Auroux, *J. Phys. Chem. B* **2001**, *105*, 10316 – 10325.
[53] F. X. Liu-Cai, B. Sahut, E. Fayadi, A. Auroux, G. Hervé, *Appl. Catal. A* **1999**, *185*, 75 – 83.
[54] L. Damjanović, V. Rakić, U. B. Mioč, A. Auroux, *Thermochim. Acta* **2005**, *434*, 81 – 87.
[55] A. Gervasini, G. Bellussi, J. Fenyvesi, A. Auroux in *New Frontiers in Catalysis* (Eds.: L. Guczi, F. Solymosi, P. Tétényi), Elsevier, Amsterdam, **1993**.
[56] D. Stošić, F. Hosoglu, S. Bennici, A. Travert, M. Capron, F. Dumeignil, J. L. Couturier, J. L. Dubois, A. Auroux, *Catal. Commun.* **2017**, *89*, 14 – 18.
[57] A. Auroux, *Top. Catal.* **1997**, *4*, 71 – 89.
[58] G. Busca, P. F. Rossi, V. Lorenzelli, M. Benaissa, J. Travert, J. C. Lavalley, *J. Phys. Chem.* **1985**, *89*, 5433 – 5439.
[59] V. Bolis, C. Busco, V. Aina, C. Morterra, P. Ugliengo, *J. Phys. Chem. C* **2008**, *112*, 16879 – 16892.
[60] M. Benaïssa, O. Saur, J. C. Lavalley, *Mater. Chem.* **1982**, *7*, 699 – 714.

Manuscript received: June 12, 2017
Revised manuscript received: July 4, 2017
Accepted manuscript online: July 7, 2017
Version of record online: August 17, 2017

Supporting Information

A comparative study of basic, amphoteric and acidic catalysts in the oxidative coupling of methanol and ethanol for acrolein production

Aleksandra Lilić,[a] Tiantian Wei,[a] Simona Bennici,[a,]† Jean-François Devaux,[b] Jean-Luc Dubois,[c] Aline Auroux[a,]†

Thermodynamic calculations

The thermodynamics of the reactions of acrolein formation from acetaldehyde and formaldehyde, and crotonaldehyde formation from acetaldehyde was examined, and the results representing the equilibrium conversions as a function of temperature for acrolein or crotonaldehyde formation are shown in Figure 8. This study was performed with help of the *Laboratoire de Génie des Procédés Catalytiques* (*LGPC*, Lyon, France). Thermodynamic data (Tables S1 and S3) were provided from ProSim software which uses enriched DIPPR database from AIChE-American Institute of Chemical Engineers.[a,b]

Thermodynamic calculations for cross-condensation of acetaldehyde and formaldehyde in gas-phase.

$$CH_3CHO\ (g) + HCHO\ (g) \longleftrightarrow CH_2{=}CH{-}CHO\ (g) + H_2O\ (g)$$

Table S1. Thermodynamic data (ideal gas state) at 25 °C under a pressure of 1 bar for the cross-condensation reactants and products in the gas phase (data from ProSim software). Heat capacity (Cp) is calculated using the following formula: $Cp=A+BT+CT^2+DT^3+ET^4$, where A, B, C, D, and E are substance-dependent constants and T is absolute temperature.

Compound	$\Delta H_f°_{IG}$ (kJ mol^{-1})	$S°_{IG}$ (J K mol^{-1})	A (J mol K-1)	B (J mol K-1)	C (J mol K^{-1})	D (J mol K^{-1})	E (J mol K^{-1})	Cp (J mol K^{-1})
Acetaldehyde	-166.4	264.2	32660.6	51.99	0.13	-1.44E-04	4.20E-08	56284.38
Formaldehyde	-108.6	218.7	34704.3	-32.93	1.60E-01	-1.36E-04	3.66E-08	35784.34
Acrolein	-81.8	297	30811.4	92.73	0.21	-2.87E-04	9.64E-08	70153.82
Water	-241.8	188.7	33693.5	-6.07	2.38E-02	-1.21E-05	1.97E-09	33695.30

For T=298.15 K, $\Delta H_R°$ *(g)*=-48.61 kJ mol^{-1}, and $\Delta S°$ *(g)*=2.86 J K mol^{-1}.

The Gibbs free energy change is equal to:

$$\Delta G = \Delta G° - RT \ln(K) \quad \text{(S1)}$$

Where R is the gas constant equal to 8.314 J (mol·K)$^{-1}$ and K is the equilibrium constant.

At the equilibrium, in the case of isothermal and isobaric transformations, the Gibbs free energy change is equal to 0 ($\Delta G=0$), therefore the equation S1 can be expressed as:

$$\Delta G° = RT \ln(K) \quad \text{(S2)}$$

It is possible to determine acetaldehyde and formaldehyde equilibrium conversion (acrolein formation by cross-condensation reaction) as a function of temperature using equations S1 and S3-S5, and thermodynamic data from Table S1. Results are shown in Figure 8 (violet curve) and Table S2.

$$\Delta G = \Delta H_T - T\Delta S_T \quad \text{(S3)}$$

$$\Delta H_T = \Delta H° + \int_{298}^{T} \Delta Cp dT \quad \text{(S4)}$$

$$\Delta S_T = \Delta S° + \ln\left(\frac{T}{298}\right) \int_{298}^{T} \Delta Cp dT \quad \text{(S5)}$$

Table S2. ΔH_T, ΔS_T, ΔG, K, and X_e (acetaldehyde and formaldehyde equilibrium conversion) calculated as a function of temperature using thermodynamic data from Table S1 and Equations S1-S5.

T (°C)	T (K)	ΔH_T (kJ mol^{-1})	ΔS_T (J K mol^{-1})	ΔG (kJ mol^{-1})	K	X_e
150	423.15	-46.95	7.50	-50.12	1539886.75	0.9992
160	433.15	-46.80	7.85	-50.20	1132131.79	0.9991
170	443.15	-46.65	8.18	-50.28	844761.54	0.9989
180	453.15	-46.50	8.51	-50.36	639100.34	0.9987
190	463.15	-46.35	8.84	-50.45	489787.52	0.9986
200	473.15	-46.20	9.16	-50.54	379917.59	0.9984
210	483.15	-46.05	9.48	-50.63	298045.91	0.9982
220	493.15	-45.90	9.79	-50.73	236311.53	0.9975
230	503.15	-45.75	10.10	-50.83	189240.75	0.9977
240	513.15	-45.59	10.40	-50.93	152972.80	0.9974
250	523.15	-45.44	10.70	-51.04	124751.31	0.9972
260	533.15	-45.29	10.99	-51.15	102585.69	0.9969
270	543.15	-45.13	11.28	-51.26	85022.70	0.9966
280	553.15	-44.98	11.56	-51.37	70990.42	0.9963
290	563.15	-44.82	11.83	-51.49	59690.52	0.9959
300	573.15	-44.67	12.11	-51.61	50522.84	0.9956
310	583.15	-44.52	12.37	-51.73	43032.28	0.9952
320	593.15	-44.36	12.63	-51.86	36870.83	0.9948
330	603.15	-44.21	12.89	-51.98	31770.24	0.9944
340	613.15	-44.06	13.14	-52.11	27522.18	0.9940
350	623.15	-43.91	13.38	-52.25	23963.70	0.9936
360	633.15	-43.75	13.62	-52.38	20966.43	0.9931
370	643.15	-43.60	13.86	-52.52	18428.62	0.9927
380	653.15	-43.46	14.09	-52.66	16269.08	0.9922
390	663.15	-43.31	14.31	-52.80	14422.64	0.9917
400	673.15	-43.16	14.53	-52.94	12836.71	0.9913

Thermodynamic calculations for self-condensation of acetaldehyde in gas-phase.

$$2CH_3CHO\ (g) \longleftrightarrow \tfrac{1}{2}\ cis\text{-}CH_3CH{=}CH\text{-}CHO\ (g) + \tfrac{1}{2}\ trans\text{-}CH_3CH{=}CH\text{-}CHO\ (g) + H_2O\ (g)$$

Table S3. Thermodynamic data (ideal gas state) at 25 °C under a pressure of 1 bar for the self-condensation reactants and products in the gas phase (data from ProSim software). Heat capacity (Cp) is calculated using the following formula: $Cp=A+BT+CT^2+DT^3+ET^4$, where A, B, C, D, and E are substance-dependent constants and T is absolute temperature.

Compound	$\Delta H_f°_{IG}$ (kJ mol^{-1})	$S°_{IG}$ (J K mol^{-1})	A (J mol K^{-1})	B (J mol K^{-1})	C (J mol K^{-1})	D (J mol K^{-1})	E (J mol K^{-1})	Cp (J mol K^{-1})
Acetaldehyde	-166.4	264.2	32660.6	51.99	0.13	-1.44E-04	4.20E-08	56284.38
***cis*-Crotonaldehyde**	-100.6	317.3	25093.4	261.40	-8.93E-02	-2.14E-05	1.44E-08	94602.64
***trans*-Crotonaldehyde**	-101.9	317.3	28631.6	244.75	-0.07	-3.23E-05	1.56E-08	94940.07
Water	-241.8	188.7	33693.5	-6.07	2.38E-02	-1.21E-05	1.97E-09	33695.30

For T=298.15 K, $\Delta H_R°$ *(g)=-10.284* kJ mol^{-1}, and $\Delta S°$ *(g)*=-22.376 J K mol^{-1}.

Acetaldehyde equilibrium conversion (crotonaldehyde formation by self-condensation reaction) was calculated as a function of temperature using equations S1 and S3-S5, and thermodynamic data from Table S3. Results are shown in Figure 8 (orange curve) and Table S4.

Table S4. ΔH_T, ΔS_T, ΔG, K, and X_e (acetaldehyde equilibrium conversion) calculated as a function of temperature using thermodynamic data from Table S3 and Equations S1-S5.

T (°C)	T (K)	ΔH_T (kJ mol^{-1})	ΔS_T (J K mol^{-1})	ΔG (kJ mol^{-1})	K	X_e
150	423.15	-8.25	-16.69	-1.19	1.40	1.4030
160	433.15	-8.09	-16.32	-1.03	1.33	1.3297
170	443.15	-7.93	-15.95	-0.86	1.26	1.2646
180	453.15	-7.78	-15.60	-0.71	1.21	1.2065
190	463.15	-7.62	-15.26	-0.55	1.15	1.1544
200	473.15	-7.47	-14.93	-0.40	1.11	1.1076
210	483.15	-7.31	-14.61	-0.25	1.07	1.0653
220	493.15	-7.16	-14.30	-0.11	1.03	1.0271
230	503.15	-7.01	-14.00	0.03	0.99	0.9924
240	513.15	-6.86	-13.71	0.17	0.96	0.9608
250	523.15	-6.72	-13.43	0.31	0.93	0.9320
260	533.15	-6.57	-13.16	0.44	0.91	0.9057
270	543.15	-6.43	-12.89	0.57	0.88	0.8816
280	553.15	-6.29	-12.64	0.70	0.86	0.8594
290	563.15	-6.16	-12.39	0.82	0.84	0.8390
300	573.15	-6.02	-12.16	0.94	0.82	0.8201
310	583.15	-5.89	-11.93	1.06	0.80	0.8027
320	593.15	-5.76	-11.71	1.18	0.79	0.7866
330	603.15	-5.63	-11.49	1.30	0.77	0.7717
340	613.15	-5.51	-11.29	1.41	0.76	0.7579
350	623.15	-5.38	-11.09	1.53	0.74	0.7450
360	633.15	-5.26	-10.89	1.64	0.73	0.7330
370	643.15	-5.14	-10.71	1.74	0.72	0.7218
380	653.15	-5.03	-10.53	1.85	0.71	0.7114
390	663.15	-4.96	-10.36	1.95	0.70	0.7016
400	673.15	-4.80	-10.19	2.06	0.69	0.6925

Physico-chemical properties

In Figures S1a and S1b, the XRD patterns of the silica-supported heteropolyacids (HPA/SiO_2) are reported and compared with bulk heteropolyacids and bare silica support. Several low intensity peaks, corresponding to the heteropolyacid crystal phase, are still present in the XRD pattern of calcined HPW/SiO_2 (Figure S1a), while in the pattern of $HSiW/SiO_2$ catalyst (Figure S1b) only a wide low intensity peak around 8° can be observed. In both samples, the amorphous phase of the silica support is present. The XRD pattern of NbP catalyst is typical of an amorphous solid and is characterized by two broad 2θ peaks at around 25° a nd 52°, as already observed by Sun et al.[c]

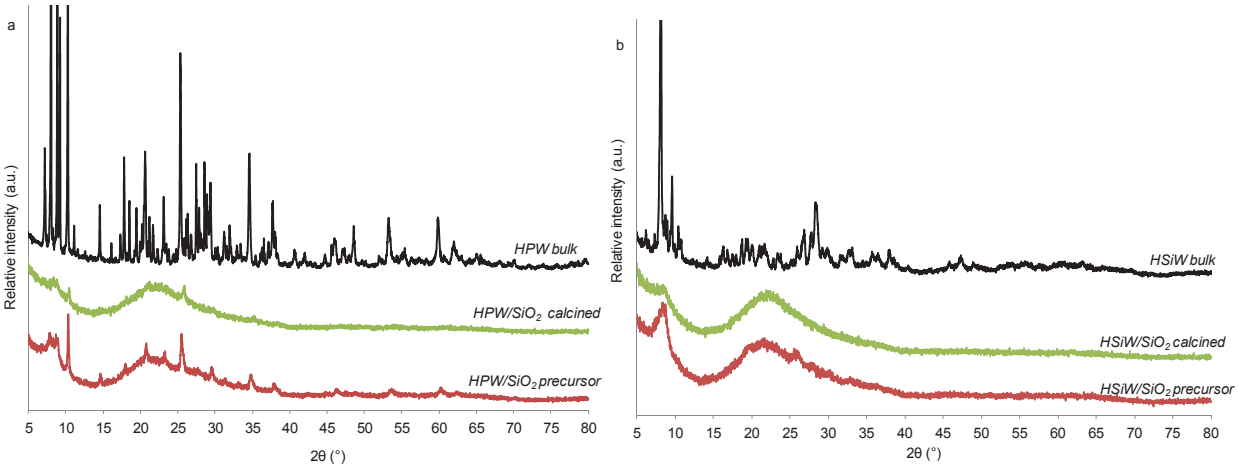

Figure S1. XRD patterns of silica-supported tungstophosphoric acid- HPW/SiO_2 (a), and silica-supported tungstosilicic acid- $HSiW/SiO_2$ (b).

Mg-Al mixed oxides (Figure 1) derived from calcination of commercial hydrotalcite-like materials (HT) lost their hydrotalcite and boehmite structure (Figure S2). Figure S2, reports the XRD patterns of non-calcined hydrotalcites (HTs). The characteristic hydrotalcite structure is dominant in the pattern of HT Mg/Al 3 (precursor of CHT Mg/Al 3 catalyst); also presence of few peaks of low intensities attributed to boehmite (AlO(OH)) was observed. HT Mg/Al 0.3 and 0.5, are characterized by peaks of both hydrotalcite (peaks of lower intensities than for Mg/Al 3) and boehmite (AlO(OH)) structure, while the precursor of sample CHT Mg/Al 0.06 (HT Mg/Al 0.06) displays only peaks attributed to alumina phase (boehmite).

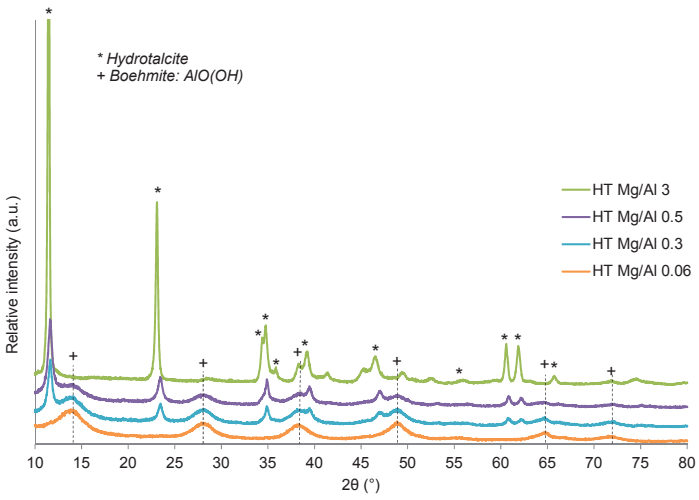

Figure S2. XRD patterns of fresh hydrotalcites (HTs).

Figure S3 presents TG-DTA curves of the four hydrotalcite precursors (HT). By mass spectrometer connected to the TG-DTA apparatus only fragments associated to the loss of water and OH^- groups (m/z=17 and 18), and CO_2 (m/z=44) were detected in the composition of the exit-stream evolved during thermal analysis. A gradual weight loss till approximately 550 °C was observed for all samples reaching 28 to 43 wt% when going from sample HT Mg/Al 0.06 to HT Mg/Al 3. Overall three main endothermic effects were observed and are in agreement with the previously reported results.[d-f] The first one, in the 25-150 °C temperature range, is attributed to the loss of hydration water from the boehmite (AlO(OH)) phase. The second one is characteristic of interlayer water departure from hydrotalcite structure (between 150 and 270 °C). The third endothermic effect (starting from 275 °C) consists in a double peak and corresponds to simultaneous migration of OH^- groups (from both boehmite phase and Mg/Al hydroxide layers in hydrotalcite phase) and decomposition of CO_3^{2-} (from brucite-like layers in hydrotalcite phase). The three types of endothermic effects were observed for HT 0.3 and 0.5 samples, in agreement with phases (boehmite and hydrotalcite) identified by XRD analysis (Figure S1), while sample HT 0.06 for which only boehmite (AlO(OH)) phase was detected (by XRD) displayed only the first and the third

endothermic peaks. With increasing Mg/Al ratio, the first peak is shifting to lower temperatures, while the second and the third peaks are shifted to higher temperatures, according with the respective structures. They are associated to the loss of hydration water and OH^- groups arising from the transition of AlO(OH) phase to Al_2O_3. Sample HT 3, which showed dominant hydrotalcite structure (XRD, Figure S1) and small quantity of boehmite, did not exhibit the characteristic endothermic peak (in the 25-150 °C range) of hydration water attributed to boehmite phase, but the two other peaks (departure of interlayer water (maximum at 250 °C), and destruction of hydrotalcite structure (maximums around 325 and 425 °C) were the most pronounced among all samples. Intensity of the endothermic peaks corresponding to hydration water (in the 25-150 °C temperature range) associated to boehmite phase diminishes with increasing Mg/Al ratio. On the other hand, the intensity of the endothermic peaks associated to the interlayer water loss (peak maximum around 250 °C) increases with increasing Mg/Al ratio. Similar trend is observed for the two peaks with maximums around 325 and 425 °C, which correspond to the decomposition of hydrotalcite structure.

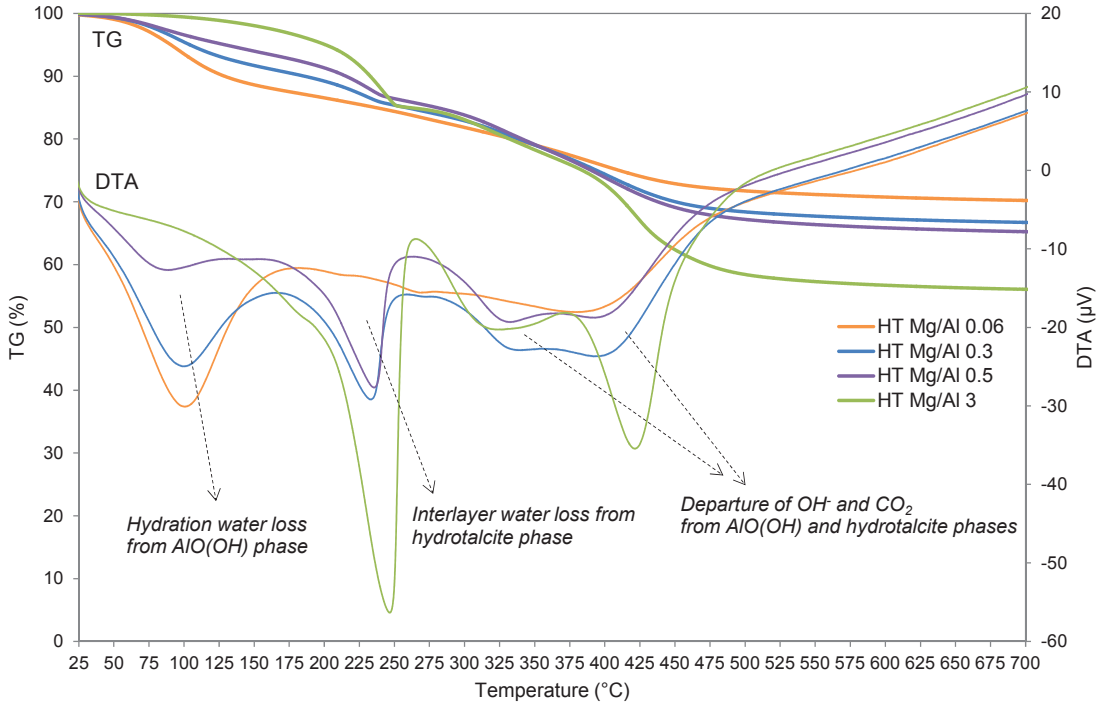

Figure S3. TG-DTA curves of the fresh hydrotalcites-HTs (MS signals not given).

Catalytic tests

Figures S4-S10 show detailed catalytic tests results for the acidic, basic, and amphoteric aldolization catalysts.

The three acidic catalysts (HPW/SiO_2, $HSiW/SiO_2$, and NbP) displayed similar catalytic behavior and the catalytic tests performed on HPW/SiO_2 are reported at Figure S4, as example. For all three catalysts the optimal working conditions were identified at 270 °C/5 000 h^{-1} with 23 mol% and 24 mol% of acrolein yield, and 7% and 6% ($CO+CO_2$) yield for HPW/SiO_2 and $HSiW/SiO_2$ catalysts, respectively. For NbP, the acrolein yield was equal to 19% with a carbon oxide yield of 8%. These results confirmed that acrolein can be generated on acidic sites. It can be stated that acrolein yield on acidic catalysts does not increase with temperature. Moreover, the presence of strong acidic sites on the catalyst surface is clearly not connected with higher production of ($CO+CO_2$).

Figure S5 presents the results obtained on MgO (basic catalyst) at the exit of the second reactor (R_2) in different conditions (various temperatures and GHSV). This catalyst exhibited the best catalytic activity among all catalysts tested in this work. For GHSV= 10 000 h^{-1}, the acrolein yield did not increase with temperature and remained constant around 20 mol%, while a gradual increase in carbon oxides production was observed at higher temperature. Similar behavior was also observed at lower contact time (GHSV=5 000 h^{-1}) at which carbon oxide production gradually increased with temperature. Acrolein yield remained constant between 270 and 300 °C (28 mol%), and then decreased to 22 mol% at 320 °C. For T≥300 °C the ($CO+CO_2$) yield was higher than 10 mol%

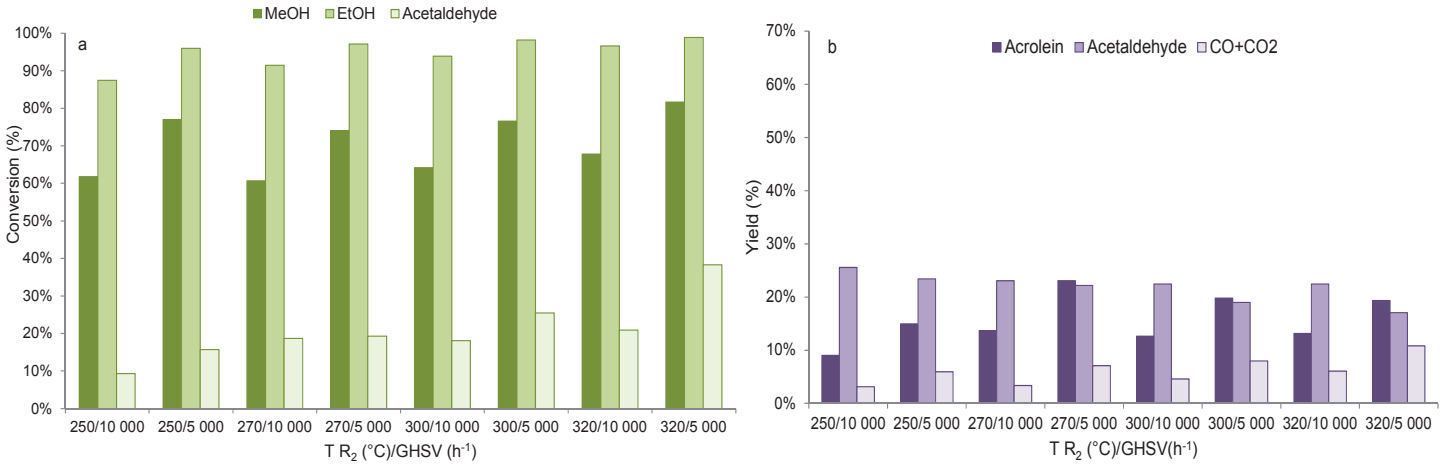

Figure S4. Catalytic performances of acidic catalysts (HPW/SiO_2) in different conditions: conversion of methanol and ethanol, and acetaldehyde conversion in the second reactor (a); yields of the main products of reaction (b).

thus limiting the possibility to further increase the reaction temperature to enhance acetaldehyde conversion and acrolein yield. Therefore, the optimal working conditions for this catalyst were identified to be 270 °C/5 000 h^{-1} and 300 °C/5 000 h^{-1} where acrolein yield was 28%, and ($CO+CO_2$) y ield 6.8 and 10%, respectively.

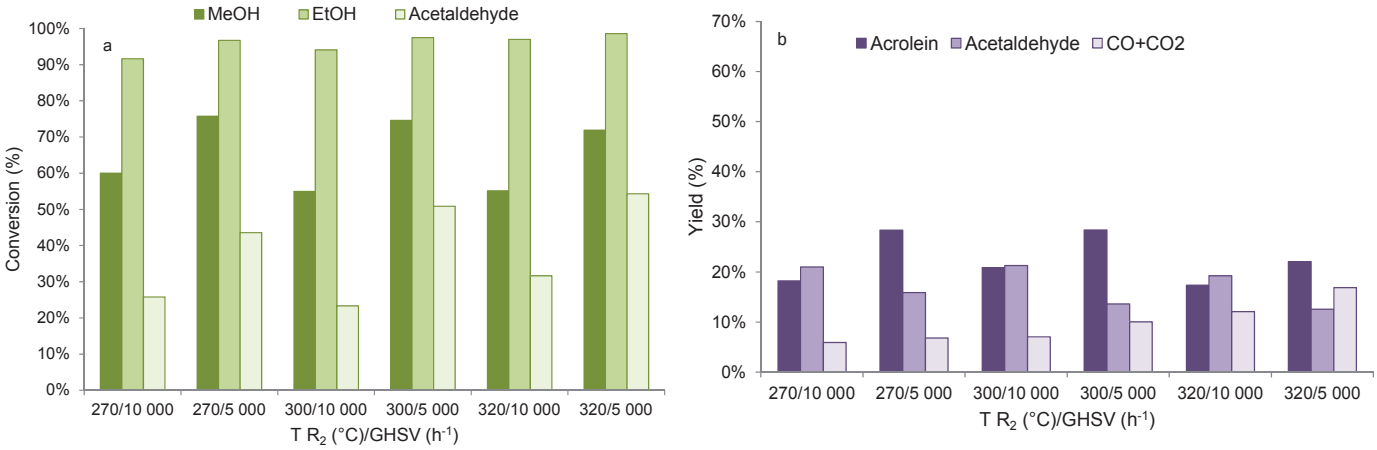

Figure S5. Catalytic performances of MgO catalyst in different conditions: total conversion of methanol and ethanol, and acetaldehyde conversion in the second reactor (a); yields of the main products of reaction (b).

Catalytic results obtained on MgO supported on alumina and alumina support are shown in Figures S6 and S7, respectively. Noticeable higher production of carbon oxides was observed for MgO/Al_2O_3 catalyst when compared to alumina support and pure MgO in all working conditions. For both MgO/Al_2O_3 and pure alumina acrolein yield was very low (below 20%), even at the identified optimal working conditions (250 °C/5 000 h^{-1} and 270 °C/10 000h^{-1}, respectively). The acrolein production was diminished due to the significant production of ($CO+CO_2$) starting from250 °C for MgO/Al_2O_3 and 270 °C for alumina. By comparing the catalytic behavior of MgO, MgO/Al_2O_3 and Al_2O_3, it can be observed that the deposition of MgO on alumina does not improve the catalytic behavior of MgO since the production of carbon oxides dramatically increased. At ($CO+CO_2$) yield ≤10% (parameter used to fix the optimal working conditions) MgO/Al_2O_3 and alumina displayed only 22 mol% (250 °C/5 000 h^{-1}) and 18% (270 °C/10 000 h^{-1}) acrolein yield, respectively.

These results arise from the fact that basicity of MgO (due to its much lower surface area) is lower than those of MgO/Al_2O_3 and Al_2O_3 (Figures 4-6 and 10), in agreement with the previously reported observation that basic sites are necessary for acrolein production, but that a too high basicity (and more precisely high amount of relatively strong basic sites) leads to over-oxidizing side reactions, which results in an increased production of carbon oxides.[g-j] Moreover by comparing these results with those obtained on MgO supported on silica and previously reported in reference g, it is clear that the deposition of MgO on alumina is not beneficial.

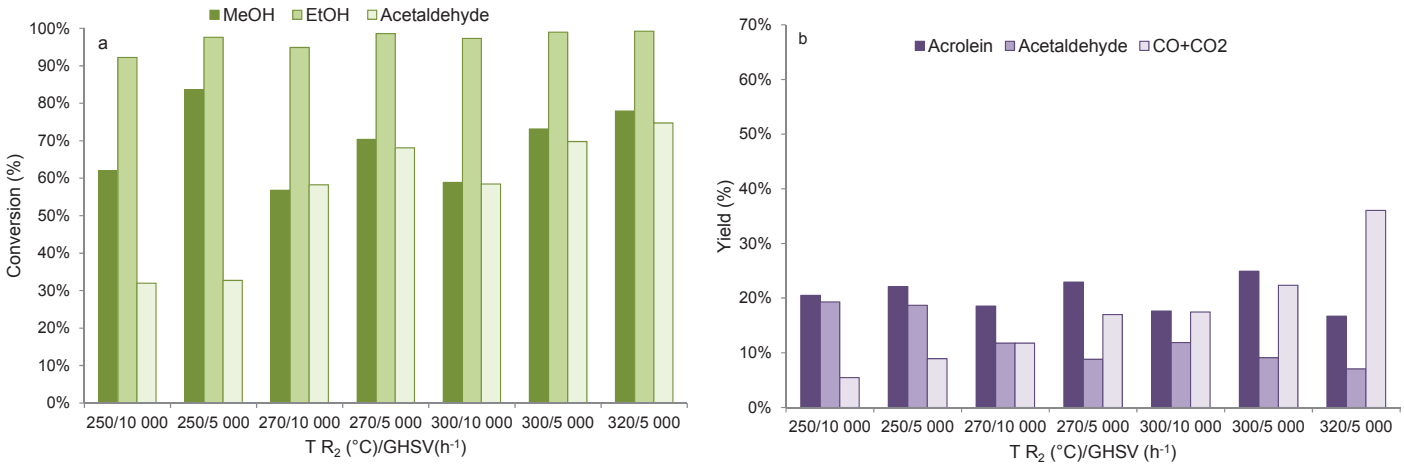

Figure S6. Catalytic performances of MgO/Al_2O_3 catalyst in different conditions: conversion of methanol and ethanol, and acetaldehyde conversion in the second reactor (a); yields of the main products of reaction (b).

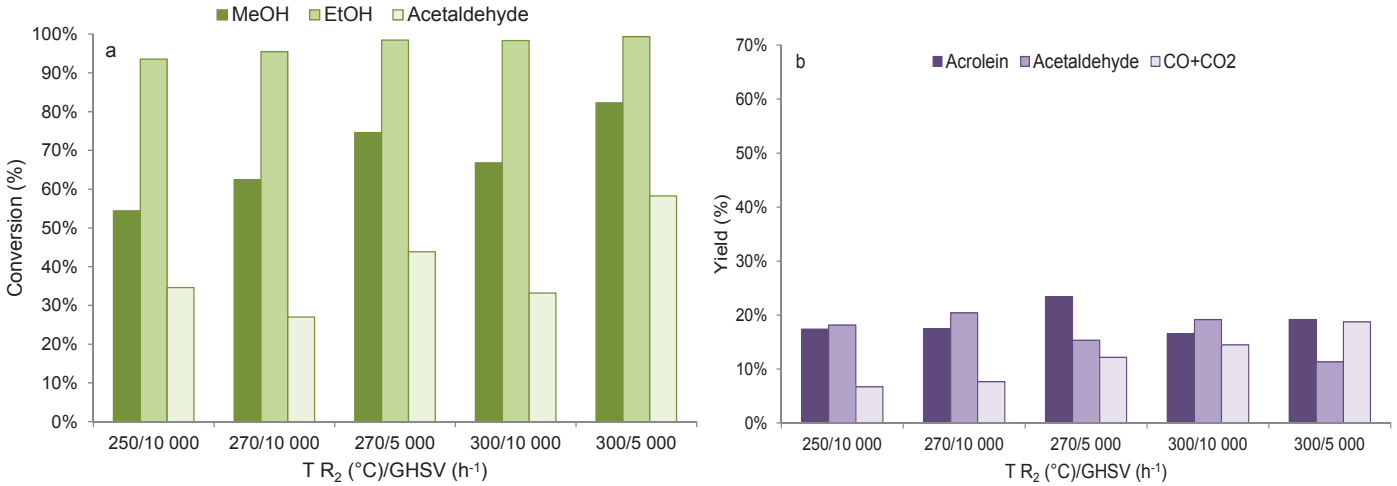

Figure S7. Catalytic performances of Al_2O_3 catalyst in different conditions: conversion of methanol and ethanol, and acetaldehyde conversion in the second reactor (a); yields of the main products of reaction (b).

Considering CHT catalysts with different Mg/Al ratios two different catalytic behaviors were observed for CHT Mg/Al 3, and for CHT Mg/Al 0.5, 0.3 and 0.06 respectively (Figures S8 and S9). Generally all CHT samples

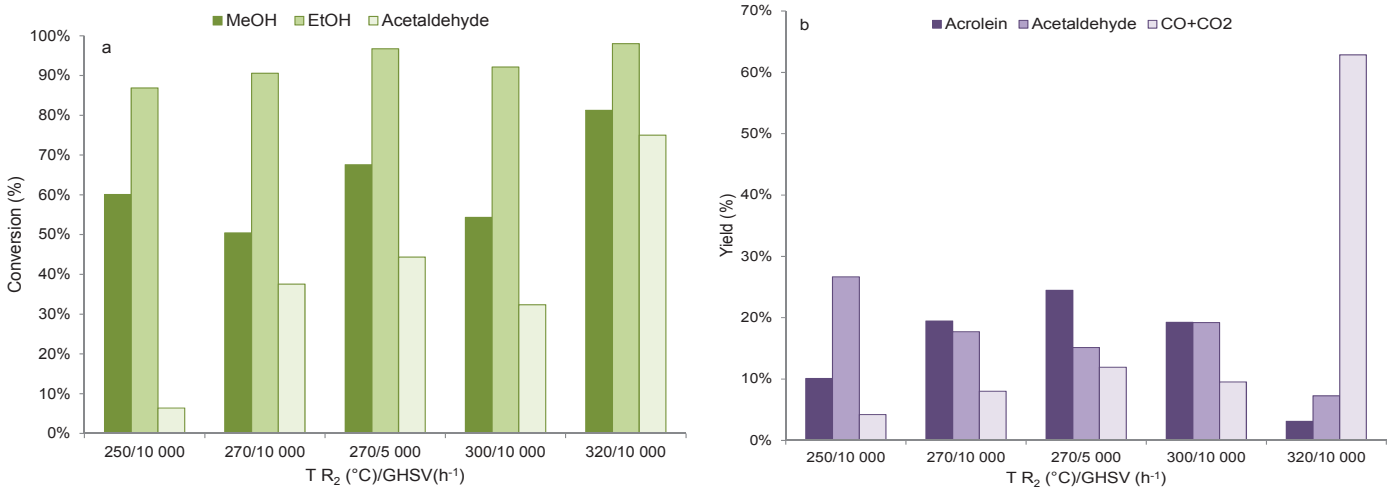

Figure S8. Catalytic performances of CHT Mg/Al 3 catalyst in different conditions: conversion of methanol and ethanol, and acetaldehyde conversion in the second reactor (a); yields of the main products of reaction (b).

exhibited acrolein yield below 25 mol%. Over-oxidizing behavior of the CHT catalysts is even more dramatic than for MgO/Al_2O_3 and alumina support. For CHT Mg/Al 3 catalyst, ($CO + CO_2$) yield started to be higher than 10% already at 270 °C/5 000 h^{-1} and further increasing of the temperature led to almost total conversion to ($CO+CO_2$) (as measured at 320 °C/10 000 h^{-1}). For the other CHT samples a very high production of carbon oxides was observed at 300 °C and 10 000 h^{-1} with a carbon oxides yield around 50%. This behavior is connected to the different basic features of these samples that arouse from the differences in their physico-chemical and structural properties. It is worth to recall that CHT Mg/Al 3 sample, which showed the best catalytic behavior among all CHT catalysts, presents a structure corresponding to homogeneous MgO phase, with aluminum cations incorporated into the matrix. Differently, the other CHT Mg/Al samples consist of two non-homogeneously mixed oxides, where alumina or Mg_xAlO_y spinel is dominant and a smaller proportion of MgO oxide is present. This enlightens the importance of MgO phase for the optimization of acrolein production.

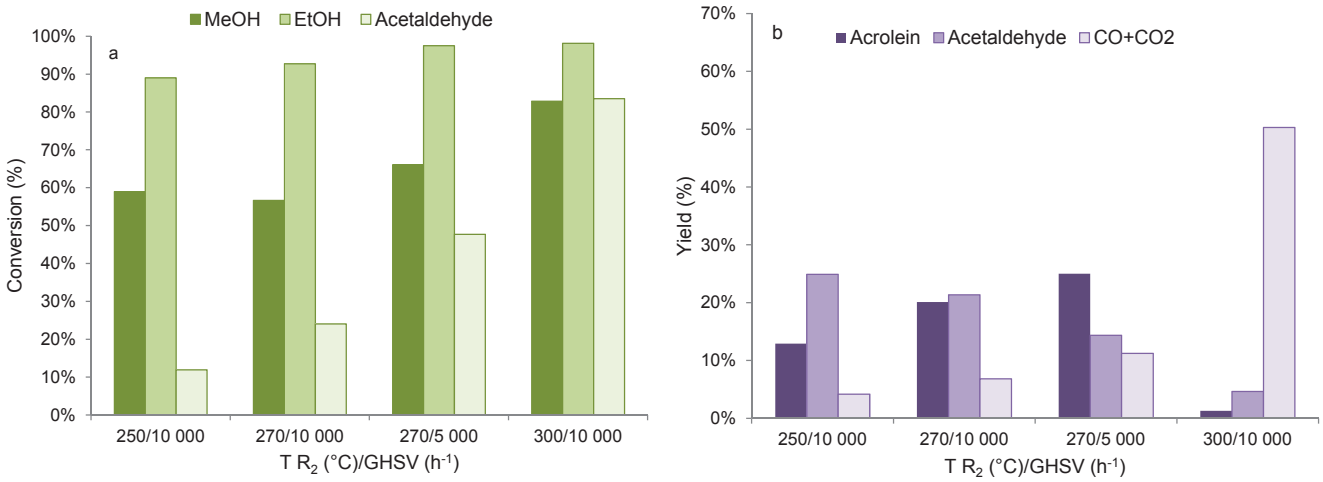

Figure S9. Catalytic performances of CHT Mg/Al 0.3 catalyst in different conditions: conversion of methanol and ethanol, and acetaldehyde conversion in the second reactor (a); yields of the main products of reaction (b).

The catalytic results obtained on ZrO_2 catalyst are represented in Figure S10; a poor production of acrolein (below 16%) was observed in all reaction conditions, while a production of carbon oxides higher than 10 mol% was measured starting from 270 °C at 5 000 h^{-1}.

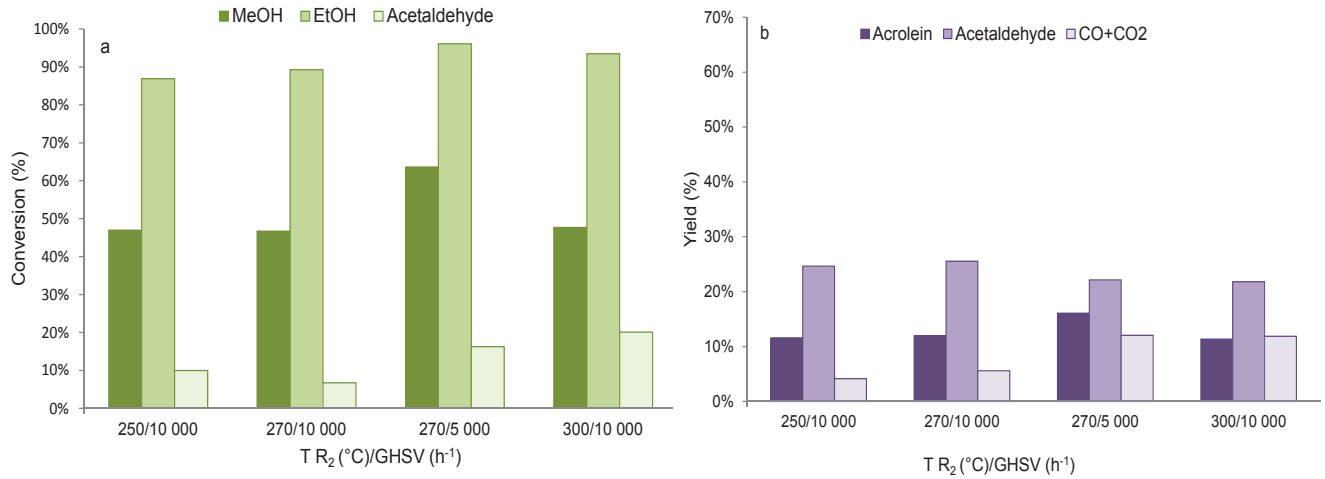

Figure S10. Catalytic performances of ZrO_2 catalyst in different conditions: conversion of methanol and ethanol, and acetaldehyde conversion in the second reactor (a); yields of the main products of reaction (b).

References

a http://www.prosim.net/bibliotheque/File/Brochures/FR_thermoprosim.pdf

b G.H. Tompson, *International Journal of Thermophysics*, 1996, **17 (1)**, 223-232.

c Q. Sun, A. Auroux, J. Shen, *J. Catal.* **2006**, *244*, 1-9.

d H.A. Prescott, Z.J. Li, E. Kemnitz, A. Trunschke, J. Deutsch, H. Lieske, A. Auroux, *J. Catal.* **2005**, *234*, 119-130.

e V. Feuillade and W. Haije, *(Characterization of hydrotalcite materials for CO_2 selective membranes)* in *Proceedings of the 9th International Conference on Inorganic Membranes*, Lillehammer, Norway, **2006**.

f S. Liu, C. Chen, Q. Liu, Y. Zhuo, D. Yuan, Z. Daib, J. Baob, *RSC Advances* **2015**, *5*, 71728-71734.

g A. Lilić, S, Bennici, J.F. Devaux, J.L. Dubois, A. Auroux, *ChemSusChem* **2017**, *10*, 1916-1930.

h M. Ai, *Bull. Chem. Soc. Jpn.* **1991**, *64*, 1342–1345.

i E. Dumitriu, V. Hulea, C. Chelaru, C. Catrinescu, D. Tichit, R. Durand, *Appl. Catal. A* **1999**, *178*, 145–157.

j E. Dumitriu, V. Hulea, N. Bilba, G. Carja, A. Azzouz, *J. Mol. Catal.* **1993**, *79*, 175–185.

Chapter 8.

Conclusions

1) Oxidation of (bio)-isobutene to (bio)-methacrylic acid: impact of the impurities on the catalysts

The impact of acid (SO_2 and CO_2) and basic (NH_3) impurities on commercial and model catalysts was investigated with the aim to understand if the existing industrial catalysts could be applied in the two step gas-phase oxidation of isobutene (IBN) to methacrylic acid (MAA), when bio-sourced isobutene, obtained by fermentation of sugars, was used instead of oil-derived IBN. The main technique, used for these ex-situ studies, was adsorption microcalorimetry. The interaction with impurities was estimated by taking into account the differential heat values of adsorption (Q_{diff}).

The 1st stage catalyst resulted to be applicable in the oxidation of IBN to methacrolein (MAL), since the main phases of the catalyst did not interact with SO_2, CO_2 and NH_3. The 2nd stage catalyst showed interaction with ammonia, and NH_3-containing compounds, formed during adsorption calorimetry, were stable up to 350-450 °C. When decomposed in inert gas, the departure of oxygenated molecules as N_2O, with the consequent reduction of the catalyst, was detected. It was found that the species interacting with ammonia involved molybdophosphoric acid components. Interaction with ammonia (in a comparable amount) occurred also when molybdophosphoric acid was replaced by another heteropolyacid (HPW, HSiMO, HSiW).

Acid-base properties of bulk oxides and heteropolyacids were determined. The most important result showed that for heteropolycids (HPW, HPMo, HSiW, and HSiMo) the pretreatment temperature significantly drives the acidic features. In Figure 8.1, the comparison of the results obtained by NH_3 adsorption microcalorimetry for the heteropolyacids pretreated at 200 °C (left) and 350 °C (right) is shown. HPW is the most acidic heteropolyacid and presented a well-defined plateau of strong sites in both cases. The plateau of differential heats of adsorption (Q_{diff}) was around 176 kJ mol^{-1} for HPW pretreated at 200 °C, and about 10 kJ mol^{-1} lower for the sample pretreated at 350 °C. The acidity of HSiW was stronger affected by the higher pretreatment temperature, and even if Q_{init} was around 180 kJ mol^{-1} in both cases and the amounts of ammonia adsorbed very similar, the plateau corresponding to sites of homogeneous strength completely disappeared after pretreatment at 350 °C. The acidity of molybdenum-containing heteropolyacids was strongly affected (Q_{diff} in the range of physisorption values) by the higher pretreatment temperature, due to decomposition of the Keggin structure responsible for superacidity of heteropolyacids.

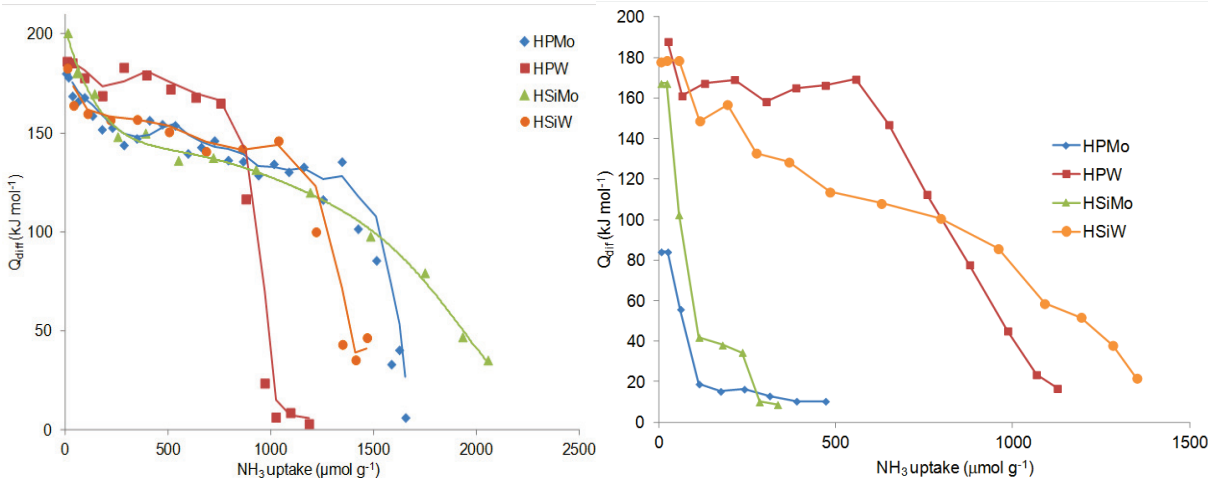

Figure 8.1. Curves of differential heats *vs.* ammonia coverage for the heteropolyacids pretreated overnight under vacuum at 200 °C (left) and 350 °C (right). Temperature of ammonia adsorption was maintained at 150 °C.

2) Acrolein production by oxidative coupling of methanol and ethanol: impact of the acid/base properties of the catalyst on acrolein production

The impact of catalyst acidity and basicity was for the first time studied for the reaction of aldol condensation of acetaldehyde and formaldehyde in oxidizing conditions.

Results, obtained after testing alkaline (Na_2O and K_2O) and earth alkaline (MgO and CaO) oxides supported on silica showed that the presence of strong basic sites (Q_{diff}>150 kJ mol^{-1}) enhances acrolein production, but that a high number of basic sites increases the production of carbon oxides. Magnesium oxide supported on silica (the only amphoteric catalyst in this series) was the most active. In this case, acrolein yield was improved thanks to the additional presence of strong acidic sites.

The impact of only acidic sites was investigated with HPW/SiO_2, HSiW/SiO_2, and NbP, and it was confirmed that acrolein production occured also on strong acidic sites, but the yields of acrolein always remained below 20 mol%. On the strong acidic sites, the production of acrolein and (CO+CO_2) did not increase with the temperature, neither by increasing the amount of acidic sites. Therefore, the sole presence of strong acidic sites is not enough to obtain high acrolein production.

Investigation of basic (MgO) and amphotheric catalysts (such as Mg-Al mixed oxides derived from hydrotalcites with different Mg/Al ratios, and MgO supported on alumina) led to the conclusion that, on strong basic sites, acrolein production increases with temperature increasing. At the same time, a high amount of strong basic sites (Q_{diff}>150 kJ mol^{-1}) brings to higher production of carbon oxides, thus diminishing the acrolein selectivity. Co-existence of strong basic and strong acidic sites in similar amount (preferably with a “strong basic sites/strong acidic sites” ratio close to 1) seems to be the best acid-base surface sites configuration for maximizing the acrolein production in oxidizing reaction conditions. On amphoteric catalysts, with enough quantity of strong acidic sites, acrolein

production is enhanced, and carbon oxides production is limited, thus allowing the catalyst to work at higher temperatures. Figure 8.2 summarizes the dependence of carbon oxides and acrolein yield on the amount of strong basic sites for basic and amphoteric catalysts. All catalysts presented dominant basic character, except MgO/SiO_2 and MgO/Al_2O_3, which show also considerable amount of strong acidic sites.

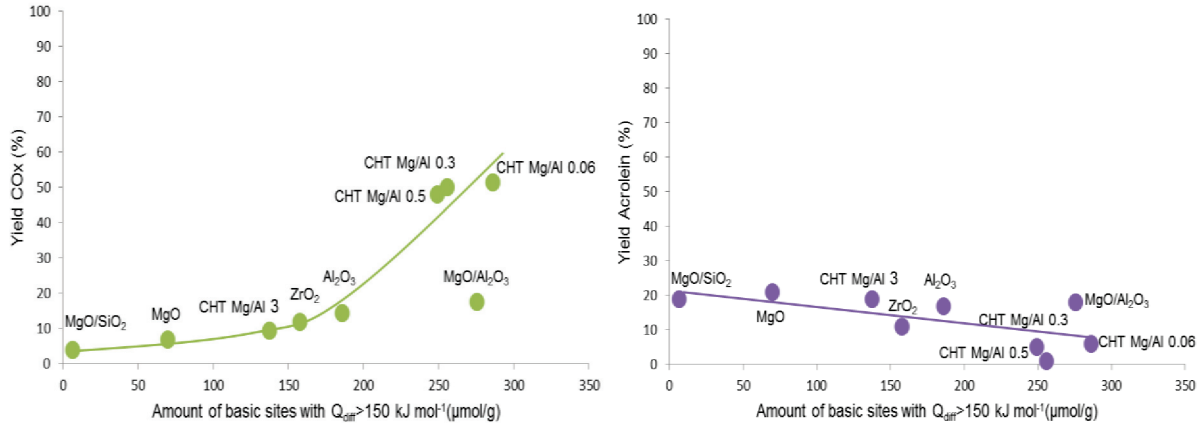

Figure 8.2. Correlation between carbon oxides (left) and acrolein (right) yield (300 °C/10 000 h^{-1}) and the amount of strong (Q_{diff}>150 kJ mol^{-1}) basic sites for basic and amphoteric catalysts.

Generally, magnesia and supported magnesia catalysts presented better results than mixed Mg-Al oxides, prepared starting from hydrotalcites (CHT, Mg/Al ratio from 0.06 to 3). CHTs showed very high carbon oxides production (at relatively low temperatures, <300 °C) and acrolein yield around 20 mol%. Thanks to a proper amount of strong basic sites (<100 µmol g^{-1}) magnesium oxide showed a good acrolein production. The catalytic performance of magnesia was improved by deposition on a silica support. This enhancement in acrolein production can be related to the creation of new acidic sites, in addition to the basicity already present on magnesia. Among all the tested catalysts, MgO/SiO_2 showed the best catalytic performance for this process. Optimal working conditions for this catalyst were found to be 320°C/5 000 h^{-1}, with an acrolein yield of 35 mol% and ($CO+CO_2$) yield 10 mol%.

Figure 8.3. shows the comparison between the amount and strength distribution of acidic and basic sites for MgO and silica and alumina-supported magnesia. MgO is a completely basic catalyst, while MgO/SiO_2 and MgO/Al_2O_3 are amphoteric. MgO/SiO_2 is characterized by a similar amount of basic and acidic sites with a slightly dominant acidic character. MgO/Al_2O_3 catalyst presented a much higher number of acidic and strong basic sites than MgO/SiO_2.

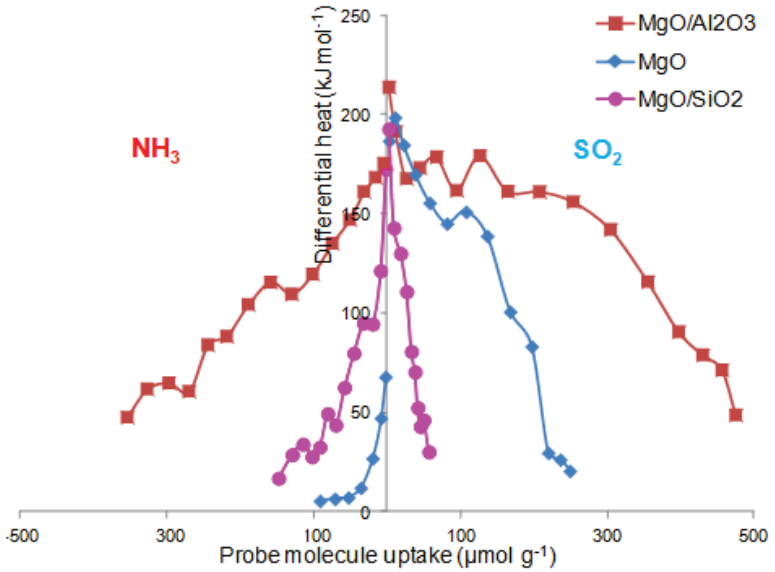

Figure 8.3. Strength distribution of MgO/SiO_2, MgO and MgO/Al_2O_3 catalysts. Izbaci slovo a iz grafika

Table 8.1. summarizes the catalytic performances of these three MgO-based catalysts at 300 °C/10 000 h^{-1}, 320 °C/5 000 h^{-1}, and at the optimal reaction conditions. Due to the high basicity, MgO/Al_2O_3 produced remarkably high amount of carbon oxides already at 300 °C. At 320 °C only MgO/SiO_2 presented good catalytic activity, with 35 mol% of acrolein yield and CO_x yield of 10 mol%. Comparing the catalytic performances of these three Mg-containing catalysts, MgO/SiO_2 showed to be the best aldolization catalyst. It can be used in a single reactor process together with FeMoOx redox catalyst. Pure MgO can be also eventually applied, while MgO/Al_2O_3 is not suitable for this reactor configuration.

Table 8.1. Comparison of catalytic tests results (feed: $(MeOH+EtOH)/O_2/N_2=(4+2)/8/86$ mol. %) over FeMoOx (R_1) + MgO/SiO_2, MgO and MgO/Al_2O_3 (R_2) catalysts. Optimal conditions= the best catalytic performance when carbon oxides yield maximum 10 mol. %.

Conditions : T(°C)/GHSV(h^{-1})	300 °C/10 000 h^{-1}		320 °C/5 000 h^{-1}		Optimal conditions
Yield (mol. %)	Acrolein	$(CO+CO_2)$	Acrolein	$(CO+CO_2)$	Acrolein
MgO/SiO_2	19	4	35	10	35
MgO	21	7	22	17	28
MgO/Al_2O_3	18	17.5	17	36	22

CO_x production increased with the amount of strong basic sites. Addition of strong acidic sites had a positive influence to limit $(CO+CO_2)$ production. Strong basic sites should be present in an amount lower than 100 µmol g^{-1}, in order to avoid the over-oxidation to CO_x, caused by too high basicity. If the amount of basic and acidic sites is similar, the acrolein yield is higher, and carbon oxides production limited. Besides, the acrolein yield decreases when the strong basic character of the catalyst increases.

3) Acid/base properties of catalytic solids determined by gas-phase adsorption microcalorimetry

The number, strength and strength distribution of the acid and base surface sites were determined by adsorption microcalorimetry, for all the solid samples used during this thesis. Then the obtained data were used to create scales of the acidity and basicity of the solids (inspired by pH scales for liquids). Since the concept of acidity and basicity of solids is more complicated than that of liquids, it is necessary to create more than one scale to be able to describe the acidity and basicity of a given solid. Scales drawn (Figures 8.4. and 8.5.) present the surface acidity (NH_3 adsorption) and basicity (SO_2 adsorption) by reporting the differential heats of adsorption and the gas-phase probe molecules uptakes. Heat of adsorption represents the strength of acidic or basic sites. Differential heats below 100 kJ mol^{-1} are attributed to physisorption phenomena (weak acidic or basic sites). Differential heats of adsorption between 100 and 150 kJ mol^{-1} are usually connected to the presence of middle-strength sites , while values of differential heats higher than 150 kJ mol^{-1} correspond to very strong acidic or basic sites. However, to have a clear idea of the acid/base properties of one solid catalyst, besides the strength of the acidic or basic sites, it is important to know their quantity (Fig. 8.5.).

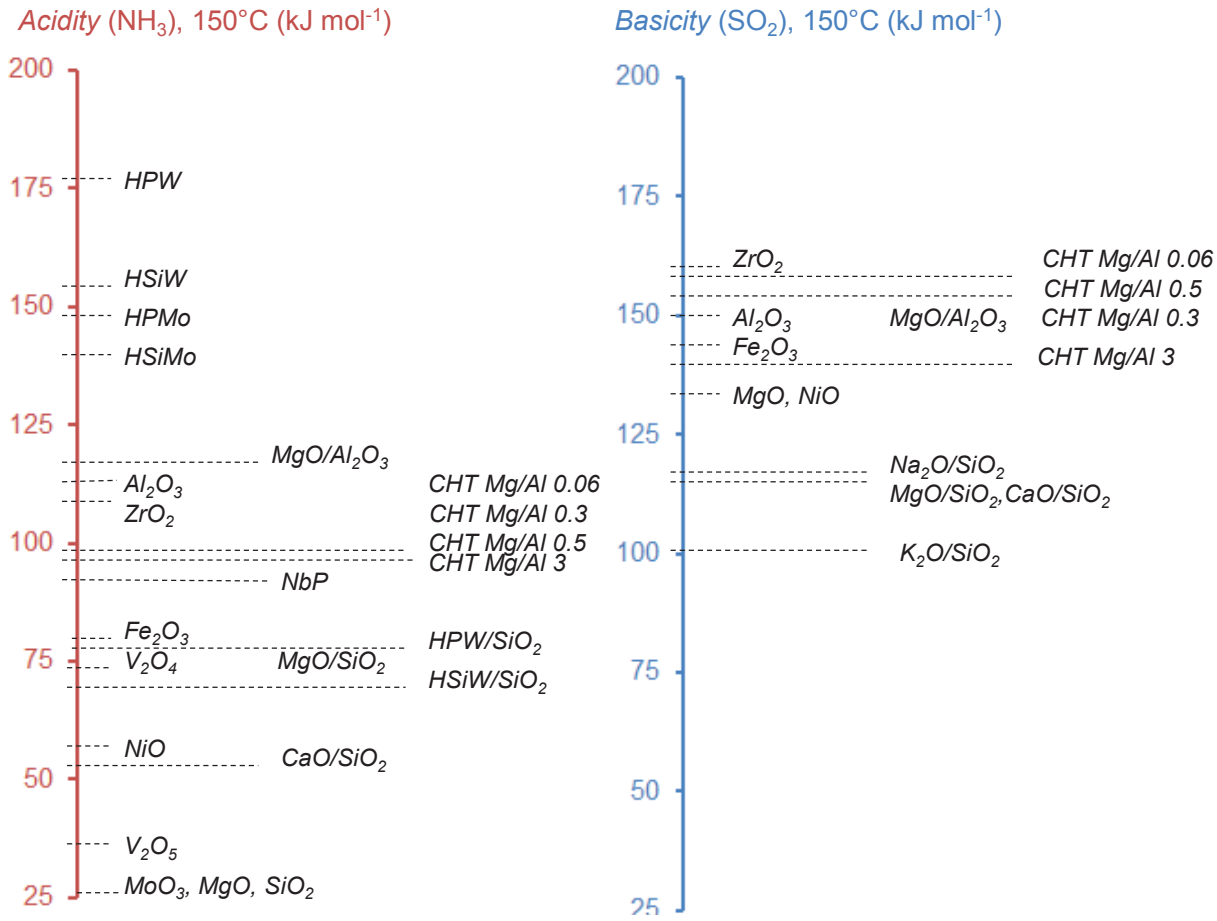

Figure 8.4. Scales of acidic and basic strength established based on the average heat of probe molecule adsorption measured at the plateau of the differential heat curve, or at half coverage when no plateau is observed.

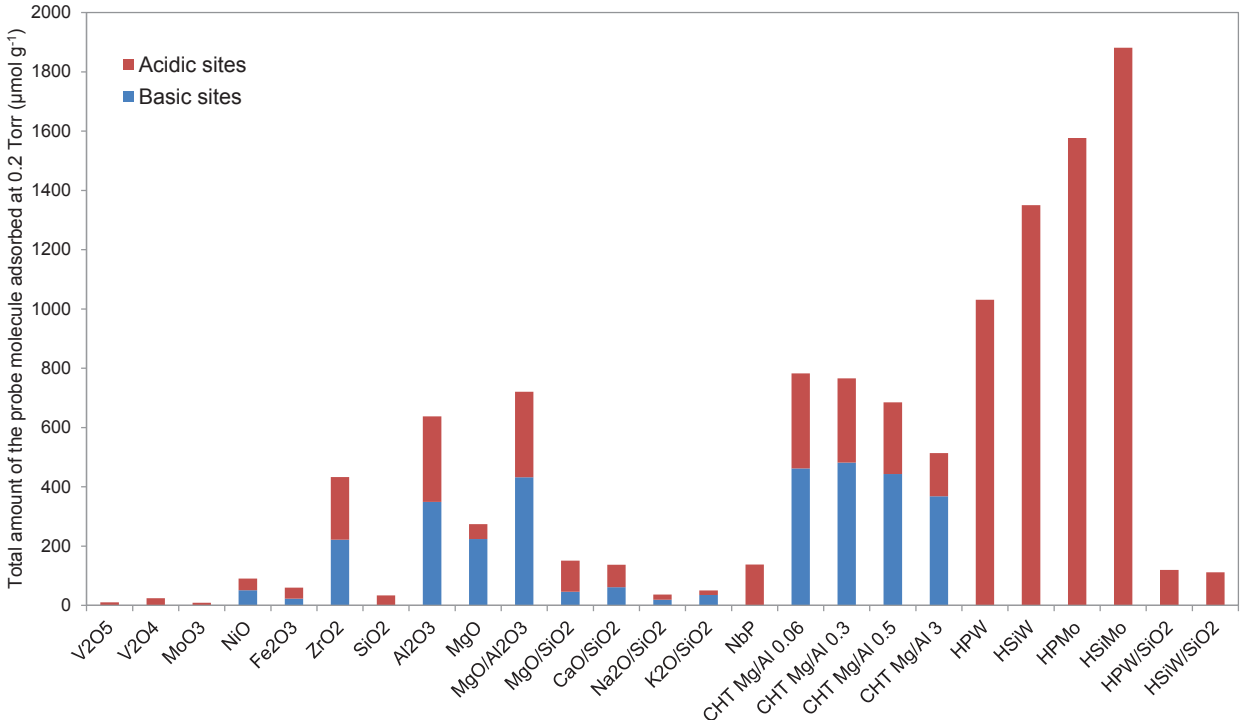

Figure 8.5. Scale of acidity and basicity obtained by measuring the total amount of probe molecules adsorbed at 0.2 Torr.

List of abbreviations *(in alphabetical order)*

^{27}Al MAS NMR	Nuclear Magnetic Resonance
ADEME	*Agence de l'Environnement et de la Maîtrise de l'Energie*
BET	Brunauer-Emmett-Teller (method for determination of specific surface area)
C.A.	Chemical Analysis (performed by ICP-OES)
ca.	Circa
Ca/Si	CaO supported on silica
CHT(s)	Calcined hydrotalcite(s)
CNRS	*Centre National de la Recherche Scientifique*
CO_x	Carbon monoxide and carbon dioxide
e.g.	For example
Eq.	Equation
EtOH	Ethanol
$FeMoO_x$	Iron molybdate redox catalyst
Fig.	Figure
GHSV	Gas Hourly Space Velocity
HPA(s)	Heteropolyacids(s)
HPMo	12-molybdophosphoric acid ($H_3PMo_{12}O_{40}$)
HPW	12-tungstophosphoric acid ($H_3PW_{12}O_4$)
HSiMo	12-molybdosilicic acid ($H_4SiMo_{12}O_{40}$)
HSiW	12-tungstosilicic acid ($H_4SiW_{12}O_{40}$)
HT(s)	Hydrotalcite(s)
IBN	Isobutene
ICP-OES	Inductively Coupled Plasma-Optical Emission Spectroscopy
i.e.	That is

IRCELYON	*Institut de Recherches sur la Catalyse et l'Environnement de Lyon*
K/Si	K_2O supported on silica
MAA	Methacrylic acid
MAL	Methacrolein
MeOH	Methanol
Mg/Si	MgO supported on silica
Na/Si	Na_2O supported on silica
OCA	Oxidative Coupling of Alcohols
PEA	Phenylethylamine
Q_{diff} (also q_{diff})	Differential heat of adsorption
Q_{init} (also q_0 or q_{init})	Initial differential heat of adsorption
R_1	Redox reactor (the first reactor)
R_2	Aldolization reactor (the second reactor)
S_{BET}	Specific surface area determined by BET method
T_1	Temperature in the first (redox) reactor (R_1)
T_2	Temperature in the second (aldolization) reactor (R_2)
Tab.	Table
TG	Thermogravimetric analysis
TG-DTA-MS	Simultaneous thermogravimetric and differential thermal analyses coupled with mass spectrometer
UCCS	*Unité de Catalyse et Chimie du Solide*
V_{irr}	Chemisorbed amount of the probe molecule on the surface
V_{tot}	Total amount of the probe molecule adsorbed on the surface
XRD	X-Ray Diffraction
XPS	X-ray photoelectron spectroscopy

Abstract (English, French)

The present work focuses on the impact of the amount and strength of acidic and/or basic sites on the yield of acrolein produced by alcohols oxidative coupling in gas phase. The influence of acid/base ratio of catalytic sites has been studied in the aldol condensation of acetaldehyde and formaldehyde to acrolein performed in oxidizing conditions. The obtained data and correlations supplied valuable information to understand which parameters have to be modified to improve the acrolein selectivity. The first reaction of the process implies methanol and ethanol oxidation respectively to formaldehyde and acetaldehyde on a FeMoOx redox catalyst. Then the cross-aldolization of the two aldehydes and the dehydration to acrolein is performed on acid/base catalysts. Because the alcohols involved in this process can be bio-sourced, this new route to produce acrolein presents a very high interest, since it can replace the current fossil-based acrolein production (nowadays industrially produced by oxidation of propylene).

The optimal catalyst should present amphoteric features with a similar amount of both basic and acidic sites. A moderate and balanced presence of acidic and basic sites improves the acrolein yield and the production of carbon oxides is significantly increased only at high temperature. Among all studied catalysts, MgO supported on silica has been identified as the best catalyst for aldol-condensation of aldehydes to acrolein in oxidizing conditions thanks to a given ratio of basic to acidic sites.

Keywords:

Biomass, Acrolein, Oxidative coupling of methanol and ethanol, Adsorption microcalorimetry, Acid/base properties, Aldol condensation of acetaldehyde and formaldehyde

_ _

Ce travail de thèse se focalise sur l'impact des propriétés acido-basiques des catalyseurs (quantité et force des sites) dans la production d'acroléine par couplage oxydant d'alcools en phase gazeuse.

L'influence du rapport entre site acides et sites basiques des catalyseurs a été étudiée dans la condensation aldolique de l'acétaldéhyde et du formaldéhyde en acroléine, réalisée en conditions oxydantes. Les données et corrélations obtenues ont donné des informations indispensables à l'identification des paramètres qui doivent être modifiés afin d'améliorer la sélectivité en acroléine.

La première réaction du procédé implique l'oxydation du méthanol et de l'éthanol respectivement en formaldéhyde et acétaldéhyde sur un catalyseur rédox de type FeMoOx.

Ensuite, l'aldolisation croisée des deux aldéhydes et la déshydratation en acroléine sont effectuées sur des catalyseurs acido-basiques.

Les alcools impliqués dans ce procédé pouvant dériver de la biomasse, cette nouvelle voie de production d'acroléine présente un intérêt élevé puisqu'elle peut remplacer la production actuelle d'acroléine basée sur des ressources fossiles (aujourd'hui l'acroléine est produite industriellement par oxydation du propylène).

Le catalyseur optimal doit présenter des caractéristiques amphotères avec une quantité similaire de sites basiques et acides. Une présence modérée et équilibrée de sites acides et basiques améliore le rendement en acroléine et déplace à plus haute température la production des oxydes de carbone. Parmi tous les catalyseurs étudiés, et grâce à ses propriétés acido-basiques spécifiques, MgO supporté sur silice a été identifié comme étant le meilleur catalyseur pour la condensation aldolique des aldéhydes en acroléine en conditions oxydantes.

Mots clés:

Biomasse, Acroléine, Couplage oxydant d'alcools, Calorimétrie d'adsorption, Propriétés acido-basiques, Condensation aldolique d'acétaldéhyde et de formaldéhyde

Résumé en français

Cette thèse a été menée dans le cadre du projet BioMA+ financé par *l'Agence de l'Environnement et de la Maîtrise de l'Energie (ADEME)* dans le cadre du programme "Investissement d'avenir". Le projet a rassemblé des partenaires de recherche français, industriels et universitaires, avec différents domaines d'expertise, y compris la biochimie, la catalyse et l'ingénierie, afin d'étendre le processus de production de l'isobutène de la biomasse (développé par *Global Bioenergies*) à l'échelle de pilote industriel. Le projet visait également à convertir cet isobutène bio-sourcé en acide méthacrylique, un composé largement utilisé dans les peintures. Pour la première fois, de l'acide méthacrylique a été effectivement produit à partir de bio-isobutène, et le succès obtenu dans le pilote industriel a permis une mise à l'échelle d'un démonstrateur récemment installé à Leuna (en Allemagne).

Mais le cœur de ce projet a été consacré à l'étude d'une nouvelle voie de production de l'acroléine à partir de méthanol et éthanol. Un tel procédé, réalisé sur des catalyseurs de type FeMoOx, a été récemment proposé par *ARKEMA* et *UCCS (Unité de Catalyse et Chimie du Solide)* et sa mise en œuvre dans un micropilote de taille industrielle ouvre de nouvelles perspectives pour remplacer l'actuel procédé de production de l'acroléine, aujourd'hui basé sur des ressources fossiles.

Les résultats obtenus au cours du projet permettront de mieux comprendre le mécanisme de réaction, et de permettre une amélioration du rendement en acroléine, envisageable dans des applications futures.

L'étude présentée dans le présent manuscrit a été réalisée grâce à un partenariat entre *l'IRCELYON (Institut de Recherche sur la Catalyse et de l'Environnement de Lyon)* et *le CRRA ARKEMA (Centre de Recherche Rhône-Alpes, ARKEMA, Pierre Bénite).*

Les recherches réalisées au cours de cette thèse de doctorat sont liées aux réactions d'oxydation de l'isobutène en acide méthacrylique et à la production d'acroléine par couplage oxydant d'alcools (méthanol et éthanol).

La production en phase gazeuse de l'acide bio-méthacrylique se fait en deux étapes (consistant en deux oxydations successives: oxydation de l'isobutène en méthacroléine suivie de l'oxydation de la méthacroléine en acide méthacrylique). Notre travail a été d'étudier l'impact d'éventuelles impuretés, contenues dans le bio-isobutène sur l'empoisonnement des sites acides/basiques des catalyseurs. En ce qui concerne la production d'acroléine, cette réaction consiste en deux étapes successives: l'oxydation des alcools en formaldéhyde et acétaldéhyde et la condensation aldolique des aldéhydes pour former l'acroléine. A l'origine cette méthode a été développée pour avoir lieu dans un seul réacteur sur des catalyseurs de type FeMoOx. Au cours de cette thèse, la réaction a été découplée et réalisée dans deux réacteurs consécutifs. De nombreux tests catalytiques, utilisant le catalyseur redox FeMoOx de référence, dans le premier réacteur (oxydation), et divers catalyseurs d'aldolisation, dans le second réacteur (aldolisation), ont été effectués et corrélés aux propriétés acido-basiques de surface. En particulier, les caractéristiques acido-basiques des catalyseurs ont été, pour la première fois, corrélées au rendement en acroléine obtenu en conditions oxydantes.

La technique principale utilisée pour étudier l'interaction des impuretés avec la surface des catalyseurs et pour l'étude de leurs propriétés acido-basiques a été la microcalorimétrie d'adsorption en phase gazeuse. D'autres techniques complémentaires comme la diffraction des rayons X (XRD), l'analyse chimique (ICP-OES) et thermique (TG et TG-DTA-MS), l'adsorption d'azote à basse température, la spectrométrie photoélectronique X (XPS) et la résonance magnétique nucléaire (RMN MAS 27Al) ont été aussi utilisées pour caractériser les catalyseurs.

Le projet BioMA+ est couvert par un accord de confidentialité jusqu'au 19/12/2026. Toutefois, en raison de l'accord donné par les participants au projet, le contenu de ce manuscrit peut être divulgué.

Le sujet et les résultats de la thèse sont présentés en huit chapitres.

Le premier chapitre intitulé «Introduction» présente le projet BioMA+ et clarifie le positionnement de cette thèse dans le projet (Section 1.1). Les principaux objectifs de la présente thèse sont définis en Section 1.2.

Le chapitre 2 présente l'état de l'art dans le domaine des réactions catalytiques impliquées dans cette thèse. La Section 2.1. fournit une brève description bibliographique de la problématique en considérant l'oxydation du (bio)-isobutène en acide (bio)-méthacrylique. Dans la section 2.2. l'aperçu des applications de l'acroléine et des méthodes de synthèse proposées jusqu'à présent est donné. Les Sections 2.3. à 2.6. sont dédiées à la production de méthanol et d'éthanol, à l'oxydation du méthanol en formaldéhyde sur des catalyseurs FeMoOx, à l'oxydation de l'éthanol en acétaldéhyde et aux réactions de couplage du méthanol et de l'éthanol en absence d'oxygène. Finalement, en Section 2.7. le nouveau procédé de synthèse de l'acroléine à partir de méthanol et éthanol est décrit en détail. Le chapitre 3 présente l'état de l'art sur l'acidité et la basicité des catalyseurs. En Section 3.1. une étude bibliographique portant sur l'influence des propriétés acido-basiques des catalyseurs sur la condensation aldolique de l'acétaldéhyde et du formaldéhyde en phase gazeuse est rapportée. De plus, un résumé détaillé de la littérature concernant la détermination des propriétés acido-basiques par microcalorimétrie d'adsorption est présenté en Section 3.2.

Le chapitre 4 (partie expérimentale) résume les informations sur la préparation des catalyseurs (Section 4.1.), les techniques expérimentales (Section 4.2.) et les essais catalytiques (Section 4.3.) effectués au cours de notre recherche.

Au cours des chapitres 5, 6, et 7, les résultats expérimentaux obtenus sont rapportés et discutés. Le chapitre 5 décrit les résultats liés à la production d'acide bio-méthacrylique par oxydation du bio-isobutène.

Les résultats les plus significatifs de cette thèse sont présentés dans les chapitres 6 et 7 et portent sur l'influence des propriétés acido-basiques des catalyseurs dans la production d'acroléine par couplage oxydant du méthanol et de l'éthanol, et plus précisément leur impact sur la condensation aldolique de l'acétaldéhyde et du formaldéhyde en phase gazeuse en présence d'oxygène. Les résultats obtenus dans l'étude d'oxydes basiques supportés sur de la silice (en tant que catalyseurs d'aldolisation) sont présentés au chapitre 6, tandis que le chapitre 7 relate l'influence de différents catalyseurs basiques, acides et amphotères sur la production d'acroléine.

Enfin, les principales conclusions de cette thèse sont résumées au chapitre 8 et ci-dessous.

- Pour l'oxydation en phase gazeuse conduite en deux étapes du bio-isobutène en acide bio-méthacrylique, l'étude de l'impact des impuretés acides (SO_2 et CO_2) et basiques (NH_3) sur les catalyseurs commerciaux a révélé que le catalyseur de la première étape est adapté à l'oxydation de l'isobutène en méthacroléine, car les principales phases présentes et identifiées n'interagissent pas avec SO_2, CO_2 et NH_3. Par contre, le catalyseur de la 2ème étape a montré une forte interaction avec l'ammoniac. Ces composés ammoniaqués sont stables jusqu'à 350-450 °C. Leur décomposition sous gaz inerte comporte le départ de molécules oxygénées (par exemple N_2O) accompagné de la réduction du catalyseur. Les espèces qui interagissent avec l'ammoniac contiennent de l'acide molybdophosphorique ou son sel de vanadium.

  L'interaction avec l'ammoniac est aussi présente lorsque l'acide molybdophosphorique est remplacé par d'autres hétéropolyacides (HPW, HSiMO, HSiW).

  Les essais catalytiques, réalisés en ajoutant différentes impuretés dans la charge standard d'isobutène, et les caractérisations des catalyseurs utilisés, ont confirmé que seule la présence d'ammoniac comme impureté dans le bio-isobutène pourrait conduire à une diminution des performances catalytiques sur le catalyseur de la 2ème étape.

- Pour la réaction d'aldolisation, différents catalyseurs, y compris des oxydes de Mg et Al, dérivés d'hydrotalcites commerciales, avec différents rapports Mg/Al, des oxydes basiques supportés sur silice et des hétéropolyacides ont été testés.

  Ces catalyseurs on été caractérisés par calorimétrie d'adsorption de NH_3, SO_2 et méthanol; la quantité, la force et la distribution de force des sites acides et basiques de surface ont pu être déterminées.

  En présence d'oxygène, la condensation aldolique d'acétaldéhyde et de formaldéhyde en acroléine s'effectue à la fois sur les sites basiques et acides.

  Sur les sites basiques forts, la production d'acroléine augmente avec la température, mais en même temps, une trop grande quantité de sites basiques forts conduit à une production plus élevée d'oxydes de carbone en diminuant la sélectivité en acroléine. Sur les sites acides forts, la production d'acroléine et celle de ($CO + CO_2$) n'augmente pas avec la température, ni avec la quantité de sites acides.

  La coexistence de sites basiques et acides forts en quantité similaire (de préférence avec un rapport sites basiques/sites acides proche de 1) semble être la meilleure configuration d'acido-basicité de surface apte à maximiser la production d'acroléine en conditions oxydantes.

  Pour les catalyseurs amphotères qui possèdent une quantité suffisante de sites acides forts, la sélectivité en acroléine est améliorée et la production d'oxydes de carbone minimisée, permettant ainsi aux catalyseurs de travailler à des températures plus élevées.

Généralement, les catalyseurs contenant du magnésium ont été les catalyseurs d'aldolisation les plus prometteurs, en particulier le catalyseur d'oxyde de magnésium supporté sur silice qui s'est avéré être le meilleur pour la condensation aldolique des aldéhydes en acroléine en conditions oxydantes grâce à ses propriétés acido-basiques spécifiques. La performance catalytique de MgO seul se trouve améliorée une fois l'oxyde supporté sur de la silice, grâce à la création de nouveaux sites acides qui s'ajoutent à la basicité originelle de l'oxyde de magnésium. L'oxyde de magnésium supporté sur alumine a montré une activité catalytique plus faible de celle de MgO pur ou de MgO supporté sur SiO_2, car la quantité de sites basiques forts était beaucoup plus élevée que celle de sites acides forts, ce qui a fortement augmenté la production d'oxydes de carbone.

- Une fois tous les catalyseurs caractérisés par calorimétrie d'adsorption de NH_3 et SO_2; et la quantité, la force et la distribution de force des sites acides et basiques de surface déterminées, les données obtenues ont été rassemblées sur des échelles uniques d'acido-basicité qui pourront servir de référence pour modéliser de nouveaux catalyseurs.